REVIEWS OF MODERN PHYSICS, VOLUME 79, OCTOBER–DECEMBER 2007

Progress in the measurement and modeling of physisorbed layers

L. W. Bruch

Department of Physics, University of Wisconsin–Madison, Madison,
Wisconsin 53706, USA

R. D. Diehl

Department of Physics, Pennsylvania State University, University Park,
Pennsylvania 16802, USA

J. A. Venables

Department of Physics, Arizona State University, Tempe, Arizona 85287, USA
and Department of Physics and Astronomy, University of Sussex,
Brighton BN1 9QH, United Kingdom

(Published 21 November 2007)

This review describes progress in the field of physisorption. Significant advances in the knowledge of microscopic structures and interactions of weakly bound adsorbates are reviewed, including the first studies for the adsorption sites of rare gases on flat metal surfaces and at surface steps, the structures of higher-order commensurate solids, collective excitations in rare-gas monolayers, molecular orientations and growth processes in alkane films, and adsorbate diffusion. The development and improvement of experimental techniques are reviewed, including high-resolution thermal desorption spectroscopy and ellipsometry for studying thermodynamics; low-temperature scanning tunneling microscopy, very low current electron diffraction, and surface x-ray diffraction for studying structures; inelastic atom scattering for studying collective excitations; quasielastic helium atom and neutron scattering and laser techniques for studying diffusion; and the quartz crystal microbalance for studying interfacial friction. The present state of knowledge of the physical adsorption potentials and the role of the van der Waals interaction are discussed in the context of the widespread use of density-functional theory. Experimental and theoretical results for many adsorption systems are described and tabulated; a few case studies are presented in which a unified picture has (nearly) been achieved by the synthesis of many contributions. Some new applications of physisorption are also presented.

DOI: 10.1103/RevModPhys.79.1381 PACS number(s): 68.43.Fg, 68.43.Jk, 68.49.Bc, 68.65.Ac

CONTENTS

0034-6861/2007/79(4)/1381(74)

I. INTRODUCTION

A. Overview

We review the present state of experimental and theoretical knowledge of physically adsorbed layers, with an emphasis on the monolayer regime and the benchmark systems of rare gases and small closed-shell molecules. These are the simplest adsorption cases and we discuss how far we have progressed in the ten years since the last comprehensive reviews and what the outstanding problems are. One of our goals is to facilitate access to this subject by a variety of workers who may want to know the accomplished science. The situation on some topics is not agreed upon and our goal there is to focus on the confrontations between various approaches. On other topics, our goal is to elicit similarities that have not been recognized or emphasized by previous workers.

Exciting developments since the mid-1990s include the discovery that rare gases often occupy low-coordination sites on metal surfaces (Diehl *et al.*, 2004), a result that was unexpected but which has important implications for the growth and dynamics of these films.[1] The utility of rare-gas films as "buffer layers" to modify the growth of metal, semiconductor, and molecular films also came as somewhat of a surprise given the metastability of such situations, but buffer-layer-assisted growth (BLAG) is now in common use to produce interfaces and nanoclusters having novel electronic characteristics, as described in Sec. VI.B.

Another major development, with accompanying surprises, was the demonstration that inelastic helium-atom scattering could determine the spectrum of collective excitations in rare-gas monolayers (Graham, 2003). It was not anticipated that the shear horizontal vibrational mode could be accessed this way. Apparently forbidden by symmetry, the mode was not expected to be observed, and therefore was erroneously identified as the longitudinal acoustic mode until high-sensitivity He-atom scattering measurements resolved both the shear horizontal and longitudinal acoustic modes for rare gases on Pt(111) (Bruch *et al.*, 2000). This experiment confirmed a basic assumption made in previous modeling of rare gases on graphite and on Ag(111), namely, that the interaction between adatoms is basically that in three-dimensional (3D) phases. The measurements described here have also opened the door to the development of new theories for adsorption, starting from electronic energies.

While progress is still being made at the fundamental level, a new frontier in physisorption is the study of complex systems, such as alkane films, where film growth involves a complex interplay of intramolecular and extramolecular interactions. Understanding such systems has utility both in the petrochemical industry and in the development of new theories that are relevant to many biological systems, where complex molecules interacting through van der Waals interactions are pervasive. Adsorption on complex substrates, such as quasicrystal surfaces, is also being explored as a new realm of systems with competing interactions.

Physisorbed layers provide many examples in which a quantitative understanding of macroscopic phenomena is achieved starting from a description in terms of interacting atoms and molecules. A large number of phases can exist in adsorbed layers, and transitions occur between these phases as the temperature T and pressure p

---

[1] We had to choose between two conventional names for the series—inert gas and rare gas. We recognize that such gases are not particularly rare. Since there are significant processes of hybridization of atomic electron states with substrate electron states in the adsorption, we concluded there was a stronger argument against the term "inert."

are varied. The variety of possible phenomena is as great as is observed in the high-pressure physics of 3D solids (e.g., Etters, 1989; Polian *et al.*, 1989). Physisorbed monolayers have been testing grounds for theories of 2D melting and for the initial stages of multilayer growth (epitaxy). Recent work on multilayers, described in Sec. VI.A, is relevant to tailoring materials such as the buffer layers described above. Multilayers are also prototype systems for friction, Sec. II.F, and for frustrated interactions, Secs. IV.A.3 and IV.C.4. Recent developments for 2D melting have occurred mostly for colloidal systems (see, e.g., Baumgartl *et al.*, 2004; Babič *et al.*, 2005), which we do not review here, although we discuss melting studies of individual adsorption systems. Another direction that we do not pursue is ordering in yet lower dimensions, as discussed, for example, by Calbi *et al.* (2001), Widdra (2001), Dash (2002), and Phillips and Dash (2005).

Many of the discoveries described here have resulted from advances in experimental techniques. The development of high-resolution thermodynamic techniques and of the ability to make measurements with several techniques simultaneously has led to unprecedented precision in the measurement of thermodynamic properties of films. These improvements, along with the development of more perfect and pure samples, have facilitated contact between results for adsorbate excitations, diffusion barriers in monolayer transport, and monolayer friction. The high-brightness synchrotron x-ray sources and improved instrumentation have permitted the use of ever-smaller samples or adsorbates having lower atomic numbers. Significant advances in the energy resolution of neutron spectrometers have allowed high-precision measurements of vibrational and diffusional properties of adsorbates. Improvements in both the sensitivity and energy resolution in He-atom scattering have provided the basis for many of the lattice-dynamical measurements for rare gases in the past decade. A deeper understanding of these phenomena is being facilitated by the development of new theoretical methods, particularly the application of *ab initio* methods and simulations. It is characteristic of this field that a thorough account of specific systems has been constructed from the complementary contributions of several experimental and theoretical techniques.

We are building on the contributions of many during the period 1970–1995. That knowledge is consolidated in a monograph-length summary of the work in physical adsorption (Bruch *et al.*, 1997) and a textbook (Venables, 2000) on surface and thin-film processes. Earlier books of Steele (1974) and Dash (1975) remain valuable for their presentation of the basic concepts. Then the emphasis in this field was on phase transition and universal phenomena (e.g., Dash, 1975). There was a very fruitful juxtaposition of thermodynamic experiments (volumetric measurements, adsorption isotherms) and precise (of order ±0.1%) lattice parameter measurements (diffraction), of the type illustrated in Figs. 1 and 2, that located phase changes and identified the structures that were involved. The theory that developed in parallel with the experiments made use of recent developments in computer simulations and approximations to continuous phase transitions. Those lines of work continue.

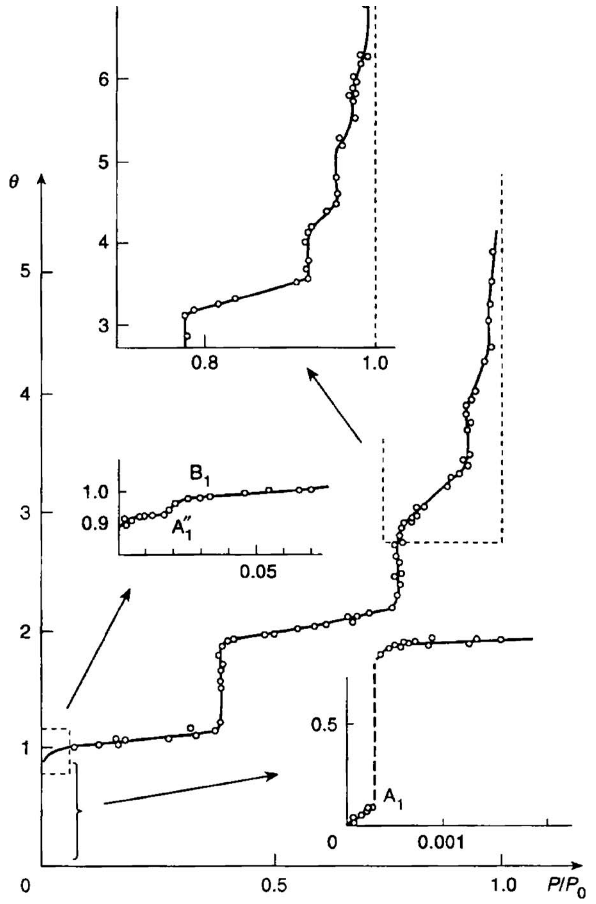

FIG. 1. Krypton multilayer adsorption isotherms. Adsorption of Kr multilayer films on exfoliated graphite at 77.3 K, from Thomy *et al.* (1981). Coverage (in layers) as a function of the relative pressure (p_0 is the saturated vapor pressure). The expanded scales in the insets present the submonolayer and multilayer transitions at p/p_0 less than 0.001 and greater than 0.8 more clearly. The points B_1 and A_1'' are signatures of monolayer phase transitions. From Bruch *et al.*, 1997.

Lately, much of the work has been conceived more as an extension of work on 3D rare-gas and simple molecular solids, which has been reviewed, *inter alia*, by Klein and Venables (1976, 1977) and Polian *et al.* (1989), respectively. There is an increasing emphasis on elucidating the mechanisms of interactions and dynamics and a much closer interplay between electronic-structure theory and the rare-gas monolayer solids, as described in Secs. III.A.2 and IV.B.2.

There is a wide range of science that could be covered in this review, but length and time constraints prevent us from treating all topics in a balanced fashion. We have organized the review into brief sections consisting of a citation of a relatively recent review and leading references and with longer sections on subjects where we have attempted to synthesize results from a variety of sources. The length of each section does not, however, represent a view on the relative importance of the subjects.

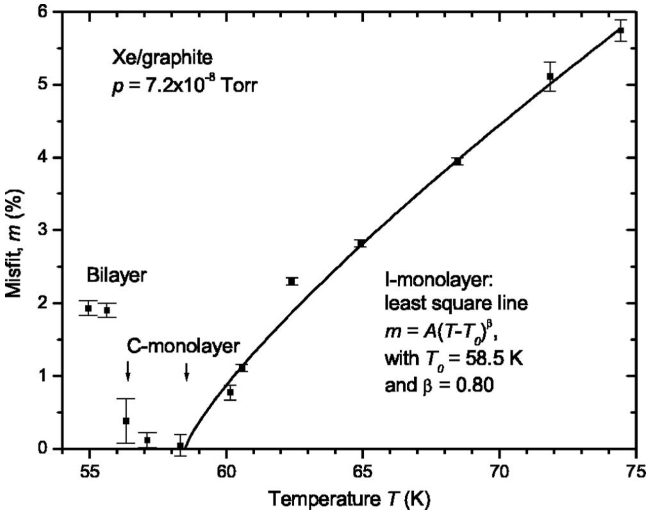

FIG. 2. I-C and monolayer-bilayer phase transitions for Xe/graphite as they appear in lattice constants measured by THEED at 3D pressure $p = 7.2 \times 10^{-8}$ Torr. The misfit $m = (L - L_c)/L_c$ is the difference in lattice parameter of the adsorbed layer relative to the commensurate $\sqrt{3}$ structure. As the temperature is lowered at constant pressure, the monolayer misfit decreases continuously from 6% at 74 K to zero at $T = 58$ K. About 2 K lower, the bilayer condenses with a misfit around 2%. Adapted from Hamichi *et al.*, 1989.

In concluding, we comment on how the review is organized. To make it easier for the reader, we have put basic background material into three appendixes on thermodynamics (Appendix A), crystallography (Appendix B), and lattice dynamics (Appendix C). We have found it instructive to make more than one cut through the subject. For instance, we treat diffusion as a topic in itself in Sec. V, but cite some results in the physical examples in Secs. IV.A.6 and IV.E.2. Similarly, recent advances in experimental technique are described in Sec. II, but the same papers are often reviewed in the sections concerned with individual adsorption systems. Considerable effort has gone into assembling the 15 tables of parameters and data.

B. Recent reviews

There have been recent comprehensive reviews by Suzanne and Gay (1996) and Bruch *et al.* (1997), and a critical compilation of adsorption data for rare gases on metals by Zeppenfeld (2001). Topical reviews include inelastic helium-atom scattering by Gumhalter (2001), Jardine *et al.* (2002), and Graham (2003), of imaging of physisorbed layers by Cyr *et al.* (1996) and Giancarlo and Flynn (1998), of adsorption site determinations by Diehl *et al.* (2004), and of adsorption on nanotubes (Calbi *et al.*, 2001; Gatica *et al.*, 2007; Migone, 2007). Reviews on the relation to friction include Gomer (1990), Israelachvili (1992), Maboudian (1998), Gnecco *et al.* (2001), Ala-Nissila *et al.* (2002), and Carpick and Batteas (2004). Larher (1992) reviewed physisorption on lamellar halides. Marx and Wiechert (1996) reviewed the literature on the adsorption of N_2 and CO on graphite and BN, while Wiechert (2003) did this for adsorption of H_2.

II. INNOVATIONS IN EXPERIMENTAL TECHNIQUES

Most of the advances in the experimental study of physisorbed systems have occurred with the development of new techniques and by increases in the precision or sensitivity of existing techniques. In this section, we review those techniques that have either made a significant impact on this field in the past 10 years or which promise to do so in the next 10 years. The section is divided into subsections that review the advances in studies of the thermodynamic properties of physisorbed films, including their adsorption energies (Sec. II.A), structural studies, including diffraction and imaging techniques (Sec. II.B), laser-based techniques that are used to study desorption and diffusion (Sec. II.C), spectroscopic techniques using infrared radiation (Sec. II.D), vibrations, phonons, and diffusion (Sec. II.E), and frictional properties (Sec. II.F).

A. Thermodynamic studies and TPD

Historically, large area techniques based on finely powdered samples or exfoliated layer compounds, such as graphite or lamellar halides, have formed the core of thermodynamic studies, especially of adsorption isotherms. These techniques were perfected in the period 1960–1980 and were reviewed by Larher (1992) and Thomy and Duval (1994). High-resolution single surface thermodynamic studies are a more recent development.

1. Large-surface-area materials

For the thermodynamic applications, it is important that materials can be prepared that have large surface-to-volume ratios and yet are rather homogeneous in their adsorption energies. There has been remarkable progress in this direction with carbon materials, but other substrates are available too, as summarized in Table I. The more modern materials enumerated in Table I generally are more homogeneous than the earlier ones.[2]

Reviews of high specific surface area carbon materials have been given by Avgul and Kiselev (1970) and by Godfrin and Lauter (1995). The experiments with these high surface area materials typically deal with a few millimoles of adsorbed material. In this review, we are interested in the refined physical data for adsorbed layers that became available with the advent of the highly homogeneous substrates. 2D monolayers on graphite, MgO, BN, and aerogels and quasi-1D packings on single-wall nanotubes (SWNT) and zeolites have been realized in this way.

---

[2] Very large specific surface areas (500 m^2/gm for silica gel and 800 m^2/gm for charcoal) were already available in 1938.

TABLE I. Some high specific area materials, given as surface area per mass. For the SWNH example, the adsorbing area corresponds to the adsorption of 2 millimoles of xenon per gram.

Material	m^2/gm	Source
Grafoil (carbon)	18–24	Bretz *et al.* (1973)
ZYX (carbon)	2	Bretz (1977)
SWNT[a] (carbon)	160	Zambano *et al.* (2001)
SWNH[b] (carbon)	250	Zambano *et al.* (2002)
Lamellar dihalides[c]	10–50	Larher (1992)
MgO	9	Coulomb *et al.* (1984)
MgO[d]	10	Freitag and Larese (2000)
BN	5	Alkhafaji *et al.* (1994)
Aerogel[e]	200–1000	Chan *et al.* (1996)
Zeolites[f]	>250	Martin *et al.* (1998)
Porous gold	100–200	Yoon and Chan (1997)

[a] Bundles of single-walled carbon nanotubes.

[b] Aggregates of single-walled carbon nanohorns.

[c] Prepared by sublimation, e.g., $CdCl_2$, $NiCl_2$, $FeCl_2$.

[d] Prepared in a patented process: Kunnmann and Larese (2001).

[e] The specific area depends on the porosity. For aerogel of 94% porosity it is 580 m^2/gm, Kim *et al.* (1993).

[f] Used in studies of quasi-1D mobility, Martin *et al.* (1996).

Physical adsorption has been applied to make nondestructive measurements of the surface area and homogeneity of materials, exploiting the fact that some adsorbates, e.g., Kr, Xe, and N_2, form monolayers having areas per atom (molecule) that are the same to within 10% on various substrates and make minimal perturbations of the host. An adsorption isotherm in the monolayer domain can determine the effective area for adsorption[3] and the energy or energies for the adsorbing sites. The rounding of the step in the adsorption isotherm at a first-order monolayer condensation can provide an estimate of the size of adsorbing terraces, assuming that it can all be attributed to finite-size effects (Larher, 1979). However, this assumption sometimes leads to size estimates that are smaller than the sizes inferred from broadening of monolayer diffraction spots, since diffraction intensities are dominated by the larger domains (Dash and Puff, 1981).

2. Automation of thermodynamic studies

Qualitative improvements in the extent and detail of experimental data, arising from automated thermal analysis, have produced precise values for quantities that depend on the slopes of isotherms, such as the isothermal compressibility (Suter *et al.*, 1987; Gangwar *et al.*, 1989; Yang *et al.*, 1991; Mursic *et al.*, 1996). A high-resolution isotherm for N_2 on graphite covering the liquid-to-solid transition and the derived compressibility are shown in Fig. 3. Zhang and Larese (1995) combined x-ray scattering with high-precision isotherm measurements to study freezing and layering transitions, starting from the monolayer-bilayer transition for Xe/graphite; a description of the automated apparatus has been given by Mursic *et al.* (1996). For the amount of detailed physics that can be extracted from these data using a suitable model see the work of Phillips and Larese (1997). Applications to the physics of multilayers are reviewed in Sec. VI.A.

Very-high-resolution ellipsometry (VHRE) has also been utilized in such thermodynamic studies, primarily for the multilayers. The VHRE technique is extremely sensitive to the average film thickness and can detect differences in coverage of 1% of a monolayer (Volkmann and Knorr, 1989; Hess, 1991; Volkmann *et al.*, 1998). It has been applied for some years to the study of wetting and film growth of rare gases and simple molecules (Faul *et al.*, 1990; Hess, 1991). More recently it has been applied to the study of alkane films (Volkmann *et al.*, 2002; Kruchten *et al.*, 2005). A VHRE study of n-$C_{32}H_{66}$ adsorption on SiO_2 found that the first one or two layers adsorb with the molecular axes parallel to the surface. Subsequent layers form with their axes perpendicular to the surface, finally followed by bulk crystallite formation (Volkmann *et al.*, 2002). A subsequent x-ray specular scattering measurement supported this interpretation (Mo *et al.*, 2003). VHRE has also been used fruitfully in conjunction with neutron diffraction to characterize the structure, growth, and wetting of pentane on graphite (Kruchten *et al.*, 2005); Fig. 4 shows an example of the isotherms.

3. Thermal desorption measurements

A rather different, but related, set of techniques has been developed around thermal desorption, notably temperature programmed desorption (TPD). This technique is sometimes called thermal desorption spectroscopy (TDS) and is closely related to other techniques in which (chemical) reactions take place on the surface, as in temperature programmed reaction spectroscopy (TPRS). Laser-induced thermal desorption (LITD) is another related technique, discussed in Sec. II.C.

In TPD, the adsorbed layer is initially deposited on the surface at rather low T where the equilibrium vapor pressure is very low. Then the temperature is ramped up slowly but linearly in time; various desorption peaks are observed as a function of time, most effectively by tracking the relevant mass numbers by quadrupole mass spectrometry. The great virtue of this technique is that it is rapid and easy to understand in outline, as phases that are more weakly bound desorb at a lower T than the more strongly bound ones.

Over the past ten years, TPD has evolved from a mostly qualitative technique, where the primary aim was to determine the order of the desorption reaction [the exponent n in Eq. (1)], to a quantitative technique that

---

[3] For a description of the BET (Brunauer *et al.*, 1938) isotherm model for determining the area at monolayer completion, see Appendix A.2.

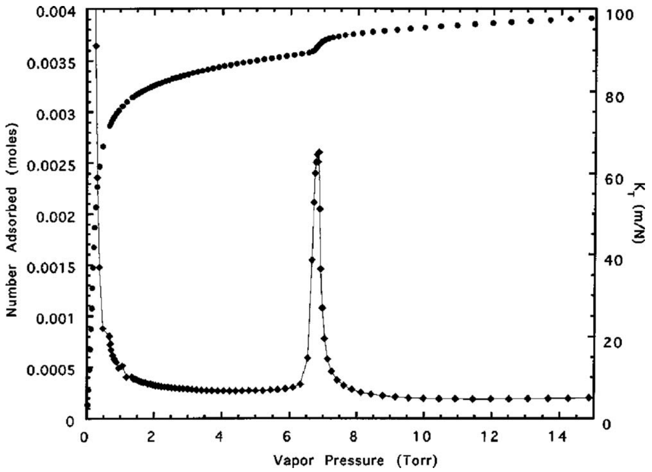

FIG. 3. Monolayer adsorption of N_2 on graphite at T close to 78 K. The small "substep" near the monolayer completion indicates a liquid-solid transition. The compressibility of the film, shown with a solid line as a guide to the eye, was calculated from the data. From Mursic *et al.*, 1996.

can complement detailed adsorption isotherms and other equilibrium thermodynamic measurements. It can be applied to more tightly bound species where equilibrium measurements may be difficult because of the propensity of the vapor to stick to other surfaces in the experimental chamber. In particular, it has been used for studies of adsorbed alkanes, see Sec. IV.A.6 (see also Weaver *et al.*, 2003).

Early thermal desorption experiments have been described and reviewed by King (1975), Menzel (1975, 1982), and Bauer *et al.* (1977). Subsequently, Menzel's group developed a high-resolution TPD instrument (Schlichting and Menzel, 1993a, 1993b) and applied it to the physisorption of Xe/Ru(0001) (Schlichting and Menzel, 1992) and other systems. Widdra *et al.* (1998) used it to study xenon adsorption on flat Pt(111) and stepped Pt(997) surfaces; Kimmel *et al.* (2003) used it to investigate the effects of adsorbate layer compression for the case of Ar/Pt(111).

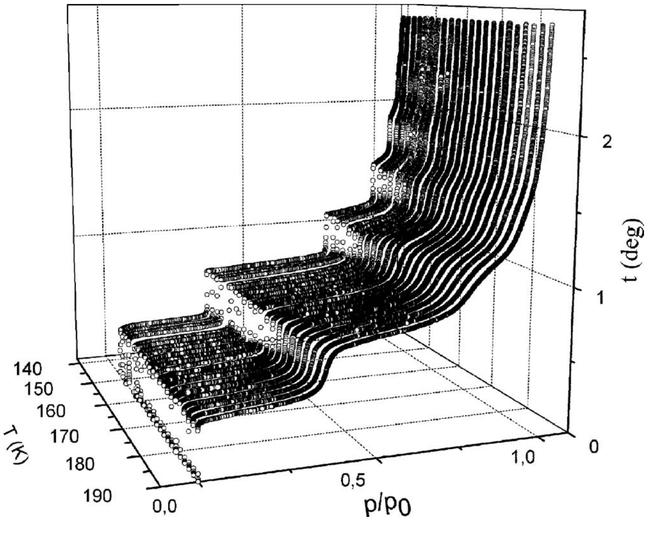

FIG. 4. A series of ellipsometric adsorption isotherms in the fluid regime of pentane on graphite. The optical thickness t (proportional to a phase delay, in degrees) is shown as a function of the relative vapor pressure (p_0 is the saturated vapor pressure at the stated T). Each isotherm terminates in a very thick film and these films completely wet the substrate. From Kruchten *et al.*, 2005.

Examples of high-resolution TPD spectra are shown in Fig. 5. The high quality of the spectra is evident in the logarithmic scale of the desorption rate; on the Arrhenius plot of Fig. 5(a), the common leading edge is essentially a straight line, shown toward the left for the bilayer and the right for the monolayer. The convenience of the technique is shown by the relatively rapid heating rates; each experimental run took no more than 70 s for Fig. 5(a) or 100 s for Fig. 5(b). These results are discussed further in Secs. II.A.4, IV.A.2, and IV.B.3.

4. Thermal desorption modeling

Early TPD observations showed that solid Xe monolayers on graphite desorb via a dilute (e.g., 2D gas) phase with zero-order kinetics (Venables and Bienfait, 1976; Bienfait and Venables, 1977); after all the dense phase had desorbed, first-order desorption was observed. Several monolayer and multilayer models were developed in the 1980s to explain zero-order desorption by relating the kinetics to the chemical potentials of the adsorbed and bulk phases. These required that the local equilibrium on the surface (i.e., within the adsorbed layer) is achieved more rapidly than desorption into the vapor.

In a series of theoretical papers, Asada and coworkers used a lattice-gas model to justify zero-order kinetics from condensed monolayer phases when desorption occurs via the intermediary of dilute phases, both within and on the first monolayer (Asada and Masuda, 1989), and later in multilayers (Asada and Sekito, 1992). Ruiz-Suarez *et al.* (1991) developed a bilayer model and analyzed Xe/graphite helium scattering data, also in the context of zero-order desorption.

Over the same period, Nagai and co-workers developed similar models, including effects of lateral interactions in a transition state theory and aiming to predict the dependence on coverage. Most of the work concentrated on systems of catalytic interest and was sometimes controversial. Several of the leading papers in the controversy are Nagai (1985, 1988), Zhadanov (1986), and Cassuto (1988). From the standpoint of physisorption, the main result is in the discussion of high temperatures, where the desorbing species is not strictly confined to well-defined layers. Then the desorption may be more complex than that treated with simple layered models. There still does not seem to be a consensus on the validity of Nagai's result for the density dependence near monolayer completion (e.g., Pitt *et al.*, 1995; Rudzinski and Panczyk, 2002).

Detailed modeling is required to extract physical parameters from TPD data, and there have been several stages of refinement. Most analyses start from the

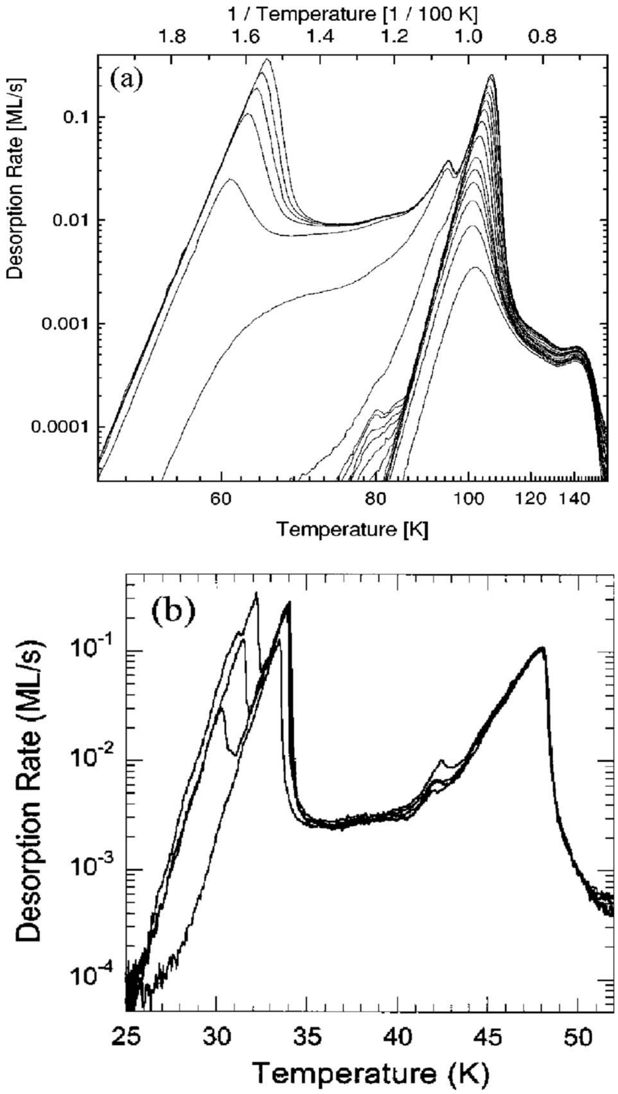

FIG. 5. Experimental TPD spectra for rare gases on Pt(111) at several coverages. The desorption rates are given on a logarithmic (Arrhenius) scale. (a) Xe in the range up to 1.8 monolayer and $50 < T < 160$ K, with a heating rate of 2 K s^{-1}. From Widdra *et al.*, 1998. (b) Ar in the multilayer range and $25 < T < 52$ K, rate 0.25 K s^{-1}. From Kimmel *et al.*, 2003.

Polanyi-Wigner equation, which phenomenologically expresses the rate of change of the coverage in the form

$$\dot{\theta} = -\theta^n \nu(\theta) \exp[-E(\theta)/k_B T], \tag{1}$$

where n is the reaction order and ν is the frequency factor. Within the field of physisorption, interest has centered primarily on first- and zero-order reactions, with the possibility of intermediate order. An empirical form for the zero-order desorption rate k $[\dot{\theta}]$ that is frequently applied is

$$k = \nu \exp(-E_{\mathrm{des}}/k_B T); \tag{2}$$

it has a decomposition into a nearly constant prefactor ν and an activation energy for desorption. It is now recognized (Fichthorn and Miron, 2002; Tait *et al.*, 2005) that the prefactor can vary by several orders of magnitude following a molecular series such as the n-alkanes, in large part because of the difference in the molecular rotational entropy in the adsorbed phase and in the 3D vapor. The values E_{des} from fits using Eq. (2) are commonly taken to be good estimates of the adsorption energies q. That is, the activation barrier to desorption E_{des} is identified with the adsorption energy, at least for small rigid molecules (Gellman, 2005). We compare thermodynamic and kinetic estimates for several cases in Table II, where it is evident that the empirical foundation for such an identification is mixed, as there are several large unresolved discrepancies between q and E_{des}.

TABLE II. Comparison of thermodynamic energies q and desorption energies E_{des} for several adsorbate-substrate combinations. The monolayer phase identifications are as follows: I for triangular incommensurate solid; C for simply commensurate solids; dense fluid; and dilute 2D gas ($\vartheta \approx 0$). The thermodynamic energy q for the solid is the monolayer heat of condensation q_1, and for the fluid and gas it is q_{st}. Energies are given in meV and nearest-neighbor spacings L in Å.

System	Phase	L	q	E_{des}
Xe/graphite[a]	I	4.3–4.4	239	260±17
Xe/Ag(111)[b]	I	4.42	225±5	224
Xe/Pt(111)[c]	C	4.80	298±22	270–280
Xe/Pd(111)[d]	C	4.75		320±10
Xe/Pd(001)[e]	Fluid		273	300
Kr/Pt(111)[f]	I	≈4.1	155	134
Ar/Pt(111)[g]	I	3.8	95	140
CH_4/Ag(110)[h]	$\vartheta \approx 0$		220	130

[a] From Bienfait and Venables (1977).

[b] From Unguris *et al.* (1979) and Behm *et al.* (1986).

[c] From Widdra *et al.* (1998) and Lehner *et al.* (2002). The heats quoted from different measurements may be for different coverages (Zeppenfeld, 2001) and this should be recognized in comparing heats of adsorption on different substrates.

[d] From Zhu *et al.* (2003).

[e] From Miranda *et al.* (1983) and Moog and Webb (1984).

[f] From Kern and Comsa (1991) and Carlsson and Madix (2001).

[g] From Kern and Comsa (1991) and Kimmel *et al.* (2003); see also Frieß *et al.* (2007).

[h] From Elliott *et al.* (1993); see also Sec. IV.A.5.

Most of the above analyses have been cast within the lattice-gas model and assumed that the desorbing layer is in equilibrium everywhere, i.e., the rate of lateral diffusion does not enter explicitly. Some lattice-gas models have included lateral interactions and diffusion. For example, Lehner *et al.* (2000, 2002) developed Monte Carlo simulations of such models and applied them to the TPD experiments of Widdra *et al.* (1998) on Xe/Pt(111) and Xe/Pt(997). It is notable that even quite weak, and particularly long-range, lateral interactions (Lehner *et al.*, 2003a, 2003b) have a strong effect on the order of desorption, increasing the trend towards zero-order desorption. This is because clustering is the first stage en route to phase separation, where the higher- and lower-

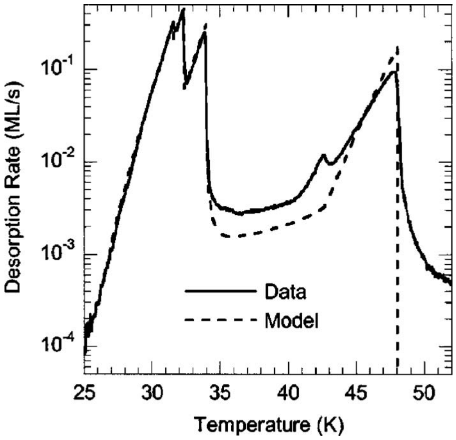

FIG. 6. Experimental and calculated TPD spectra for Ar/Pt(111). Note the nearly temperature-independent desorption rate for the compressed first monolayer from 34 to 41 K in both the experimental and calculated spectra. From Kimmel *et al.*, 2003.

density phases are spatially separated. Similar effects arise for adsorption at steps, see, e.g., Sec. IV.B.3.

Models based on surface phonons, which have the potential for describing nonequilibrium effects, have been developed by Kreutzer and co-workers (Kreuzer and Payne, 1988a, 1988b; Payne and Kreuzer, 1988, 1989), and reviewed by Kreuzer and Payne (1997). These models have been applied to Xe/Pt(111) and Xe/Pt(997) by Widdra *et al.* (1998), where several lateral interactions in the adsorbed layers have been fitted to the predicted TPD curves. Stampfl *et al.* (1999) made an even more elaborate application to the chemisorption system O/Ru(0001). The lattice-gas model is constructed in terms of a sequence of higher-order commensurate structures, thus requiring many lateral interaction parameters, specific to the sequence chosen. While the level of agreement obtained is impressive, it is hard to believe that the solution is unique.[4]

Also, lattice-gas models do not properly describe layers that have finite compressibility, as noted by Phillips and Larese (1997). In rare-gas adsorption, the work of compression is one of the main components in the increase of chemical potential μ between the gas-solid monolayer and the bilayer line; it gives rise to a finite, almost constant, desorption rate between the second- and first-layer thermal desorption peaks. In lattice-gas models, even with large numbers of terms (see, e.g., Woodruff and Delchar, 1994; Widdra *et al.*, 1998; Stampfl *et al.*, 1999), this region of the spectrum is typically underestimated. This issue has been specifically confronted by Kimmel *et al.* (2003) for Ar/Pt(111), as shown in Fig. 6, where the compression between bilayer and monolayer desorption is high, estimated to be between 10 and 15%. Their model does include compression, although the actual extent is underestimated, and can serve as a basis for future work of this type.

An extreme case of a compressible monolayer system is He/Pt(11). TPD experiments on He/Pt(111) at $2 < T < 6$ K also show almost constant desorption rates for temperatures below the main peak near 4 K. These phenomena are explained by a mixture of thermal and photon-induced desorption (Niedermayer *et al.*, 2005).

There are several more directions for future work. Multiphonon models for surface diffusion and adsorption-desorption are in development (Azzouz *et al.*, 2002), but are not yet readily available for analysis of experimental data. The thermal desorption theory of large molecules poses special problems arising from effects of internal conformational isomerism and entropy (Fichthorn and Miron, 2002; Gellman, 2005; Becker and Fichthorn, 2006), as discussed for alkanes in Sec. IV.A.6. There is also some concern that TPD models have not yet been fully related back to *a priori* theory (Alfè and Gillan, 2006). Nonetheless, it is worth reemphasizing that TPD, LITD, and related techniques are extremely useful, especially for initial surveys and for complex systems where each desorbing species can be followed separately by mass spectrometry.

B. Structure and imaging, including STM

Lander and Morrison (1967) showed that low-energy electron diffraction (LEED) could provide structural information for the adsorbed phases on single-crystal surfaces. Since then, the structure of adsorbed films has been investigated by diffraction using probe beams of x rays, electrons, neutrons, and atoms, especially helium atoms. Standard surface techniques are described in several textbooks (see, e.g, Rivière, 1990; Woodruff and Delchar, 1994). By use of suitable geometries, many of these probes can be made sufficiently surface sensitive to investigate the adsorbed layer on a single surface. Neutron scattering is an exception, because of the very long mean free path in the substrate, and powdered or exfoliated samples, similar to those in most thermodynamic measurements, are used.

1. Diffraction versus imaging

Diffraction techniques are central to structure determination, including adsorbed monolayers. They enable both lattice parameters and lattice orientation to be determined with high precision, particularly for adsorption on single-crystal substrates. Quantitative intensity observations, such as LEED $I(E)$ spectra, enable detailed structural analyses and have been the basis of many recent determinations of the adsorption sites in commensurate monolayers, see Sec. IV.B.

On the other hand, imaging presents the structures in real, rather than reciprocal, space and gives the actual microstructure with some spatial resolution, including any structural variations in time. As spatial resolution has improved dramatically in recent years, the balance of work has shifted from diffraction to imaging. How-

---

[4] Lei *et al.* (2004) noted that desorption temperatures for alkanes/Ag(111) can be fit with different parameterizations of Wetterer *et al.* (1998) and Fichthorn and Miron (2002).

ever, there frequently are differences in the state of the adsorbate in the applications and difficulties in relating one set of results to another. Two examples from the recent physisorption literature will illustrate these points.

Several scanning tunneling microscope (STM) experiments have been performed for submonolayer amounts of Xe condensed onto metal surfaces. One involved experiments at liquid helium temperatures (4 K) in which the STM tip was used to move the Xe atoms over a Ni(110) surface. This enabled Eigler and Schweitzer (1990) to put the initials of their employer on the surface of a nickel crystal. In these experiments, the atoms stay where they are pushed or put for hours. At $T=4$ K, the time scale for true thermodynamic equilibrium laterally over the surface, and even more so with the 3D vapor, is much longer than the experimental time scale. Consequently, we cannot make realistic comparisons with other adsorption measurements.[5]

The second example is the detailed T-dependent study of Xe/Pt(111) by Horch *et al.* (1995a, 1995b). High-resolution images obtained below 30 K show 2D islands of solid monolayer Xe; above 30 K, however, the motion of Xe atoms over the surface led to blurred STM images. At 30 K, 2D equilibrium may be possible, but the T is well below that needed for 3D equilibrium. Therefore, what is observed for Xe with STM at low T is really the first stage of crystal growth, rather than equilibrium adsorption. In viewing the dramatic images, we need to bear in mind that we typically do not know the pressure; therefore we may not be able to relate the observations directly to the phase diagrams obtained via thermodynamic or diffraction measurements. Note that even when the STM image is blurred due to the short-range motion of Xe, observations of the average (ordered) structure are still quite feasible with diffraction techniques.

2. Recent developments in imaging

Several new imaging studies have been performed on physisorbed films because of the increasing availability of stable low-temperature and variable-temperature STM's. Horch *et al.* (1994) produced atomically resolved images of Xe/Pt(111) near monolayer coverage at 13 K. The orientation of the Xe lattice with respect to vacancy islands on the Pt(111) surface was observed, as were individual vacancies in the Xe monolayer. These vacancies were observed to anneal out and 2D islands coalesced at $T\simeq 27$ K. A more extensive study followed (Horch *et al.*, 1995a, 1995b), discussed in Sec. II.B.1. Park *et al.* (1999) made a similar study for Xe/Cu(111), covering growth below $T=20$ K, followed by a tunneling spectroscopy experiment on this system (Park *et al.*, 2000). Reihl, Hövel, and co-workers used STM to observe the domain-wall structure of incommensurate Xe/graphite at $T=5$ K (Hövel *et al.*, 1998; Grimm *et al.*, 1999, 2000). Brunet *et al.* (2002) studied Ar, Kr, and Xe on Pt(111). The results of these STM experiments are discussed in Secs. IV.B.3, IV.E.1, and V.B.1. STM experiments on physisorbed molecular layers were reviewed by Cyr *et al.* (1996) and Giancarlo and Flynn (1998).

Atomic force microscopes (AFM) are increasingly available for use under the ultrahigh vacuum and low-T environments necessary to study physisorbed films. One AFM application was to investigate the structure of films of intermediate-length alkanes (Trogisch *et al.*, 2005). Schwarz *et al.* (2002) have described a new AFM that was used to obtain atomic-resolution images of Xe(111). Ashino *et al.* (2004) applied this microscope to the carbon atom honeycomb net of a SWNT. The microscopes are also used for friction studies (Gnecco *et al.*, 2001; Carpick and Batteas, 2004; Park *et al.*, 2005).

von Przychowski *et al.* (2003) have also examined adsorption and desorption of Xe/graphite by photoemission electron microscopy (PEEM). This technique does not approach atomic resolution, but it has the advantage that real-space images can be followed in real time at temperatures of 40–75 K. In this it parallels earlier TEM and THEED work on condensed Xe, but the PEEM imaging is successful on a single monolayer. The images confirm the understanding of zero-order desorption kinetics as arising from the coexistence of monolayer solid and fluid phases (Venables and Bienfait, 1976), see Sec. II.A.4. The images span one-phase and two-phase coexistence conditions and show the presence of coexisting commensurate and incommensurate monolayer solid phases,[6] a topic discussed in Sec. IV.E.1 in the context of the phase diagram for Xe/graphite.

Finally, we note that STM images of Xe and Kr on graphite have been simulated using density-functional theory (DFT) by Chen, Zhou, *et al.* (2003) and Chen *et al.* (2003b), in work stimulated by low-temperature (4–7 K) STM observations of these systems by Matsui *et al.* (2002). This brings rare-gas layers into line with many other systems that have been imaged by STM and simulated by DFT starting from the model of Tersoff and Hamann (1983, 1985). However, the calculations necessarily are carried through for a small lateral repeating unit and, therefore, take both Kr and Xe to be in the C phase. A full simulation of complete images in the I phase, such as those in Sec. IV.E.1, is not to be expected in the immediate future.

3. Recent developments in electron and x-ray diffraction

LEED is the most commonly used technique for the quantitative determination of surface structures, but its

---

[5] In contrast, Weiss and Eigler (1992) found that single Xe atoms on Pt(111) at 4 K move ballistically across the surface, stabilizing at surface step or other defect sites. They proposed that the basis for the Xe transport across the Pt(111) surface is a lack of energy accommodation for motion parallel to the surface plane.

[6] The coexistence is interpreted as evidence for a first-order C-I transition. The role of different thermodynamic paths for Xe/graphite is discussed in Sec. IV.E.1.

application to physisorbed layers has been relatively sparse. This is partly due to beam-induced desorption that necessitates the use of low (<1 μA) beam currents for species that are more weakly bound than Xe. Low-current LEED systems have been used for some time (Chinn and Fain, 1977; Diehl and Chandavarkar, 1989; Ogletree *et al.*, 1992) and typically operate at currents of 0.1–10 nA. Even these currents are too high for sustained observation of certain adsorbates such as molecular hydrogen (Cui *et al.*, 1988). Recently, there have been two new developments in LEED detectors that are promising for studies of weakly bound or electron-sensitive adsorbates such as hydrocarbons. The first of these is a delay line detector in conjunction with microchannel plates (Human *et al.*, 2006), which allows LEED patterns to be acquired with a much lower total electron exposure than with previous channel plate LEED detectors. Typical electron beam currents are 0.3 fA to 0.15 pA. This system has been used to study the structure of hydrogen-stabilized MgO, which would be subject to beam damage and charging in a conventional LEED instrument (Poon *et al.*, 2006). The delay line detector also provides higher spatial resolution of the pattern than other detectors, leading to better resolution in momentum transfer. The transfer width of this instrument ranges from 260 to 610 Å depending on the beam current used, compared to about 150 Å for a typical LEED system. The second type of detector developed recently (Driver and King, 2007) utilizes a continuous fiber-optic coupling between the phosphor screen and a CCD detector. The screen is the front face of the fiber-optic element, which tapers and demagnifies the LEED image toward the detector. A fiber-optic viewport transmits the image from a tapered fiber optic element to a third fiber-optic element, which is bonded to a slow-scan CCD camera. Typical beam currents are in the nA range.

The higher momentum-transfer resolution achieved in x-ray diffraction makes this technique particularly applicable to phase transitions and, in fact, the first application of x-ray diffraction to physisorbed films was to the phase transitions of rare gases on polycrystalline graphite (Nagler *et al.*, 1985; Birgeneau and Horn, 1986). Synchrotron sources provided a great boost to the applicability of x-ray scattering to adsorbed films because the increased brightness permits the use of single-crystal substrates. A thorough review of x-ray scattering studies of surfaces using synchrotron radiation has been given by Daillant and Alba (2000). The x-ray diffraction studies of Xe on single-crystal graphite (Hong *et al.*, 1987, 1989; Nuttall *et al.*, 1993, 1994, 1995) contributed precise determinations of overlayer rotational epitaxy and melting that were not feasible using high-surface-area polycrystalline substrates. X-ray scattering studies of physisorbed films were extended to physisorbed films on single-crystal metal substrates by Dai *et al.* (1999). X-ray reflectivity measurements complement diffraction and can provide valuable information on film morphology, roughness, and growth, as demonstrated for dotriacontane films (Mo *et al.*, 2004). As these latter studies demonstrate, x-ray scattering has the advantage of less beam damage to organic molecules than typically occurs using low-energy electrons. The new third-generation synchrotron sources (e.g., the APS at Argonne, NSLS-II at Brookhaven National Laboratory, or Diamond in the UK) provide even higher brightness, raising the possibility of studying individual molecules on surfaces (Robinson, 2007).

C. Laser-based techniques

Laser techniques, such as laser-induced thermal desorption (LITD) and linear optical diffraction (LOD), increasingly have been used to study physisorbed species. In LITD, a laser pulse is used to desorb the gas in a well-defined region and a second pulse at a later time is used to desorb the gas that migrates onto this region in the interim. The amount of this desorbed gas is then measured using a mass spectrometer and the time dependence of the refilling of the region can be established by successive measurements. Because of the relatively large (compared to FEM) area sampled, the diffusion properties measured using this technique almost necessarily include diffusion across some number of surface defects such as steps. LITD has been used to study the diffusion of Xe and Kr on Pt(111) and Pt(11,11,9) (Meixner and George, 1993a, 1993b; Sneh and George, 1994) as discussed in Sec. V.B.

An example of using LITD in conjunction with ellipsometry (Faul *et al.*, 1990) is the study of Ar/graphite by Bär *et al.* (1997), where differences in recondensation rates after desorption were measured as a function of supersaturation $\Delta\mu$. At low T, high $\Delta\mu$, where the adsorbed Ar was either solid or just into the fluid range, zero-order adsorption was found, but at higher T, lower $\Delta\mu$, nonlinear effects were found and ascribed to nucleation at steps.

LOD has been used to study the diffusion of rare gases on metal surfaces. In LOD, an interference pattern from laser light is used to desorb the adsorbate, resulting in a 1D density grating of gas adsorbed on the surface (Zhu, 1992). The grating has a line spacing of a few microns, i.e., appropriate for optical diffraction. After the grating is formed, the rare gas diffuses into the bare regions and the diffraction intensity from the grating is measured as a function of time. The evolution of the diffraction intensity can then be used to extract the diffusion rate. This technique has been used to study Xe adsorption on both Ni(111) (Nabighian and Zhu, 2000) and Nb(110) (Thomas *et al.*, 2003). Although LOD also measures diffusion over relatively macroscopic distances, it has the advantage of being able to orient the grating in any direction, which facilitates the measurement of anisotropy in diffusion.

D. Infrared spectroscopy

High-sensitivity polarization Fourier transform infrared spectroscopy (FTIR) became widely available about

20 years ago. Most of the early physisorption studies were performed in transmission mode and were limited mainly to NaCl and MgO substrates (Heidberg, Kampshoff, *et al.*, 1990; Ewing, 1993). Many measurements of structures, molecular orientations, thermodynamics, vibrations, and phase transitions were performed for physisorbed small molecules. Enhancement of the infrared signal using an attenuated total internal reflection technique made possible recent measurements on extremely weak infrared absorbers such as H_2 on NaCl and enabled a direct comparison between the experiment and quantum-mechanical models for the vibration-orientation-translation motions of the molecules. The difference between the adsorption energies for *ortho* and *para* H_2 on NaCl(100) was thus determined to be 6 ± 2 meV, in agreement with calculations (Heidberg *et al.*, 1999).

Infrared reflection absorption spectroscopy (IRAS or IRRAS) has been applied to physisorbed molecules on graphite surfaces. Although it was predicted that there would be a distortion of adsorbate absorption peaks on graphite (Leitner *et al.*, 2003), such distortions have not been observed in monolayer or few-layer films. The orientations of CF_2Cl_2 and CH_3Cl molecules in various phases were found to change with coverage (Nalezinski *et al.*, 1995, 1997). A later study of CO at $20 < T < 40$ K expanded on an early IRAS work (Heidberg, Warskulat, *et al.*, 1990). Earlier studies had identified three different structural phases in which the CO molecules are nominally flat (herringbone, commensurate orientationally disordered, and incommensurate orientationally disordered). The newer IRAS measurements give average tilt angles (relative to flat) of 12°, 17°, and 23° for these phases, respectively. Simultaneous ellipsometry measurements enabled the unambiguous assignment of the CO bilayer signal and found that the bilayer has a structure with a pinwheel arrangement in each layer, similar to that of the bulk α-CO structure (Boyd *et al.*, 2002). Therefore IRAS can provide unique information about the orientations of physisorbed molecules. It can also detect interesting vibrational phenomena such as the tunable Fermi resonance found for C_2F_6 on graphite (Hess, 2002). The polarization modulation technique (Green *et al.*, 1991) allows experiments to be performed at higher pressures and improves the measured signal; it has been employed fruitfully in the study of mixtures of physisorbed gases (Boyd *et al.*, 2004; Hess *et al.*, 2005, 2006).

E. Dynamics and excitations

Two techniques that are commonly used to study the dynamical properties of surfaces are neutron scattering and helium-atom scattering (HAS), which also happen to be the least surface-sensitive and most surface-sensitive of scattering techniques, respectively. There has been a tremendous improvement in both due to recent innovations; for physisorbed films these improvements are most evident in studies of surface diffusion. Measurement of surface diffusion using quasielastic scattering provides a measure of the diffusion behavior of single atoms or molecules over a very short time scale, unlike a technique such as LITD (Sec. II.C), which measures diffusion behavior over a much larger area and time scale.

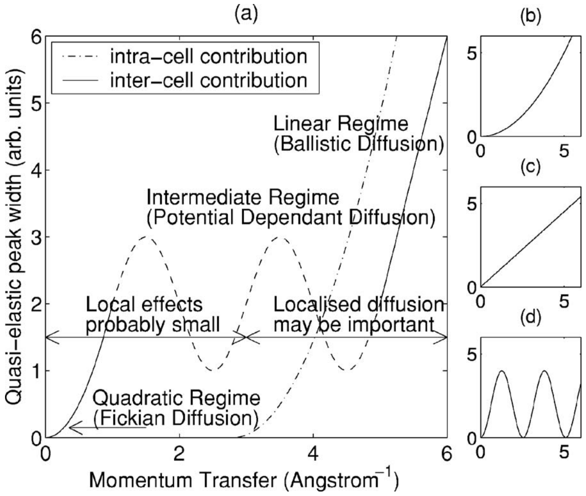

FIG. 7. Contributions to the quasielastic peak shape. (a) The generalized dependence of the quasielastic peak width upon momentum transfer $[E(K)]$ for a surface lattice constant of 2.55 Å. There are contributions due to both intracell and intercell diffusion, which may only be distinguished using high-resolution measurements. (b), (c), and (d) The $E(K)$ characteristics expected for continuous diffusion, ballistic diffusion, and jump diffusion, respectively, which together give rise to the overall form in (a). In general, continuous diffusion is expected over long length scales (small K) and ballistic motion over very short length scales (large K). In between, the surface potential affects the diffusion mode, often leading to jump behavior. From Jardine, Ellis, *et al.*, 2004.

In quasielastic scattering, the small energy exchanges between incident particles and diffusing adatoms or molecules produce a Doppler-like energy broadening of the elastic peak. This broadening of the quasielastic peak is measured as a function of the parallel momentum transfer $\Delta\mathbf{k}$. The peak shape and dependence on $\Delta\mathbf{k}$ can be used to distinguish the single-particle diffusion mode.

The limiting modes of diffusion normally considered are continuous Brownian diffusion, discrete jump (or hop) diffusion, and ideal gas diffusion. In continuous Brownian diffusion, the adatoms perform random-walk motions along the surface. This is also the case for discrete jump diffusion, except that then adatoms are restricted to jumping between discrete sites on the surface. In ideal gas diffusion, adatoms move unimpeded by the substrate, as expected for a 2D ideal gas (Jardine *et al.*, 2002). For the first two of these modes, the quasielastic peak has a Lorentzian line shape, whereas for the third, it has a Gaussian line shape. The dependences of their widths on $\Delta\mathbf{k}$ are quite different from each other, as shown in Fig. 7. Brownian diffusion produces a parabolic dependence, jump diffusion is oscillatory, and ideal gas diffusion has a linear dependence (Jardine *et al.*, 2002). In practice, diffusion can be a combination of the different types and/or have a combination of jump lengths. Examples of these cases are given in Sec. V. Because of the complexity of typical diffusion processes, computer simulations have become an integral part of the interpretation of experimental data (Ellis and Graham, 1997; Jardine *et al.*, 2002; Jardine, Ellis, *et al.*, 2004; Enevoldsen, Hansen, Diama, Taub, *et al.*, 2007).

The traditional method for measuring the energy transfer in both neutron scattering and HAS is the time-of-flight (TOF) method. Using this technique, the limits imposed by both the incident beam properties and the detection of the scattered beams restricted the range of measurements, but recent innovations for both quasielastic neutron scattering (QNS) and quasielastic helium-atom scattering (QHAS) have dramatically increased the accessible range of surface diffusion.

1. Neutron scattering

The development of neutron backscattering spectrometers has resulted in an increase in energy resolution to the order of μeV, an improvement by more than an order of magnitude over the best TOF instruments (Bée, 2003; Meyer *et al.*, 2003). With this technique, backscattering geometries are used at both the monochromator and the analyzer. Under these conditions, only the spreads of lattice spacing of the monochromator and analyzer crystals contribute to the energy spread in the beam. The energy of the beam can be varied by thermal expansion of the monochromator or by fast translation of the monochromator. The energy shifts in the scattering process are thus measured by varying the energies set by the monochromator and analyzer crystals. Backscattering spectrometers can operate over a wide range of momentum transfer simultaneously and can access time ranges between 100 ps and 0.01 μs. Examples of the applications in physical adsorption include measuring (i) diffusive motions of HD molecules on graphite powders (Wiechert *et al.*, 2003), (ii) methane mobility in (SWNT) carbon nanotubes (Bienfait *et al.*, 2000), and (iii) diffusive motions of conformational defects in adsorbed alkanes (Hansen *et al.*, 2004).

A second innovation in QNS is the use of the spin-echo technique to achieve the measurement of much smaller energy transfers, down to tens of neV (Bée, 2003). The spin-echo technique uses the Larmor precession of the neutron magnetic moment as a clock for scattered neutrons. It has also been applied to QHAS and is described in the next section. The spin-echo technique was first applied to neutron scattering about 25 years ago, but so far has been used to study diffusion mainly in bulk systems (Bée, 1988).

2. Helium-atom scattering

a. Inelastic scattering

Helium-atom beams are generated by nozzle jets and typically have velocity spreads of 1% and less for ^{4}He. As for neutron scattering, the dynamics and excitations in adsorbed films are probed using inelastic and quasielastic scattering. Such experiments typically have used a TOF technique to measure the energy transfer. An energy resolution of about 0.3 meV is achieved for inelastic scattering of ^{4}He beams of about 10 meV initial energy (Graham, 2003). This enables informative measurements of monolayer collective excitations with energies in the range of 1–2 meV (Graham *et al.*, 1997; Gerlach *et al.*, 1998; Šiber *et al.*, 1999; Bruch *et al.*, 2000; Boas *et al.*, 2003). In contrast to the results of inelastic neutron scattering for monolayers on high specific surface area powders, which typically give densities of states (see, e.g., Hansen *et al.*, 1990), inelastic helium-atom scattering directly gives dispersion curves in the analogue of 3D single-crystal experiments for neutrons. Graham (2003) reviewed many of these experiments, some of which are described in Sec. V. Implementation of the inelastic scattering theory is reviewed in Sec. III.B.

b. Quasielastic scattering

The typical energy widths of He beams restrict the measurement of diffusion processes using the TOF technique to those having characteristic times shorter than tens of ps. The spin-echo technique now extends the accessible range of characteristic times to hundreds of ns and can also be applied to inelastic scattering measurements, e.g., to measure phonons (Alexandrowicz and Jardine, 2007). Here we discuss it in the context of quasielastic scattering.

The spin-echo technique overcomes the intrinsic energy resolution of the beam by utilizing a similar spin-echo method to that employed in nuclear magnetic resonance. To apply the spin-echo technique to HAS requires that the He atoms have a half-integer spin, which is achieved by using ^{3}He. The first ^{3}He spin-echo instrument was built in Heidelberg (DeKieviet *et al.*, 1995) and a later version that is more optimized to study surface dynamics was built in Cambridge (Jardine *et al.*, 2001).

A schematic diagram of the Cambridge instrument is shown in Fig. 8. With this instrument, the ^{3}He beam is produced with the usual expansion technique and has a nominal energy of 8 meV and an energy spread of about 0.5 meV. The beam is then spin aligned in a direction perpendicular to its velocity, using a succession of magnets, and the spin-polarized beam enters a primary solenoid (B field along its axis) and begins a Larmor precession. The amount of Larmor precession achieved by the time the atom gets to the other end of the solenoid depends on how long the He atom stays in this solenoid (inversely proportional to its speed) and the strength of the B field (proportional to the solenoid current). After emerging from the solenoid, the beam scatters from the sample and then enters another identical (spin-echo) solenoid with its B field in the opposite direction to the first. Therefore, the He spin precession direction is opposite to that in the primary solenoid. After they emerge

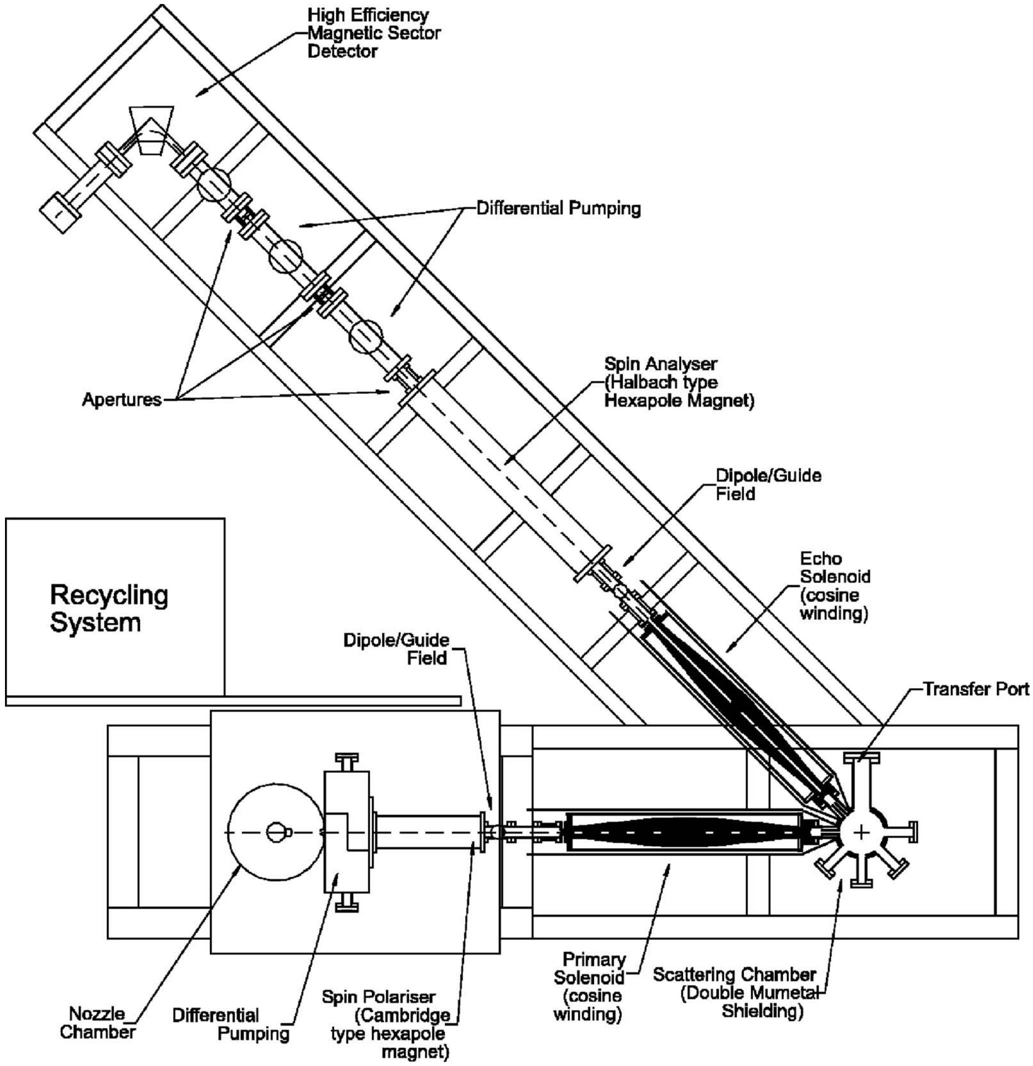

FIG. 8. Top down schematic of the complete ^{3}He spin-echo spectrometer. The overall design follows a 45° fixed scattering geometry for sufficient momentum transfer on scattering. The recycling beam source (bottom left) produces the ^{3}He beam and passes it through two differential pumping stages, prior to polarization. The polarizer focuses the beam to parallel, improving the intensity and reducing the aberrations within the solenoid. The scattered beam is passed through an identical solenoid and an analyzer magnet, which focuses the selected polarization from the crystal to the detector. From Alexandrowicz, 2005.

from the second solenoid, the He atoms enter a spin analyzer and are then detected.

In a spin-echo QHAS experiment, the time of flight is not measured. Instead, the polarization of scattered He atoms is measured as a function of the current through the solenoids, with the currents fixed to always be equal and opposite to each other. The measurement can be understood by considering what happens to the He spins in two different cases.

(1) The speeds of He atoms that scatter elastically from the surface are the same through each of the solenoids. Therefore, the precession angle accrued in the spin-echo solenoid is equal and opposite to that in the primary solenoid. This is true no matter what current is used in the solenoids, as long as they are the same. It is also true for every He atom in the beam, even though there is a distribution of initial velocities. Therefore, the detected atoms all have a total precession angle of zero and the polarization is the same as in the original beam.

(2) For He atoms that scatter quasielastically from the surface, the speeds in the spin-echo solenoid will be slightly faster (slower) than in the primary solenoid. Therefore, the detected spins will have total precession angles slightly smaller (larger) compared to the elastically scattered atoms. The average polarization of the scattered atoms will be in the same direction as the incident beam, but with a somewhat smaller magnitude that depends on the width of the polarization angle distribution. The actual change of spin angle for any given atom is proportional to the energy lost or gained in the scattering process, and the proportionality constant is called the spin-echo time t.

The net precession angle is proportional to the difference in time spent in the two solenoids. At zero current,

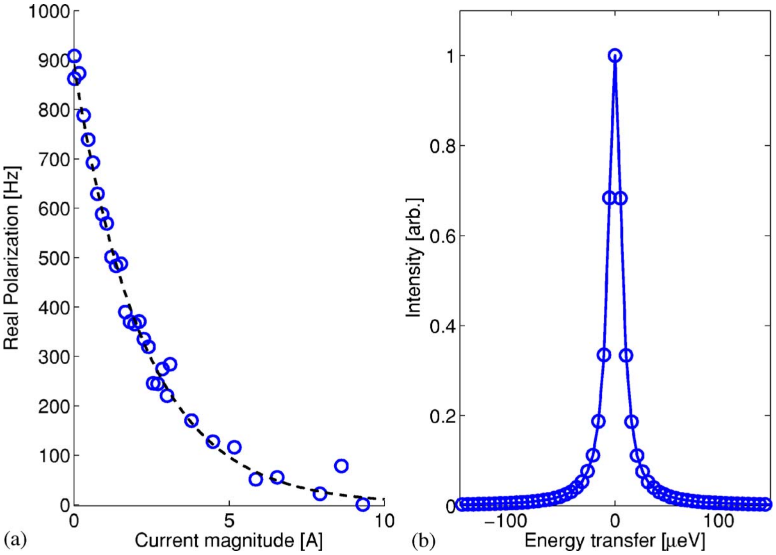

FIG. 9. (Color online) Detected polarization signal vs solenoid current (left) and its Fourier transform (right) for ^{3}He scattering from a 0.02 coverage of Na on Cu(001) at 155 K. The decay constant of the exponential is proportional to the inverse lifetime of the diffusion process and the FT is analogous to a time-of-flight spectrum, where the peak width is the quasielastic broadening.

the change in spin angle is zero and all spins are polarized in their original direction, whether they have scattered elastically or inelastically. For a nonzero current, the spins of quasielastically scattered atoms are rotated from the original direction by an amount proportional to their energy change, giving a distribution of polarization directions that becomes broader as the current is increased. Therefore, the total polarization of the scattered beam will decrease as the current is increased or, equivalently, as the spin-echo time is increased. A typical measurement of this decay is shown in Fig. 9(a).

As long as there are no other processes such as phonon scattering within the time range of interest, the decay of the polarization can be directly fitted to an exponential function, for which the decay constant is proportional to the inverse lifetime, which in turn is proportional to the quasielastic broadening. Alternatively, since the spin-echo time is the Fourier conjugate of the energy difference, the decay spectra can be Fourier transformed and analyzed as if they were time-of-flight spectra. Figure 9(b) shows the Fourier transform of the polarization decay scan in Fig. 9(a) and represents the quasielastic peak that would be measured in a very-high-resolution TOF experiment.

A diffusion process that has a very narrow quasielastic peak will produce a very broad (slow) decay of polarization versus spin-echo time and, therefore, the energy resolution of the measurement depends on the longest spin-echo time that can be measured. This is the spin-echo time corresponding to one revolution of precession, which corresponds to 3 μeV for the Cambridge instrument, an improvement of a factor of about 100 compared to TOF QHAS. In practice, much higher resolutions can be achieved by precisely fitting the spin-echo curve [Fig. 9(a)] and, for example, quasielastic peak widths of 20 neV were achieved for CO on Cu(100) (Alexandrowicz, 2005). This improvement over TOF QHAS effectively allows much slower diffusion processes to be measured, giving much greater scope for observing the diffusion of weakly bound adsorbates.

F. Interfacial friction

The quartz crystal microbalance (QCM) enables one to determine adsorbed masses and adsorption isotherms by measuring the shift in resonance frequency of a thin film on a high-Q quartz crystal. Amounts as small as nanomoles of adsorbed material are readily detected (see, e.g., Daly and Krim, 1996). A significant extension of this technique is to measure sliding friction by including analysis of the width of the resonance too, especially for rare gases sliding on metallic films bonded to the quartz crystal (Daly and Krim, 1996; Carlin *et al.*, 2003; Coffey and Krim, 2005). The time scale for damping in such experiments is on the scale of nanoseconds, while the linewidths for damping of vibrating adatoms tend to have damping times of a few picoseconds (Fuhrmann and Wöll, 1996). Although there is a large gap in these time scales, there is some modeling of the sliding friction of monolayers in terms of the processes that give the damping for adsorbate spectroscopy. In particular, there has been much discussion about whether coupling to phonon or electron degrees of freedom of the substrate (Persson and Nitzan, 1996; Tomassone *et al.*, 1997; Persson *et al.*, 1999; Liebsch *et al.*, 1999) is more important in the first stage of dissipation.

There has been an attempt to disentangle the phonon and electron contributions to sliding friction by looking for changes in the friction as the temperature of the metallic film passes through the superconducting transition (Dayo *et al.*, 1998; Mason *et al.*, 2001; Highland and Krim, 2006). The interpretation of these experiments is still controversial because similar experiments by others have found that the monolayer does not slip at such low temperatures. These differences have been discussed in terms of the presence or not of surface defects, but no clear explanation has emerged (Renner *et al.*, 2001; Carlin *et al.*, 2003; Bruschi *et al.*, 2006).

TABLE III. Parameters of the potential well of homonuclear diatomic molecules from ultraviolet spectroscopy. The ΔG and $\omega_e x_e$ are parameters[a] of the vibrational level spectra. $\hbar\omega_e$ is the energy quantum of the harmonic oscillator fit at the potential minimum. r_e is the equilibrium separation derived from analysis of the rotational energy levels and D is the depth of the pair potential there. The values of D and r_e are nearly identical to the values ϵ and $R_{\min}$ used by Tang and Toennies (2003) in constructing their semiempirical pair potentials. $K=(m/2)\omega_e^2$ (in $\mathrm{J/m^2}$) is the spectroscopic value for the curvature d^2V/dr^2 at r_e. K_{TT} (in $\mathrm{J/m^2}$) is the curvature calculated for the Tang-Toennies potentials.

Pair	$\Delta G(\frac{1}{2})$ (meV)	$\omega_e x_e$ (meV)	$\hbar\omega_e$ (meV)	r_e (Å)	D (meV)	K[b]	K_{TT}[b]
Xe_2[c]	2.39	0.066	2.53	4.377	24.3	1.62	1.72
$^{84}\mathrm{Kr}_2$[d]	2.65	0.133	2.92	4.017	17.1	1.37	1.47
$^{40}\mathrm{Ar}_2$[e]	3.19	0.317	3.79	3.761	12.3	1.10	1.21
$^{20}\mathrm{Ne}_2$[f]	1.71		>1.71	3.094	3.65		0.515

[a] In terms of the vibrational energy levels, $\Delta G(v+\frac{1}{2})=E(v+1)-E(v)\simeq\omega_e-2\omega_e x_e(v+1)$. The experimental data for ω_e and $\omega_e x_e$ were reported in cm^{-1} and have been converted to meV using $1\ \mathrm{cm}^{-1}=0.1240$ meV.

[b] Curvature at the pair potential minimum, in $\mathrm{J/m^2}$: K evaluated from ω_e and K_{TT} from the Tang-Toennies (2003) semiempirical pair potentials.

[c] ΔG, ω_e, $\omega_e x_e$ for an average of isotopomers, from Freeman *et al.* (1974) and Wüest *et al.* (2004).

[d] From LaRocque *et al.* (1986).

[e] From Colbourn and Douglas (1976) and Herman *et al.* (1988).

[f] From Wüest and Merkt (2003). Only $\Delta G(\frac{1}{2})$ was determined (only two vibrational levels in the ground-state potential) and so there is no direct measure of $\omega_e x_e$ and K.

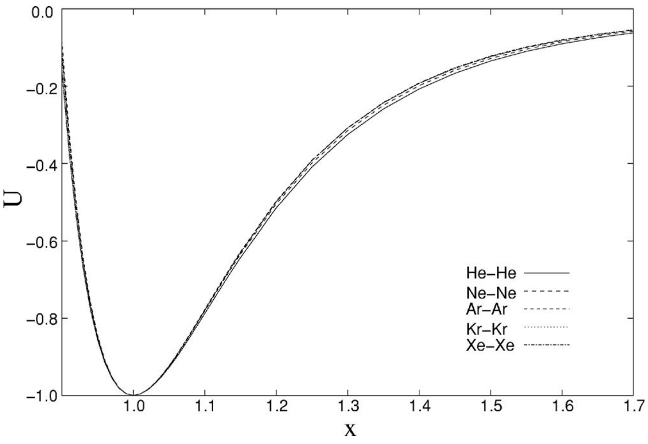

FIG. 10. Potential wells for He_2 to Xe_2 presented in scaled, corresponding states, form. The pair potentials of Tang and Toennies (2003) are plotted in the form $U=V(r)/\epsilon$ vs $x=r/R_{\min}$, where ϵ and $R_{\min}$ are the depth and position of the potential minimum, respectively. The curves for Ar-Ar, Kr-Kr, and Xe-Xe are indistinguishable on this scale.

III. DEVELOPMENTS IN THEORY

A. Interactions

We first review the status of the knowledge on the potential energy of homonuclear rare-gas pairs and then the calculations of rare-gas (primarily xenon) adsorption on metals.

1. Rare-gas pairs

The attractive potential well of the interaction $V_{XX}(r)$ of rare-gas atoms in the dimer X_2 is determined to within 5% for separations r that are important for the cohesion of solid and fluid phases of the species X. This has come about through the convergence of semiempirical constructions (Hepburn *et al.*, 1975; Tang and Toennies, 2003) based on calculations of van der Waals energy coefficients and short-range repulsions and refined with experimental data such as ultraviolet spectroscopy of the dimers. A summary of information for Ne_2 to Xe_2 is given in Table III. One of the surprises has been how closely the series He_2 to Xe_2 follows the hypothesized principle of corresponding states (Hirschfelder *et al.*, 1964), where the potential is assumed to have a scaled form $V=\epsilon f(r/R_{\min})$, in which the depth ϵ and separation $R_{\min}$ at the potential minimum are values specific to the pair X_2. That this in fact is the situation for the rare gases was shown convincingly first by Farrar *et al.* (1973) in an analysis of atom-atom differential scattering cross sections. In Fig. 10, we show the scaled pair potentials from the construction of Tang and Toennies (2003) for the five pairs He_2 to Xe_2; there is scarcely any distinction visible for the five potential curves in this format.

Calculating the pair potentials remains a challenge for density-functional theories because of the significant contributions from nonlocal van der Waals terms. The most primitive level of such calculations, the Gordon and Kim (1972) electron gas approximation (GKA), does give an attractive potential well, but systematic attempts at improving on the calculation give quite erratic results. We summarize several such attempts in Table IV, where the separation r_e (i.e., $R_{\min}$), depth D (i.e., ϵ), and curvature K for the potential minimum are given. For comparison, precise empirical and semiempirical values for these parameters are given in Table III. The sequence GKA, LDA-PW91, GGA-PW91, GGA-PBE, GGA-TPSS, PBE+vdW, and vdw-DF is believed to have an increasing degree of physical accuracy, but a comparison to the observed potential well parameters in Table III shows that there is not a monotonic improvement in the final interaction energies. The fair agreement of the LDA-PW91 results for ϵ and $R_{\min}$ is considered to be coincidental and the local-density approximation (LDA) has a tendency to serious overbinding.

Because of the small energy scale of the van der Waals binding in rare-gas dimers, details of the calculation become significant in comparing and appraising the approximations. It is evident from Table IV that results are sensitive to the various "flavors" of the generalized gradient (GGA) approximation. Furthermore, there is a sensitivity to basis-set size and to basis-set superposition error (BSSE) that is more pronounced in a derivative

TABLE IV. Potential wells of homonuclear rare-gas dimers evaluated in various flavors of density-functional approximations. D (meV) is the depth and r_e(Å) is the separation of the potential minimum. K is the curvature in $\mathrm{J/m^2 = N/m}$.

Case	GKA[a]	LDA-PW91[b]	GGA-PW91[c]	GGA-PBE[d]	GGA-TPSS[e]	PBE+vdW[f]	vdW-DF[g]
Ne_2							
D	3.53	19.9	14.3	5.6	3.0		
r_e	2.99	2.64	3.42	3.61	3.26		
K		4.0	1.6	0.9	0.7		
Ar_2							
D	10.9	28.9	14.2	6.1	3.3		20
r_e	3.63	3.01	3.96	4.29	4.3		3.9
K		4.0	0.9	0.7	0.5		
Kr_2							
D	15.5	33.5	14.3	6.6	3.3	25.3	25.4[45.5]
r_e	3.88	3.08	4.03	4.36	4.64	3.92	4.25 [3.91]
K		3.9	0.8	0.6	0.7	1.93	1.50 [3.22]
Xe_2							
D	26.1	37.4	14.1	9.4			
r_e	4.13	4.14	4.79	4.83			
K		2.4	0.4	0.4			

[a] GKA: Gordon-Kim approximation (Gordon and Kim, 1972), as evaluated by Clugston (1978).

[b] LDA-PW91: Local-density approximation with Perdew-Wang functional, evaluations by Patton and Pederson (1997) and Pederson (private communication).

[c] GGA-PW91: Generalized gradient approximation with Perdew-Wang functional, evaluations by Patton and Pederson (1997) and Pederson (private communication).

[d] GGA-PBE: Generalized gradient approximation with Perdew-Burke-Ernzerhof functional, evaluations by Patton and Pederson (1997) and Pederson (private communication). See also Tao and Perdew (2005) for corrections for basis-set superposition errors.

[e] GGA-TPSS: Generalized gradient approximation with Tao, Perdew, Staroverov, and Scuseria functional, evaluations by Tao and Perdew (2005).

[f] PBE+vdW: Density functional as in footnote d, but with van der Waals energy added as a fragment term, from Lazić *et al.* (2005, 2007).

[g] vdW-DF: Density-functional calculation with "seamless" inclusion of van der Waals terms (nonlocal correlation), calculation of Dion *et al.* (2004) for Ar_2 using revPBE exchange and Lazić *et al.* (2007) for Kr_2 using revPBE exchange and, in [ ], using PBE exchange.

property such as the curvature K, Table III, than in ϵ or R_{min} (Tao and Perdew, 2005). Recent work (Dion *et al.*, 2004; Lazić *et al.*, 2005, 2007) attempts to include the nonlocal character of the van der Waals forces; the first results, Table IV, are encouraging.

2. Atom-metal interactions

Satisfactory models of the adatom-substrate potential for physisorption on graphite and on graphene sheets have been constructed from pairwise sums of adatom-carbon potentials (Steele, 1974; Bruch *et al.*, 1997; Gatica *et al.*, 2007). However, such a formulation is expected not to be useful for adsorption on metals (see, e.g., Kirchner *et al.*, 1994). Thus the modeling of atom-metal interactions almost immediately becomes dependent on calculations at some level of quantum chemistry, and there are many parallels between the calculations for chemisorption and physisorption (Brivio and Trioni, 1999). Since the energies involved in physical adsorption typically are a small fraction of the total electronic energy, the modeling turns out to be dependent on details of the approximations and there has been much opportunity for coincidental successes.

We first note the progress in understanding the repulsive branch of the atom-metal potential that determines scattering phenomena at energies of 50–100 meV. Early experiments for He scattering by the (110) surfaces of several fcc metals were analyzed in terms of spatial corrugations for the metal surface (height variations for a given potential energy) that were much larger than anticipated by calculations based on the unperturbed metal and atom charge densities. Annett and Haydock (1984, 1986) proposed a resolution of the problem based on hybridization of He electron orbitals with metal electron states (i.e., the He is not inert in this picture) and noted that the consequence even could be a reversal, "anticorrugation," of the potential energy contours in some cases. Rieder *et al.* (1993) confirmed the existence of the anticorrugation for He scattering by two metal surfaces, but found (and gave a qualitative explanation) that the corresponding scattering for Ne showed the normal corrugation. Petersen *et al.* (1996) confirmed this difference using density-functional calculations for the repulsive potential energy of He and Ne with Rh(110) (the difference arises from the different angular symmetries of the outermost atomic electrons, $1s$ for He and $2p$ for Ne). Jean *et al.* (2004) showed for He/Cu(111) that the contours change from anticorrugation to corrugation as the scattering energy increases. The calculations incorporate realistic electron densities of states of the metals and there are large differences between the predicted phenomena for copper and aluminum.

Experimental measurements of the van der Waals energy for an adatom interacting with a substrate show an encouraging level of agreement with the near-field, nonretarded theory values (Panella *et al.*, 1996). Related experiments are the high-resolution measurement of selective adsorption resonance energies for Ne/Cu(110) by Linde and Andersson (2006) and the measurement of the difference in the He/Ni(001) and He/Cu(001) potentials by Huang *et al.* (2006). Further, semiquantitative agreement of experiment and theory has been achieved for ideal geometries in a NCAFM (noncontact atomic force microscope) measurement for a silicon tip and a carbon SWNT (Ashino *et al.*, 2004; Bruch, 2005) and a silicon tip and Pd clusters (Fain *et al.*, 2006). Another direction of work has been to adapt the theory to the calculation of forces between dielectric nanoclusters (Kim *et al.*, 2007)

Next we survey the status of calculations relevant to the properties of an adsorbed monolayer of the more massive rare gases. Quantitative comparison of the calculations with experimental data is given in Sec. IV.B. We take as our starting point Müller's calculation (1990) of the interaction of Xe with a cluster of Pt atoms. This was a calculation in the local-density approximation (LDA) and was the first electronic-structure calculation to find a top-site potential minimum for adsorbed xenon.[7] It was 10 years before his result was confirmed in another density-functional calculation (Betancourt and Bird, 2000) that also included the results for the generalized gradient approximation (GGA).

Recent work (Da Silva *et al.*, 2003, 2005; Lazić *et al.*, 2005) attempts to improve on the treatment of the Xe/Pt(111) system, to treat other Xe/metal cases, and to develop a qualitative understanding of the top-site adsorption. There is fair agreement between calculations for the adsorption energies and the Xe-metal distance in the LDA approximation, but in view of the remarks in Sec. III.A.1 this may be coincidental. The simple GGA (Betancourt and Bird, 2000; Da Silva *et al.*, 2003, 2005) severely underbinds xenon. Both the LDA and GGA are expected to apply only for xenon near the metal, and, for instance, the curvature at the potential minimum and hence the perpendicular frequency ω_S are given poorly. The calculation of Lazić *et al.* (2005) adds the van der Waals energy (in the fragment approximation) to the GGA-PBE energy and restores fair agreement for the adsorption energy of Xe/Pt(111). These recent calculations show that there is significant charge redistribution in the metal during the xenon adsorption and there must then be an adsorption-induced dipole moment, which is very sensitive to the Xe-metal spacing and is larger in the calculations than in experimental measurements (Ostertag *et al.*, 1996). The features of rather strong binding, atop site adsorption, and charge rearrangement are consistent with a picture of weak chemisorption for Xe/Pt(111) and there are long-standing proposals that there are elements of chemistry in xenon adsorption (Ishi and Viswanathan, 1991). However, the cluster calculation for Xe/Cu(111) by Bagus *et al.* (2002) finds that most of the adsorption-induced dipole moment can be understood with a self-consistent-field (SCF) calculation.

While the energy scale for Xe on Pd(111) and Pt(111) and the top site adsorption phenomenon are suggestive of chemisorption, the overall behavior of these monolayers is similar to the traditional physisorption systems (Bruch *et al.*, 1997). However, besides the semantic problem of assigning a sharp boundary to a continuous gradation between physisorption and chemisorption, one should note that the charge rearrangement in the hybridization of adatom and substrate electron wave functions may lead to other measurable effects such as adsorption-induced dipole moments and work-function changes (Zeppenfeld, 2001). Yang and Phillips (2007) calculated the work-function change for a monolayer of Ar/Ag(111) and found agreement with the data of Hückstädt *et al.* (2006).

There are also attempts to get quantitative and qualitative insights into other systems starting from commercial quantum chemistry packages. Yang *et al.* (2006) obtained reasonable agreement with experimental data for the energies and vibrational frequencies of methane adsorbed on graphite. Thomas *et al.* (2003) estimated diffusion barriers for Xe/Nb(110).

B. Atomic scattering

Inelastic scattering of a thermal energy (10s of meV) rare-gas atom by a monolayer or by a clean substrate surface is nondestructive of the target. Such experiments are analogous to inelastic thermal neutron scattering by 3D single crystals (Brockhouse, 1995), but the atom scattering case is a strong-coupling problem (in fact this is how it becomes a surface-sensitive probe) and the implementation of the theory has involved major recent developments and surprises. For the topics treated in this

---

[7] This was a pioneering calculation, at the frontier of what was then feasible, and some features of the results have been criticized (Da Silva *et al.*, 2005). For instance, the minimum energy height of Xe in Müller's calculation is larger atop a Pt atom than at the threefold hollows (Bruch, 2001) while later calculations by Da Silva *et al.* (2005) for Xe/Pt(111) and Kirchner *et al.* (1994) for Ar/Ag(111) give the reverse ordering.

review, the theoretical development is considered to begin with Manson and Celli (1970). There were quite detailed analyses of the diffraction of ^{4}He by xenon monolayers in the late 1980s (Gibson *et al.*, 1988; Aziz *et al.*, 1989). Then, with systematic data on dispersive monolayer phonons in physisorbed systems[8] in the 1990s, there was a renewed effort at achieving quantitative theories of the inelastic scattering process.

The theory has been developed in time-independent and time-dependent versions. In both, there are many coupled diffraction channels, even for incident energies of only 10 meV. Gumhalter (2001) reviewed the time-independent theory, and applications to inelastic scattering by xenon monolayers and multilayers were given by Šiber *et al.* (1999, 2001). The most extensive results are for single-phonon excitations, but there also are some results for the relative intensities of multiphonon excitations of Kr/Pt(111) that are in good agreement with experiment (Li *et al.*, 2002). The time-dependent version uses a wave-packet description of the incident beam (Tribe, 2006) and has been applied to the inelastic scattering of ^{4}He by Xe, Kr, and Ar monolayers on Pt(111) (Bruch and Hansen, 2005). A closely related application of the wave-packet formulation is to determine the lifetimes of selective adsorption resonances (Hernández *et al.*, 1994).[9]

There are now several measurements of dispersive monolayer phonon branches by inelastic helium-atom scattering (Graham *et al.*, 1997; Braun *et al.*, 1998; Gerlach *et al.*, 1998; Bruch *et al.*, 1998, 2000; Šiber *et al.*, 1999); an example is shown in Fig. 11. In principle, these provide direct tests of models of the interatomic potentials in the monolayer. However, the assignment of the experimentally observed modes is critical to this analysis (Bruch and Hansen, 2005; Lazić *et al.*, 2005). The problem is that the experiments are performed along near-symmetry azimuths of the monolayer, and analogies to the selection rules for inelastic neutron scattering led to the expectation that modes with polarization perpendicular to the momentum transfer [the shear horizontal (SH) branches] would be excited with low probability, if at all. Nonetheless observed dispersion relations could be fit in many cases to SH branches using adatom forces transported from 3D rare-gas solid phenomena. In the case of Xe, Kr, and Ar adsorbed on Pt(111), there are three observed branches, as expected for the modes of a monatomic Bravais lattice. Since the two dispersive branches for the gases on Pt(111) are fit by the transported interactions, using identification as SH and LA branches as in Fig. 12, there is now no doubt that the SH branch can be excited in such experiments. In fact, there are cases in which the experimental intensity of the SH phonon is larger than that of the LA phonon. Bruch and Hansen (2005) explained the effect as arising from a small misalignment of the scattering plane relative to symmetry axes of the monolayer solid, and the departure from systematic trends based on analogies to neutron scattering as arising because the theory of the HAS experiment is a strong-coupling theory. The unsettled state of the interpretation for other adsorbate/substrate combinations arises because (i) frequently only one dispersive branch was observed and (ii) the experiments were not configured to measure very small (e.g., 0.5°) misalignments of the scattering plane.

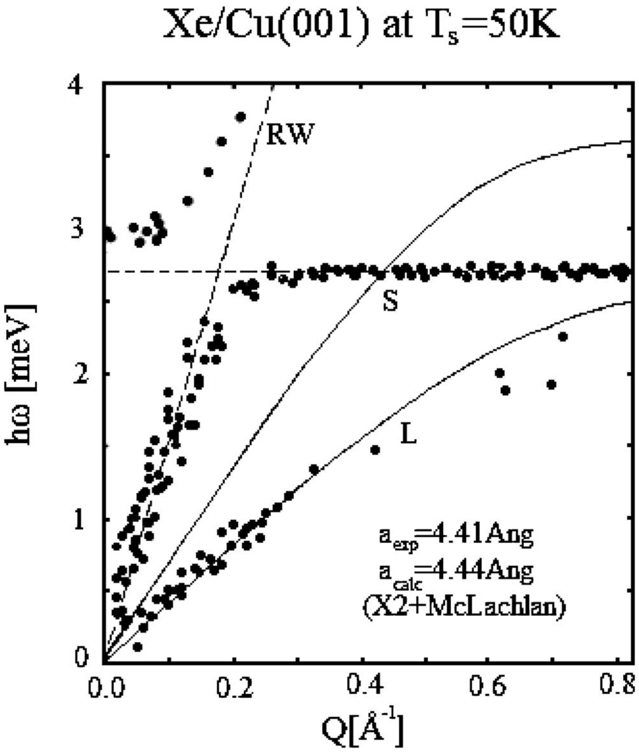

FIG. 11. Monolayer phonon energies for Xe/Cu(001) at 50 K. The filled circles are the inelastic HAS data of Graham *et al.* (1997) at a beam energy of 8.1 meV. The labels RW (Rayleigh wave), *S* (perpendicular monolayer vibration), and *L* (longitudinal mode) are those assigned in the original experiment. The solid lines are the results of model calculations using the Barker X2 Xe-Xe potential augmented by the McLachlan substrate mediated dispersion energy (see Bruch *et al.*, 2000). The lower solid line, which runs through the dispersive branch, has shear horizontal polarization; the upper solid line has longitudinal acoustic polarization. The mixing of the *S* branch with the copper Rayleigh wave at $Q \approx 0.2$ Å^{-1} is an example of the damping by a Fano resonance treated by Hall *et al.* (1989).

The theory of molecule-surface scattering is distinctly more difficult (Moroz *et al.*, 2004) because of the need to treat very different time scales for the center-of-mass

---

[8] Dispersive phonons have frequencies that depend on the wave number. The dependence arises from adsorbate-adsorbate interactions and, for geometrical reasons, is negligible for monolayer phonons with vibrations polarized perpendicular to the plane. An early HAS experiment showed a dispersive branch for Xe/KCl(100) (Mason and Williams, 1984).

[9] The lifetimes might be used to construct models of the corrugation potential. However, it is only recently that experiments on selective adsorption states have high enough resolution, linewidths of order 0.1 meV for He/LiF(001) and Ne/Cu(110), to seriously constrain the models (Jardine, Dworski, *et al.*, 2004; Linde and Andersson, 2006; Riley *et al.*, 2007).

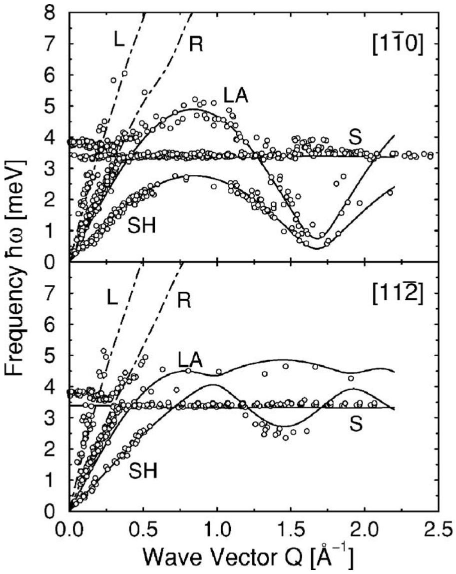

FIG. 12. Phonon-dispersion curves for a monolayer of xenon on Pt(111) for the [1$\bar{1}$0] and [11$\bar{2}$] azimuths of the Pt substrate, at an angle of 2.6° to the Γ*K* and Γ*M* azimuths of the triangular incommensurate xenon monolayer with nearest-neighbor spacing 4.33 ± 0.01 Å. The experimental points, denoted by circles, were obtained with inelastic helium-atom scattering at energies from 6 to 17 meV and a surface temperature of 50 K. The solid lines are the result of calculations with realistic Xe pair potentials and the McLachlan dispersion energy. The xenon branches are designated SH (shear horizontal), LA (longitudinal acoustic), and *S* (perpendicular to the monolayer plane) and two branches of the Pt(111) are also indicated (*R*, Rayleigh and *L*, longitudinal resonance). From Bruch *et al.*, 2000.

and internal molecular motions, but there is good agreement with experiment for such properties as the angular distribution of CH_4 scattered from LiF(001) at 100–500 meV.

IV. MONOLAYER SOLIDS

We begin with a survey of monolayer solids, updating the reviews of Suzanne and Gay (1996), Bruch *et al.* (1997), and Zeppenfeld (2001) and extending the coverage to adsorption on quasicrystals and the properties of alkane monolayers. Then there is a comprehensive review of site determinations in commensurate monolayers and on stepped surfaces. This is followed by a review of recent applications of the lattice-dynamical theory of monolayer solids and of estimates of the monolayer compressibility. Finally, Xe/graphite, Xe/Pt(111) [with Xe/Pd(111)], and Xe/Cu(110) are discussed to illustrate what has been, and remains to be, accomplished.

A. Survey of monolayer solids

1. Rare gases and small molecules on graphite and dielectrics

The adsorption of rare gases on graphite and graphitic substrates is a rather large subject in itself and we limit our presentation to giving a few leading references and to topics that are closely related to the rest of this review. Reviews of adsorption on graphite as of the mid-1990s were given by Suzanne and Gay (1996) and Bruch *et al.* (1997). Since then, there has been extensive work with adsorption on carbon nanotubes, reviewed by Calbi *et al.* (2001), Bienfait *et al.* (2004), Gatica *et al.* (2007), and Migone (2007). The monolayer phase diagram for Xe/graphite is presented in Sec. IV.E.1, with references to the literature. A closely related system is xenon on a graphene sheet studied for its sliding friction by Coffey and Krim (2005). The argon/graphite system exhibits rather complex phenomena at temperatures near monolayer melting. Johnson *et al.* (1997) looked at the possibility that the monolayer solid expanded to a commensurate structure just before melting, but found no evidence for that. Flenner and Etters (2002, 2006) gave a new interpretation of a specific-heat anomaly near the melting, ascribing it to a transition to another state of orientational epitaxy. However, the Kr monolayer phase diagram was essentially completed before 1995, nor has much work been done since on Ne/graphite.

Boron nitride is available in homogeneous powders of large surface to volume ratio (see, e.g., Alkhafaji *et al.*, 1994) and provides interesting parallels to graphite because the surface symmetry is the same, but the lattice constant is 2% larger, $\ell=2.50$ Å (Marx and Wiechert, 1996). Morishige *et al.* (1996) made an x-ray study of monolayers of Kr, N_2, and Xe. In contrast to the adsorption on graphite, commensurate monolayers of Kr and N_2 on BN form only in very limited regions of coverage and temperature. This may not be a great surprise, because the dilation of the corresponding commensurate monolayers on graphite relative to the spacing in the 3D solids was already 6.5%. However, no commensurate monolayer of Xe is observed for BN down to 72 K, in contrast to the situation for graphite, and this would only have required a compression of 1% beyond the nearest-neighbor spacing in the 3D solid. The triple point temperature for Xe/BN is 102 K (Regnier *et al.*, 1979), close to the value 99 K for Xe/graphite, and the lattice constant of the Xe/BN monolayer at the melting curve at 110 K is 4.53 Å,close to the value 4.56 Å for Xe/graphite at melting at 116–134 K reported by Hong *et al.* (1989).

Marx and Wiechert (1996) gave a comprehensive review of the adsorption of N_2 and CO on graphite and on BN. Later theoretical work for N_2/graphite addressed signatures of monolayer diffusion of fluid N_2/graphite (Hansen and Bruch, 2001) and the monolayer melting transition (Etters and Kuchta, 1998). A planar herringbone lattice is also observed for C_2H_2/KCl(001) (Glebov *et al.*, 2000); a rather advanced interaction model was required to produce this result theoretically. C_2H_2/MgO(001) was also found to form a 2-sublattice (2×2) structure using both neutron diffraction (Coulomb *et al.*, 1994) and LEED (Ferry *et al.*, 1997). Both studies were consistent with a herringbonelike structure with planar or nearly planar molecular axis orientations, in agreement with semiempirical calculations (Ferry *et al.*, 1997). The rotational tunneling of monolayer CH_4 was studied earlier for adsorption on graphite and now (Larese *et al.*, 2001; Drummond *et al.*, 2006) for adsorption on MgO(100).

The monolayer Xe/NaCl(001) was determined by low-energy electron diffraction (LEED) (Schwennicke *et al.*, 1993) to have a distorted hexagonal UIC structure. This was later identified as a $c(10\times2)$ HOC structure using HAS and its phonons were measured by Gerlach *et al.* (1998) (see also Sec. IV.C.1). Xenon and krypton were used to titrate the different adsorption sites on reconstructed Si(111)-(7×7) using low-temperature STM in conjunction with TDS (Li *et al.*, 2002, 2003; Takeuchi and Shigekawa, 2003). The gases were found to bind somewhat more strongly to the faulted half of the unit cell (adsorption energies for Xe of 220 meV versus 200 meV). Interestingly, Xe initially adsorbs as dimers, whereas Kr adsorbs as trimers.

2. Rare gases on metals

Zeppenfeld (2001) gave a critical review of the energies and structures of adsorbed rare gases. Since then, Hückstädt *et al.* (2006) have made systematic measurements of the work function changes for argon, krypton, and xenon on Cu(111), Ag(111), and Au(111) that will be useful for an improved understanding of the adsorption-induced changes in charge distributions.

a. Xenon

Several monolayer systems have been studied, including xenon on Ag(111) and Pb(111); Pd(111) and Pt(111); Cu(111), (100), and (110); Pd(100) and Nb(110). The Xe/Pt(111) and Xe/Pd(111) cases are reviewed in Sec. IV.E.2 and Xe/Cu(110) in Sec. IV.E.3, respectively.

The case of Xe/Ag(111) was well-studied rather early (Unguris *et al.*, 1979; Gibson and Sibener, 1988) and found to be an excellent realization of an intrinsic monolayer solid. Recent work supports this view (Leatherman *et al.*, 1997; Igarashi *et al.*, 2003; Tosaka and Arakawa, 2006). A thorough understanding of its thermodynamic properties permitted its use as a 2D manometer to measure the spreading pressure, and hence the interatomic forces, in alkali-metal overlayers over a wide range of densities (Leatherman and Diehl, 1997b). Because so much is known about Xe/Ag(111), it was the subject of early sliding friction experiments (Daly and Krim, 1996). However, interpretation in terms of dissipation mechanisms (Persson and Nitzan, 1996; Tomassone *et al.*, 1997; Liebsch *et al.*, 1999) is hampered by the fact that only rough estimates (e.g., Coffey and Krim, 2005) are available for the corrugation energy amplitude V_{g0} of Xe moving on Ag(111).

Xe on Pb(111) condenses into an incommensurate hexagonal structure with a lattice constant similar to those observed on Ag(111) (Ferralis *et al.*, 2007). An adsorption isotherm measured with a QCM (Mason *et al.*, 2001) leads to a "normal" q_1.[10] Experiments looking for the effects of substrate superconductivity in sliding friction have investigated Xe/Pb(111), but find no effect (Highland and Krim, 2006).

There are extensive data for xenon adsorption on three crystal faces of copper. Xe on Cu(111) condenses as a commensurate $\sqrt{3}$ structure between about 50 and 90 K and an incommensurate structure was observed at lower T (Jupille *et al.*, 1990; Seyller *et al.*, 1998). Structurally, it appears to have normal interactions. However, the interpretation of vibrational spectra is in dispute. Some workers (Braun *et al.*, 1998; Šiber *et al.*, 1999) interpreted inelastic HAS data to show that the Xe-Xe van der Waals forces are strongly perturbed by the adsorption.[11] An alternative analysis (Bruch *et al.*, 1998, 2000) fits the Xe/Cu(111) data with normal Xe-Xe forces, but with a different polarization assignment of the spectra, as shown in Fig. 13. Similarly, there is much experimental evidence that Xe/Cu(100) has normal interactions.Chesters and Pritchard (1971) showed that there is a hexagonal monolayer lattice with nearest-neighbor spacing of 4.50 ± 0.1 Å at 77 K and Glachant and Bardi (1979) showed that the monolayer condensation behavior was that of a system with attractive lateral intereractions. The monolayer compressibility (Bruch, 1997) is also similar to that of other monolayer Xe systems with the same area per adatom. However, the assignment of an observed dispersive branch as LA (rather than SH) led to the conclusion that the forces between Xe atoms were strongly perturbed by the adsorption (Graham *et al.*, 1997; Šiber *et al.*, 1999). The fit as an SH branch with normal xenon forces is shown in Fig. 11. The Xe/Cu(110) case is discussed in Sec. IV.E.3.

In some cases, the Xe-Xe van der Waals forces may be disrupted by adsorption, although other mechanisms disrupting monolayer ordering are possible. The main experimental manifestation is the failure to form well-ordered submonolayer or monolayer solids at low temperature. It is known that the presence of impurities can both impede the ordering of a monolayer and cause additional ordered structures to form that do not form in the pure system, as demonstrated for Xe/Pd(111) by Zhu *et al.* (2003). However, there are cases in which the ordering is impeded even for the pure system, for example, Xe/Pd(100) (Miranda *et al.*, 1983; Moog and

---

[10] For xenon, a rare gas with $\xi_{\text{int}}=1$, Eq. (A13) can be used to estimate a monolayer heat of adsorption q_1 from the pressure and temperature at monolayer condensation. This has been done with QCM data of Mason *et al.* (2001) for Xe/Pb(111) at 77 K. The result, $q_1\approx200$ meV, puts the energetics of that xenon monolayer in a similar range to that of xenon on several other metals (Bruch *et al.*, 1997) and is support for modeling of the sliding friction (Smith *et al.*, 1996; Tomassone *et al.*, 1997; Bruch, 2000). The value for Xe/Pb(111) measured by Ferralis *et al.* (2007) is $q_1\simeq191$ meV.

[11] A recent calculation for commensurate Xe/Cu(111) by Lazić *et al.* (2005) offers a less dramatic picture. The authors attribute lowered force Xe-Xe constants to strong anharmonic effects in a dilated lattice, which is still a subject of discussion.

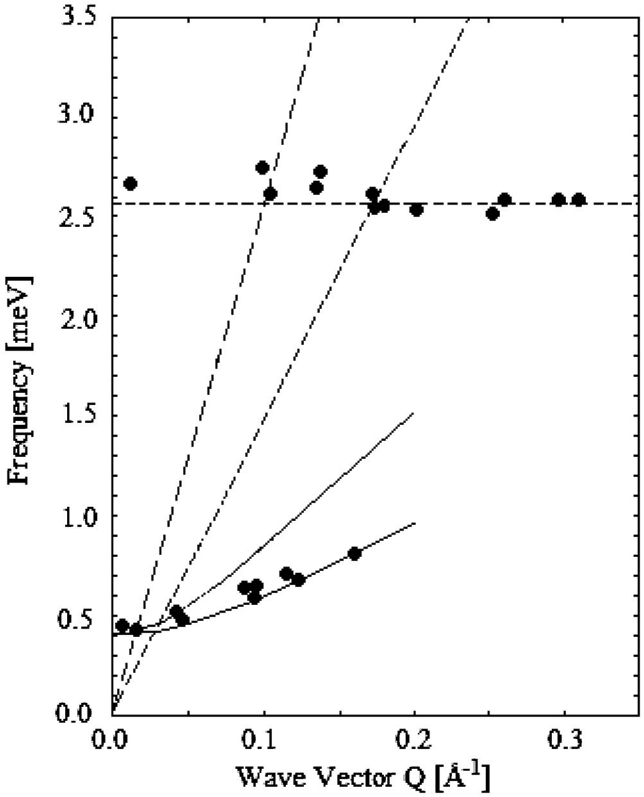

FIG. 13. Phonon energies for the commensurate $(\sqrt{3}\times\sqrt{3})R30°$ monolayer solid of Xe/Cu(111) at $T\approx 60$ K. The filled circles are the inelastic HAS data of Braun *et al.* (1998) at a beam energy of about 10 meV. The two solid lines are the SH (lower curve) and LA (upper) branches calculated with the HFD-B2 Xe-Xe potential augmented by the McLachlan energy and fitted to a zone-center gap of 0.4 meV.

Webb, 1984) and Xe/Nb(110) (Thomas *et al.*, 2004).

Two early studies for Xe/Pd(100) (Miranda *et al.*, 1983; Moog and Webb, 1984) found no ordering of the Xe at $T>10$ K for submonolayer coverages, although a close-packed structure was observed at monolayer completion. A more recent study for Xe on Nb(110) at 33–100 K indicates that the monolayer does not order at all and that long-range order only occurs when the third layer of Xe adsorbs (Thomas *et al.*, 2004). For $40<T<54$ K, a bulklike Xe film grows in the step-flow mode, whereas at 33 K, the layer growth is kinetically hindered and proceeds in a 3D island mode. DFT calculations (Thomas *et al.*, 2004) indicate that the top site is preferred and the lateral variation in the Xe-Nb(110) potential energy is about 50–70 meV compared to the adsorption energy of 247 meV. Apparently the rather large energy variation, along with the substrate-overlayer lattice mismatch, hinders the long-range ordering to a much larger extent than in other xenon monolayers. A similar situation is observed in simulation studies of the smaller rare gases on a quasicrystalline substrate (Setyawan *et al.*, 2006, 2007; Diehl *et al.*, 2007) as discussed in Sec. IV.A.3.

Monolayer Xe/Ru(10$\bar{1}$0) appears to be an intermediate system with several ordered structures, but with first-order desorption kinetics suggesting repulsive Xe-Xe interactions (Schmidt and Christmann, 2001; Kerner, Stein, *et al.*, 2005).

b. Argon

Ar/Ag(111) is the only rare gas adsorbed on silver to have a commensurate lattice (Caragiu *et al.*, 2001) as discussed in Sec. IV.C.4. Compressed monolayer solids of Ar/Pt(111) were studied with elastic and inelastic HAS (Zeppenfeld *et al.*, 1992; Bruch *et al.*, 2000). The SH and LA phonon branches for a nearest-neighbor spacing of 3.79 Å were fit using 3D gas phase pair potentials. However, the calculated chemical potential increase to compress the monolayer to 3.79 Å was already larger (Bruch *et al.*, 2000) than the range allowed by the adsorption energy q_1 reported by Kern and Comsa (1991), Table II. Thus, an earlier observation of a yet more compressed Ar/Pt(111) monolayer with 3.69 Å (Zeppenfeld *et al.*, 1992) became quite puzzling. The energies E_{des} from recent TPD experiments for Ar/Pt(111) (Kimmel *et al.*, 2003; Frieß *et al.*, 2007) are considerably greater than the q_1, Table II, and might drive a much larger calculated compression.

3. Rare gases on quasicrystals

It is anticipated that atomically thin layers on quasicrystal surfaces may have quite small friction because of the extreme incommensurability of the adlayer and the substrate (see, e.g., Park *et al.*, 2005). Studies are now beginning on the evolution of ordering for thin films of rare gases on quasicrystals. Ferralis *et al.* (2004) demonstrated the hindered hexagonal ordering of Xe on the quasicrystalline AlNiCo surface. In this case, the substrate has fivefold symmetry and LEED does not detect ordering of the monolayer, although a bulklike hexagonal structure begins to form at the onset of the second-layer adsorption. Grand canonical Monte Carlo (GCMC) simulations were performed for this system, using an adsorption potential that was constructed from semiempirical Lennard-Jones interatomic potentials (Trasca *et al.*, 2004) and has a lateral variation of about 50 meV. They indicate sitewise ordering for submonolayer coverages followed by a transition to a hexagonal structure near monolayer completion, with subsequent bulk growth. The multilayer structure aligns with the fivefold directions of the quasicrystal, i.e., five rotational domains of the sixfold structure are observed in both the experiment and the simulation. The simulations suggest that the rotational domains are mediated by fivefold defects in the Xe structure and, therefore, are intrinsic to the film (Curtarolo *et al.*, 2005; Diehl *et al.*, 2006). While there is necessarily a lattice mismatch in this case, the average row spacing for this quasicrystal surface is close to the Xe row spacing of Xe(111), which apparently facilitates the ultimate conversion to a hexagonal film. Similar GCMC simulations for other gases (Ne, Ar, Kr) that do not have such a fortuitous relationship with the substrate spacing exhibit fivefold ordered structures in the first monolayer, but with no transition to a long-range ordered hexagonal structure within at least the first two layers (Setyawan *et al.*, 2007).

4. Monolayer quantum solids

Several monolayer quantum solids are formed from the isotopic helium and molecular hydrogen series. Recent reviews are those of Godfrin and Lauter (1995) for helium adsorbed on graphite and Wiechert (2003) for molecular hydrogen isotopes adsorbed on graphite and BN. Higher-order-commensurate lattices of bilayer helium on graphite are discussed in Sec. IV.C.4.

The sliding friction of helium on graphite (Hosomi *et al.*, 2004, 2005), on Au(111) (Wataru *et al.*, 2005), and on Pb(111) (Highland and Krim, 2006) has been studied using QCM. A very different type of study was done for He/Pt(111) by Niedermayer *et al.* (2005), using thermal desorption and photodesorption spectroscopies at temperatures near 3 K. First-order desorption and nearly ideal 2D gases of ^{3}He and of ^{4}He were observed in a certain coverage range, followed by dense monolayer phases, but it is not yet known whether these are liquid or solid. The desorption energies are estimated to be in the range 90–120 K (8–10 meV), significantly larger than the ground-state energy of He on other metals.[12]

The main developments not covered in Wiechert's review (2003) are the results of experiments for monolayer hydrogen using new applications of surface-sensitive techniques. Infrared spectroscopy has been applied to the adsorption on NaCl(001) by Briquez *et al.* (1998) and Heidberg *et al.* (1999). Inelastic HAS was applied to H_2 on MgO(001) (Skofronick *et al.*, 2003), on NaCl(001) (Traeger and Toennies, 2004), and on LiF(001) (Toennies and Traeger, 2007). Inelastic neutron scattering has been used to measure the dynamical response of H_2/MgO(100) (Larese *et al.*, 2006). Photodesorption becomes significant for some cases such as H_2/Cu(510) (Hassel *et al.*, 2002).

5. Small molecules on metals

The most extensive results are for N_2 and a continuing puzzle is the scarcity of herringbone lattices in contrast to the N_2/graphite case (Marx and Wiechert, 1996). Leatherman and Diehl (1997a) studied N_2/Ag(111) and found a monolayer solid with molecular centers of mass arranged in a triangular incommensurate lattice.[13] Molecular-dynamics simulations (Bruch and Hansen, 1997) suggested that there would be a herringbone ordering at a temperature of 17–20 K, below their experimental range, and that a signature of this would be a transition to a rectangular lattice. N_2/Cu(110) is found to have novel packing into a pinwheel ordering[14] for the monolayer solid (Marmier *et al.*, 1997; Zeppenfeld *et al.*, 1997). N_2/Pt(111) (Zeppenfeld *et al.*, 2000) also has multimolecule unit cells.[15] The only reported herringbone for nitrogen on a metal is the system N_2/Ag(110) (Ramseyer *et al.*, 1998). An interesting variant on the Pt(111) case is the report (Gustafsson and Andersson, 2006) of a physisorbed monolayer of N_2 on chemically inert Pt(111)(1×1)H, which is said to have only minor differences from N_2/Pt(111).

There is an increasing amount of information on methane (CH_4) adsorbed on metals. Some data for the desorption energy of monolayers are summarized in Table V. Sakurai and Yamada (2005) reported a higher-order-commensurate monolayer solid of CH_4/Ag(111), discussed in Sec. IV.C.4. Kevan and co-workers used an electron-energy-loss spectroscopy technique for the C-H stretch mode to monitor low methane coverage on two metals in a density range where a virial expansion for the 2D methane gas is applicable.[16] Elliott *et al.* (1993) obtained an initial isosteric heat $q_{st}(0) \simeq 220$ meV for CH_4/Ag(111). However, their fit to an activation energy for desorption at low coverage gave 130 meV; they concluded that some of the assumptions used to identify the activation energy with the adsorption energy must fail in this case. The corresponding adsorption energy for CH_4/Cu(001) is (Wei *et al.*, 1996) $q_{st}(0) \simeq 165$ meV.

Sulfur hexafluoride on gold SF_6/Au(111) is a potentially interesting molecular system, since bulk SF_6 is a plastic crystal with octopolar coupling between molecules; there is a first report of inelastic helium-atom scattering from the monolayer (Rosenbaum *et al.*, 2006). It is curious that, at the temperature of the measurement (80 K), the monolayer was found to be disordered whereas several well-ordered monolayer solids were observed for SF_6/graphite at similar temperatures (Marti *et al.*, 1986).

6. Alkanes on graphite and metals

Flexible chain molecules have internal degrees of freedom that are believed to play an important role in determining the structure of the dense phases, in phase transformations such as melting, and in the dynamics of

---

[12] For ^{4}He/Pt(110), the ground-state energy obtained from selective adsorption resonances is 6 meV (Krzyzowski *et al.*, 1995).

[13] They found that CO/Ag(111) also orders in a triangular incommensurate lattice, but with a lattice constant 5% smaller than N_2/Ag(111), and inferred that the axes of the CO molecules are tipped out of the monolayer plane.

[14] The pinwheel for N_2/Cu(110) probably has seven molecules per unit cell (Marmier *et al.*, 1997) as does a pinwheel for N_2O/graphite (Leinböck *et al.*, 2000). For N_2/Pt(111) there are unit cells with four and seven molecules (Zeppenfeld *et al.*, 2000), both with in-plane ordering at low temperatures, although simulations suggest there may be a pinwheel structure for the seven-molecule cell at a higher temperature.

[15] We note that these authors also report $\omega_{\perp(s)} = 5.0–5.2$ meV for N_2/Pt(111) primarily devoted to structure.

[16] The 2D second virial coefficient B_2 extracted from the data and discussed in terms of proposed adsorption-mediated methane-methane interactions (McLachlan, 1964; Elliott *et al.*, 1993; Wei *et al.*, 1996). There was only qualitative success in accounting for large modifications to the interactions.

TABLE V. Adsorption energies, in meV/molecule, for alkanes. q_{sub} is the sublimation energy of bulk adsorbate. Entries for graphite include the monolayer heat of adsorption q_1 and the zero coverage isosteric heat $q_{st}(0)$ in [ ] for the shorter alkanes and desorption energies for the series. For MgO there are thermodynamic entries for q_1 of methane, ethane, and hexane. All other entries are activation energies for thermal desorption.

Name	Symbol	q_{sub} (bulk)	Graphite	MgO(001)	Au(111)	Pt(111)
Methane	CH_4	101[a]	147,[d] 200[b] [139[b]]	120,[c] 126[d]	151[e]	158,[d] 167[f]
Ethane	C_2H_6	214[g]	256,[d] 252[g] [120[h]]	185,[c] 231[d]	251[e]	300,[d] 383[f]
Propane	C_3H_8	296[j]	334,[d] 320[i] [235[h]]	290[d]		432,[d] 428[f]
n-Butane	C_4H_{10}	373[j]	424,[d] [290[h]]	363[d]	421[e]	529,[d] 350–600[f]
n-Pentane	C_5H_{12}	437[j]	675,[k] [350[h]]			443[f]
n-Hexane	C_6H_{14}	528[j]	655,[d] 765[k] [410[h]]	377,[c] 482[d]	581[e]	830,[d] 642[f]
n-Heptane	C_7H_{16}	602[j]	850[k] [543[h]]	440[c]	652[e]	690[f]
n-Octane	C_8H_{18}	708[j]	755,[d] 920[k] [580[h]]	654[d]	725[e]	749[f]
n-Nonane	C_9H_{20}	~760[j]	[640[h]]		782[e]	772[f]
n-Decane	$C_{10}H_{20}$	~870[j]	950,[d] 1050[k] [725[h]]	810[d]	833[e]	803[f]
n-Tetracosane	$C_{24}H_{50}$	~2140[l]	1810[k]			
n-Dotriacontane	$C_{32}H_{66}$	~2850[l]	2140[k]			

[a] From Colwell *et al.* (1963).

[b] $q_{st}(0)$ from Inaba *et al.* (1986) and $q_1 = 200 \pm 37$ meV for 2D gas-monolayer solid at 54–58 K. From Gay, Dutheil, *et al.* (1986).

[c] q_1 values for condensation to monolayer liquid from Arnold *et al.* (2005) and Arnold, Cook, *et al.* (2006) for C_2 at 91–144 K and C_1 at 70–96 K; Yaron and Larese (2006) for C_6 at 195–255 K; Fernandez-Canoto and Larese (2007) for C_7 at 205–275 K.

[d] Desorption energies by TPD from Tait *et al.* (2005, 2006).

[e] TPD energy at monolayer coverage from Wetterer *et al.* (1998).

[f] Values from Weaver *et al.* (2003).

[g] From Regnier *et al.* (1981).

[h] From Avgul and Kiselev (1970) and Kiselev and Poshkus (1976). Values from the Western literature differing by 10% from these are assembled in Lal and Spencer (1974).

[i] TPD energy for HOPG (highly oriented pyrolitic graphite) from Zhao *et al.* (2002).

[j] From Chickos and Acree (2002).

[k] TPD energy at monolayer coverage using HOPG, from Paserba and Gellman (2001).

[l] From Chickos and Hanshaw (2004a, 2004b).

the dense phases. The alkane series[17] offers a family of such molecules in which to observe systematic variations as the balance between components of the interactions is changed by changing the number of atoms in the alkane chains. Further, they promise a connection to biophysical systems: the chains in lipid bilayers typically have 14–18 carbons (Douliez *et al.*, 1995). The alkane chains already investigated have reached this scale (Hansen *et al.*, 1999).

Experiments on diffusion in alkane monolayers are reviewed in Sec. V.C. Here we review the information on energetics, structures, and phase transitions of adsorbed alkanes. The composition in the series is C_NH_{2N+2}, with a frequent shorthand notation CN for this species.

Molecularly thin films of alkanes present an increased complexity familiar for generic molecular solids: there are the possibilities of isomorphism, plastic crystals, and liquid crystals. Also, limited layer growth (Stranski-Krastanov growth mode) is a frequent occurrence, see Bai *et al.* (2007) and Sec. VI.A. However, the phenomenon of triple point wetting, in which a very thick film of adsorbate is formed at its bulk triple point temperature, has been demonstrated for pentane on graphite (Kruchten *et al.*, 2005), see Fig. 4. Further examples of novel phenomena are as follows: (i) Different monolayer structures created by deposit of an alkane from vapor and from solution [Herwig *et al.* (1995) for dotriacontane/graphite and Mo *et al.* (2004) for tetracosane/graphite, C32 and C24]. (ii) A plastic monolayer crystal of C24/graphite with rotation around the long molecular axis (Taub *et al.*, 2004). (iii) A phase for C24/graphite that is similar to a smectic liquid crystal (Hansen *et al.*, 2004). (iv) Intermediate phases between 2D crystal and isotropic fluid for ethane/graphite (Gay, Suzanne, *et al.*, 1986) and alkanes on Pt(111) and Ag(111) (Firment and Somorjai, 1977, 1978; Hostetler *et al.*, 1995).

Perspective on adlayers is provided by the energetics and structures of the corresponding dense 3D phases. It

---

[17] Alkanes on graphite and several noble metal surfaces are classified as physisorbed systems. For longer alkane chains, the adsorption energy per molecule exceeds the 0.4 eV usually held to be the dividing line between physisorption and chemisorption. A recent empirical construction of the interaction of *n*-alkanes with Ag(111) (Jalkanen and Zerbetto, 2006) makes the distinction on the basis of adsorption energies per carbon atom, with energies in the range 100–200 meV/carbon assigned as physisorption.

is only recently that comprehensive reviews of 3D data have been given for the *n*-alkane series up to $N=38$ (Lemmon and Goodwin, 2000; Chickos and Acree, 2002). Table V surveys heats of adsorption of alkanes on various substrates. One internal consistency check is available for the adsorption on graphite, where heats of adsorption at very low coverage and at monolayer condensation are available. The difference between these is the energy of lateral interactions among the alkanes; it is on the scale of one-half of the bulk sublimation energy, in accord with the expectation that the number of nearest-neighbor molecules in the monolayer is about half of the number in the 3D solid.

TPD experiments are a major source of information of the heats of adsorption for alkanes, but there is still vigorous discussion on the analysis of the data. The measured desorption rate is decomposed into a frequency prefactor[18] and an Arrhenius exponential activation factor, following Eq. (2). Some assumed prefactors may have distorted results for the desorption energy (Fichthorn and Miron, 2002), and systematic trends, in particular whether the adsorption energy scales linearly with N, are still not agreed upon (Gellman, 2005; Tait *et al.*, 2005). The trends observed for $N=1-10$ seem to change qualitatively for longer chains. The rotational entropies, whose effect has been confirmed for the shorter chains (Tait *et al.*, 2005, 2006), are at least partially balanced by conformational entropies for $N>10$ and may lead to relatively constant prefactors for long chains (Gellman, 2005; Becker and Fichthorn, 2006). Tait *et al.* (2006) have reanalyzed some of the TPD data in light of recent theoretical developments. The technical issue of heating rates has also been addressed, as has the evidence for a transition from zeroth- to first-order desorption for the larger N arising from a failure to reach 2D equilibrium in the adsorbate.

Arnold, Dong, *et al.* (2002) and Arnold, Thomas, *et al.* (2002) made a systematic determination of the structures of the alkane monolayers on graphite, up to $N=15$. Arnold, Chanaa, *et al.* (2006) and Arnold, Cook, *et al.* (2006) have begun such a survey for alkanes on MgO(001). For alkanes on Ag(111), there remain some differences in assigned structures between the early work of Firment and Somorjai (1978) and the more recent work of Wu *et al.* (2001).

The melting of monolayer alkanes presents qualitatively new phenomena relative to observations for rare gases and small closed-shell molecules. Thermally excited intramolecular motions (creating *gauche* defects) play an important role in the melting of the tetracosane and dotriacontane monolayers on graphite (Hansen *et al.*, 2004). There are even major static distortions of a branched alkane, squalane/graphite, at low temperature (Enevoldsen, Hansen, Diama, Criswell, *et al.*, 2007). An overview of the trends in melting temperatures is given in Table VI. The discussion is in terms of ideas familiar from classical discussions of melting in three dimensions, where the concept of free volume is used (Hirschfelder *et al.*, 1964). In the alkane series, the mechanism by which free volumes are increased (i.e., the footprint on the plane is reduced) changes as the molecule gets longer. For butane/graphite (Herwig *et al.*, 1997), the free volume is increased by a tilting of the molecule relative to the plane of the surface. For hexane/graphite (Herwig *et al.*, 1997), some *gauche* defects are generated at the ends of the molecule at temperatures just below the melting temperature.[19] The situation becomes extreme for tetracosane/graphite. Then the melting occurs in a temperature range where there is an abrupt increase in the number of *gauche* defects in the central part of the alkane chains, and intramolecular and translational order are disrupted simultaneously.[20]

A pleasant surprise for the modeling is that the experimental melting temperatures so far are reproduced rather well by spontaneous instabilities in molecular-dynamics simulations (Velasco and Peters, 1995; Herwig *et al.*, 1997; Hansen *et al.*, 2004; Roth *et al.*, 2005).

Alkane monolayers have been used to demonstrate the improved capability of inelastic neutron scattering instrumentation to probe dynamics on time scales of 1 ns. Over the course of the experiments reviewed here, the energy resolution for the quasi-elastic neutron scattering experiments has improved from 70 μeV (Herwig *et al.*, 1997) to 1 μeV (Hansen *et al.*, 2004; Enevoldsen, Hansen, Diama, Taub, *et al.*, 2007).

There also are inelastic HAS data for alkanes on metals, mostly for the S-mode frequencies, which are used in the discussion of damping of adlayer vibrations and the relation to energy dissipation in monolayer friction (Fuhrmann and Wöll, 1996, 1998; Fuhrmann *et al.*, 1999; Persson *et al.*, 1999; Graham, 2003). Octane/Cu(111) is an example where there are QCM sliding friction experiments (Coffey, 2004) and for which an estimate of

---

[18] The role of the prefactors is crucial in the analysis and the adsorption energy for the longer alkanes is very different from the estimate $30k_BT_d$, with T_d the desorption temperature (Bruch *et al.*, 1997), that is so useful for rare-gas adsorption.

[19] The adsorbed alkane monolayers, at least at low coverages, have the dihedral carbon-carbon bonds in a zigzag pattern lying in the monolayer plane. This is termed the *trans*-conformation. For a *gauche* defect there is a rotation around the dihedral bond by approximately 120° to another local minimum potential energy of the conformation (Hansen and Taub, 1991).

[20] Fuhrmann and Graham (2004) observed a sharp change in the S-mode frequency of C24/Pt(111) as the temperature increased, which they interpreted as a signature of the onset of conformational disorder in the C24. They did not see this effect in the S-mode frequency of squalane/Pt(111), which differs from C24 by having six methyl side chains. However, Enevoldsen, Hansen, Diama, Criswell, *et al.* (2007) interpreted diffraction experiments for C24 and squalane on graphite as showing the occurrence of a transition to conformational disorder in both systems and attributed the absence of the S-mode shift for squalane/Pt(111) to offsetting effects in conformational distortions.

TABLE VI. Melting temperatures (in K) of alkanes in bulk and monolayers on the designated substrates. Several of these entries are for deuterated materials, as noted.

Alkane	T_t	T_m(graphite)	T_m[Ag(111)]	T_m[Cu(111)]	T_m[Pt(111)]
CH_4	90.7	$\sim$56[a]			
C_2H_6	89.8	S_1[b] 65; I_1 95			
		S_2 57; I_2 95			
		S_3 85			
C_3H_8	85.5	67[c]			
n-C_4H_{10}	135	116[d]	112[e] [125,…][k]		[125,160][l]
n-C_5H_{12}	143	100,[c] 99–105[i]	[100,175][k]		[170,195][l]
n-C_6H_{14}	178	170[d]	152[e] [170,215][k]		[187,210][l]
n-C_7H_{16}	182	137[c]	165[e] [175,215][k]		[215,230][l]
n-C_8H_{18}	216		[205,230][k]	163[j]	[212,240][l]
n-$C_{24}H_{50}$	324	340[f]			
n-$C_{32}H_{66}$	342	350[g]	345–348[h]		

[a] From Coulomb *et al.* (1981).

[b] S_1, S_2, and S_3 are monolayer solid phases while I_1 and I_2 are well-correlated liquids, from Gay, Suzanne, *et al.* (1986).

[c] Deuterated material, from Matthies (1999).

[d] From Herwig *et al.* (1997).

[e] From Wu (1997).

[f] Monolayer crystal to smectic phase transition at ~215 K followed by melting at 340 K, from Hansen *et al.* (2004).

[g] Deuterated material, vapor-deposited low-density monolayer, from Hansen *et al.* (1999).

[h] From Mo (2004).

[i] Deuterated material, from Kruchten *et al.* (2005).

[j] From Fuhrmann *et al.* (1999).

[k] Temperatures T_1 and T_2 for transition from 2D to 1D order and then for complete loss of 1D order, from Firment and Somorjai (1978).

[l] As in footnote (k), from Firment and Somorjai (1977) and Hostetler *et al.* (1995).

20–35 meV for the barrier to translation has been made using the inelastic HAS data (Bruch, 2004).

B. Adsorption sites

1. Experiments

During the past 10 years, experiments to determine the adsorption sites of rare gases on metals have shown that a preference for low-coordination sites is the rule rather than the exception for Xe on metal surfaces and there is some evidence that this preference extends to Kr and Ar (Diehl *et al.*, 2004). This was an unexpected development in the field, since weak physisorption bonds were believed to be nondirectional and therefore to favor high coordination. Although an early helium-atom diffraction measurement (Kern, Zeppenfeld, Palmer, *et al.*, 1987; Gottlieb, 1990) for an incommensurate phase of Xe on Pt(111) suggested a preference for the low-coordination top site, and this result was curious enough to attract theoretical attention (Müller, 1990; Barker and Rettner, 1992; Rejto and Andersen, 1993), it was not until 1995 that an experiment on a commensurate phase of Xe/Pt(111) was performed (Potthoff *et al.*, 1995). The result of that study, which showed Xe to be in a high-coordination site [using spin-polarized low-energy electron diffraction (SPLEED)], dampened enthusiasm for more experiments. Four years later this result was shown to be wrong (Seyller *et al.*, 1999) in a low-energy electron diffraction study that determined that Xe occupies the top sites, not the hollow sites.[21] Additional experimental studies carried out in the late 1990s and early 2000s produced more experimental determinations for rare-gas adsorption sites, which are summarized in Table VII.

We note that for Xe on close-packed metal substrates, the adsorption site for commensurate structures is always found to be the top site. In these structures, there is little or no reconstruction of the substrate. Where it is observed, the substrate atom directly beneath the Xe atom is pushed slightly inward (toward the bulk) by up to 0.02 Å.

---

[21] It is not clear why the initial SPLEED studies gave erroneous results, although a later study for Xe on Pd(111) found that some structures observed in the SPLEED study were due to contamination of the surface (Zhu *et al.*, 2003). It has also been proposed that the errors in the SPLEED results could have been due to using too-small data sets and searching insufficient ranges in parameter space (Diehl *et al.*, 2004).

TABLE VII. Experimentally determined adsorption sites for rare gases in commensurate monolayers. The adsorbate, substrate face, structure, and site are given. L is the nearest-neighbor spacing in triangular lattices or average triangular lattices for the two higher-order-commensurate (HOC) cases. d_{AS} is the distance from the adatom to the surface plane and q_1 is the monolayer heat of adsorption. The values of q_1 are assembled from several sources, and the cited paper gives the determination of the site and d_{AS}. Energies in meV and lengths in Å.

Adatom	Substrate	Structure	L	Site	d_{AS}	q_1
Xe	Cu(111)	$\sqrt{3}$	4.42	top[a]	3.60	227
Xe	Ru(0001)	$\sqrt{3}$	4.69	top[b]	3.54	230
Xe	Pt(111)	$\sqrt{3}$	4.80	top[c]	3.4	298 ± 22
Xe	Pd(111)	$\sqrt{3}$	4.76	top[d]	3.07	320
Kr	Ru(0001)	3×3 HOC	4.06	1hol3int[e]	4.01	152
Ar	Ag(111)	$\sqrt{7}$ HOC	3.81	1top3br[f]	3.22	99
Xe	Cu(110)	$c(12\times2)$		row tops[g]	3.3	218
Kr	Cu(110)	$c(8\times2)$		row tops[h]	3.36	114
Xe	graphite	$\sqrt{3}$	4.26	hollow[i]	3.59	239
Kr	graphite	$\sqrt{3}$	4.26	hollow[j]	3.35	172
Ar	graphite	incomm	3.84		3.2 ± 0.1[k]	119
Kr	Ag(111)	incomm	$\simeq4.05$		3.3[l]	151
Xe	Ag(111)	incomm	$\simeq4.40$		3.55[l]	225
Xe	Pb(111)[m]	incomm	$\simeq4.40$		3.95 ± 0.10	191 ± 10

[a] Seyller *et al.* (1998).
[b] Narloch and Menzel (1997, 1998).
[c] Seyller *et al.* (1999).
[d] Caragiu *et al.* (2002).
[e] Narloch and Menzel (1997, 1998); one atom in three-fold hollow and three atoms at intermediate sites in a four-atom HOC unit cell.
[f] Caragiu *et al.* (2001); one atom in a top site and three atoms at bridge sites in a four-atom HOC unit cell.
[g] Caragiu *et al.* (2003).
[h] Seyller *et al.* (2000).
[i] Pussi *et al.* (2004).
[j] Bouldin and Stern (1982).
[k] Distance of adatom to surface plane, from Shaw *et al.* (1980).
[l] Distance of adatom to surface plane, from Unguris *et al.* (1979, 1981).
[m] Ferralis *et al.* (2007).

For Kr and Ar on close-packed surfaces, the site preference is not as clear because the two systems studied have four atoms per unit cell and not all adatoms occupy the same site. In the case of Ru(0001)-(3×3)-4Kr, one Kr atom occupies a hollow site, while three atoms occupy a location that is halfway between top and hollow sites.[22] In the case of Ag(111)-$(\sqrt{7}\times\sqrt{7})R19.1°$-4Ar, one Ar atom occupies the top site while three atoms occupy bridge sites. The perpendicular distances (d_{AS}) between the adatom and the substrate are different for nonequivalent adatoms in both cases and some degree of substrate reconstruction was observed for Ar/Ag. Unlike the situation for Xe adsorption, the Ag atom directly beneath the Ar atom was found to be slightly pulled outward (away from the bulk). We note that in all cases in which substrate reconstruction was observed, the magnitude of the displacement is equal to or smaller than the precision of the measurement. As discussed in Secs. IV.B.2 and IV.C.4, information on the site preference may be obtained in such higher-order commensurate (HOC) systems from the relative d_{AS}'s for adatoms in different sites. For Kr/Ru(0001), the Kr atom in the hollow site is located 0.02 ± 0.03 Å higher than those in the intermediate sites, whereas for Ar/Ag(111), the Ar atom in the top site is 0.06 ± 0.08 Å higher than those in the bridge sites. This suggests that Kr prefers a low-coordination site while Ar prefers a high-coordination site. It is unfortunate that the differences in these values are near the precision limit of the current LEED tech-

---

[22] The reported $Z=d_{\mathrm{AS}}$ is larger for Kr/Ru(0001) than for Xe/Ru(0001). Narloch and Menzel (1997, 1998) gave $Z_{\mathrm{Kr}}-Z_{\mathrm{Xe}}\simeq0.15$ Å while on Ag(111), Unguris *et al.* (1981) gave $Z_{\mathrm{Kr}}-Z_{\mathrm{Xe}}\simeq-0.2$ Å. The $d_{\mathrm{AS}}=4.01$ Å for Kr/Ru(0001) in Table VII is large and in fact is much larger than values 3.4–3.5 Å for Kr/Ru(0001) structures obtained by Yang and Phillips (2007) in a density-functional calculation.

nique, but other measurements might provide more enlightenment.

For both Xe and Kr on the more open Cu(110) surface, adatoms order along the tops of the rows rather than in the troughs, another example of a preference for low coordination. The structures that are formed in both cases are HOC structures, having repeat distances along the rows of 7 Xe atoms per 12 Cu atoms and 5 Kr atoms per 8 Cu atoms. In both cases, the overall Cu structure remained the same as for the clean surface, although some rumpling of both the top layer atoms and gas atoms was observed. As for the other surfaces, the magnitude of this rumple was of the same magnitude as the precision, although in the case of Kr, there appeared to be a clear indication that the Kr atom in the top site was closer to the Cu atom than the others. This suggests that the top sites are preferred by the Kr.

Contrary to the pervasive preference for top sites for Xe on metals, Xe atoms in a $(\sqrt{3}\times\sqrt{3})R30°$ structure on the basal plane of graphite were observed in a LEED study to reside in hollow sites (Pussi *et al.*, 2004). An early EXAFS measurement for Kr in the same structure led to a similar conclusion (Bouldin and Stern, 1982). These structures are similar to the vacancy-occupation structures that have been observed for alkali-metal atoms on close-packed metal surfaces (Diehl and McGrath, 1997). While alkali-metal atoms also frequently occupy top sites on close-packed metal surfaces,[23] the higher chemisorption energy gained by occupation of vacancy sites may cause the alkali metals to create and occupy vacancies on some substrates (Neugebauer and Scheffler, 1993). The physisorption energy of rare gases apparently is not high enough to create vacancies on metal surfaces, though. Nevertheless, there is evidence that such an effect occurs for the adsorption of C_{60} molecules, which ranges from strong physisorption to chemisorption depending on the substrate. A recent x-ray diffraction study showed that C_{60} induces a reconstruction on Pt(111) that consists of vacancies in a $(\sqrt{13}\times\sqrt{13})R13.9°$ array (Felici *et al.*, 2005) and the C_{60} molecules sit over the vacancies. That system has a particularly strong adsorption bond that is described as covalent. On Ag(111), C_{60} forms a weaker bond that is described as ionic and a preliminary LEED study suggests that the favored site is the top site (Li *et al.*, 2007). We note that such structure determinations are quite difficult using imaging techniques; for instance, two STM studies of C_{60} on Ag(111) found different structures from each other (Altman and Colton, 1993; Sakurai *et al.*, 1995) and both differed from the LEED study. The site preference for physisorbed small molecules such as N_2 or CH_4 remains an open question, as there are no site determinations for such systems, to our knowledge.

2. Calculations

Various theoretical approaches have been employed to address the issue of the adsorption sites of rare gases. Müller's (1990) calculation for Xe on a Pt(111) cluster found that the top site was preferred over the hollow sites by about 30 meV for one or two adsorbed Xe atoms. The site preference in this case was attributed to a mixing of the Xe $5p$ states with the empty metal d states. Betancourt and Bird (2000) extended this approach to the $(\sqrt{3}\times\sqrt{3})R30°$ structure on a semi-infinite Pt solid, with the result that the top site was lower in energy by 45 meV. They also performed a DFT-GGA analysis and still found a preference for the top site, but only by 5 meV; in both approximations d_{AS} was smaller for the top site than for the hollow site. Another DFT-GGA study was carried out for the commensurate structure Ag(100)-$c(2\times2)$-Ar, using the full-potential linearized augmented plane wave (FLAPW) method (Clarke *et al.*, 2001), and again a preference for the top site was found. As for the Müller study, the site preference was attributed to mixing of the Xe $5p$ states with the metal d states. A DFT-LDA study of Ar on a 19-atom Ag(111) cluster also indicated a lower energy for the top site (Kirchner *et al.*, 1994) and the d_{AS} was smaller for the top site than for the hollow site. In that case, the site preference was attributed to the delocalization of the valence charge of the metal, which has the effect of building up the charge in the hollow site and raising its potential relative to the top site.

A similar interpretation for the top site preference of Xe came from a recent and more extensive DFT study of Xe adsorption on close-packed metal surfaces by Da Silva *et al.* (2003, 2005). They investigated the $(\sqrt{3}\times\sqrt{3})R30°$ structures of Xe on Mg(0001), Al(111), Ti(0001), Cu(111), Pd(111), and Pt(111) using both LDA and GGA. The LDA approach resulted in stronger binding of the Xe to the surface than found in experiment, whereas the GGA had weaker binding than experiment. In general, for systems that have been studied experimentally, the binding energies and the Xe-metal distances are between those calculated using LDA and GGA. Da Silva *et al.* argued that the trends observed in the calculations remain valid and they agree with those observed in experiments. The top site was found to be the preferred site in all cases studied. The origin of the preference for the top site was attributed to two factors, both of which are related to the fact that metal electrons can move more easily from the top site region to the hollow site region. This movement of charge allows a larger dipole moment to develop on the Xe atom, increasing the attractive interaction between the Xe and the metal. The movement of charge also leads to a reduction of the Pauli repulsion at the location of the metal atoms, allowing the Xe atom to move closer to the surface compared to the hollow site. This study also found evidence for a similar situation for Ar and Kr adsorption, indicating that the top site preference is not a result of the Xe-Xe interaction.

---

[23] As for rare gases, these structures were unexpected based on coordination and their nondirectional bonding.

The origin of the interface dipole was analyzed with a Hartree-Fock calculation for a Xe atom on a 10-atom Cu cluster (Bagus *et al.*, 2002), in which the self-consistent wave functions were analyzed to separate the various contributions to the Xe-Cu interaction. The equilibrium distance found for the top site was 4.23 Å, larger than the experimental value of 3.6 Å, owing to the smaller Xe binding energy of 95.1 meV (compared to 190 meV) due to a too small van der Waals contribution in the calculation. This study concluded that the major contribution to the charge redistribution at the interface is from exchangelike forces rather than electrostatic repulsion, polarization, or chemical contributions.

The main drawback of the DFT approach for rare-gas adsorption is its failure to include the full Xe-metal van der Waals interaction. This shortcoming was addressed in a recent study for Xe on Cu(111) and Pt(111) by introducing a van der Waals term into a DFT-GGA analysis (Lazić *et al.*, 2005, 2007). In this approach, contribution from a van der Waals potential is added to the energy in the DFT calculation. The addition of the vdW term increases the Xe binding to the substrates, bringing it closer to the experimental values, although it overshoots on the d_{AS} somewhat, giving too small equilibrium values of 3.2 and 3.1 Å for Xe-Cu and Xe-Pt, respectively. The top site is still found to be more stable, however, and the agreement with vibrational frequencies is improved. DFT studies for C_{60} adsorption on the close-packed surfaces of Ag(111), Au(111), and Cu(111) (Wang and Cheng, 2004a, 2004b) suggest that the adsorption site is the hollow, whereas the LEED study on Ag(111) indicates a top site (Li *et al.*, 2007). In a simple picture, the top site would be stable because it has the highest coordination for a hexagon-down C_{60} molecule, with six C atoms surrounding a silver atom. Thus, the hollow sites found for C_{60} in the DFT study may also be due to an inadequate treatment of the van der Waals interactions.

In spite of the problems with the DFT-LDA and DFT-GGA approaches in reproducing adsorption energies, a first-principles approach appears to be the current method of choice for gaining insight into these systems. A DFT study of Xe on Nb(110) also indicated a top site preference (Thomas *et al.*, 2003). Recent DFT-LDA studies of Xe, Kr, and Ar on graphite showed a preference for the hollow (honeycomb center) sites (Chen, Zhou, *et al.*, 2003; Chen *et al.*, 2003a, 2003b).[24] The values of d_{AS} for Kr and Ar on graphite were smaller for the hollow sites than for the other sites, in accordance with the similar correlations between preferred site and adsorption height found in the DFT studies on metals. However, there was no difference in d_{AS} between honeycomb center and top site in the Xe calculation. Another study of Xe/graphite (Da Silva and Stampfl, 2007), also described as using DFT-LDA, found a difference of 0.09 Å in d_{AS} between honeycomb center and top site. The honeycomb center had the lower energy and smaller height, and this preference was attributed to the greater polarization of the Xe and C atoms in that configuration. Table VIII summarizes the results of the DFT studies for rare-gas adsorption.

The effect of site preference in HOC structures was addressed by a model calculation for Ar/Ag(111) (Bruch, 2001). The analysis is summarized in Sec. IV.C.4. The substrate corrugation leads to distinctive spatial modulations of adatom positions in the HOC unit cell that have consequences for the adsorption geometry. For the Ag(111)-$(\sqrt{7}\times\sqrt{7})R19.1°$-4Ar structure determined by Caragiu *et al.* (2001), the site preference determines the sign of relative heights of Ar atoms in the unit cell. If the top site is preferred, the atop Ar resides closer to the substrate, whereas a preference for the hollow site leads to the bridge atoms being closer. This result is consistent with the result from DFT studies that rare-gas atoms reside closer to the surface when they are in their preferred site. It also suggests that HOC structures may be used to determine site preference if the height difference can be measured. This is important for exploring adsorption properties of smaller rare gases on metal surfaces, because simple commensurate structures are difficult to achieve due to the lattice mismatch between them and most metals.

3. Stepped surfaces

Studies of Xe at surface steps have indicated differences in the preferred adsorption sites on different metals. On Pt(111), these sites are on the low-coordination (top) edges of steps (Zeppenfeld *et al.*, 1994; Horch *et al.*, 1995a), whereas on other surfaces such as Cu(110) (Dienwiebel *et al.*, 2000), Ag(111) (Hövel *et al.*, 2001), and Cu(111) (Park *et al.*, 1999), these sites are at the high-coordination (lower) edges. Such differences in the interactions at surface steps can have consequences for the subsequent growth of the films. The adsorption and desorption of Xe on Pt(997), which is a stepped surface having terraces of Pt(111) as shown in Fig. 14, have been the subject of several experimental studies (Marsico *et al.*, 1997; Pouthier *et al.*, 1997; Widdra *et al.*, 1998; Picaud *et al.*, 1999). They demonstrated that the adsorption of Xe on Pt(997) occurs row by row at certain temperatures and interpreted this as the growth of discrete rows of Xe along the step edges.

Specular intensity oscillations were observed as Xe was adsorbed on Pt(997) in a helium-atom diffraction experiment performed at grazing incidence, indicating the sequential growth of rows at the steps (Marsico *et al.*, 1997). Similar growth was observed for Kr on the same surface.[25] Various experimental measurements were made in order to determine the structure of Xe/Pt(997).

---

[24] There is a fortuitous cancellation of errors in such LDA studies, as discussed for rare-gas dimers in Sec. III.A.1 and shown for Ar/graphite by Tkatchenko and von Lilienfeld (2006).

[25] Pouthier *et al.* cite this as unpublished work of Blanc, Marsico, Kuhnke, and Kern.

TABLE VIII. Adsorption sites calculated using density-functional theory (DFT). The functionals are the local-density approximation (LDA), the generalized gradient approximation (GGA), and the GGA supplemented by an approximation for the van der Waals energy (GGA+vdW). The structure in the calculation is one adatom or a commensurate adlayer as specified. E_a is the adsorption energy per atom in the minimum energy configuration. E_{corr} is the energy difference per adatom between the top and fcc hollow sites. d_{AS} is the distance of the adatom to the surface plane. Energies in meV and distances in Å.

Adatom	Substrate	Functional	Structure	Site	d_{AS}	E_a	E_{corr}
Xe	Pt(111)	LDA	1 atom	top[a]	3.00	307	30
Xe	Pt(111)	LDA	$\sqrt{3}$	top[b]	3.11	332	45
Xe	Pt(111)	GGA	$\sqrt{3}$	top[b]	3.80	41	5
Xe	Pt(111)	LDA	$\sqrt{3}$	top[c]	3.07	367	49
Xe	Pt(111)	GGA	$\sqrt{3}$	top[c]	3.62	82	4.8
Xe	Pt(111)	GGA+vdW	$\sqrt{3}$	top[d]	3.1	300	43
Xe	Cu(111)	LDA	$\sqrt{3}$	top[c]	3.26	277	9.14
Xe	Cu(111)	GGA	$\sqrt{3}$	top[c]	4.03	40	5.91
Xe	Cu(111)	GGA+vdW	$\sqrt{3}$	top[d]	3.20	250	3.8
Xe	Mg(0001)	LDA	$\sqrt{3}$	top[c]	3.80	130	4.34
Xe	Al(111)	LDA	$\sqrt{3}$	top[c]	3.69	176	1.12
Xe	Ti(0001)	LDA	$\sqrt{3}$	top[c]	3.56	196	21.82
Xe	Ti(0001)	GGA	$\sqrt{3}$	top[c]	4.18	44	3.10
Xe	Pd(111)	LDA	$\sqrt{3}$	top[c]	2.85	453	51.22
Xe	Pd(111)	GGA	$\sqrt{3}$	top[c]	3.27	76	13.48
Xe	Nb(110)	LDA	1 atom	top[e]	3.13	294	68
Xe	graphite	LDA	$\sqrt{3}$	hollow[f]	3.60	204	4.9
Xe	graphite	LDA	$\sqrt{3}$	hollow[g]	3.50	168	6.3
Kr	graphite	LDA	$\sqrt{3}$	hollow[h]	3.35	160	8.0
Ar	graphite	LDA	$\sqrt{3}$	hollow[i]	3.20	86	9.0
Ar	Ag(111)	LDA	1 atom	top[j]	3.20	100	12

[a] Müller (1990) (LDA cluster).
[b] Betancourt and Bird (2000).
[c] Da Silva *et al.* (2003, 2005).
[d] Lazić *et al.* (2005).
[e] From Thomas *et al.* (2003); M. C. Qian, C. Y. Fong, X. D. Zhu, L. H. Yang, and S. Dag. ΔE is measured between the top site and the long bridge site.
[f] Chen, Zhou, *et al.* (2003).
[g] Da Silva and Stampfl (2007).
[h] Chen *et al.* (2003b).
[i] Chen *et al.* (2003a).
[j] Kirchner *et al.* (1994).

Helium-atom diffraction measurements from the Xe monolayer on Pt(997) indicated a small average Xe-Xe spacing of 4.1 Å parallel to the steps. For a single Xe row, however, a value of 5.5 Å was deduced from LEED (Trischberger *et al.*, 1997; Widdra *et al.*, 1998), suggesting a repulsive Xe-Xe interaction within the single row and a significant compression as the layer grows. Such an alignment of the rows with the steps indicates that the Xe monolayer on Pt(997) is aligned with the substrate, not rotated at 30° as it is on Pt(111).

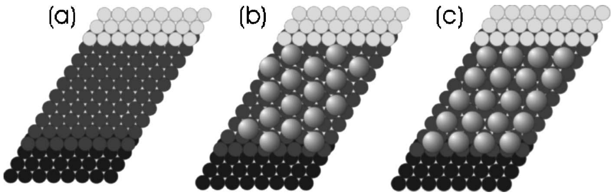

FIG. 14. Schematic of the Xe/Pt(997) structure. (a) The vicinal Pt(997) surface. (b) The $(\sqrt{3}\times\sqrt{3})R30°$ structure with eight rows per terrace. (c) $R0°$ aligned incommensurate phase with five rows per terrace. Adapted from Lehner *et al.*, 2002.

Results from the helium-atom diffraction study for Pt(997) (Marsico *et al.*, 1997) were interpreted as row growth outward from the bottoms of the steps, based on similar intensity oscillations for Ag adsorption on Pt(997). This is in contrast to an initial row forming at the tops of steps as proposed by Zeppenfeld *et al.* (1994) for Xe/Pt(111). A mean-field 2D Ising model was applied to interpret the growth results further (Pouthier *et al.*, 1997) and successfully reproduced the conclusions of Marsico *et al.*, namely, that the Xe rows grow from the bottoms of the steps. This study also found that the initial Xe-Xe distance in the first row is 5.5 Å, in agreement with the LEED study (Trischberger *et al.*, 1997). The subsequent growth in the model, however, was not consistent with experimental findings, since the layer grows as a rotated structure, ending up as eight rows of a commensurate $(\sqrt{3}\times\sqrt{3})R30°$ structure on each terrace.

Subsequently, a high-resolution thermal desorption experiment was performed and interpreted using a lattice gas model (Widdra *et al.*, 1998). The fitting of the TPD data allowed determination of the binding energies of three different sites on the terraces, as well as the lateral Xe-Xe interaction within the terrace and along the steps. The result was that the binding energies for the Xe were 264, 398, and 287 meV for adsorption on the terrace, at the top of the step, and at the bottom of the step, respectively. The Xe-Xe nearest-neighbor interaction is repulsive along the top of the step (15.9 meV) and attractive on the terraces (−11.2 meV). These interactions lead to a growth mode in which the tops of the steps are first occupied. The Xe then adsorbs at the bottoms of the steps and grows out to cover the terraces. The final structure is incommensurate and consists of five rows of Xe, which is consistent with the LEED data.

Lehner *et al.* (2002) used a discrete event kinetic Monte Carlo simulation to model growth of Xe on Pt(997). The study included different interaction models, which were judged by how well the sequential growth of the first two Xe rows, observed in the HAS experiments and inferred from the TPD experiments, was reproduced. There was evidence for the preferential adsorption of two rows at the step edges, consistent with the HAS result, but with one at the top of the step and one at the bottom. The same set of parameters was found to be consistent with the experimental results for Xe adsorption on Pt(111). Therefore, the weight of evidence now favors a picture for Xe adsorption at steps on Pt(111) and Pt(997) in which the low-coordination tops of the steps are occupied first, followed by the high-coordination bottoms of the steps, followed by occupation of the terraces.

This is quite different from Xe adsorption at steps on other surfaces. A low-temperature STM study of Xe on Ag(111) found that Xe grows islands that are attached to the bottom edges of surface steps (Hövel *et al.*, 2001). A low-temperature STM study of the growth of Xe on Cu(111) also found that the high-coordination bottoms of the steps are the first adsorption sites (Park *et al.*, 1999). In that case, although the first Xe atoms occupy the step-bottom sites, they also start to occupy the upper step edges after one Xe atomic row is almost complete, as shown in Fig. 15. As more Xe is adsorbed, it grows row by row from the bottom of the step edge. The Xe also grows from the top step edges, but instead of a row-by-row growth, the Xe forms 2D clusters dispersed along the step edge. The interaction between Xe atoms at the top step edges appears to be attractive rather than repulsive as it is on Pt(111), since the Xe grows as clusters from these sites. Park *et al.* (1999) conjectured that the difference in the initial adsorption sites for Cu(111) and Pt(111) is due to a difference in the balance of the dipole-dipole repulsion between the Xe and the step

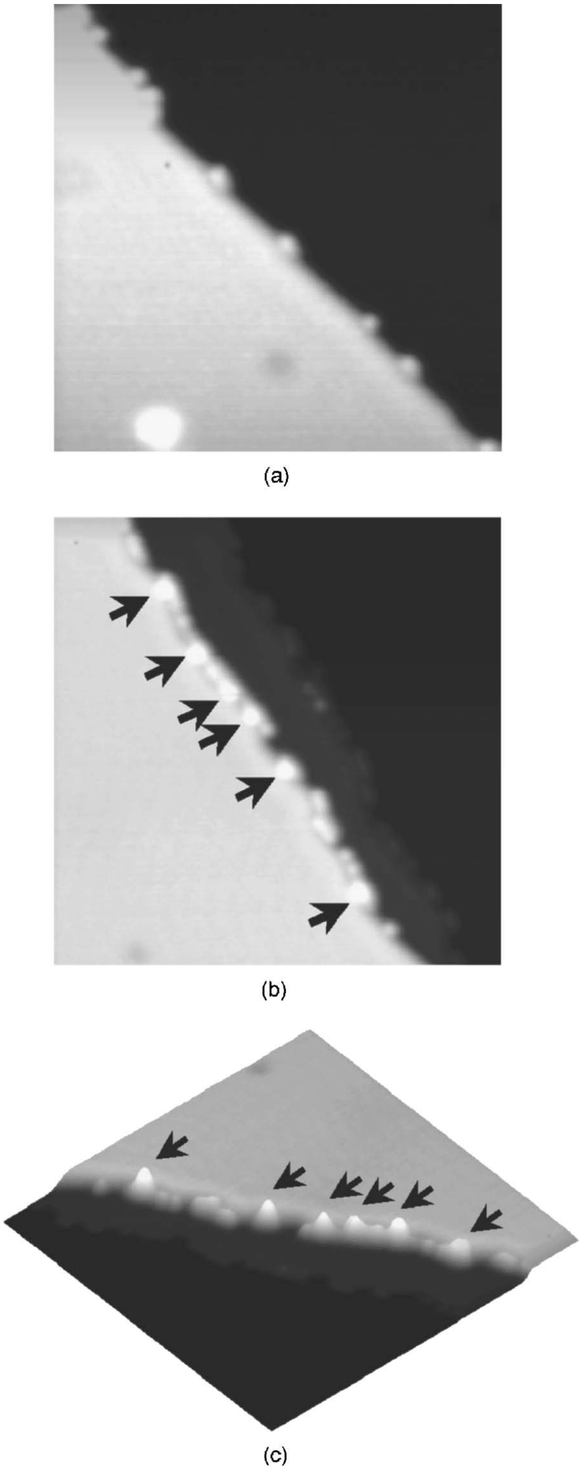

FIG. 15. STM image of the low-coverage adsorption of Xe/Cu(111), $T=10$ K. (a) All Xe adsorbed at the lower step edge, panel 200 Å × 200 Å. (b) Almost all Xe adsorbed at Cu steps, with some Xe at the upper step edges as marked by arrows, panel 300 Å × 300 Å. (c) Another perspective on (b), with arrows marking the same Xe atoms. From Park *et al.*, 1999.

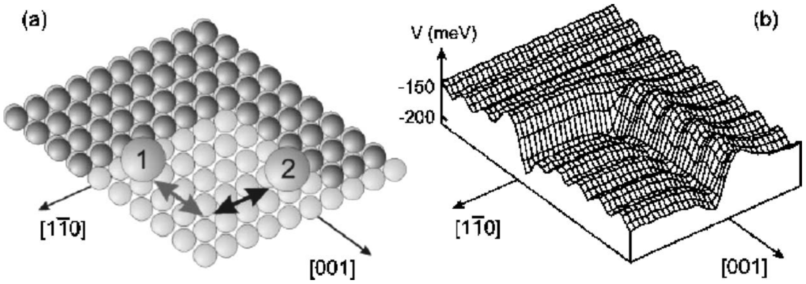

FIG. 16. Cu(110) surface. (a) Schematic model showing steps along the [1$\bar{1}$0] and [001] directions. (b) Potential energy map for a single adsorbed Xe atom on this configuration. From Dienwiebel *et al.*, 2000.

edge and the expected higher attraction at the step bottoms due to the coordination.

An STM experiment for Xe on Cu(110) (Dienwiebel *et al.*, 2000) indicated an even more complex scenario. The adsorption of Xe depended on the orientation of the surface steps and the temperature. At 13 K, the first Xe to adsorb was observed to nucleate and grow at steps that were kinked and did not run in any particular direction, but consisted of [001] and [1$\bar{1}$0] segments. The Xe growth occurred along the [001] segments of these steps, at the bottoms of the step edges. Xe islands also started to grow from the top edges of those segments after the lower edge had been decorated. In contrast, there is almost no nucleation at [1$\bar{1}$0] steps. At 40 K, however, the first Xe atoms adsorb preferentially at the bottom edges of the [1$\bar{1}$0] steps, forming rectangular-shaped islands. No nucleation at the upper edges of steps was observed at this temperature. It was inferred that different behavior at the two temperatures is a consequence of the restricted mobility at the low temperature. At low temperature, the Xe atoms diffuse mainly along the easy [1$\bar{1}$0] direction (see Fig. 16), leading to a decoration of the [001] step edges, where at higher temperature, the diffusion along [001] becomes thermally activated and Xe can reach the energetically preferred [1$\bar{1}$0] step edges.

C. Lattice dynamics

Experiments that determine the dispersion curves of monolayer solids, e.g., Fig. 12, have been discussed in Secs. II.E and III.B. The results are at the center of discussions of the forces among atoms in physisorbed monolayers. The lattice-dynamical theory is readily generalized to multilayer films (Šiber *et al.*, 2001) and to the coupled dynamics of monolayer and substrate (Boutchko and Bruch, 2004). Also, monolayer solids with many atoms in the Bravais unit cell and in different substrate environments have been treated (Boutchko and Bruch, 2004). The damping of phonons that arises from dynamic coupling to substrate vibrations has been treated for several systems (Hall *et al.*, 1989; Bruch and Hansen, 1997; Lewis *et al.*, 1998; Persson *et al.*, 1999).[26]

Here we present results for two special cases of the frequency spectrum at small wave number q and two applications of the full characterization (frequencies and polarization vectors) of the normal modes. In particular, results for commensurate lattices consisting of rather small superlattices are given in quite compact form, see Sec. IV.C.4. To formulate the lattice-dynamical theory in the form widely used for commensurate monolayers, we express the external potential for the adatom in the presence of the periodic substrate lattice as a Fourier series,

$$V_s(\mathbf{s},z) = V_0(z) + \sum_{\mathbf{g}} V_{\mathbf{g}}(z)\exp(\imath \mathbf{g}\cdot\mathbf{s}), \tag{3}$$

where $\mathbf{r}=(\mathbf{s},z)$ is a decomposition into Cartesian coordinates parallel and perpendicular to the substrate plane and $\mathbf{g}$ are reciprocal-lattice vectors of the substrate surface. Conventionally, $\mathbf{s}$ is measured from the position of a substrate surface atom for a Bravais cubic lattice and from the honeycomb center for adsorption on the basal plane surface of graphite. Frequently, $V_{\mathbf{g}}$ is taken to be real and to depend only on $|\mathbf{g}|$. However, when it is necessary to distinguish between the hcp and fcc stacking sites on the fcc(111) surface, a useful model is

$$V_{\mathbf{g}}(z) = V_g^{(1)}(z) + V_g^{(2)}(z)\exp(-\imath \mathbf{g}\cdot\boldsymbol{\rho}), \tag{4}$$

where $\boldsymbol{\rho}=(\mathbf{a}_1+\mathbf{a}_2)/3$ is the position of a substrate atom in the first underlying layer of the substrate, so that $\mathbf{s}=\boldsymbol{\rho}$ is the hcp-stacking position and $\mathbf{s}=2\boldsymbol{\rho}$ is the fcc-stacking position. In principle, the sum in Eq. (3) is over as many 2D reciprocal-lattice vectors $\mathbf{g}$ as are needed to describe the corrugation of the potential adequately. Typically, only the leading shell of reciprocal-lattice vectors, $|\mathbf{g}| = g_0$, is retained and only one amplitude V_{g0}. This simplification is driven by the limited empirical information and by the expectation, based on models, that the magnitudes $|V_g|$ decrease rapidly with increasing $|\mathbf{g}|$.

The substrate corrugation V_g is an important parameter for the modeling of phonon damping processes and of sliding friction experiments, see Sec. II.F. A major source for estimates of the corrugation is the analysis of

---

[26] The damping is much greater for Xe/graphite than for Xe/Pt(111) and Xe/Cu(001). This was observed in the experiments of Toennies and Vollmer (1989) and shown to be a consequence of the much smaller mass density of the graphite using an elastic continuum theory (Bruch and Hansen, 1997).

TABLE IX. Minimum energy barrier to motion from zone-center frequency gap $\omega_{0\parallel}$. $\omega_{0\parallel}$ is fitted to one Fourier amplitude V_{g0}. g_0 is the corresponding reciprocal-lattice vector, in Å^{-1}. $\Delta E = V(\text{bridge}) - E(\text{site}) = 8|V_{g0}|$ for site equal to the atop site on fcc(111) and the honeycomb center on the basal plane surface of graphite.[a] It is $4V_{g0}$ for the fcc(110) and fcc(100) cases. q_1 is the heat of adsorption for monolayer condensation. Energies in meV. Data from Bruch (1991, 2003), Vidali *et al.* (1991), and Zeppenfeld (2001).

Case	g_0	$\omega_{0\parallel}$	V_{g0}	ΔE	q_1	$(\Delta E/q_1)^{\text{b}}$
Xe/Pt(111)	2.62	1.3	−2.6	20.8	~300	0.067
Xe/Cu(111)	2.84	0.4±0.15	−0.2	1.6	227[c]	0.008
Xe/Cu(110)	1.74	0.7	−2.6	10.4[d]	220	0.045
Kr/graphite	2.95	0.86	0.57	4.6	172	0.026
N_2/graphite	2.95	1.6[e]	−0.7	5.6	110	0.051
CD_4/graphite	2.95	1.2	0.27	2.1_5	200±30	0.011
H_2/graphite	2.95	4.08	−0.6	4.8[f]	43	0.112
H_2/MgO(001)	2.12	2.5	−0.47	1.9	28.8	0.065
H_2/NaCl(001)	1.69	7.0	5.6_4	22.6	31	0.73
H_2/LiF(001)	2.21	4.5	-1.4_3	5.7_2	17.3	0.33
^{4}He/graphite	2.95	1.0	−0.13	1.04	12.1	0.086

[a] Another measure of the corrugation is the total excursion E_{corr} on the minimum energy surface. Retaining only one Fourier amplitude, this is $E_{\text{corr}} \simeq 9|V_{g0}|$ for the fcc(111) and graphite surfaces and $E_{\text{corr}} \simeq 8|V_{g0}|$ for the fcc(100) surface.

[b] A widely used rule of thumb (Antczak and Ehrlich, 2005) is that the barrier to motion is approximately 1/3 of the heat of adsorption. The construction from $\omega_{0\parallel}$ avoids lateral interaction contributions.

[c] Based on Jablonski *et al.* (1986), who did not establish the heat of adsorption for Xe/Cu(111), but identified it to be between the heats of adsorption for Xe/Ag(111) and Xe/Ru(0001), which are reported to be 225 and 230 meV, respectively. We take an intermediate value 227 meV for the heat of adsorption of Xe/Cu(111).

[d] A stability estimate for UIC by Bruch (1985, $r_0 = 4.5$ Å case) gave $\Delta E = 10$ meV; the diffusion barrier (in the slow direction [001]) from Dienwiebel *et al.* (2000) is 11.4 meV.

[e] $\omega_{0\parallel}$ was measured for orientationally ordered solid, but V_g and ΔE are derived assuming spherical adsorbate at honeycomb center.

[f] Activation energies for isotopes of H_2 at the bulk surface are summarized in Sec. V.B.2.

Brillouin-zone-center gaps in adsorbate spectroscopy; see Sec. IV.C.2 and Table IX. This parameter also enters in the evaluation of the Brownian friction of a single adatom on a fluctuating substrate (Boutchko and Bruch 1999, 2004).

1. Acoustic branches

When $V_{\mathbf{s}}$ does not depend on $\mathbf{s}$ (no corrugation, $V_g = 0$), the SH and LA frequencies go to zero as $q \to 0$. In fact, the frequencies then depend linearly on q (Graham *et al.*, 1997) unless the forces are very long ranged (charged particle oscillations, not treated here).

These acoustic-phonon branches have a special significance because the absence of a frequency gap at $q = 0$ is related to the translational symmetry of the adlayer center of mass. The slopes in the $q \to 0$ limit are given by the sound speeds of the monolayer solid, $\omega \simeq cq$. A triangular lattice is elastically isotropic so the speed c of the wave is independent of azimuth and can be estimated by combining the macroscopic compressibility with relatively few model-dependent assumptions, as in Eq. (7).

The speeds of the LA and SH acoustic waves in an isotropic elastic planar medium of mass density ρ and a spreading pressure ϕ are given in terms of elastic constants C_{ij} (with a Voigt notation in which $1 = xx$, $2 = yy$, and $3 = xy$) (Born and Huang, 1954; Bruch and Gottlieb, 1988),

$$c_{\text{LA}}^2 = [C_{11} - \phi]/\rho, \quad c_{\text{SH}}^2 = [C_{33} - \phi]/\rho. \tag{5}$$

The isothermal bulk modulus B_T is the reciprocal of the isothermal compressibility K_T. The elastic isotropy gives

$$1/K_T = B_T = C_{12} + C_{33} = C_{11} - C_{33}. \tag{6}$$

Thermodynamic stability places a requirement $B_T > 0$ and hence the relations of the triangular lattice imply $c_{\text{LA}} > c_{\text{SH}}$. Thus when two acoustic branches are observed, as in experiments for incommensurate Xe, Kr, and Ar monolayers on Pt(111) (Bruch *et al.*, 2000), the lower-frequency branch at small wave vector must be the SH branch.

Further relations arise for Cauchy solids, defined by $C_{12} = C_{33}$. In particular, the Cauchy solid condition holds

TABLE X. Isothermal compressibility of monolayer solids in m^2/J at specified temperatures T in K and area A per atom (molecule, N_2) in $Å^2$.

Substrate	Xe			Kr			Ar			N_2		
	T	A	K_T	T	A	K_T	T	A	K_T	T	A	K_T
Pt(111) $[1\bar{1}0]$[a]	50	16.2	0.79 ± 0.15	50	14.5	1.25 ± 0.22	23	12.4	1.58 ± 0.3			
$[11\bar{2}]$			0.73 ± 0.15			1.13 ± 0.22			1.42 ± 0.3			
Pt(111)[b]	88	19.0	1.70									
	88	18.6	0.79									
Ag(111)[c]	76	17.7	1.22 ± 0.15	50	14.7	1.23 ± 0.19	41	13.2	2.02 ± 0.30	35–40	14.6	2.9[d]
	56	16.5	0.71 ± 0.12	40	14.0	0.68 ± 0.19	32	12.3	1.25 ± 0.26			
Graphite	68	16.7	1.5[e]	48	14.2	1.2[e]	42.2	13.2	2.8 ± 0.14[f]	35–40	14.6	2.8[d]
				54.3	14.5	1.4[g]	42.2	12.9	2.0 ± 0.14[f]	~80	~15	20–30[h]
Cu(110)	72	16.5	1.1 ± 0.1[i]									
Cu(001)	70	17.2	1.3 ± 0.5[j]									
Pb(111)	75	17.2	0.76 ± 0.13[k]									
NaCl(001)	60	17.4	1.2 ± 0.22[l]									
MgO(001)										30	~13	2.6[d]

[a] Evaluated using Eq. (24) along the specified Pt azimuths. $[1\bar{1}0]$ is close to the ΓM azimuth for the Xe and Kr lattices and the ΓK azimuth for the Ar lattice. From Bruch *et al.* (2000).

[b] Using Eq. (22) along an isotherm for uniaxially incommensurate xenon lattice. Data of Kern, David, *et al.* (1988) analyzed by Gottlieb and Bruch (1991).

[c] Along isobars using Eq. (23). From Unguris *et al.* (1981).

[d] From Bruch and Hansen (1998). N_2/graphite value from a model calculation.

[e] Along isobars using Eq. (23). Data of Schabes-Retchkiman and Venables (1981). The temperature range is 57–77 K for Xe and 40–50 K for Kr.

[f] For an isotherm, as reanalyzed in Shaw and Fain (1980).

[g] For an isotherm, Chinn (1977).

[h] Probably fluid. Isotherm data of Chung and Dash (1977) at 76 K and Chan *et al.* (1984) at 85 K.

[i] For an isobar, from 64 to 79 K, with $A=16.1-16.8$. From Glachant *et al.* (1984).

[j] For an isobar from 62 to 78 K, with $A=16.8-17.7$. From Bruch (1997).

[k] From isobar data of Ferralis *et al.* (2007).

[l] From isotherm data of Schwennicke *et al.* (1993).

in classical mechanics if the monolayer has only pair potential interactions (even carried to distant neighbor shells). Then $c_{LA}/c_{SH}=\sqrt{3}$ at zero spreading pressure. Under compression, the ratio c_{LA}/c_{SH} increases, but the spreading pressures in the monolayer are limited by the value at which the bilayer condenses (about 0.05–0.07 J/m^2 for xenon monolayers) and the increase is small. The ratio c_{LA}/c_{SH} from experimental data for the acoustic branches of incommensurate rare-gas solids on Pt(111) (Bruch *et al.*, 2000) is 1.64 ± 0.1 for Xe, 1.75 ± 0.15 for Kr, and 1.60 ± 0.12 for Ar. These all agree well with $\sqrt{3}\simeq1.732$.

The speed of the LA wave can be estimated (Bruch, 1997) from K_T without much model-dependent information.[27] The relation is (with $\mathcal{R}\equiv c_{LA}^2/c_{SH}^2$)

$$c_{LA}^2 = 1/K_T\rho(1-\mathcal{R}). \tag{7}$$

The value of $\mathcal{R}$ is 1/3 for the Cauchy solid at zero spreading pressure. Since C_{12} is positive for classical solids, the normal range for $\mathcal{R}$ is $1/3<\mathcal{R}<1/2$.

2. Zone-center gap

For commensurate lattices, there is a net energy contribution of the corrugation amplitudes V_g and the broken symmetry for translations is manifested by a nonzero frequency at $q=0$, as shown for Xe/Cu(111) in Fig. 13. Explicit results can be given for the Brillouin-zone-center frequency gap $\omega_{0\parallel}$ if the corrugation series is truncated at the first shell $|\mathbf{g}|=g_0$.

a. Graphite basal plane

The Bravais lattice is triangular, with lattice constant $\ell\simeq2.46$ Å. There are six primitive vectors $\mathbf{g}$ of length $g_0=4\pi/\ell\sqrt{3}$. For a simply commensurate lattice, such as the $(\sqrt{3}\times\sqrt{3})R30°$ lattice, and adsorption at the honeycomb center site $V_{g_0}<0$, the zone-center gap is isotropic and has the value

---

[27] A similar analysis, using the compressibilty derived from Schwennicke *et al.* (1993), Table X, fits the acoustic branch of Xe/NaCl(001) measured by Gerlach *et al.* (1998) as a SH branch.

$$\omega_{0\parallel} = (3g_0^2|\bar{V}_{g_0}|/m)^{1/2}. \tag{8}$$

In Eqs. (8)–(11), $\bar{V}_{g_0}$ denotes an average over the z motions.

b. fcc(111)

The reciprocal lattice for the fcc(111) surface plane is triangular with six primitive vectors of length $g_0 = 4\pi/\ell\sqrt{3}$, where ℓ is the nearest-neighbor distance of like atoms in the substrate. For atop site adsorption in a $(\sqrt{3}\times\sqrt{3})R30°$ lattice, such as arises for Xe/Pt(111) and Xe/Cu(111) (Diehl *et al.*, 2004), $\omega_{0\parallel}$ is again given by Eq. (8).

c. fcc(001)

The reciprocal lattice for the fcc(001) surface plane is square with four primitive vectors of length $g_0 = 2\pi/\ell$, where ℓ is the nearest-neighbor distance of atoms in the substrate. Then the zone-center gap for vibrations in the simply commensurate direction of a lattice such as $c(4\times 2)$ H_2/MgO(001) is

$$\omega_{0\parallel} = (2g_0^2|\bar{V}_{g_0}|/m)^{1/2}. \tag{9}$$

d. fcc(110)

The reciprocal lattice for the fcc(110) surface plane is rectangular with length ℓ along $[1\bar{1}0]$ and $\ell\sqrt{2}$ along [001]. The two smallest reciprocal-lattice vectors have length $g_0 = 2\pi/\ell\sqrt{2}$ along [001], and the zone-center gap for vibrations of uniaxially commensurate lattices along this axis is given by Eq. (9).

e. Zero-point averaging

In quantum solids such as the monolayer He and H_2 solids, the lateral vibrations $\mathbf{u}$ about the commensurate positions are large enough that the effective corrugation amplitude is significantly reduced. For Eq. (8), the reduction can be estimated by an average in the ground state using (Bruch, 1994)

$$\bar{V}_{g_0} \to \bar{V}_{g_0}\langle \exp(i\mathbf{g}_0\cdot\mathbf{u})\rangle \simeq \bar{V}_{g_0}\exp(-g_0^2\langle u^2\rangle/4). \tag{10}$$

For uniaxial commensurate solids with a zone-center gap along an axis $\hat{x}$, the corresponding modification to Eq. (9) is

$$\bar{V}_{g_0} \to \bar{V}_{g_0}\langle \exp(ig_0x)\rangle \simeq \bar{V}_{g_0}\exp(-g_0^2\langle x^2\rangle/2). \tag{11}$$

Here $\bar{V}_{g_0}$ denotes the expectation value of $V_{g0}(z)$ in the vibrational ground state of z motion.

3. Debye-Waller factor

The Debye-Waller factor F_{DW} expresses the reduction of diffraction and inelastic scattering intensities from a solid arising from the fact that the target lattice is not static. For monolayer solids, the 2D character of lateral correlations leads to marked changes in the line shape of the scattering that we do not review here (e.g., see Sec. 4.2 of Bruch *et al.*, 1997). We discuss two points about the Debye-Waller factor for the systems treated in the present review: (i) the inclusion of the Beeby correction (Beeby, 1971; Gumhalter, 2001) in thermal energy atomic scattering, and (ii) order-of-magnitude agreement for the mean-square displacements inferred from analyses of LEED experiments (Diehl *et al.*, 2004).

Assume that the displacements $\mathbf{u}_j$ of monolayer atoms from the equilibrium sites are small enough that the harmonic approximation to the energy change is valid. The Debye-Waller factor for scattering with wave-vector transfer $\Delta\mathbf{k} = \mathbf{k}_f - \mathbf{k}_i$ is defined as the thermal average

$$F_{\mathrm{DW}} = |\langle \exp(i\Delta\mathbf{k}\cdot\mathbf{u}_j)\rangle|^2 = \exp(-\langle[\Delta\mathbf{k}\cdot\mathbf{u}_j]^2\rangle), \tag{12}$$

where the harmonic approximation has been used in the second equality. Then for $\Delta\mathbf{k} = \Delta k_z\hat{z} + \mathbf{g}$, where $\mathbf{g}$ is a reciprocal-lattice vector of the monolayer, and neglecting the coupling of perpendicular and parallel vibrations, the expression for F_{DW} simplifies to

$$F_{\mathrm{DW}} = \exp[-(\Delta k_z)^2\langle z^2\rangle - \mathbf{g}\cdot\langle\mathbf{u}_\parallel\mathbf{u}_\parallel\rangle\cdot\mathbf{g}]. \tag{13}$$

In particular, for a dispersionless S mode, the z average depends simply on ω_s,

$$\langle z^2\rangle = \frac{\hbar}{2m\omega_s}\coth(\beta\hbar\omega_s/2), \tag{14}$$

while the average $\langle\mathbf{u}_\parallel\mathbf{u}_\parallel\rangle$ depends on the frequencies and polarizations of in-plane vibrations.

The dependence of F_{DW} on $(\Delta k_z)^2$ has been used (Diehl *et al.*, 2004) to get estimates of ω_s from the intensities of LEED patterns and the results agree well with direct determinations of ω_s by inelastic helium-atom scattering. A refinement that arises for the Debye-Waller factor of thermal energy atomic beams (mass m_a) is the Beeby correction (Beeby, 1971), where the effect of an attractive well of depth D near the monolayer is estimated by introducing the effective kinetic energy of normal motion,

$$(\Delta k_z)^2 \to (\Delta k_z')^2 = (\Delta k_z)^2 + 2m_aD/\hbar^2. \tag{15}$$

Gumhalter (2001)emphasized that, while this is justified in the limit of impulsive scattering, corrections are to be expected in other cases. Still, it is a qualitative way to treat the effect of the attractive potential on scattered intensities at low energy.

Most of the momentum transfer in the LEED experiments is perpendicular to the monolayer. Although the measured intensities are relatively insensitive to the parallel motions, there is fair agreement between the experimental and calculated parallel root-mean-square displacements for two of the commensurate lattices in Table IX (Diehl *et al.*, 2004). For Xe/Cu(111) at 50 K, experiment gives $\sqrt{\langle u_x^2\rangle} = 0.29 \pm 0.14$ Å while the lattice-dynamics calculation gives 0.19 Å, using $\omega_{0\parallel} = 0.4$ meV. For Xe/Pt(111) at 80 K, experiment gives $\sqrt{\langle u_x^2\rangle} = 0.23 \pm 0.06$ Å and the calculation gives 0.32 Å, using $\omega_{0\parallel} = 1.3$ meV.

TABLE XI. Higher-order commensurate lattices with length scales for adsorption on the (111) face of the designated (fcc) metals. Lengths L and ℓ in Å. ℓ is the nearest-neighbor distance in the 3D solid at 50 K and the other lengths are the nearest-neighbor distances in the average triangular adatom lattice. Some typical monolayer spacings are 3.75–3.85 Å for Ar, 4.00–4.10 Å for Kr, and 4.35–4.50 Å for Xe. ϑ is the angle that the primitive vector $\mathbf{b}_1$, of the average adlayer lattice, makes with the substrate $\mathbf{a}_1$. For more general structures, see Tkatchenko (2007).

Substrate		$L, \sqrt{3}$	$L, \sqrt{7}-4$	$L, \sqrt{7}-3$	$L, \sqrt{19}-7$
ϑ	ℓ	30°	19.1°	10.9°	4.3°
Cu(111)	2.548	4.41[a]	3.37	3.89	4.20
Ni(111)	2.486	4.31[b]	3.29	3.80	4.10
Pd(111)	2.744	4.75[c]	3.63	4.19[d]	4.52[e]
Pt(111)	2.769	4.80[f]	3.66	4.23	4.56
Ag(111)	2.878	4.98	3.81[g]	4.40[h]	4.74

[a] Observed for Xe/Cu(111) (Braun *et al.*, 1998; Seyller *et al.*, 1998; Šiber *et al.*, 1999).

[b] Observed for Xe/Ni(111) (Wong and Zhu, 1996).

[c] Observed for Xe/Pd(111) (Caragiu *et al.*, 2002; Zhu *et al.*, 2003).

[d] Disputed occurrence for Xe/Pd(111) (Vogt *et al.*, 1991; Zhu *et al.*, 2003).

[e] Disputed occurrence for Xe/Pd(111) (Hilgers *et al.*, 1995; Zhu *et al.*, 2003).

[f] Observed for Xe/Pt(111) (Poelsema *et al.*, 1983; Seyller *et al.*, 1999).

[g] Observed for Ar/Ag(111) (Caragiu *et al.*, 2001).

[h] Possibly present for Xe/Ag(111) (Leatherman *et al.*, 1997).

4. Higher-order commensurate lattices/modulated unit cells

Many subtle coincidences arise in matching adlayer structure to substrate. The triangular adlayer on a rectangular or centered-rectangular substrate surface lattice gives an important set, but there are only limited recent experimental data for such cases in physical adsorption. Work for a triangular adlayer lattice on a bcc(110) substrate was reviewed by Bruch and Venables (1984) and extended by Paik and Schuller (1990). Here we treat the more limited, but still very rich, series of coincidence lattices for the triangular adlayer on the triangular substrate surface, for which there has been significant progress in experiments and modeling. We use the theoretical formulation to highlight similarities and contrasts for the systems studied experimentally.

Table XI gives an overview of the commensurate lattices discussed here. We note that the alignments of rare-gas monolayer lattices are extremely sensitive to the presence of small amounts of impurity at the surface, whether put there intentionally or not (Kern *et al.*, 1986; Leatherman *et al.*, 1997; Kern, Zeppenfeld, David, and Comsa, 1988; Zhu *et al.*, 2003).

In general, there are several contributions to the stabilization energy of higher-order commensurate (HOC) lattices. Terms arise both from the periodic repeat of the superlattice cell (first order in some Fourier amplitudes V_g)[28] and from the modulation of positions within the superlattice cell (roughly, second order in some of the amplitudes). We review the $(\sqrt{7}\times\sqrt{7})\,R19.1°$ triangular lattice on a triangular substrate, with four atoms in the unit cell, in some detail to illustrate the phenomena that may arise. There are experimental data for three systems with this structure: Ne/graphite, He/He/graphite, and Ar/Ag(111) (Calisti *et al.*, 1982; Godfrin and Lauter, 1995; Caragiu *et al.*, 2001). The (3×3)Kr/Ru(0001)$R0°$ lattice (Narloch and Menzel, 1997, 1998) has a closely related theory.

a. $(\sqrt{7}\times\sqrt{7})\,R19.1°$*-4 lattice*

The following treatment implicitly assumes the substrate is rigid, so that deformations occur only in the monolayer. Experimentally, the substrate atom displacements driven by a physically adsorbed monolayer can scarcely be resolved (Diehl *et al.*, 2004). The formulation begins with a definition of the coordinate axes. The substrate primitive vectors are denoted $\mathbf{a}_1=\ell\hat{x}$; $\mathbf{a}_2=(\ell/2)(\hat{x}+\hat{y}\sqrt{3})$ and the leading reciprocal-lattice vectors are $\mathbf{g}_1=(g_0/2)(\hat{x}\sqrt{3}-\hat{y})$; $\mathbf{g}_2=g_0\hat{y}$; $\mathbf{g}_3=-\mathbf{g}_1-\mathbf{g}_2$, with $g_0=4\pi/\ell\sqrt{3}$. The primitive vectors of the superlattice are $\mathbf{c}_1=3\mathbf{a}_1-\mathbf{a}_2$; $\mathbf{c}_2=\mathbf{a}_1+2\mathbf{a}_2$, of length $\ell\sqrt{7}$ and with $\mathbf{c}_1$ at 19.1° to $\mathbf{a}_1$. The average adlayer lattice is generated by the vectors $\mathbf{b}_1=\mathbf{c}_1/2$; $\mathbf{b}_2=\mathbf{c}_2/2$ with a corresponding pair of reciprocal-lattice vectors $\mathbf{t}_1,\mathbf{t}_2$. The misfit wave vectors $\mathbf{q}_j$ between $\mathbf{g}_i$ and $\mathbf{t}_i$ correspond to midpoints (M) of the hexagonal boundary of the first Brillouin zone of the average adlayer lattice, e.g., $\mathbf{q}_1\equiv\mathbf{t}_1-\mathbf{g}_1=-(\mathbf{t}_1+\mathbf{t}_2)/2$, with $\mathbf{q}_2$ and $\mathbf{q}_3$ given as successive 120° rotations of $\mathbf{q}_1$.

Positions in the modulated adlayer lattice are given by

$$\mathbf{r}_j=\bar{z}\hat{z}+\mathbf{s}_j+\mathbf{d}_0+\sum_{\alpha=1}^{3}\mathbf{d}_\alpha\exp(\imath\mathbf{q}_\alpha\cdot\mathbf{s}_j), \tag{16}$$

where the uniform monolayer positions are $\mathbf{s}_j=j_1\mathbf{b}_1+j_2\mathbf{b}_2$, there is a displacement $\mathbf{d}_0$ relative to the substrate, and the modulation amplitudes are $\mathbf{d}_\alpha$.

The stabilization energy can be estimated with a perturbation expansion (McTague and Novaco, 1979; Bruch 1988, 2001) of the dependence of the V_0 and V_{g0} terms on $\mathbf{d}_\alpha$. Then the minimum modulation energy for given positioning $\mathbf{d}_0$ is

$$E_{\mathrm{mod}}/N=-2\epsilon_\perp+6V_{2g_0}+\frac{\tilde{\epsilon}}{3}\sum_{j=1}^{3}[1-\cos(2\mathbf{g}_j\cdot\mathbf{d}_0)], \tag{17}$$

$$\tilde{\epsilon}=\epsilon_\perp-\epsilon_\parallel-6V_{2g_0}, \tag{18}$$

with

$$\epsilon_\perp=3\frac{(dV_{g_0}/dz)^2}{m\omega_s^2},$$

---

[28] The discussion here retains only a few amplitudes V_g in Eq. (3). Tkatchenko (2006, 2007) has formulated a more complete description.

$$\epsilon_{\|} = 3\frac{g_0^2 V_{g_0}^2}{7m}\left(\frac{4}{\omega_{\mathrm{LA}}(M)^2} + \frac{3}{\omega_{\mathrm{SH}}(M)^2}\right). \tag{19}$$

At this level of approximation, there are two cases for the energy minimum. For $\tilde{\epsilon} > 0$ ($\mathbf{d}_0 = 0$), which is the one observed for Ag(111)-$(\sqrt{7}\times\sqrt{7})R19.1°$-4Ar (Caragiu *et al.*, 2001), one adatom is atop a surface Ag atom and three adatoms are at bridge sites. It has been argued (Bruch, 2001) that the V_{2g_0} term is negligible in Eq. (18) and that the energy amplitude of parallel modulation $\epsilon_{\|}$ is smaller than the $\epsilon_{\perp}$ to make $\tilde{\epsilon} > 0$ for Ar/Ag(111). On the other hand, the Ne/graphite case is believed to have $\epsilon_{\|} > \epsilon_{\perp}$ and $\tilde{\epsilon} < 0$, because the rather dilated Ne lattice has smaller frequencies $\omega_{\mathrm{LA,SH}}(M)$. Then the displacement would be $\mathbf{d}_0 = (\mathbf{a}_1 + \mathbf{a}_2)/6$ or $(\mathbf{a}_1 + \mathbf{a}_2)/3$, with one adatom at the fcc or hcp stacking site. Notice that a quantitative treatment of $\tilde{\epsilon}$ requires an estimate of dV_g/dz; using $dV_{g_0}/dz \simeq -g_0 V_{g_0}$ seems to be good to about 50% at the equilibrium overlayer height.

In the $\tilde{\epsilon} > 0$ case, adatoms of the uniform adlayer lattice have zero lateral forces, but this will be modified when the $V_g^{(2)}$ term is included. For $\tilde{\epsilon} < 0$, three of the four atoms in the uniform unit cell are in low-symmetry positions and experience forces arising from $V_g^{(1)}$. Hence, it is expected that the modulation of relative separations will be larger for $\tilde{\epsilon} < 0$.

The lateral positioning in the $\tilde{\epsilon} > 0$ case does not itself decide that the minimum energy adsorption site is an atop site. However, in the approximation to V_s used here, $V_{g_0} < 0$ corresponds to a minimum energy atop site and, further, the overlayer height at the atop site is smaller than at the bridges and, in turn, smaller than at the threefold sites. The experiments (Caragiu *et al.*, 2001) did not establish a net difference in heights at the atop site and the bridges, so the issue of optimal one-adatom site remains open for Ar/Ag(111).

The $\sqrt{7}$ lattice also occurs for the second-layer solid of helium adsorbed on a monolayer of helium on graphite, in particular ^{3}He/^{3}He/graphite (Godfrin and Lauter, 1995) and ^{3}He/^{4}He/graphite (Matsumoto *et al.*, 2004; Ziouzia *et al.*, 2004). It is a bit startling that such a subtle commensurate structure occurs for quantum solids with large zero-point vibrations that are likely to reduce greatly the average corrugation energies. The $(\sqrt{7}\times\sqrt{7})R19.1°$ second-layer lattice is found to be stable in calculations for ^{3}He/^{3}He/graphite (Abraham *et al.*, 1990) and ^{4}He/^{4}He/graphite (Pierce and Manousakis, 1999). However, the positioning of the unit cell is different in the two calculations. For the unit cell of ^{3}He/^{3}He/graphite, one of the four second-layer atoms is at an atop site and three are at bridge sites, paralleling the Ar/Ag(111) structure and corresponding to $\tilde{\epsilon} > 0$ in the perturbation theory. For the unit cell of ^{4}He/^{4}He/graphite, one atom is at a threefold site and the other three are in low-symmetry environments, paralleling what is believed to be the Ne/graphite structure and corresponding to $\tilde{\epsilon} < 0$ in the perturbation theory. To interpret the difference in positioning in terms of corrugation terms and phonon energies will require advances in the state of the art for simulating the properties of bilayer helium films (Whitlock *et al.*, 1999).

b. $(\sqrt{3}\times\sqrt{3})\,R0°$*-4 lattice*

A related unit cell is observed for Ru(0001)-$(3\times3)R0°$-4Kr (Narloch and Menzel, 1997, 1998). The primitive vectors of the superlattice are $\mathbf{c}_1 = 3\mathbf{a}_1$; $\mathbf{c}_2 = 3\mathbf{a}_2$, aligned with the axes of the triangular substrate surface unit cell. The average adlayer lattice is generated by the vectors $\mathbf{b}_1 = \mathbf{c}_1/2$; $\mathbf{b}_2 = \mathbf{c}_2/2$ with a corresponding pair of reciprocal-lattice vectors $\mathbf{t}_1 = (2/3)\mathbf{g}_1$, $\mathbf{t}_2 = (2/3)\mathbf{g}_2$. The misfit wave vectors $\mathbf{q}_j$ are at the M points of the average adlayer Brillouin zone, e.g., $\mathbf{q}_1 \equiv \mathbf{t}_1 - \mathbf{g}_1 = -\mathbf{t}_1/2$. The perturbation theory analysis goes through as in Eqs. (16)–(19), but the evaluation of $\epsilon_{\|}$ changes because the misfit wave vectors $\mathbf{q}$ are parallel to the corresponding $\mathbf{g}$,

$$\epsilon_{\|}(\mathrm{Kr/Ru}) = 3g_0^2 V_g^2 / m\,\omega_{\mathrm{LA}}(M)^2. \tag{20}$$

Narloch and Menzel (1997, 1998) found that the unit cell of the krypton layer has one atom at a threefold (hcp or fcc) site and three at near-top sites, which is the $\tilde{\epsilon} < 0$ case of the perturbation theory.[29] They also determined that the "Kr atoms above the hollow sites are pushed up with respect to the other Kr atoms by 0.03±0.04 Å (hcp) and 0.02±0.03 Å (fcc)." While not a statistically compelling discrimination, this suggests that the minimum energy adsorption site for a single Kr is the atop site, as found for Xe on several metals, see Sec. IV.B.

Sakurai and Yamada (2005) reported a four-molecule $(3\times3)R0°$ structure for CH$_4$/Ag(111) at 37 K. The separation of molecular centers is 4.33 Å, which is in the range of calculations for a floating methane solid at this temperature (Phillips, 1984). However, the adsorption energy and the modulations of the four-molecule unit cell have not yet been determined.

c. Other cases

We describe two higher-order-commensurate structures that have less extensive experimental support. First, there is a $(\sqrt{7}\times\sqrt{7})R19.1°$ HOC lattice with three atoms in the unit cell, proposed for Xe/Pd(111) (Vogt *et al.*, 1991). The triangular average adatom lattice is generated by primitive vectors $\mathbf{b}_1 = (4\mathbf{a}_1 + \mathbf{a}_2)/3$ and $\mathbf{b}_2 = (-\mathbf{a}_1 + 5\mathbf{a}_2)/3$, with $\mathbf{b}_1$ at 10.9° to $\mathbf{a}_1$. The relation of the substrate reciprocal-lattice vectors to leading reciprocal-lattice vectors of the average adatom lattice is $\mathbf{g}_1 = (4\boldsymbol{\tau}_1 - \boldsymbol{\tau}_2)/3$; $\mathbf{g}_2 = (\boldsymbol{\tau}_1 + 5\boldsymbol{\tau}_2)/3$. Then the $V_{g_0\sqrt{3}}$ energy amplitude

---

[29] It is hard to get $\epsilon_{\|} > \epsilon_{\perp}$ from the available information for Kr/Ru. The nearest-neighbor Kr-Kr distance in the average lattice is 4.06 Å, close to the length 4.09 Å of the Kr/Pt(111) lattice for which $\omega_{\mathrm{LA}}(M) \approx 4.1$ meV (Bruch *et al.*, 2000). ω_s is 2.95 meV for Kr/Ag(111) (Gibson and Sibener, 1985) and 3.9 meV for Kr/Pt(111) (Bruch *et al.*, 2000). If the value for Kr/Ru(0001) is in this range, to get $\tilde{\epsilon} < 0$ requires either a large effect of V_{2g_0} or a rather small magnitude for $|d \ln V_{g_0}/dz|$.

contributes in first order[30] in the modified form of Eqs. (17) and (18), and the misfit wave vectors for the V_{g_0} terms are at K points of the Brillouin zone.

Second, there is a $(\sqrt{19}\times\sqrt{19})R23.4°$ HOC lattice with seven atoms in the unit cell, also proposed for Xe/Pd(111) (Hilgers *et al.*, 1995). The primitive vectors of the unit cell are $\mathbf{c}_1=3\mathbf{a}_1+\mathbf{a}_2;\mathbf{c}_2=-\mathbf{a}_1+5\mathbf{a}_2$ and the primitive vectors of the triangular average adatom lattice are $\mathbf{b}_1=(11\mathbf{a}_1+\mathbf{a}_2)/7$ and $\mathbf{b}_2=(-\mathbf{a}_1+12\mathbf{a}_2)/7$, with $\mathbf{b}_1$ at 4.3° to $\mathbf{a}_1$. The effect of the leading V_g terms is evaluated using the nondegenerate perturbation theory of McTague and Novaco (1979), in contrast to the other HOC cases described thus far.

Finally, we mention two other cases with large unit cells. The $(5\times5)R0°$-12 superlattice of Kr/Pt(111) with 12 Kr atoms per unit cell and average lattice spacing $L=4.00$ Å was observed at monolayer completion (Kern, Zeppenfeld, David, and Comsa, 1987; Kern and Comsa, 1988). The perturbation theory analysis of this subsection would not give a lock-in energy to stabilize the structure (Gordon, 1986), but experimentally it is stable against thermal expansion (Kern and Comsa, 1988). Zeppenfeld *et al.* (1992) observed the $(4\times4)R0°$-9 compressed lattice of Ar/Pt(111) with nine Ar atoms per unit cell and an average lattice spacing of 3.70 Å.

D. Equation of state

In principle, a thorough knowledge of the equation of state of the form $\mu=\mu(n_2,T)$ for the chemical potential or $E=E(L,T)$ for the internal energy of a solid with lattice constant L or 2D density n_2 would do much to confirm or refine the knowledge of interactions in the monolayer. The present situation is much less advanced, especially because there are few direct thermodynamic measurements for adsorption on metals.[31] Instead diffraction measurements[32] of the monolayer lattice constants are used to get partial information on the isothermal compressibility K_T of monolayer phase x,

$$K_T=[n_x\,\partial\,\phi/\partial n_x|_T]^{-1}. \qquad (21)$$

Two methods have been used for most evaluations of K_T. Measurement of the variation of the 3D gas pressure along an isotherm directly gives

$$K_T=\ 1/n_x^2 k_B T\,\partial\,\ln p/\partial n_x|_T, \qquad (22)$$

when equilibrium between the 3D gas and the monolayer phase x, $d\mu_g=d\mu_x$, is maintained. This has been applied with automated adsorption isotherm measurements on samples with large surface-to-volume ratio; see Sec. II.A.2 (see, e.g., Alkhafaji and Migone, 1991; Mursic *et al.*, 1996). Shaw and Fain (1980) derived K_T from diffraction measurements of the lattice constant of Ar/graphite along an isotherm. A second method is to transform diffraction measurements of monolayer lattice constants along an isobar using a form of Eq. (A7),

$$K_T=(T/q_{\mathrm{st}})\frac{\partial}{\partial T}(1/n_x)|_p. \qquad (23)$$

Then an estimate for q_{st} is needed and a frequent choice, probably good to 10%, is $q_{\mathrm{st}}\simeq q_1$. Using the lattice constant observed in diffraction to measure the areal density (coverage) has an implicit assumption, discussed in Appendix A.1.a, that there are negligible concentrations of vacancies in the monolayer and negligible second-layer gas density. The coverage measure has been confirmed to 1% for rare gases on Ag(111) (Unguris *et al.*, 1979, 1981) (for Xe at $T<80$ K, Kr at $T<65$ K, and Ar at $T<45$ K).

A third method is to combine the measured speeds of sound (initial slopes of acoustic phonon branches) for monolayer triangular lattices using Eqs. (5) and (6),

$$1/K_T=B_T=\rho(c_{\mathrm{LA}}^2-c_{\mathrm{SH}}^2). \qquad (24)$$

Table X lists the monolayer compressibility for several adsorbate/substrate combinations. K_T for Kr/graphite was evaluated by two methods at similar $A=1/n_x$ and the results agree to 15%. For given adsorbate, the K_T values are similar in magnitude, with smaller K_T for smaller area A. There is even a similarity in K_T for triangular lattices of xenon and three uniaxial incommensurate cases of xenon [Xe/Pt(111), Xe/Cu(110), and Xe/NaCl(001)]. This type of evidence has been cited as support for the transferrability of interactions from 3D to physically adsorbed layers.

Compressibilities at higher temperatures tend to be larger than the values given in Table X. For solid Xe/graphite at the melting curve, from 115 to 140 K, the values are (Gangwar *et al.*, 1989) 6–8 m^2/J. The 2D liquid compressibility of Ar/graphite near the 2D melting curve for 60–80 K is in the range 8–10 m^2/J, while the 2D solid there has $K_T\approx3-5$ m^2/J (Zhang and Larese, 1991). The 2D liquid compressibility for Ar/BN near solidification at 72 K is (Alkhafaji and Migone, 1991) about 9 m^2/J, rather similar to that for Ar/graphite. All these values are derived from high-resolution adsorption isotherm data in experiments whose main goal was to elucidate transitions in multilayer films (Phillips and Larese, 1997).

We have emphasized the near-classical regime and data derived from diffraction experiments. The thermodynamic data for atomic helium and molecular hydrogen on graphite are reviewed elsewhere (Bruch *et al.*, 1997; Wiechert, 2003). Monolayer solids of these quantum gases have large compressibilities and span a wide range of densities.

---

[30] Another example to show the need for case-by-case analysis is that the V_{g0} amplitude contributes at first order in the energy of the $(\sqrt{21}\times\sqrt{21})R10.9°$-7 HOC lattice proposed for N$_2$O/graphite (Leinböck *et al.*, 2000).

[31] In fact, comprehensive treatments of the equation of state are rare also for monolayer adsorption on graphite. See the reviews in Bruch *et al.* (1997, Chap. 6).

[32] Inelastic helium-atom scattering may provide direct tests of models of the interactions in the monolayer, but diffraction results are still the only checks for many cases.

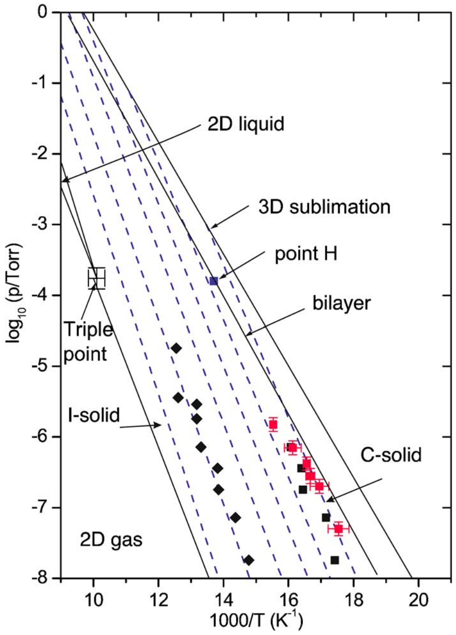

FIG. 17. (Color online) log(p)-T^{-1} phase diagram of Xe/graphite. The solid lines indicate the phase boundaries between 2D gas and I-solid, 2D gas and 2D liquid, 2D liquid and I-solid, monolayer and bilayer, and the 3D sublimation curve. The 2D triple point is also indicated. The squares are experimental points locating the I-C transition (Schabes-Retchkiman and Venables, 1981; Hamichi *et al.*, 1989). The diamonds are experimental points locating the coverage =0.92 isostere (where coverage =1 for the C structure). The dashed lines are isosteres from coverage =0.90 to 1.0 in increments of 0.02, calculated from a multiparameter potential model using Einstein vibrations for the vertical motion and the cell model for lateral motion (Schabes-Retchkiman and Venables, 1981). Point H on the bilayer line is from Hong *et al.* (1989) as described in the text.

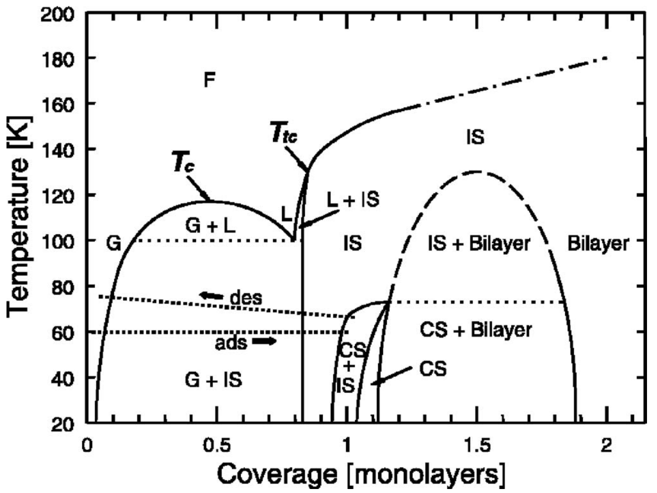

FIG. 18. θ-T phase diagram of Xe/graphite in the 0–2 layer regime from von Przychowski *et al.* (2003), adapted from Hong *et al.* (1987). Note that this plot emphasizes coexistence regions, e.g., CS+IS, where IS denotes incommensurate solid, CS denotes commensurate solid, G denotes 2D gas, L denotes 2D liquid, and F denotes fluid phases. The adsorption and desorption paths studied by von Przychowski *et al.* (2003) are shown as dot-dashed lines.

E. Case studies

1. Xe/graphite

In this case study, we review diffraction results and thermodynamic data, produce an updated phase diagram, and comment on remaining uncertainties. This incorporates an immense amount of work.

A great deal of information on the Xe/graphite system was available by the mid-1990s (Thomy and Duval, 1994; Suzanne and Gay, 1996). Some recent work fits easily into this same framework, e.g., the imaging of hexagonal domains for incommensurate Xe/graphite (Grimm *et al.*, 1999, 2000). The preferred adsorption site of commensurate Xe/graphite is one of maximum coordination at the center of a carbon honeycomb; this assumption has been confirmed by Pussi *et al.* (2004), as emphasized in Sec. IV.B.1 and Table VII.

An early proposal for the log(p)-T^{-1} phase diagram for T below about 100 K was given by Schabes-Retchkiman and Venables (1981). Their phase diagram, including the original cell model calculations and updated with later experimental points, is shown in Fig. 17. Another presentation is the coverage-temperature (θ-T) phase diagram of von Przychowski *et al.* (2003) shown in Fig. 18, which is based on that of Hong *et al.* (1989). The different cuts through the phase diagram look very different and emphasize different aspects of the data sets; neither includes the transition between incommensurate aligned (IA) and incommensurate rotated (IR) monolayer solids. The θ-T phase diagram, Fig. 18, emphasizes two-phase coexistence regions and magnifies into broad regions those parts of the three-dimensional parameter space that are indicated by lines on a log(p)-T^{-1} phase diagram, Fig. 17.

There are substantial differences, both qualitative and quantitative, in the treatment of the commensurate (C) phase in Figs. 17 and 18. The latter has a region of two-phase coexistence of the C and I monolayer solids, as supported by the diffraction line shapes recorded by Hong *et al.* (1987, 1989). However, the lattice constants measured in the THEED experiments indicated a continuous transition, Fig. 2, and no coexistence. The intersection of the I-C phase transition line with the I-bilayer line is markedly different in the various experiments. Using THEED, Hamichi *et al.* (1989) placed the intersection at $T=62.5\pm1$ K and $p=2\pm0.5\times10^{-6}$ Torr,[33] while Hong *et al.* (1987, 1989) found the intersection to be at $T\simeq73$ K for a filling $f=1.16$ (denoted H in Fig. 17). The thermodynamic paths through p,θ,T were quite different in the THEED and x-ray experiments.

To clarify what is going on in these various experiments, we consider what is being measured in each case

---

[33] To be consistent with the literature, we quote pressures in Torr. The conversion to SI units is 1 Torr=1.33 mbar =133 Pascal.

and what interpretations are based on assumptions. In particular, it can be difficult to compare the coverages. The coverage measured in the THEED experiment, e.g., Fig. 17, was deduced from the average lattice parameter, which assumes that the film is a uniform, perfect single-phase monolayer solid with no vacancies or higher layers present. This coverage is not the same as that in a volumetric measurement, which is the total amount of adsorbate on the surface, irrespective of whether the film has vacancies or second-layer atoms. The two will generally coincide for perfect low-temperature monolayer solids. However, the distinction can be important, particularly at higher T or near phase transition lines, as emphasized by Hamichi *et al.* (1989, 1991). In many x-ray experiments, the lattice parameter or misfit $m = (L - L_c)/L_c$ has been measured at constant filling by using a closed-cell arrangement. (This can be done even with single crystals by using a ballast surface of high-surface-area polycrystalline graphite.) Filling (e.g., $f = 1.16$ for point H in Fig. 17) is determined in the same way as the coverage in a volumetric experiment, but it typically is determined at only one T and p. Thus, the constant filling in the x-ray experiments does not imply a constant coverage as T varies.[34] Comparing the pressures between different experiments can also be problematic. In x-ray experiments on single crystals at constant filling, the pressure is set indirectly whereas in other diffraction experiments such as THEED and LEED it is usually measured directly. Aside from calibration issues, there is not a consensus on whether this measured pressure should be corrected to account for the difference in the T of the gas at the surface and in the gauge. These rather technical issues, and the possibility of kinetic restrictions at low temperatures, mean there are several possibilities for obtaining path-dependent results. Therefore, the experimental power-law dependencies (β) of misfit on $T - T_0$ near the C-I transition are not easily related to universal phenomena. The values $\beta = 0.33 \pm 0.08$ from Hong *et al.* (1987) and $\beta = 0.80 \pm 0.03$ from Hamichi *et al.* (1989) arise from very different experimental paths through the (θ, p, T) variable space.

We now attempt to make a quantitative unification of the diffraction-based results with thermodynamic data. Our summary presentation is a μ-T phase diagram in two parts, Figs. 19(a) and 19(b). In Fig. 19(a), we plot the basic phase diagram. The bulk solid sublimation (solid-vapor), vaporization (liquid-vapor), and melting (solid-liquid) lines and the 3D triple point all are known from classic data on bulk Xe from Crawford (1977). There is also agreement on much of the monolayer phase domain and its boundary with the bilayer. Figure 19(b) shows experimental data that support the phase boundaries in Fig. 19(a) and additional experimental points that are discussed below.

The monolayer triple (T_t) and critical (T_c) points in Fig. 19(a) were determined by volumetric isotherm measurements (Thomy *et al.*, 1981). The position of the 2D solid-liquid (melting) phase boundary was also set by several volumetric isotherm experiments stretching to $T = 160$ K, as shown in Fig. 19(b) (Tessier and Lahrer, 1980; Thomy *et al.*, 1981; Tessier 1984; Gangwar *et al.*, 1989). The isotherms have vertical risers characteristic of a first-order transition, except for the last four points at $T \geq 152$ K, where the slight rounding of the risers is taken to indicate second-order transitions.

The heat capacity and volumetric melting line data of Jin *et al.* (1989)[35] agree with these data. However, Jin *et al.* argued that melting is first order at least up to $T = 156.5$ K, with half-widths of order 1.3 K. The same authors extended their experiments into the multilayer regime, where the half-width of the melting transition ranged from ~0.9 K at $T = 161.2$ K to 2 K at 186.7 K; thus the transition width is not getting dramatically wider as the temperature is raised. Later studies, included in Sec. VI.A, indicate that a solid first layer is in equilibrium with a fluid second layer as the bilayer line is approached in this region.

Two points from the simultaneous x-ray scattering and volumetric isotherm measurements of Zhang and Larese (1995) are indicated as filled squares near the bilayer line in Fig. 19(b). Their bilayer critical point ($T = 136.8 \pm 0.2$ K, $p = 40 \pm 1$ Torr) is marked, and also their point at 145 K, for which an inflection point in the adsorption isotherm was observed at $p = 83$ Torr.[36] Their data for n-layer films with $n = 3 - 5$ are for states in the narrow space between the bilayer and 3D sublimation lines in Fig. 19(b) and are not shown there.

We next review the diffraction studies, starting with the 2D gas-monolayer phase boundary. Two of the many LEED data points from Suzanne *et al.* (1974, 1975) and some data points from THEED diffraction studies by Schabes-Retchkiman and Venables (1981) are shown as open squares in the bottom left corner of Fig. 19(b). Along this phase boundary, the electron diffraction data (LEED and THEED) are systematically displaced downwards in pressure by about 15–30 % from the Thomy-Duval triple point. This is likely to be due to the difference in the experimental setup (directed gas beams, with no thermomolecular correction, versus volumetric measurements). Notably the single Thomy-

---

[34] A related issue arises for the experimental determination of the lattice constant L of the ground state of Xe/graphite. Hong *et al.* (1989) reported $L = 4.32$ Å at the lowest temperature (25 K) for their smallest filling. In the experiments of Mowforth *et al.* (1986), the corresponding values are $L = 4.43$ Å at $T = 20$ K. Ellis *et al.* (1985) measured the lattice constant for several ways of preparing the monolayer and their largest value at $T = 15$ K is $L = 4.42$ Å. Presumably the condition closest to the ground state of an unconstrained monolayer solid is that with the largest L.

[35] These data were taken with a closed cell configuration and so they nominally correspond to constant coverage and a different trajectory through the phase diagram.

[36] These values are based on data reported by Phillips and Larese (1997).

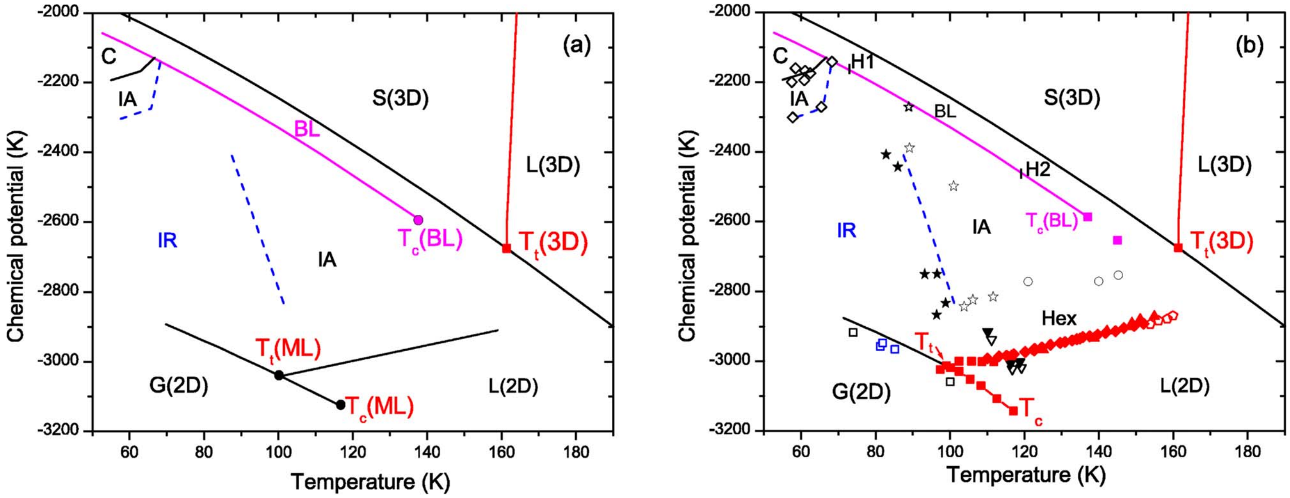

FIG. 19. (Color online) Composite μ-T phase diagram for Xe/graphite at temperatures that span the 2D monolayer, bilayer, and 3D bulk phases and the monolayer melting transitions. (a) Phase diagram containing the phases and phase boundaries discussed in the text. The 2D gas is at the lower left. A monolayer condensation line, which contains the 2D triple and critical points, separates the 2D gas from the 2D liquid and incommensurate monolayer solid phases. The 2D melting line extends from the 2D triple point toward higher T. A bilayer adsorption line ends in a bilayer critical point, and the 3D bulk sublimation line (with the 3D triple point) separates the 2D film from the 3D bulk. The phase boundary between 3D solid and liquid extends up from the 3D triple point. Within the monolayer domain, there are additional phase boundaries between the incommensurate aligned (IA) and rotated (IR) monolayers (dashed lines) and between the IA and commensurate (C) solid phase (solid line). (b) The same phase diagram with some of the supporting experimental data. The filled symbols on the 2D gas-liquid line and the monolayer melting line are from volumetric isotherms by Thomy *et al.* (1981) (squares), Tessier (1984) (diamonds), and Gangwar *et al.* (1989) (triangles). The open pentagons at the high-T end denote second-order melting (Tessier, 1984). The gas-solid transition line is supported by electron diffraction observations (Suzanne *et al.*, 1975; Schabes-Retchkiman and Venables, 1981) (open squares). Electron diffraction was also used to locate C-IA-IR transition (Hamichi *et al.*, 1989) (open diamonds) and the reentrant IA-IR phase boundary (Zerrouk *et al.*, 1993) (closed and open stars for the IR-IA states, respectively). IA-hexatic transitions were observed with electron diffraction (Zerrouk *et al.*, 1994) (filled inverted triangles) and x-ray diffraction (Nuttall *et al.*, 1995) (open circles). Hexatic-liquid transitions were also observed by Zerrouk *et al.* (open inverted triangles). The IA-IR transitions observed by Hong *et al.* (1989) are denoted by $H1$ and $H2$. Two bilayer points of Zhang and Larese (1995) (filled squares) are also shown.

Duval sublimation point also lies on the line, which suggests that these data may correspond to slightly lower overall coverage; i.e., information may be coming from large patches of unconstrained monolayer Xe, rather than from complete layers. This is possible because the diffraction data correspond to the first or last appearance of diffraction spots while heating or cooling at a small but finite rate. von Przychowski *et al.* (2003) have seen such monolayer patches of condensed Xe directly during adsorption and desorption, by photoemission electron microscopy as described in Sec. II.B.2.

This brings us to the nature of high-temperature solid and the question of whether melting proceeds in two stages via a hexatic phase (Strandburg, 1988). THEED studies by Zerrouk *et al.* (1994) near the melting line found strong evidence for two-stage melting via the hexatic phase. In Fig. 19(b), their points for the IA-hexatic transition, shown as filled inverted triangles at 110–120 K, fall very close to the thermodynamic melting line, as do x-ray data of diffraction data of Dimon *et al.* (1985) at 116–134 K and of Heiney *et al.* (1983) at 150 K. There is no doubt that these varied experiments are dealing with the same transition. According to Zerrouk *et al.*, there may actually be two transitions, from solid-to-hexatic and hexatic-to-liquid, with phase boundaries separated by only $\Delta T \simeq 1$ K. The locations of the second transition are shown as open inverted triangles.

However, the later high-resolution x-ray diffraction experiment of Nuttall *et al.* (1994, 1995) places the boundary for melting of the IA solid phase at much higher chemical potentials for T in 120–145 K. The points of Nuttall *et al.* in Fig. 19(b) (open circles) fall some way above the thermodynamic monolayer melting line set by thermodynamic measurements (Tessier, 1984; Jin *et al.*, 1989) and previous x-ray determinations (Heiney *et al.*, 1983; Dimon *et al.*, 1985). Specifically, at $T = 145$ K, the Nuttall *et al.* experimental pressures are in the range $40 \leq p \leq 70$ Torr and approach that of a supercritical bilayer point at $p = 83$ Torr (Zhang and Larese, 1995). They are well above the volumetric melting point at $p = 14$ Torr (Tessier, 1984). The consequence of these data for locating the solid-hexatic phase boundaries at intermediate and high T is as yet unclear.

The locations of the C-IA and IA-IR transitions at the left side of Fig. 19 are based exclusively on electron and x-ray diffraction data. At the lowest temperatures, around 60 K, the C phase occurs close to the bilayer line and the IA (aligned) phase occupies a narrow region (Hamichi *et al.*, 1989, 1991). However, most of the region consists of the IR (rotated) monolayer phase.[37] An interesting point about this central region of the monolayer phase diagram is that the IA phase is reentrant. It reappears at higher T, so that the monolayer melts from the IA phase essentially along the entire melting line. The transition from IR to IA before the solid melts is shown in THEED experiments of Zerrouk *et al.* (1993) and x-ray experiments of D'Amico and Moncton (1986) and D'Amico *et al.* (1990). In the x-ray experiments, the pressure was measured only in a few cases and further analysis is needed to test whether the THEED and x-ray data are mutually consistent. A more detailed examination of this region, correlating lattice parameter and rotation angle with μ and T, is warranted. At present the IR-IA reentrant phase transition boundary is not precisely determined.

The corresponding data plotted on Fig. 19(b) are the steeply sloping phase boundary line accompanied by a few star symbols from Zerrouk *et al.* (1993). These sets of constant pressure data exhibit both the IA and IR phases, where the IA phase data shown (black open stars) correspond to diffraction spots with an angular broadening of ≤0.2° and the IR phase (filled stars) has a maximum rotation of 1.2°. The reentrant IA phase was also found in x-ray diffraction by Hong *et al.* (1987, 1989) and D'Amico *et al.* (1990), but a pronounced asymmetry between cooling an I-layer and heating a C-layer was reported. On cooling from the 2D liquid phase, an IA phase forms first, then abruptly becomes an IR phase [indicated by point $H2$ in Fig. 19(b)], and then becomes aligned again (at point $H1$) before the I-C transition. On reheating the C phase through the C-IA phase transition, the layer stays aligned and does not form the IR phase before melting.

The phenomena described in the previous paragraph must mean that the kinetics of various transitions are important and that metastability is rife in this portion of the phase diagram. In particular, the difficulty of generating the geometrically necessary Kosterlitz-Thouless dislocations, to create two rotated domains in the IR phase from a highly perfect IA or C phase (Venables and Schabes-Retchkiman, 1978; Hamichi *et al.*, 1991), must play a decisive role.

The domain-wall structure of incommensurate Xe/graphite at $T=5$ K is shown (Hövel *et al.*, 1998; Grimm *et al.*, 1999) in Fig. 20. The domain walls are rotated from the atomic lattice orientation by about 11°, corresponding to an angular rotation of the Xe lattice from the $(\sqrt{3}\times\sqrt{3})R30°$ structure of about 0.5°. This angle is close to those observed in the diffraction experiments where rotations of up to 0.4° (Hamichi *et al.*, 1989, 1991) or 0.75° (D'Amico *et al.*, 1990) were observed in the temperature range 60–80 K. The image in Fig. 20 also shows alternate expanded and contracted nodes in the domain-wall network, in an analogous manner to those naturally occurring in graphite sheets [and in fcc(111) layers generally]. This feature is well known from TEM studies over many years (Amelinckx and Delavignette, 1960; Howie and Swann, 1961; Venables and Schabes-Retchkiman, 1978). Subsequently, Grimm *et al.* (2000) observed changes in the domain structure taking place during observation at $T=5$ K as shown by the STM images in Fig. 21. Such changes were only observed in monolayers that had a distorted domain-wall structure, which was formed by introducing impurities that create local strain in the layer. Grimm *et al.* found the domain-wall activity, on a time scale of tens of minutes, at such a low temperature to be surprising and suggested that a mechanism might be the spontaneous creation of mobile dislocations in weakly incommensurate structures pre-

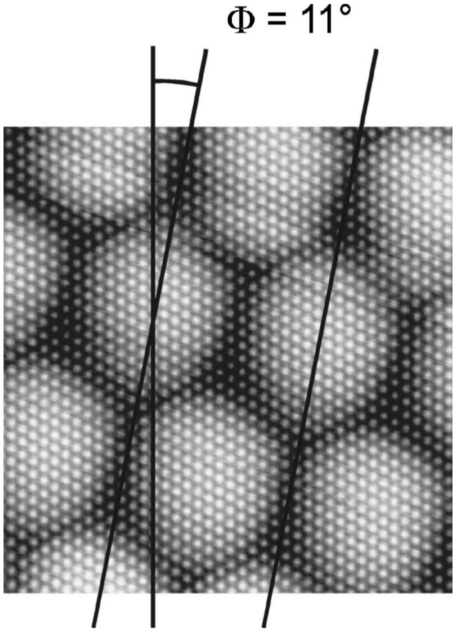

FIG. 20. STM image of Xe on graphite, showing atomically resolved hexagonal domains arranged in a honeycomblike structure. The image size is 16×16 nm^2. The distance between two opposite domain walls is about 5 nm. From Grimm *et al.*, 1999.

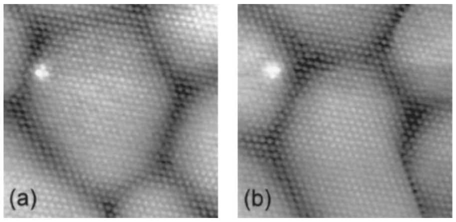

FIG. 21. Close-up STM images of Xe on graphite, showing atomically resolved hexagonal domains that change between frames. In (b), a dislocation has been formed, resulting in a changed domain structure. The image size is 14×14 nm^2. Time to scan each image was 10 min. From Grimm *et al.*, 2000.

---

[37] The upward slope of the IA-IR phase boundary toward the bilayer line corresponds to the (statistically measured) kink in the Hamichi coverage data above $p=10^{-6}$ Torr, but the total coverage may not be quite as sharply varying as that, which would lead to a point at higher T as the intersection with the bilayer line.

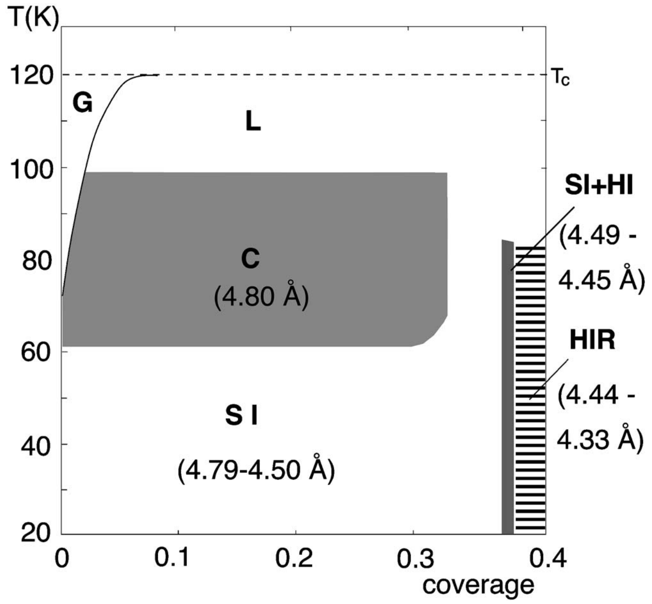

FIG. 22. Phase diagram of Xe/Pt(111) monolayer with temperature T and coverage ϑ as the axes. The $\sqrt{3}$-monolayer coverage has $\vartheta = 1/3$. The phases are 2D gas (G), liquid (L), commensurate solid (C), uniaxial incommensurate solid (stripe, SI), hexagonal incommensurate aligned solid (HI), and hexagonal incommensurate rotated solid (HIR). A two-phase coexistence region of SI and HI is noted. Adapted from Kern, David, *et al.*, 1988.

TABLE XII. Measures of energy barrier to motion or activation energies for Xe/Pt(111). The measure used for the barrier in the calculations is the substrate property most closely related to the energy to create a domain wall in the monolayer solid.

Method	Estimate (meV)	Source
Δq_{st}	30	Kern, David, *et al.* (1988)
$\omega_{0\parallel}$, HAS	21	Bruch (2003)
QHAS	<10	Ellis *et al.* (1999)
LITD	~20[a]	Meixner and George (1993a, 1993b)
Stability		
	4.0[b]	Gottlieb and Bruch (1991)
	23.7[b]	Barker and Rettner (1992)
	15.1[c]	Rejto and Andersen (1993)
A priori theory		
	33[d]	Betancourt and Bird (2000)
	45[d]	Da Silva *et al.* (2005)

[a] Value extrapolated to zero xenon coverage.

[b] Model with minimum energy atop site A, value is $E(\text{bridge}) - E(A)$.

[c] Model with minimum energy threefold site fcc, value is $E(\text{bridge}) - E(\text{fcc})$.

[d] Density-functional calculations in the local-density approximation; minimum energy site is atop, value is $E(\text{bridge}) - E(A)$.

dicted by Coppersmith *et al.* (1982). Also, they used the phrase domain-wall dynamics in a different sense to that in the adsorption literature, where the domain walls are known to have "breathing modes" (Shrimpton and Joos, 1989) and to contribute to the entropy of the layer (Villain and Gordon, 1983; Kariotis *et al.*, 1988).

In summary, it is clear that a great deal is known about the phase diagrams of adsorbed Xe on graphite. However, kinetic effects can make it difficult to determine both the C-IA and IA-IR phase boundaries. Detailed statistical models of several of these phase boundaries are also currently lacking.

2. Xe/Pt(111) and Xe/Pd(111)

Xe/Pt(111) has been the subject of an extensive effort (partially reviewed in Comsa *et al.*, 1992; Lehner *et al.*, 2002; Boutchko and Bruch, 2004) in which a unified picture has resulted from a detailed interplay of theory and experiment. The phase diagram, with coverage-temperature axes (ϑ-T), is shown in Fig. 22 (Kern and Comsa, 1988, 1991; Kern, David, *et al.*, 1988). A comparison with Xe/Pd(111) is made at the end of this subsection.

The monolayer phases include a commensurate lattice, a striped phase (unaxially incommensurate solid, not observed for Xe/graphite), and triangular incommensurate solids in aligned and rotated phases. The (dilated) commensurate solid becomes stable above about 60 K, i.e., by thermal expansion. In contrast to the case of Xe/graphite, direct thermodynamic measurements such as adsorption isotherms, compressibility, and specific heat are scarcely available for Xe/Pt(111). Information on the monolayer comes mostly from electron diffraction and helium atom scattering experiments.

From early observations of a dilated commensurate Xe/Pt(111) lattice with nearest-neighbor spacing 4.80 Å (Poelsema *et al.*, 1983), it was evident that a large corrugation energy was needed to stabilize it.[38] However, it was not until 1990 that it was recognized that the large corrugation carried another surprise (the atop site adsorption) with it. After that, albeit with irregularities described in Sec. IV.B, there was steady progress. Several estimates of the energy barrier to Xe motion on the Pt(111) surface are summarized in Table XII. The best estimate for the full Xe/Pt(111) energy surface remains the Barker-Rettner model (Barker and Rettner, 1992).

It is instructive to examine the ambiguities in the methods used for the estimates in Table XII. The first estimate (Kern, David, *et al.*, 1988) assigned an increment in the isosteric heat of adsorption at the commensurate-to-incommensurate transition to a barrier to xenon motion. However, domain walls are created in that process and their energy includes a balance

---

[38] Nevertheless, the ground state of the monolayer solid at low temperatures is an incommensurate triangular lattice, as demonstrated by a STM image of the submonolayer solid (Brunet *et al.*, 2002), with $L = 4.45 \pm 0.02$ Å at 8 K, consistent with Fig. 22.

TABLE XIII. Diffusion parameters for rare gases. Unless otherwise noted, the coverage ϑ is the ratio of adatoms to top-layer substrate atoms. The MC and MD methods are computer simulations based on realistic adatom-substrate potential surfaces. Data are grouped as single adatom diffusion, diffusion in the presence of condensed phases, and diffusion in the presence of substrate surface steps.

Substrate	Adsorbate	ϑ	T (K)	E_{dif} (meV)	D_0 ($\text{cm}^2\,\text{s}^{-1}$)	Method
Single adatom						
Pt(111)	Xe[a]	0.017	105	≤ 10		QHAS
With dense 2D phases						
W(110)	Xe[b]	0.3	54–72	50 ± 10	7×10^{-8}	FEM
W(110)	Xe[b]	0.9	67–83	50 ± 10	$10^{-9}-10^{-8}$	FEM
Pt(111)	Xe[c]	0.02	80	~20		LITD
Pt(111)	Xe[c]	0.08	80	52 ± 9	$3.4\times10^{-4\pm0.5}$	LITD
Pt(111)	Xe[c]	0.333	80	56 ± 4	$1.1\times10^{-4\pm0.2}$	LITD
Ni(111)	Xe[d]	0.04	30–60	14.3 ± 0.9	2×10^{-9}	LOD
Ni(111)	Xe[d]	0.16	30–60	17.4 ± 1.7	3×10^{-8}	LOD
Nb(110)	Xe[e]	0.235	48–70	54	1.7×10^{-6}	LOD
Pt(111)	Kr[f]	0.47	45	48	1.5×10^{-4}	LITD
Pt(111)	Kr[f]	0 (extrap)	45	18	1.5×10^{-4}	LITD
Pt(111)	Xe[g]	2D cluster	65–80	51 ± 5		MC
Si(100)	Xe[h]	0.5	40–150	31.1 ± 0.6	$(8.6\pm0.5)\times10^{-5}$	MD
				33.6 ± 0.9 ($\perp$)	$(8.0\pm1.0)\times10^{-5}$	
				30.0 ± 0.8 ($\parallel$)	$(9.9\pm1.1)\times10^{-5}$	
With substrate steps						
Pt(11,11,9)	Xe[i]	0–0.4	59–92	120 ($\parallel$)	50	LITD
Pt(11,11,9)	Xe[i]	0–0.4	59–92	195 ($\perp$)		LITD

[a] $\gamma\leq0.25\ \text{ps}^{-1}$, Eq. (26), from Ellis *et al.* (1999).

[b] $\vartheta=1$ is $n=5.5\times10^{14}/\text{cm}^2$, from Chen and Gomer (1980).

[c] Meixner and George (1993b).

[d] Nabighian and Zhu (2000).

[e] Thomas *et al.* (2003).

[f] Meixner and George (1993a); see also Carlsson and Madix (2001), who estimate the activation energy for migration of Kr on Pt(111) terraces at low coverage to be 23 meV.

[g] Sholl and Skodje (1995).

[h] See the discussion in Sec. V.B.1, from Utrera and Ramirez (1992).

[i] Sneh and George (1994).

of Xe-Xe forces and Xe-Pt forces. This balance is included in the stability calculations (Gottlieb and Bruch, 1991; Barker and Rettner, 1992; Rejto and Andersen, 1993) cited in the table, and the increment can be reproduced with rather different energy barriers, depending on the model used for Xe-Xe interactions. Second, the barrier estimated from the activation energy for surface diffusion of the xenon has a strong dependence on coverage, as shown in the values cited in Table XIII and recognized in other analyses of surface diffusion. In fact, the energy barrier and the activation energy in an Arrhenius fit to the diffusion constant were found to differ by 30% in a model calculation (Sholl and Skodje, 1994) for Xe/Pt(111). Third, the energy barrier for motions in the low-density 2D Xe gas inferred from QHAS (Ellis *et al.*, 1999), discussed in Sec. V.A, is very low and differs from the value inferred from $\omega_{0\parallel}$ in another HAS experiment (Bruch *et al.*, 1998).

Inelastic helium-atom scattering has measured the phonon-dispersion curves in the commensurate solid and in the compressed monolayer solid just before bilayer condensation (Bruch *et al.*, 1998, 2000). The in-plane dispersion relation for the commensurate solid has a zone-center gap from the broken translational symmetry and only a small amount of dispersion, because the 4.80 Å nearest-neighbor spacing is within 1% of the spacing of the inflection point in the Xe-Xe pair potential (Dham *et al.*, 1990). Observation and analysis of the three branches of the monolayer phonon-dispersion curves (Bruch *et al.*, 2000), Fig. 12, give the most direct proof that the Xe-Xe interactions are normal that is available for any of the physisorbed monolayers.

The Xe/Pt(111) system also has been used to demonstrate the effects of hybridization of adlayer motions with the platinum substrate (Hall *et al.*, 1989). Lehner *et al.* (2002) made a study of TPD experiments on this system and showed that the activation energy for desorption agreed well with the monolayer heat of condensation, Table II.

Xe/Pd(111) is an adsorption system that has many parallels to Xe/Pt(111) (Caragiu *et al.*, 2002; Zhu *et al.*, 2003). It has been the subject of a recent investigation by Zhu *et al.* (2003); see also the discussion in Sec. IV.B and entries in Tables VII and VIII. There is a $(\sqrt{3} \times \sqrt{3})R30°$ solid at monolayer condensation for temperatures from 40 to 80–100 K. Incommensurate solids form when the layer compressed for 40–70 K. However, no uniaxially incommensurate lattice is observed, in contrast to Xe/Pt(111), and the succession of solid phases is triangular commensurate, triangular incommensurate-aligned, and triangular incommensurate-rotated, similar to the succession of phases observed for Kr on graphite; see Bruch *et al.* (1997). It appears the Xe is more strongly bound to Pd(111) than to Pt(111) and this correlates well with the values for d_{AS} in Table VII.

3. Xe/Cu(110)

In contrast to Sec. IV.E.2, there is not an agreed unified picture for Xe/Cu(110), in spite of a long and intensive experimental effort (reviewed in Boas *et al.*, 2003).

The 2D monolayer solids observed for Xe/Cu(110) are uniaxially incommensurate lattices (Glachant *et al.*, 1984) or HOC $(n \times 2)$ lattices simply commensurate along the [001] direction (Zeppenfeld *et al.*, 1996). The stability along [001] implies a large energy corrugation perpendicular to the Cu atom rows. The barrier to xenon motion along [001] inferred from the zone-center frequency gap, see Table IX, is 10.4 meV and agrees well with the 11 meV inferred from observations of surface diffusion (Dienwiebel *et al.*, 2000). It also agrees with an estimate of 7–10 meV for the barrier based on a zero-temperature calculation of stability with unperturbed Xe-Xe interactions (Bruch, 1985). Finally, LEED experiments established that the uniaxially incommensurate xenon rows are adsorbed above rows of copper atoms (Caragiu *et al.*, 2003); see Table VII.

Two experiments indicate the Xe-Xe interactions for Xe/Cu(110) are similar to those for Xe/Pt(111). First, the 2D heat of sublimation is found (Ramseyer *et al.*, 1994) to be 47±9 meV, rather close to the value 48±5 meV (Poelsema *et al.*, 1983) for the 2D sublimation from the $(\sqrt{3} \times \sqrt{3})R30°$ solid of Xe/Pt(111). Second, the monolayer compressibilities in Table X, at comparable area per xenon, are equal for the two systems to within the substantial (20%) uncertainties in the values derived from experiments (Bruch *et al.*, 2000). Further, there has been much success in modeling the properties of the HOC lattices using normal Xe-Xe interactions (Zeppenfeld *et al.*, 1996; Ramseyer *et al.*, 1997).

However, Boas *et al.* (2003) assigned the dispersive branches observed in their inelastic helium-atom scattering experiments on Cu(110)-$c(26 \times 2)$-30Xe at $T=35$ K to a xenon monolayer solid with much reduced Xe-Xe force constants. That assignment can be used to estimate the monolayer compressibility, in a manner analogous to the construction for triangular lattices with Eq. (24). For this, assume that the xenon atoms interact by central pair potentials ϕ and that substrate corrugation along the $[1\bar{1}0]$ direction can be neglected. Then the bulk modulus for uniaxial compressions along this direction is, with A the area per adatom,

$$B_T(UI) = (1/2A)\sum_j \{(R_x^4/R^2)[d^2\phi/dR^2 - (1/R)d\phi/dR] + (R_x^2/R)d\phi/dR\}|_{R=s_j}. \quad (25)$$

Similarly the speed c_ℓ of the longitudinal acoustic (LA) branch for wave vector $\mathbf{q}$ aligned along $[1\bar{1}0]$ can be calculated from $B_T(UI)$ using $mc_\ell^2 = AB_T(UI)$.

The $c(26 \times 2)$Xe/Cu(110) lattice is quasihexagonal with a nearest-neighbor distance of 4.42 Å along the $[1\bar{1}0]$ direction and area $A=15.9$ Å^2. Boas *et al.* assigned a phonon branch with $c=6.1 \times 10^2$ m/s to the LA mode, although there are a few points at small q with $c=9.5 \times 10^2$ m/s that agree with earlier calculations of Ramseyer *et al.* (1994, 1997) for a LA branch. The corresponding values of the isothermal compressibility are 2.0 and 0.8 m^2/J, respectively. The latter is close to the values for Xe/Pt(111) at $A=16.2$ Å^2 in Table X. The former is distinctly larger than the value of Glachant *et al.* (1984) for uniaxial compression of Xe/Cu(110) from $A=16.8$ to 16.1 Å^2, although for smaller area per adatom it would normally be expected to be smaller than 1.1 m^2/J. Thus there may have been a misassignment of the observed $[1\bar{1}0]$ branches (Bruch, 1997). The energies of phonons observed with $\mathbf{q}$ along the [001] axis do not become understood with a reassignment, though.

This puzzle is largely distinct from a dispute (Boas *et al.*, 2001; Zeppenfeld *et al.*, 2001) over the assignment of a very energetic mode at 3.7 meV. Zeppenfeld *et al.* fitted their inelastic helium scattering data for the mode to a model with normal gas-phase xenon interactions. Boas *et al.* instead assigned the mode as an extrinsic effect arising from (large) contamination by carbon monoxide (CO) and do not consider it to be a signature of the xenon interactions.

V. DIFFUSION OF PHYSISORBED GASES

Virtually all processes that occur on surfaces involve some transport of atoms or molecules and, therefore, understanding surface mobility is an important part of understanding surfaces. Both the theoretical (Ala-Nissila *et al.*, 2002) and experimental aspects (Barth, 2000) of surface diffusion have been reviewed recently. These reviews survey the wide range of experimental and theoretical studies of surface diffusion, but we concentrate here on aspects of surface diffusion of physisorbed species.

Adatoms experience a lateral variation in potential energy due to the atomic lattice of the substrate, and diffusive motion involves the traversal of this corrugated potential surface. The range of the variation in potential energy along a diffusion path is called the diffusion barrier. An adatom whose thermal energy is very small compared to the diffusion barrier will tend to be mostly confined to potential minima (adsorption sites) with occasional hops from site to site that are driven by thermal energy fluctuations. For isolated adatoms, these hops will be random. If the thermal energy is comparable or large compared to the corrugation, the lateral motion of the adatoms will be largely unaffected by the substrate structure, and motion will consist of lateral jumps that are dictated by (random) fluctuating adatom-substrate energy exchanges, as in Brownian motion (Barth, 2000). Increasing the coverage to values where the adatoms interact with each other leads to many more possibilities that depend on the nature of the interadsorbate interactions (Ala-Nissila *et al.*, 2002). The measurement and modeling of the diffusion of physisorbed species, therefore, provide a way to obtain a more complete description of the adsorbate-substrate interaction, including information on the frictional damping that is part of the adsorbate-substrate energy exchange, and on adatom-adatom interactions.

A temperature-dependent diffusion coefficient D is one parameter used to describe single-particle diffusion. It is the proportionality constant between particle current and concentration gradient. For the limiting case in which the thermal energy is large compared to the diffusion barrier, the diffusion coefficient is given by

$$D = k_B T / m\gamma, \tag{26}$$

where γ is a frictional parameter associated with the particle motion. When the thermal energy is small compared to the diffusion barrier, the situation is described by a hopping model in which the isolated particle (also called tracer and self) diffusion coefficient is expressed as

$$D = (1/2d)\langle\lambda\rangle^2 \Gamma_h = D_0 \exp(-E_{\mathrm{dif}}/k_B T), \tag{27}$$

where $\langle\lambda\rangle$ is the mean jump length, Γ_h is the jump rate, E_{dif} is the diffusion barrier energy, and d is the dimensionality of the diffusion process. The prefactor D_0, often called the diffusivity, is equal to $(1/2d)\langle\lambda\rangle^2 \nu_0$, where ν_0, the attempt frequency, is related to the lateral vibrational frequency of a localized adatom, another measurable parameter.

The diffusion properties of single adatoms or admolecules are very difficult to measure, because most experimental techniques do not follow the motion of a single particle; rather, they measure the evolution of concentration gradients. Although experimental data for the diffusion coefficient usually are interpreted using Eq. (27), D_0 and E_{dif} thus obtained must be recognized as complicated averages over local configurations. The presence and interaction of other adatoms also change the measured diffusion properties, which complicates the interpretation but also provides the potential for measuring interadsorbate interactions through their diffusion properties. That is, when experimental data for the monolayer diffusion constant are fitted with Eq. (27), the inferred energy E_{dif} generally includes contributions from adsorbate-adsorbate interactions as well as from the substrate surface corrugation energy.

The diffusion of physisorbed gases has been studied using several experimental techniques, including field emission microscopy (FEM), laser-induced thermal desorption (LITD), linear optical diffraction (LOD), quasielastic helium-atom scattering (QHAS), and quasielastic neutron scattering (QNS), and also by simulations. Each technique has its strengths and weaknesses and these will be discussed along with the findings. The FEM, LITD, and LOD studies generally obtain diffusion parameters by the measurement of concentration gradients while QHAS and QNS study single-particle diffusion, with or without the presence of other ad-particles.

Some other estimates of the barriers to diffusion are based on the thermodynamic stability of commensurate phases and values deduced from measurements of the zone center energy gap for overlayer phonons polarized parallel to the surface (see Sec. IV.C.2 and Table IX). A measure of the diffusion barrier has also been obtained from density-functional theory calculations for adsorbed gases by calculating their configurational energies for adsorption on different sites (DaSilva *et al.*, 2003, 2005; Da Silva and Stampfl, 2007).

As discussed in Appendix A.1.a, the coverage measure ϑ is the ratio of the number of adatoms to the number of atoms in the top substrate layer.

A. Single adatom diffusion of rare gases in the 2D gas phase

The diffusion of Xe atoms in the 2D gas phase on Pt(111) was studied using QHAS and employing a time-of-flight technique (Ellis *et al.*, 1999). The experiments were carried out at the relatively high temperature of 105 K and the low coverage of $\vartheta = 0.017$ in order to avoid the formation of islands. The measured quasielastic peak shape is Gaussian and Fig. 23 shows that the peak width Γ (FWHM) for the gas phase of Xe on Pt(111) varies linearly with momentum transfer $\hbar\Delta k$. This dependence of Γ is consistent with an ideal gas under these conditions (Ellis *et al.*, 1999), for which

$$\Gamma = 2\sqrt{\ln 2}\,\hbar v \Delta k, \tag{28}$$

where v is the root-mean-square adatom speed. The straight line through the data in Fig. 23 uses the value $v = 115\ \mathrm{m/s}$ expected for a 2D Xe gas at 105 K. Molecular-dynamics simulations for the QHAS experimental conditions were performed in order to determine upper limits for the frictional coupling parameter and the diffusion barrier; these were found to be $\gamma \leq 0.25\ \mathrm{ps}^{-1}$ and $E_{\mathrm{dif}} \leq 10\ \mathrm{meV}$. This bound on E_{dif} is much smaller than the 20–30 meV range of most estimates for monolayer Xe/Pt(111); see Table XII. The length scale probed in these QHAS studies is of the order of the interadsorbate distances and, therefore, the effect of any relatively widely dispersed surface defects, such as steps, on adatom diffusion will be negligible.

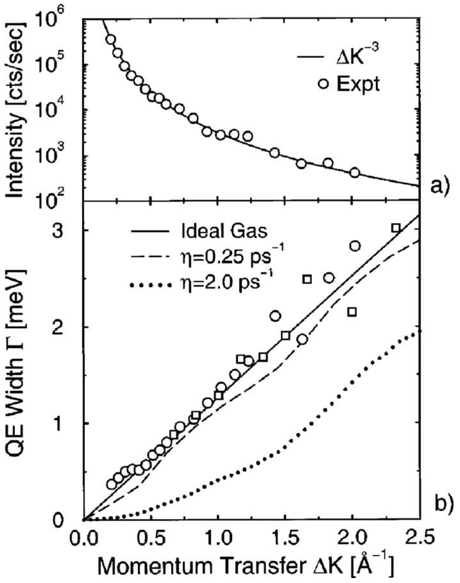

FIG. 23. Diffusion of 2D Xe gas on Xe/Pt(111) at $T_s=105$ K by QHAS. (a) The momentum transfer dependence of the QHAS peak intensity at $\Delta E=0$, $E_i=10.15$ meV. (b) Measured momentum dependence (circles, $E_i=10.15$ meV; squares, $E_i=26.85$ meV) of the peak width (FWHM) compared to calculations for an ideal 2D gas and for a 2D gas on a flat surface with specified friction coefficients. From Ellis *et al.*, 1999.

B. Diffusion of adsorbed gases in the presence of 2D condensed islands

1. Adsorbed rare gases

Table XIII summarizes the measured diffusion parameters for rare gases. The diffusion barrier energy and diffusivity, E_{dif} and D_0, are related to the measured translational diffusion constant D by Eq. (27). The experiments on which these are based are reviewed in this subsection. It is evident from Table XIII that there are marked discrepancies for some of the systems. For instance, the values of E_{dif} reported for Xe on Pt(111) vary from <10 to 56 meV and span other estimates for the energy barrier given in Table XII. Much of the variation can be attributed to measuring the overlayer under different conditions, but at this time there is still no clear picture of how to understand the differences in E_{dif} in terms of the multiple and complex diffusion modes that may occur.

The earliest measurements of diffusion of physisorbed gases employed a FEM shadowing technique, whereby the spreading of an adsorbate into a section of clean surface is investigated. Gomer (1990) reviewed these and other FEM studies of physisorbed gases. In the experiments, Xe adatoms moving into the clean area were almost certainly detaching from islands of condensed Xe. It was observed that the diffusion barriers for rare gases on tungsten surfaces were small, in the range of 1/4–1/2 of the heat of adsorption (Ehrlich and Hudda, 1959; Gomer, 1959; Antczak and Ehrlich, 2005). The fluctuation method of FEM, developed later, allowed more systematic and precise measurements. Then fluctuations of the emission current, which are related to fluctuations of the adsorbed density, are measured for a small surface area. The buildup or decay of these density fluctuations is statistically related to the diffusion coefficient D through its relaxation time $\tau_0=r_0^2/4D$, where r_0 is the radius of the surface area being measured. Chen and Gomer (1980) obtained a diffusion barrier for Xe/W(110) of $E_{\mathrm{dif}}=50\pm10$ meV for coverages of 0.3 and 0.9 saturated monolayers with such measurements. Their value for the diffusivity D_0 was several orders of magnitude lower than expected, a result that is still unexplained (Barth, 2000).

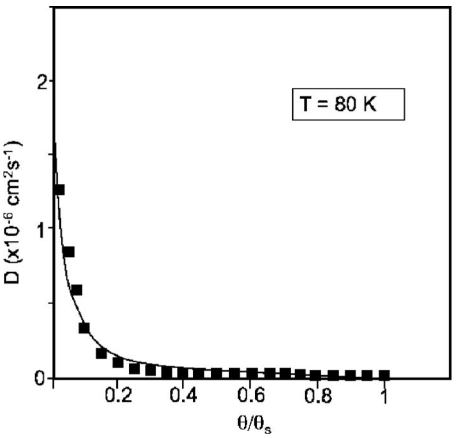

FIG. 24. Surface diffusion coefficient of Xe/Pt(111) at 80 K. Monolayer coverage is 5×10^{14} cm^{-2}. The data points show the actual diffusion constants and the solid lines are the results of calculations with a simple model for a coverage-dependent activation barrier for diffusion. Adapted from Meixner and George, 1993a.

The laser-induced thermal desorption (LITD) technique has been used to study the diffusion of Xe and Kr on Pt(111) (Meixner and George, 1993a, 1993b). The diffusion coefficients of Kr/Pt(111) at 45 K and of Xe/Pt(111) at 80 K were found to decrease sharply with increasing coverage, as shown for Xe in Fig. 24, indicating a sharp drop in the mobility of the adatoms. This was interpreted as an indication of attractive interactions between adatoms, consistent with the HAS (Kern and Comsa, 1988, 1991) and STM (Zeppenfeld *et al.*, 1994; Horch *et al.*, 1995a; Brunet *et al.*, 2002) experiments that show island formation at low submonolayer coverages. Later measurements on a stepped Pt(11,11,9) surface (Sneh and George, 1994) provided strong evidence that the coverage dependence of diffusivity is indeed due to island formation, suggesting that the diffusion parameters deduced from the flat surface studies include processes such as detachment and attachment of adatoms to the edges of islands. The diffusion of Xe on Pt(11,11,9) was also found to be highly anisotropic, with the diffusion coefficient perpendicular to the steps being two orders of magnitude lower than that parallel to the steps at 90 K. These values imply a coefficient for diffusion on the terrace that is three orders of magnitude larger than that for diffusion across the step. The barrier for diffusion across the step was estimated to be about 195 meV.

Surprisingly, the barrier for diffusion parallel to the step was measured to be about 120 meV (Sneh and George, 1994), i.e., more than twice as large as the values obtained in the earlier measurements on the flat Pt(111) surface (Meixner and George, 1993b). This apparently anomalous value may arise from something more complicated than simple terrace diffusion; e.g., diffusion along the step edges would be consistent with the row growth at the step edges observed using HAS (Marsico *et al.*, 1997; Pouthier *et al.*, 1997), Sec. IV.B.3.

Diffusion of entire Xe islands on Pt(111) was studied using Monte Carlo simulations (Sholl and Skodje, 1995). This work used the Xe-Pt(111) potential of Rejto and Andersen (1993), in which the hollows are the preferred adsorption sites, and diffusion of islands of the commensurate $(\sqrt{3}\times\sqrt{3})R30°$ structure was studied. The diffusion barrier for an isolated Xe atom in this model[39] was 22 meV and adatoms were constrained to single site hops. The main finding was that the primary mechanism for diffusion of Xe islands was by evaporation of atoms having two nearest neighbors to the surrounding 2D gas and condensation of Xe atoms at the edges of the islands; the barrier for this process was $E_{\mathrm{dif}}=51\pm5$ meV. The fact that the adsorption site array used was a honeycomb array having nearest-neighbor sites separated by 1.6 Å may affect how well it describes Xe/Pt(111), which has been shown since to have a preference for top sites, in a triangular array of sites separated by 2.77 Å (Seyller *et al.*, 1999).

The linear optical diffraction (LOD) technique has been applied to the diffusion of Xe on other metal surfaces (Nabighian and Zhu, 2000; Thomas *et al.*, 2003). On Ni(111), measurements were made between 30 and 60 K for coverages $0.04<\vartheta<0.16$ (Nabighian and Zhu, 2000), while the saturation monolayer coverage is $\vartheta=0.33$ (Wong and Zhu, 1996). The evolution of the grating gave the temperature-dependent diffusion constant $D(T)$, and D_0 and E_{dif} were determined by fitting to Eq. (27). The results are shown in Table XIII. The values for D_0 are very small and similar to the earlier values obtained for Xe/W(110) using FEM (Chen and Gomer, 1980), which themselves are not explained. Little is known about the submonolayer structure evolution of Xe on Ni(111) (Wong and Zhu, 1996), but to the extent that the behavior is similar to Xe on Pt(111), some island formation is likely at these temperatures and coverages. It was noted that the diffusion barrier measured in this study is close to the energy required to break a Xe dimer on Ni(111); if dimers form in collisions, their breakup may be the rate-limiting step in the surface diffusion. Such an effect would slow the diffusion process that is measured in an experiment of this type, as would the formation of islands.

Thomas *et al.* (2003) measured a much larger barrier for Xe on Nb(110), at temperatures between 48 and 70 K and a coverage $\vartheta=0.235$ using LOD. No overlayer order was observed by LEED for submonolayer coverages, suggesting that island formation may be hindered. There is some evidence that the first two layers have a lower density than the bulk planes of Xe (Thomas *et al.*, 2004). The derived parameters E_{dif} and D_0 for Xe/Nb(110) are given in Table XIII. In the same study, a DFT calculation gave a diffusion barrier of 51 meV, compared to the experimental value of $E_{\mathrm{dif}}=54$ meV, for hopping across the short bridges between top sites, which were found to be preferred (Thomas *et al.*, 2004). The values of E_{dif} are similar for Xe/Nb(110) and Xe/Pt(111) at similar coverages, although the diffusion process might be quite different due to differences in the structures. However, D_0 for Xe/Nb(110) is two orders of magnitude smaller than that for Xe/Pt(111).

Diffusion of Xe on Si(100)-(2×1), i.e., a surface with dimer row reconstruction, was studied using molecular-dynamics simulations (Utrera and Ramirez, 1992). The total mean-square displacements as a function of time for motion displacements parallel (y) and perpendicular (x) to the dimer rows were calculated and used to evaluate diffusion constants. The corresponding E_{dif} and D_0 are given in Table XIII. The simulations were carried out at a Xe coverage corresponding to 60% of the monolayer saturation coverage; i.e., the ratio of Xe to surface Si atoms is $\vartheta=0.5$, and it was found that the Xe-Xe interactions greatly reduce the anisotropy of the diffusion constant.

2. Molecular hydrogen

There are also some measurements of the diffusion of isotopes of molecular hydrogen, performed at such low temperatures that the molecules are in the ground rotational state and therefore effectively spherical.

Wiechert *et al.* (2003) measured the diffusive motion in the 2D liquid and solid phases of HD on graphite using QNS, to clarify the nature of the (reentrant) fluid phase intermediate to the commensurate and incommensurate monolayer solids, although the diffusion parameters were not reported. Bloss and Wyatt (2000) studied the diffusion of H_2 on solid H_2 at 2.5–3.0 K using heater-induced thermal desorption (another density gradient technique). They obtained $D_0=4.03\pm0.25$ cm^2/s (much larger than for rare gases on flat metal surfaces) and $E_{\mathrm{dif}}=43\pm7$ K (3.7 ± 0.6 meV), which includes contributions of lateral H_2-H_2 interactions. Other measures for activation energies at the bulk surface are 16.1 K for HD activation (Maruyama *et al.*, 1993) and 23 ± 2 K for H_2/H_2 and 47 ± 3 K for D_2/D_2 (Classen *et al.*, 1996). These values are in the range of the barriers to motion for isolated H_2 molecules on several dielectrics reported in Table IX.

---

[39] The static barrier on the Rejto-Andersen surface is 15.2 meV and it led to an activation barrier $E_{\mathrm{dif}}=22$ meV in calculations with a continuous diffusion model (Sholl and Skodje, 1994). Sholl and Skodje (1995) took this activation barrier to be the diffusion barrier in their jump diffusion simulation.

TABLE XIV. Translational diffusion parameters for alkanes. Coverage θ is given as a fraction of a saturated layer. E_{dif} is the diffusion barrier in meV. D is the diffusion constant, given over stated ranges of θ and T.

Substrate	Adsorbate	θ	Phase	T (K)	E_{dif}	D (10^{-5} cm^2/s)	Method
Cu(111)	octane[a]	1	liquid	200		7.5	QHAS
Graphite	methane[b]	0.3–0.63	liquid	61.7		$(3.7\pm0.7)-(4.6\pm0.5)$	QNS
Graphite	methane[b]	0.4–0.63	liquid	71.5		8.3 ± 0.8	QNS
Graphite	methane[b]	0.45	fluid	91.5		22 ± 4	QNS
Graphite	methane[b]	0.70	fluid	91.5		12 ± 2	QNS
Graphite	methane[b]	0.72	fluid	81.5–101.5		$(10\pm2)-(12\pm2)$	QNS
Graphite	methane[b]	0.9	fluid	81.5–101.5		$(3.2\pm1.0)-(6.3\pm0.5)$	QNS
Graphite	ethane[c]	0.54	I1 liquid	66.4–84.1		$\leq0.01-(0.34\pm0.06)$	QNS
Graphite	ethane[c]	0.4,0.63	I1 liquid	87,122	61	$(0.5\pm0.1),(5\pm1)$	QNS
Graphite	ethane[c]	1.3	S3 fluid	87,122		0.2,1.4	QNS
Graphite	butane[d]	0.88	fluid	121–149		$(1.0\pm0.05)-(1.7\pm0.4)$	QNS
Graphite	butane[d]	~1	fluid	$(0.99-1.29)\times T_m$		2.4–4.4	MD
Graphite	hexane[d]	0.95	fluid	190–270		$(0.14\pm0.07)-(3.5\pm0.7)$	QNS
Graphite	hexane[d]	~1	fluid	$(1.02-1.59)\times T_m$		0.3–9.3	MD
MgO(001)	methane[e]	0.8	fluid	88		0.5– 0.6	QNS
MgO(001)	methane[e]	0.8	fluid	97		1.2	QNS
Pt(111)	methane[f]	0.02		69	<2		QHAS
Pt(111)	methane[g]	0–1		45	23	0.1	LITD
Ru(0001)	propane[h]	0–1		90–116	130	0.001–0.03	LITD
Ru(0001)	*n*-butane[h]	0–1		105–140	152	$(8\times10^{-4})-(3\times10^{-2})$	LITD
Ru(0001)	*n*-pentane[h]	0–1		130–160	195	$(8\times10^{-4})-(3\times10^{-2})$	LITD
Ru(0001)	*n*-hexane[h]	0–1		150–190	208	$10^{-3}-6\times10^{-2}$	LITD

[a] Fuhrmann and Wöll (1997).
[b] Coulomb *et al.* (1981).
[c] Coulomb and Bienfait (1986).
[d] Herwig *et al.* (1997).
[e] Bienfait *et al.* (1987).
[f] Jardine *et al.* (2002).
[g] Meixner and George (1993a).
[h] Brand *et al.* (1990).

C. Diffusion measurements for adsorbed alkanes

The adsorption energies and melting temperatures of monolayer alkanes are reviewed in Sec. IV.A.6 and in Tables V and VI. Summaries of information on the diffusion, reviewed in this subsection, are presented in Tables XIV and XV. The molecule C_NH_{2N+2} is often denoted CN.

1. Methane

QHAS was used to study diffusion for methane on Pt(111) at very low coverages ($\vartheta=0.02$) and $T=69$ K, and large broadenings of the quasielastic peak were observed, as for Xe/Pt(111). A linear dependence on momentum transfer was found for the quasielastic peak width (Jardine *et al.*, 2002), indicating that CH_4 diffuses as a 2D gas at low coverages. Using simulations, the data led to a bound for the diffusion barrier of $E_{\mathrm{dif}}\leq2$ meV and the friction parameter in Eq. (26) of $\gamma\leq0.5$ ps^{-1}. Therefore, the diffusion behavior of CH_4 on Pt(111) at low coverages appears to be very similar to that of Xe (Ellis *et al.*, 1999; Jardine *et al.*, 2002). However, the effective mass required for the linear fit was 54 amu, rather than the expected 16 amu for CH_4. It was speculated that this may indicate that the CH_4 diffuses primarily as clusters. LITD studies of CH_4 on Pt(111) at 45 K found that the diffusion coefficient was independent of coverage, while TPD also suggested little or no interaction between molecules (Meixner and George, 1993a). The TPD study produced values of $E_{\mathrm{des}}=156\pm7$ meV and $\nu=1.9\times10^{11\pm0.6}$ s^{-1} for the desorption rate, Eq. (2).

The results of QNS studies of translational and rotational diffusion of CH_4 on both graphite and MgO are summarized in Tables XIV and XV. The motion in the 2D liquids appeared to be 2D Brownian diffusion for CH_4 on graphite(0001) (Coulomb *et al.*, 1979) and single-site jump diffusion for CH_4 on MgO(100) (Bienfait *et al.*, 1987). On both graphite and MgO(001), CH_4 exhibited isotropic rotational diffusion in the 2D solid phase (Thorel *et al.*, 1982; Bienfait *et al.*, 1987). Later, the tunneling between different rotational states of CH_4 on MgO was studied with inelastic neutron scattering (INS)

TABLE XV. Rotational diffusion parameters for alkanes from quasielastic neutron scattering experiments (QNS) and molecular-dynamics simulations (MD).

Substrate	Adsorbate	Coverage	T (K)	D_r (s^{-1})	Method
Graphite	methane[a]	0.6–0.9	55	$(6\pm1)\times10^{11}$	QNS
Graphite	ethane[b]	0.5	66–87	$(5\pm1)\times10^{10}$	QNS
Graphite	butane[c]	0.88	121–149	$(1.3-7.9)\times10^{9}$	QNS
Graphite	butane[c]	1?	$(0.99-1.29)T_m$	$(25-38)\times10^{9}$	MD
Graphite	hexane[c]	0.95	150–270	$(6.6-59)\times10^{9}$	QNS
Graphite	hexane[c]	1?	$(0.77-1.59)T_m$	$(0-52)\times10^{9}$	MD
MgO(001)	methane[d]	0.8	72	~0	QNS

[a] From Thorel *et al.* (1982).
[b] From Coulomb and Bienfait (1986).
[c] From Herwig *et al.* (1997).
[d] From Bienfait *et al.* (1987).

at $T=1.5$ K (Larese *et al.*, 2001). The measured splitting of the librational ground state enabled the determination of the equilibrium orientation of the molecule. The CH_4 molecule ordered with a dipod-down orientation and the C_{2v} axis normal to the surface. A later DFT study (Drummond *et al.*, 2006) concurred with this orientation assignment and also found that the most stable configuration has the methane molecules located directly above the surface Mg atoms, with pairs of H atoms oriented along the lattice lines that include adjacent surface O atoms. In this structure, neighboring methane molecules are rotated by 90° to reduce the H-H steric interactions.

2. Ethane

The diffusive motions of ethane ($N=2$) on graphite were studied using QNS (Coulomb and Bienfait, 1986). Ethane on graphite has three different solid phases at submonolayer coverages (Suzanne *et al.*, 1983). In the S1 structure, which forms for coverages up to about 0.75 saturated monolayer, the ethane molecules are ordered in a commensurate structure with the molecules lying flat on the surface and their molecular axes ordered in a herringbone arrangement. At higher coverages in the S3 structure, the molecules stand up with their axes perpendicular to the surface, with the molecules all having the same orientation. The S2 structure is intermediate to S1 and S3. At about 60–65 K, these solids melt into several fluid phases having various degrees of order. The I1 fluid phase exists for T between about 65 and 95 K and coverages below about 0.75 saturated layer. Above 95 K, this phase converts into an isotropic liquid. The diffusion parameters for ethane were measured between 66.4 and 122 K for the S1 and S3 phases and for the I1 phase. Uniaxial rotations about the C-C axis occur between 57 and 67 K for the S3 phase and between 10 and 53.5 K for the S1 phase. At higher temperature, when the structures have melted, the same type of uniaxial rotation is observed in the higher-density melt of the S3 phase, whereas the rotations are isotropic in the melted S1 phase. Translational diffusion was measured in the fluid phases. In the higher-density fluid, the molecules exhibit Brownian translational diffusion. In the lower-density fluid, the diffusion is activated with a diffusion barrier of 61 meV. The measured diffusion parameters are given in Tables XIV and XV.

3. Propane to hexane

The $N=3-6$ linear alkanes on Ru(0001) were studied using LITD (Brand *et al.*, 1990) and the diffusion parameters determined are given in Table XIV. The parameters for the desorption rate Eq. (2) obtained from the accompanying TPD measurements ranged from $E_{\mathrm{des}}=477$ meV and $\nu=3.1\times10^{16}$ s^{-1} for propane to $E_{\mathrm{des}}=651$ meV and $\nu=8.0\times10^{14}$ s^{-1} for n-hexane. The behavior in a later MD study (Cohen and Zeiri, 1992) for a series of alkanes ($N=3$, 6, 10, and 20) on W(100) using empirical potentials agreed qualitatively with the LITD study: (i) the diffusion coefficient can be described by an Arrhenius expression, (ii) the activation energy for diffusion scales with chain length, and (iii) the prefactors were essentially independent of N.

Butane/graphite forms a monolayer structure in which the butane molecules have their long axes parallel to the surface and arranged in a herringbone pattern (Herwig *et al.*, 1994). QNS studies from Herwig *et al.* (1997) indicated that the butane monolayer melts abruptly to a liquid phase in which the molecules in their *trans* (i.e., linear or normal) state rotate isotropically about their centers of mass while diffusing translationally. The measured diffusion parameters are given in Tables XIV and XV. Herwig *et al.* also reported MD simulations at experimental conditions that qualitatively agree with the QNS measurements.

A QNS study for hexane on graphite (Herwig *et al.*, 1997) found that the diffusive motion is strongly associated with the creation and annihilation of *gauche* defects in the hexane molecules. The *trans* conformation of hexane corresponds to a state in which the molecule is linear, whereas the *gauche* conformation corresponds to a state in which the molecule is folded back onto itself, forming a more globular shape. An earlier neutron dif-

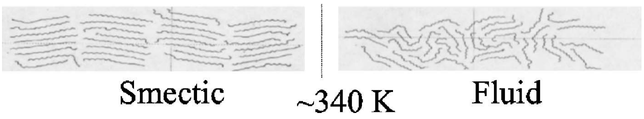

FIG. 25. Results of an MD simulation of monolayer tetracosane (C24) on graphite. The left panel shows a smectic phase at 230 K and the right panel shows the fluid phase at 350 K. The transition temperature is ~340 K. From Hansen *et al.*, 2004.

fraction study (Hansen and Taub, 1992) suggested that the melting of a hexane monolayer on graphite is initiated by a change from *trans* to *gauche* conformation of the hexane. The QNS study was performed to look for evidence for this in the quasielastic scattering below the melting point. A quasielastic component appeared at T near $0.9T_m$, whereas an elastic component was present up to about $1.3T_m$. With the help of MD simulations, the interpretation of these findings is that at $T<0.9T_m$ most molecules are in the *trans* state and the structure is ordered in a herringbone configuration. At $T=0.9T_m$, a small fraction of the hexane molecules, which are apparently in the *gauche* conformation, diffuse rotationally about a fixed center of mass. At T_m, the rotating molecules also diffuse translationally. The fraction of molecules that are mobile then increases with T, until at $T=1.3T_m$, all molecules are mobile and increasing T results in a fluid phase of predominantly *gauche* molecules. The diffusion constants determined from these experiments are given in Tables XIV and XV.

4. Octane, nonane, and decane

Monolayers of *n*-octane, *n*-nonane, and *n*-decane ($N=8-10$) on Cu(111) were studied using HAS and LEED (Fuhrmann and Wöll, 1997; Fuhrmann *et al.*, 1999). Similar to the situation for the shorter alkanes on other surfaces, these formed ordered 2D lattices with molecular axes parallel to the surface at $T<160$ K and, furthermore, with the C-C-C planes parallel to the surface. At higher temperatures, the structures disordered into liquidlike states at transition temperatures that increased slightly with the alkane length. For octane, the diffusion coefficient of this liquid was measured using QHAS to be 7.5×10^{-5} cm^2 s^{-1} at 200 K. The vibrational excitations showed evidence for the creation of *gauche* conformers at the transition, similar to the case of hexane on graphite studied by QNS.

5. Tetracosane

QNS experiments in conjuction with MD simulations (Hansen and Taub, 2004; Taub *et al.*, 2004) for monolayer *n*-tetracosane (C24) on graphite determined that the molecule begins to rotate about its long axis at 160 K and that the 2D crystalline phase has its molecular axes parallel to the substrate at low T and transforms at about 215 K to a smectic phase, shown in Fig. 25. Additional broadening of the quasielastic peak above 230 K is interpreted as rotation about other axes as well as translational diffusion. At this point, the molecules are no longer linear but have *gauche* defects that are dynamically created and annihilated, contributing to the observed rotational diffusion. These relatively slow diffusive motions occur on a time scale of order 0.1–4 ns (Hansen *et al.*, 2004).

Recent QNS experiments have studied the molecular diffusive motion in thin fluid films of C24 adsorbed on graphite (Diama *et al.*, 2007). They demonstrated that molecules in the third layer of the trilayer film have different dynamical properties from the first two layers and from the bilayer at 330 K, about 10 K below the monolayer melting point.

6. Heptane on dotriacontane

Fuhrmann *et al.* (2000) performed a QNS study on a heptane (C7) monolayer that was vapor deposited over a dotriacontane (C32) monolayer on exfoliated graphite. This system was of interest because it was expected to represent the diffusive processes in selective adsorption. At 294 K, the translational and rotational diffusion constants were found to be $D=1.2\pm0.2\times10^{-5}$ cm^2 s^{-1} and $D_r=(22\pm5)\times10^9$ s^{-1}, respectively. The value for D is the same as found for bulk heptane.

VI. EXTENSIONS TO OTHER SYSTEMS

A. Multilayer growth

Physisorbed multilayers of rare gases have been used to trace the evolution of adsorbed films from atomically thin to near bulk (Dash, 1988; Zhu and Dash, 1988). The phenomena which occur include wetting, limited wetting, surface melting, and preroughening. Tartaglino *et al.* (2005) gave a broad overview with only limited emphasis on the observations and analysis of physisorbed layers. Here we summarize what has been accomplished for multilayers of rare gases. Some aspects of the monolayer phases repeat in the next few layers and there is evidence for solid, liquid, and gas phases. For instance, in the bilayer and trilayer of Ar/graphite, transitions corresponding to melting of the topmost layer are identified and a triple point for that layer is determined (Day *et al.*, 1993). The most striking developments have been for the layering transitions of thicker films.

Adsorption isotherms for Ar, Kr, and Xe adsorbed on graphite or boron nitride powders show several successive sharp layer condensations (steps) as the pressure increases, as illustrated for Kr/graphite in Fig. 1 and for Ar/graphite in Fig. 26. The steps become rounded as the temperature increases. Critical temperatures for each layer condensation are determined and seem to approach a limit as the layer index increases from 2 to 5–7. For a long time, it was thought that the sequence of layer critical temperatures would have the roughening temperature of the bulk solid as its limit (e.g., De-Oliveira and Griffiths, 1978; Larher and Angerand, 1988). However, around 1990 it was shown that the ex-

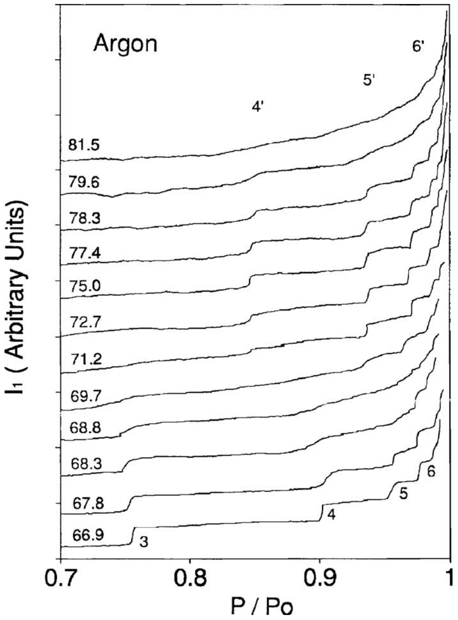

FIG. 26. Multilayer adsorption isotherms for Ar/graphite measured by ellipsometry and illustrating the phenomenon of reentrant layering. Coverage as a function of reduced pressure (p_0 is the saturated vapor pressure at the stated temperature, at the left axis). The integer indices number the layering transition and the primed indices identify the offset resumption of discontinuous layering. From Youn *et al.*, 1993.

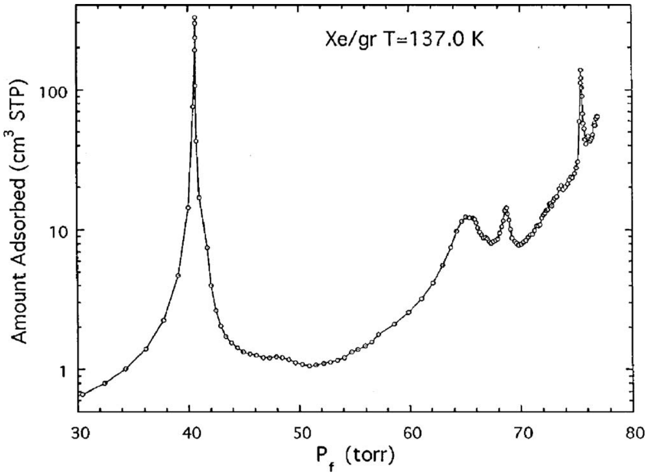

FIG. 27. Derivative of the adsorbed amount as a function of pressure for Xe/graphite at 137 K. The ordinate is $\partial N_{\mathrm{ads}}/\partial \ln p|_T$, where 10 cm^3 STP is 4.5×10^{-4} mol. The film goes through a layering sequence with increasing pressure and sharp peaks correspond to nearly vertical steps in the adsorption isotherm. The peak at 40 torr reflects the condensation of a solid second layer. The succeeding peaks are as follows: at 66 torr, condensation of liquid third layer; at 70 torr, freezing of third layer under a liquid fourth layer; and a sharp (reentrant step) peak at 76 torr for the freezing of layer four under a liquid fifth layer. From Phillips and Larese, 1997.

perimental situation is richer and a rather different picture emerged involving preroughening and surface melting (Bienfait and Gay, 1991; den Nijs, 1991; Hess, 1991). For thick enough films, at the limit of the layer critical points, there is a solid multilayer with top layer of fluid.[40] The transition at which this fluid layer (of half the density of the underlying layers, in the ideal case) forms is called the preroughening transition. At higher temperatures, but still below the 3D triple point temperature T_t, the thickness of the fluid layer increases, a process termed surface melting. The roughening transition, in which the solid surface develops a large interfacial width, does not seem to have been demonstrated for rare-gas multilayers yet, although it may be associated with the limit of the critical points of reentrant layering (Youn *et al.*, 1993). For Ar, Kr, and Xe, the characteristic temperatures scale with the 3D T_t (83.81, 115.76, and 161.39 K, respectively).

The relaxation of lattice constants in the initial stages of multilayer solid has been demonstrated for layers of xenon on Ag(111) by Dai *et al.* (1999) for $T/T_t<0.4$. A closely related experiment by Igarashi *et al.* (1998), using a combination of low-energy electron diffraction and ellipsometry, demonstrated a lack of roughening for thick films of Xe/Ag(111) at 35–57 K, $T/T_t=0.21-0.35$. Kerner, Stein, *et al.* (2005) gave a proof that the top layer of a multilayer solid of $\mathrm{Xe/Ru}(10\bar{1}0)$ is solid by demonstrating that there was no detectable diffusion from the grating created in an LOD experiment for $T/T_t<0.4$. At the other limit, Rieutord *et al.* (1997) demonstrated the onset of a fluid layer atop an argon multilayer, Ar/MgO(001), at 70 K ($T/T_t\approx 0.84$) and a divergent thickness of liquid layer as $T\rightarrow T_t$. Argon followed the scenario of a preroughening transition because the initial liquid layer amounted to approximately a half-layer jump in adsorbed mass.

The phenomenon of reentrant layering (Hess, 1991; Day *et al.*, 1993; Migone *et al.*, 1993; Youn *et al.*, 1993) was first demonstrated in adsorption isotherms. In this case, at temperatures above the critical temperature for the layering transition, there is a resharpening of the isotherm at total coverages offset from the nominal integer multiples of monolayer coverage by about one-half unit, as shown in Fig. 26. The signatures of the transitions can be made more prominent by plotting the compressibility along an isotherm, as shown for Xe/graphite at 137 K ($T/T_t=0.85$) in Fig. 27. There has been much discussion about how universal the reentrant layering phenomenon is and what process is giving rise to the evident thermodynamic singularities (Day *et al.*, 1993; Youn *et al.*, 1993; Choi *et al.*, 2005, 2006). For films about

---

[40] In the language of lattice gases, the transition in the top layer is from ordered to disordered flat (DOF). In the DOF phase, the top layer is only partially complete and lacks positional order. There is a proliferation of unit height steps (a step liquid), but the height-height correlation function remains quite limited (the steps compensate) instead of developing the divergence that is associated with the roughening transition. In atomistic models, with continuous displacements, the top layer becomes a medium density fluid with a substantial population of vacancies in the solid layer below it and a small population of adatoms in a layer of 2D gas above it.

three layers thick, there seems to be a correlation with a melting transition in the layer just below a half-filled surface fluid layer, i.e., a liquid layer freezes under compression driven by the condensation of the next (partial) layer. The melting transitions in the bilayer and trilayer show up in the specific-heat measurements of Day *et al.* (1993) on Ar/graphite. It is expected that universal behavior should be observed for the layering and reentrant layering of thick films, but there are differences for two to five layer films between adsorption on graphite and on boron nitride (summarized in Diama and Migone, 1999).

The modeling of reentrant layering poses major problems for computer simulations. Phillips and Larese (1997) were able to reproduce layer-melting transitions and the major qualitative features of data of Zhang and Larese (1995) for multilayer Xe/graphite at $T/T_t = 0.85$ and 0.90. However, their simulations used the canonical ensemble (constant N) and so questions remained about whether some of the conditions were two-phase coexistence. A later simulation by Celestini *et al.* (2000) in the grand-canonical ensemble reproduced the phenomenon of top layer solidification right after it is covered by the next half-layer of fluid. That condensation transition had half occupancy of the new top fluid layer, agreeing with the preroughening scenario. Another simulation for a Lennard-Jones fcc(111) surface by Jayanthi *et al.* (2000) gave estimates of $T/T_t = 0.83$ for the preroughening transition and $T/T_t = 0.94$ for the roughening transition. The data of Youn *et al.* (1993) for Ar, Kr, and Xe on graphite gave estimates of $T/T_t = 0.81 - 0.83$ for the limit of the layer critical temperatures and $T/T_t = 0.92 - 0.94$ for the limit of the terminal temperatures of the reentrant layer transitions. Thus, the reentrant layering may well be associated with a surface roughening transition.

However, methane multilayers (3D $T_t = 90.69$ K) follow a different pattern. The solid layers of $CH_4/MgO(001)$ form with an fcc(001) surface. The limit of layer critical points from the data for layers 2–4 is $\simeq 85$ K, $T/T_t \simeq 0.94$ (Freitag and Larese, 2000), but quasielastic neutron scattering (Bienfait *et al.*, 1988) shows the top layer of a nominal 10-layer film disorders already at 72 K. The limit of the layer critical points for layers 2–5 of an fcc(111) CH_4/graphite film is $\simeq 87.5$ K, $T/T_t \simeq 0.96$ (Larher and Angerand, 1988; Lysek *et al.*, 1993). Quasielastic neutron scattering (Bienfait *et al.*, 1990) shows a disordered surface layer on a nominal 10-layer fcc(111) film at 84.1 K. The translational diffusion within the quasiliquid surface layer is anisotropic, with the diffusion coefficient parallel to the surface about 5–7 times larger than that perpendicular to the surface for quasiliquid layer thicknesses of 1–4 layers (Stocker *et al.*, 1997). Reentrant layering has not been observed for methane multilayer films (Diama and Migone, 1999), but the extrapolated limit of the layer critical points is (perhaps coincidentally) close to the Jayanthi *et al.* (2000) estimate of a roughening transition and certainly is higher than the temperature for the onset of surface melting.

The more traditional question of conditions for limited layer growth versus extended layer-by-layer growth continues to be explored. A useful guide is that limited layer growth is likely to occur when the monolayer or bilayer is a poor template for growth of the 3D solid. However, new conditions are being encountered. The growth mode of long alkanes on SiO_2 surfaces can be remarkably different (Schollmeyer *et al.*, 2002, 2003) from the Stranski-Krastanov limited layer growth for rare gases or small molecules. Those usually have a few layers of rather similar packing; this is also found for short alkanes (Wu *et al.*, 2001). However, the long C32 alkane has two flat layers and then one layer in perpendicular stacking before bulk nucleation (Mo *et al.*, 2003, 2004; Trogisch *et al.*, 2005), as described in Sec. II.A.2.

A new line of research has determined the phase diagram of multilayers with coadsorbates and displacive/substitutional transitions (Weber and Goodstein, 1999, 2002, 2006). Combinations that have been studied include CH_4/CCl_4 and Kr/CCl_4 on graphite.

B. Buffer layers

In 1989, an experiment showed that it was possible to grow Co films on top of Xe films on GaAs (Waddill, Aldao, *et al.*, 1989; Waddill, Vitomirov, *et al.*, 1989). This buffer layer of Xe was then slowly desorbed, providing a soft landing for Co onto GaAs(110). The motivation for this application of physisorbed films was that earlier it had been impossible to make abrupt metal-insulator interfaces due to substrate restructuring that occurs when the metal was evaporated directly onto the semiconductor. The nearly perfect interfaces produced with this technique show unique electronic characteristics without the metal-induced gap states that typically were observed with other deposition methods (Waddill *et al.*, 1990). This technique has now been developed and extended to the production of size-selected metal nanocrystal arrays (Huang *et al.*, 1998), whose characteristics can be controlled by adjusting the thickness of the Xe layer. The thermodynamic processes involved in the formation of such films have been analyzed, leading to the conclusion that the motion of the nanoparticles is driven by phonons in the semiconductor and metal film and is controlled by the friction between the metal and the rare-gas buffer layer (Antonov *et al.*, 2003, 2004). The electronic properties of suspended metal nanoparticles on metal surfaces have been studied using photoemission. For Xe thicknesses of 60 layers, metal clusters were decoupled from the substrate. The electronic levels of the clusters were referenced to the vacuum level of the substrate, rather than to its Fermi level. This allowed the observation of filled electronic states in the cluster that are above the Fermi level of the substrate for the case of Pb clusters on Au(111) (Irawan *et al.*, 2006).

The so-called BLAG (buffer-layer-assisted growth) technique has been extended for use in laser patterning of metal films and, for instance, has been shown to allow the production of a submicron gold grating on Ru(0001) (Kerner and Asscher, 2004; Kerner, Horowitz, *et al.*,

2005) and the formation of magnetic nanostructures (Gai *et al.*, 2002; Shen *et al.*, 2003). It has also been extended to the use of reactive physisorbed layers, i.e., by depositing a material that chemically reacts with the physisorbed film. Thus, it is possible to grow MoC particles on Au(111) by adsorbing Mo onto a physisorbed ethylene film on the gold surface (Horn *et al.*, 2005). The same technique has been employed to grow MgO films on Au, by depositing Mg onto a physisorbed O_2 overlayer (Kim *et al.*, 2004). Other studies have used the physisorbed buffer layer technique to grow semiconductor nanoclusters (Yoo, Li, *et al.*, 2003; Yoo, Zhang, *et al.*, 2003) and metals on insulators (Gai *et al.*, 2002; Yan *et al.*, 2002). The use of buffer layers was recently extended to the growth of semiconducting clusters on Si surfaces (Antonov *et al.*, 2006). It was demonstrated that photoluminescent CdSe quantum dots and rods could be self-assembled and delivered to the Si surface, opening the door to the synthesis of optoelectronic nanodevices such as UV-visible range quantum dot lasers and high-efficiency solar cells (Antonov *et al.*, 2006).

VII. DISCUSSION AND CONCLUSIONS

The field of physical adsorption has shown steady progress during the past 10 years. There is a core of established results and some topics are quite thoroughly developed while others are still in a period of rapid change. In particular, there has been considerable progress in the understanding of fundamental interactions in simple atomic physical adsorption during the past 10 years. This has come about largely as a result of coupled experimental and theoretical efforts. New experiments on adsorption kinetics, thermal properties, lattice dynamics, and adsorption geometries have provided important input for the development of more realistic potentials, and the first steps have been taken to describe physisorption interactions using *ab initio* methods. In some areas, the body of experimentally derived quantities is now sufficient for identifying trends among different systems, such as Xe on close-packed metals, and for making connections between different measurements of the same system, as shown for Xe on graphite. The higher precision and sensitivity in experiments coupled with improvements in theoretical modeling have led to a much more complete description of physisorption in some cases, as described for Xe on Pt(111).

At the same time, the domain of physisorption studies has expanded to include ever more complex systems, in terms of both substrates and adsorbates. Studies of adsorption on vicinal surfaces, which can be thought of as having well-characterized defects, have provided insight into adsorption on more heterogeneous surfaces as well as probing the properties of steps on metal surfaces. Studies of adsorption on more complex substrates such as quasicrystals may begin to bridge the gap between perfect and realistic surfaces. Physisorbed multilayer films provide examples of equilibrium epitaxial growth. The studies of alkanes are beginning to connect with studies of self-assembled films and have identified growth and excitation mechanisms that are likely to have an impact on the broader field of soft condensed matter. Physisorbed gases are already being used to assist and mediate growth of more complex films, as in buffer layer growth processes.

There still are fundamental questions to be answered about the interactions. A quantitative understanding of the adsorption energies of physisorbed gases, and what determines the preferred adsorption sites, exists only for a few systems and then only for high substrate perfection and specific coverages. It is still not possible to predict what structures will occur for any given gas on any given substrate. It is not even possible to accurately predict the binding energies of simple gases to metal surfaces. There are many unresolved issues in existing studies. What impedes the formation of long-range hexagonal order in some overlayers, such as Xe on Pd(100) and Nb(110)? Computer simulations of rare-gas adsorption on a quasicrystalline surface suggest that long-range ordering can be prevented by a large substrate corrugation that has no length scale or symmetry in common with the adsorbate, but there are no systematic studies for such an effect on periodic substrates.

Much remains to be accomplished in areas of kinetics and dynamics. Only a few atomistic studies for diffusion of simple gases have been performed, but such studies can provide important information on macroscopic surface phenomena such as friction. Some problems in the analysis of temperature programmed desorption (TPD) and inelastic helium-atom scattering (HAS) seem to be focused enough that they will be resolved in the near future. A more thorough understanding of the adsorbate dynamics and the dynamical effects of the coupling of adsorbate and substrate motions has relevance to improved control of dissipation mechanisms.

Physical adsorption is not an independent basic subject, nor is it one with sharp demarcations relative to related fields of adsorption and growth. Workers with a wide range of skills have contributed to the knowledge, as is evident from the bibliography. In our view, one of the main characteristics of work in this field is that the topics lend themselves very well to quantitative understanding in terms of atomic and molecular scale phenomena. In this way, one develops an improved understanding of the processes and also of experimental and theoretical methods that are applied much more broadly. We expect this pattern of activity to continue.

ACKNOWLEDGMENTS

We have benefited from discussions with G. Alexandrowicz, W. Allison, S. Clarke, J. Ellis, G. Hess, A. Jardine, W. J. Nuttall, and P. Zeppenfeld. We are grateful to A. P. Graham, A. Jardine, and R. Kariotis for unpublished figures. We thank several authors for communicating results prior to publication: C. T. Campbell, K. Fichthorn, B. Gumhalter, F. Y. Hansen, J. Z. Larese, M. R. Pederson, J. M. Phillips, and H. Taub. We thank K. Hanna and M. Winokur for help. R.D.D. acknowledges support under NSF Grant No. DMR-0505160 and the

Fulbright Foundation for a US-UK Distinguished Visiting Scholar Award.

APPENDIX A: NECESSARY THERMODYNAMICS

The application of thermodynamics to adsorbed layers has a long history, stretching back to J. W. Gibbs in the 19th century, with many details for thin layers developed in the period 1970–1980 (Larher, 1971; Steele, 1974; Price and Venables, 1976). The thermodynamic relations needed for an understanding of the terminology and notation used in this review are given in this appendix, which is based on Venables (2000), especially Chap. 4 and Appendix E.

1. Phase diagrams and derived quantities

Several formats of phase diagram are useful in studies of one-component adsorbed layers. There are three thermodynamic variables, temperature T, 3D gas pressure p or chemical potential μ, and monolayer coverage θ or number density n_2. Typically the phase diagram is projected onto a plane. Then the corresponding third piece of information either may not be known, may be discarded, or it may be given as a parameter.

a. Coverage units

The equilibrium equation of state for (2D) adsorbed layers gives the coverage as a function of pressure and temperature, $\theta = f(p, T)$. The coverage (number density n_2 of atoms or molecules per unit area) frequently is expressed as fractions of a monolayer.

The units and notation used for monolayer coverage are not standard among workers in the field. We adopt a definition that the coverage ϑ is the ratio of the number of atoms or molecules in the layer to the number of atoms (or sometimes sites) in the top substrate layer, assuming a perfect crystal. With this definition, 1 monolayer, i.e., $\vartheta = 1$, is usually different from one layer of adatoms, but it gives an absolute scale that does not depend on the conditions. Another commonly used definition is that one monolayer unit, $\theta = 1$, consists of one complete layer of atoms or molecules on the surface, sometimes referred to as a physical monolayer. This definition is used in Fig. 1. Although quite intuitive, it can be ambiguous since the number of atoms or molecules in a complete monolayer can be different under different conditions due to the thermal expansion and compressibility of the layer.

Another measure of coverage is based on the (2D) lattice parameter L of an adsorbed solid. However, transforming L to ϑ for a monolayer depends on the assumptions that the first crystalline monolayer is perfect and that the second layer coverage either is known or is very low; this issue arises in Secs. IV.D and IV.E.1. There is also a problem with identifying the coverage for nominal constant filling trajectories through the p, T parameter space in some x-ray diffraction experiments (Specht *et al.*, 1987; Hong *et al.*, 1989).

b. Phase diagrams and projections

In phase diagrams with intensive thermodynamic variables as coordinates, e.g., (p, T) or (μ, T), there typically are large single-phase regions. In the monolayer domain, these may be 2D gases, liquids, and solids and have sublimation, vaporization, and melting lines as the boundaries. Further, there may be several 2D solid phases that are either commensurate (C) or incommensurate (I) with the substrate lattice; in many cases a C-I phase transition occurs. The incommensurate solids are designated as incommensurate aligned (IA) or incommensurate rotated (IR) according to the orientation of the 2D solid relative to the substrate.[41] In a phase diagram with $\ln(p)$ and $1/T$ as the axes, a phase boundary (e.g., for gas-solid or monolayer-bilayer transitions) frequently becomes a straight line. The slope of the line gives the latent heat of the corresponding phase transition. Another presentation has T and μ as the axes: this emphasizes the adsorbed phase, while the coexisting 3D gas phase is reflected in the value of μ. In both formats, the coverage information typically is lost.

Adsorption isotherms, e.g., Fig. 1 for multilayers, present the coverage θ as a function of $\ln(p)$, with T as the parameter, and may include two-phase coexistence. A variant on this is to use the chemical potential μ, which is proportional to $\ln(p)$ at constant T, as the abscissa. Isobars and isosteres are different cuts through a given set of isotherms.

An isobar is a constant pressure path and gives a plot of $\theta(T)$ with $\ln(p)$ or μ as the independent variable. In many single-crystal surface experiments, a beam directed at the substrate establishes a steady-state concentration. In other experiments, the experimental chamber is filled with gas at a constant pressure. Such procedures produce almost a true 2D-3D equilibrium, but the temperature of the 3D gas T_b often is not the same as that of the adsorbate T_a. There then is a question of whether to correct the pressure for this thermomolecular effect, of order $(T_a/T_b)^{1/2}$.

An isostere is a constant-coverage path on a (p, T) diagram. Typically $\ln(p)$ varies linearly with $1/T$ and the energy q_{st} derived from the slope is called the isosteric heat of adsorption. This energy depends on the coverage and includes contributions from the adsorption energy and lateral binding energies, their derivatives with respect to coverage, and various terms related to the atomic vibration.

The layers are usually, but not always, in equilibrium with the 3D vapor phase. In equilibrium, the adsorbed layer a has a chemical potential equal to that of the vapor, $\mu_a = \mu_v = \mu$. In the monolayer regime, the vapor is at sufficiently low pressure p that it forms an ideal gas with known chemical potential. Then it is simple to reexpress the equation of state as $\theta = f(\mu, T)$. By increasing

---

[41] The incommensurate rotated phase was discovered for Ar/graphite using LEED (Shaw *et al.*, 1978). An introduction is given by Venables (2000, Sec. IV.D).

the 3D vapor pressure p, the adsorbed phase can be compressed, which changes the balance between attractive and repulsive forces within the adsorbed layer so that phase transitions occur within a monolayer or between layers.

c. Thermodynamic calculus

We present some results for the very common limiting case in which the thin physically adsorbed layer is treated as a distinct thermodynamic phase coexisting with a dilute 3D gas. Ordinarily, the 3D gas, which coexists with a physically adsorbed monolayer, is at such a low density that it is essentially an ideal gas and Boyle's law holds,

$$p = n_g k_B T, \tag{A1}$$

where k_B is Boltzmann's constant and p and n_g are the gas pressure and number density, respectively. The chemical potential of the 3D monatomic ideal gas of spin zero atoms is

$$\mu_g = k_B T \ln(n_g \lambda^3), \tag{A2}$$

with the thermal wavelength for particles of mass m defined by $\lambda = \sqrt{2\pi\hbar^2/mk_BT}$. The differential of the (3D) μ_g is

$$d\mu_g = -s_g dT + (1/n_g)dp \simeq -s_g dT + k_B T d\ln p, \tag{A3}$$

where Boyle's law has been used in the last step.

The corresponding thermodynamic differential for an isotropic monolayer phase x is

$$d\mu_x = -s_x dT + a d\phi. \tag{A4}$$

The spreading pressure ϕ is defined to be the negative of the derivative of the free energy with respect to area a per admolecule or adatom, $n_x = 1/a$ is a 2D number density, and s_x is the entropy per adatom (or molecule).

Heats of adsorption are defined in terms of the slopes of phase boundaries and isosteres. The heats of condensation, also called integral heats of adsorption, are

$$q_i = -k_B \left.\frac{\partial \ln p}{\partial(1/T)}\right|_{i\text{-layer}}, \tag{A5}$$

where the heat of first-layer condensation is denoted q_1 and of second-layer condensation is denoted q_2. Similarly, the isosteric heat for a line of constant coverage in a single phase region is

$$q_{\mathrm{st}} = -k_B \left.\frac{\partial \ln p}{\partial(1/T)}\right|_{n}. \tag{A6}$$

An example of the transformations possible with the thermodynamic calculus is the expression for the monolayer isothermal bulk modulus of a phase with area a per molecule,

$$\begin{aligned} B_T &= -a \left.\frac{\partial\phi}{\partial a}\right|_T = -\left.\frac{\partial\mu}{\partial a}\right|_T = -k_B T \left.\frac{\partial \ln p}{\partial a}\right|_T \\ &= k_B T \left.\frac{\partial \ln p}{\partial T}\right|_a \left.\frac{\partial T}{\partial a}\right|_p = (q_{\mathrm{st}}/T) \left.\frac{\partial T}{\partial a}\right|_p. \end{aligned} \tag{A7}$$

We next give expressions for q_1 and q_{st} in terms of monolayer thermodynamic functions, to show the relation between them. Two monolayer phases (subscripts α and β) in equilibrium have equal chemical potentials and equal spreading pressures, $\mu_\alpha = \mu_\beta$; $\phi_\alpha = \phi_\beta$. The adsorbate phases are also in mass-transfer equilibrium with the vapor phase, $\mu_\alpha = \mu_\beta = \mu_{3\mathrm{D}}$. Then (Bruch *et al.*, 1997; Venables, 2000) the monolayer heat of condensation is

$$q_1 = h_{3\mathrm{D}} - (n_\alpha u_\alpha - n_\beta u_\beta)/(n_\alpha - n_\beta), \tag{A8}$$

where $h_{3\mathrm{D}}$ is the enthalpy per particle of the 3D phase ($=\frac{5}{2}k_BT$ for a dilute monatomic gas) and n_x and u_x are the number density and thermodynamic internal energy per particle, respectively. For the condensation from 2D gas (α) to 2D solid (β), the great difference in number densities ($n_\alpha \ll n_\beta$) enables a reduction to $q_1 \simeq h_{3\mathrm{D}} - u_{2\mathrm{Dsolid}}$; then q_1 is a direct measure of the cohesive energy of the 2D solid. The isosteric heat for an adsorbed phase x is

$$q_{\mathrm{st}} = h_g - \frac{\partial}{\partial n_x}(n_x u_x)|_T. \tag{A9}$$

Thus it includes a contribution from a lateral stress term $n\partial u/\partial n$. The parallelism between the derivative in Eq. (A9) and the finite difference in Eq. (A8) gives rise to the terminology differential and integral heats of adsorption for q_{st} and q_1, respectively.

An approximate representation for the $\ln p - 1/T$ phase boundary of monolayer condensation, based on Eq. (A5), is

$$k_B \ln p_1 = -\frac{q_1}{T} + B_1. \tag{A10}$$

The corresponding relation for the sublimation pressure p_S of the 3D solid has q_S and B_S. Then the ratio of the pressures is

$$p_1/p_S = \exp([B_1 - B_S]/k_B)\exp(-\beta[q_1 - q_S]). \tag{A11}$$

However, Larher (1971) used simplifying approximations for the thermodynamic relations at the 2D and 3D sublimation curves to obtain

$$\begin{aligned} k_B T \ln(p_1/p_S) \simeq{}& [u_{2\mathrm{Dsolid}} - u_{3\mathrm{Dsolid}}] \\ &- T(s_{2\mathrm{Dsolid}} - s_{3\mathrm{Dsolid}}). \end{aligned} \tag{A12}$$

In Eq. (A12), s_α are the entropies per atom/molecule in the corresponding monolayer and bulk phases. Comparing to Eq. (A11) shows that the prefactor B_1 gives a measure of the entropy difference in the two phases.

Thus, understanding the thermodynamics of 2D sublimation enables one to measure both the cohesive energy of the 2D adsorbed solid, which appears in Arrhenius-type exponentials, and the entropy of adsorption, which is related to the preexponential factor, Eq. (A11). This results in an estimate of the change in vibration frequencies between the adsorbed 2D phase and the bulk 3D phase. In the case of Xe/graphite, the entropy change is negative (Suzanne *et al.*, 1974), because the effective vibration frequencies are higher in the adsorbed state than in the bulk phase (Price and Venables, 1976). However, Debye models and computer simulations do give larger entropy for an incommensurate monolayer solid than for the 3D solid at sufficiently low temperature (Bruch, 1986).

Equation (A2) can be used to estimate a monolayer heat of adsorption q_1 from the pressure p_1 and temperature at monolayer condensation. Generalizing to molecules, we write

$$-q_1 \simeq \mu_{3D}(T,p_1) = k_B T \ln[p_1 \lambda^3 / k_B T \xi_{\mathrm{int}}], \tag{A13}$$

where $\lambda = \sqrt{2\pi\hbar^2/Mk_BT}$ is the thermal wavelength for molecular mass M and ξ_{int} is the internal partition function for the molecule in the dilute 3D gas. This type of application arises in the discussion of quartz crystal microbalance (QCM) experiments, where single isotherms typically are measured at the working temperature, rather than the family of isotherms that would be needed for Eqs. (A5) and (A6).

2. Statistical thermodynamics

Empirically, the coverage in the submonolayer domain is proportional to the pressure of the 3D gas, Henry's law. This result is recovered, and approximate expressions for the approach to saturation coverage are given, in two elementary models for the isotherms by Langmuir and by Brunauer, Emmett, and Teller (BET), which we now review (see also Bruch *et al.*, 1997). The low-coverage limit is also accessible to analytic atomic-scale statistical mechanical theory and it has been an important source of information on gas-surface interactions (Steele, 1974). The properties of the intermediate density adsorbed 2D gas can be expressed in terms of virial coefficients that incorporate the adatom-adatom potentials (Steele, 1974; Venables, 2000), and the presence of adsorption-induced interactions is inferred from analysis of the leading virial coefficients (Elliott *et al.*, 1993; Wei *et al.*, 1996). The treatment of dense monolayers (Schabes-Retchkiman and Venables, 1981; Bruch *et al.*, 1997) has a similar flavor to the theory of 3D rare-gas solids, and analytically based approximations are combined with interaction models in computations that achieve a good description of large bodies of experimental data. For multilayers, the treatments rely heavily on computer simulations (Phillips and Larese, 1997) and the state of the art is a simulation of the layering transitions as a function of chemical potential using the grand ensemble (Celestini *et al.*, 2000).

The Langmuir isotherm model takes the surface to consist of N_0 possible adsorption sites with a binding energy ϵ_0 for adatoms. Then the fractional coverage at temperature T and 3D gas pressure p is given by

$$\theta = N/N_0 = \frac{p}{p + p_L}, \tag{A14}$$

where the pressure scale is set by

$$p_L = (g/z\beta\lambda^3)[\exp(\beta\epsilon_0)]. \tag{A15}$$

In Eq. (A15), we have introduced two refinements, namely the spin degeneracy factor g and the one-particle partition function z for excitations at the site (which is a way to include effects of adatom vibrations at the site). In this model, the limiting configuration at large pressure is a saturated monolayer.

The BET isotherm model (Brunauer *et al.*, 1938) is a generalization that allows for coverage exceeding a monolayer and was constructed to improve on previous methods of determining monolayer coverage. An old method to estimate the surface area of porous and finely divided substances uses the so-called point B to determine the area at monolayer completion. A typical adsorption isotherm has a concave shape for adsorbed mass as a function of pressure at low pressure, then a sharp increase in adsorbed mass at monolayer condensation (monolayer "riser" or "step"), and then a convex shape as the monolayer is completed, followed by a linear dependence as higher layers begin to be populated. Point B is defined to be the point at which the convex shape joins the linear dependence. As might be anticipated, identifying point B in a set of experimental data can be ambiguous, and the BET isotherm model provides another method of determining the monolayer coverage. Their method is as follows: Let the volume of gas required to form a complete monolayer be v_m and the pressure and saturation vapor pressure of the gas be p and p_0, respectively. Then with binding energies in the monolayer and the bulk liquid denoted E_1 and E_L and $c \equiv \exp(\beta[E_1 - E_L])$, the BET isotherm for the volume of adsorbed gas v can be written as

$$\frac{p}{v(p_0 - p)} = \frac{1}{v_m c} + \frac{c-1}{v_m c}\frac{p}{p_0}. \tag{A16}$$

From the slope and intercept of the straight line in p/p_0, the constants v_m and c can be determined.

A more systematic approach that is explicit and accurate for the initial stage of adsorption relies on an expansion in powers of the 2D number density, $n_2 = N/A$ for N adsorbed particles on area A. The leading term for a classical monatomic adsorbate is

$$n_2 = (\beta p/A)\int_0^\infty dz \int_A d^2r[\exp\{-\beta V(\vec{r},z)\} - 1], \tag{A17}$$

where $V(\vec{r},z)$ is the adatom-substrate potential for perpendicular distance z and lateral (vector) position $\vec{r}$ relative to a planar adsorbing surface of area A.

As mentioned at the beginning of this subsection, the quantitative statistical mechanical theory for adsorbate coverage has been extended algebraically to higher powers of the density n_2 and, with computer simulations, to

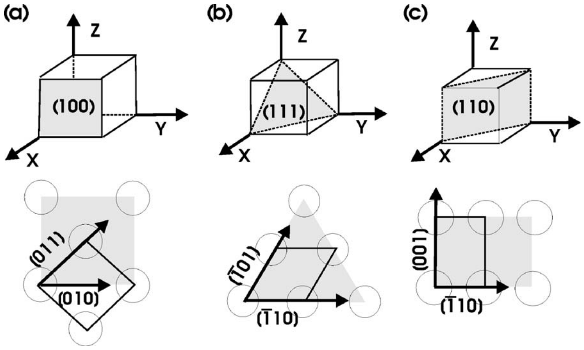

FIG. 28. The orientation of three planes in a cubic crystal and the surface lattice of the corresponding planes for an fcc crystal. The (100), (111), and (100) planes are shown in (a), (b), and (c), respectively. The labels for the primitive vectors of these surface lattices are also given.

nonuniform adsorbed films many layers thick. Some of the physical phenomena that arise in the latter case are discussed in Sec. VI.A.

APPENDIX B: SURFACE CRYSTALLOGRAPHY NOMENCLATURE

The nomenclature for planes and directions associated with the surfaces of crystals is the same as that used in the bulk crystals. For instance, the direction in a lattice that is specified by $[uvw]$ is along the vector $\mathbf{r}(uvw)=u\hat{a}+v\hat{b}+w\hat{c}$, where $\hat{a}$, $\hat{b}$, and $\hat{c}$ are unit vectors of the Bravais unit cell. In most lattices, several directions are equivalent, since a symmetry operation will transform them into each other. A group of such equivalent directions is denoted $\langle uvw\rangle$. For example, the equivalent directions corresponding to $\langle 100\rangle$ in a cubic crystal are [100], [$\bar{1}$00], [010], [0$\bar{1}$0] [001], and [00$\bar{1}$].

A lattice plane (hkl) is any one of the set of equivalent planes, denoted by $\{hkl\}$; this plane is perpendicular to the direction $[hkl]$ in a cubic crystal, but not in general. In an experiment, the specification of the surface plane, e.g., (100) versus (010) versus (001), etc., is usually arbitrary and an accepted practice is to specify the plane in curly brackets (Woodruff and Delchar, 1994); e.g., Pt{100} specifies one of the planes equivalent to the Pt(100) plane. However, the (hkl) notation is often used in place of the $\{hkl\}$ notation, as in this review.

Figure 28 shows the orientation of three planes in a cubic crystal and the lattices in those planes. Panel (a) shows the conventional unit cube with one of the family of (100) planes shaded. Panel (b) shows the (111) plane, with the surface lattice for an fcc crystal. Panel (c) shows the (110) plane and its surface lattice for an fcc crystal. While the low-index surfaces of most materials are generally easy to visualize and draw, high-index surfaces present more of a challenge. One tool to help in the visualization of surfaces is called Surface Explorer. The Surface Explorer is a web interface (written by Fritz Rammer, FHI) to the Balsac visualization software (written by Klaus Hermann, FHI) and running at the Fritz-Haber Institute. It allows one to visualize surfaces of the most common single crystals of any Miller index orientation. Surface images can be downloaded as PostScript files of publication-ready quality.

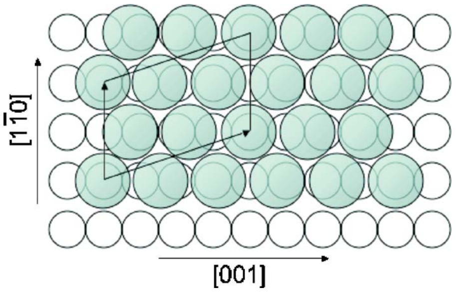

FIG. 29. (Color online) Schematic drawing of the Cu{110}-$c(8\times 2)$-10Kr structure. The open circles are the top-layer Cu atoms, the shaded circles are Kr atoms. The oblique primitive cell, denoted by Cu{110}-$\begin{pmatrix}4&1\\0&2\end{pmatrix}$-5Kr, is indicated.

Two main methods are used to describe surface structures. The more compact and commonly used of these is the Wood notation (Wood, 1964). This notation can be used when the included angle of the surface unit mesh is the same as that of the substrate unit mesh. The form of the notation is $S\{hkl\}(p\times q)R\phi°-nA$, where $S\{hkl\}$ is the substrate surface, p and q are the lengths of the surface structure unit cell vectors relative to the substrate unit cell vectors, ϕ is the rotation angle (omitted if $\phi=0$) of the surface structure unit cell relative to the substrate unit cell, n is the number of overlayer atoms or molecules per cell, and A is the name of the adsorbate.

As an example, the structure that forms for Kr on Cu{110} is shown in Fig. 29. The Wood notation for this structure is Cu{110}-$c(8\times 2)$-10 Kr, where c refers to the fact that the unit cell is a *centered* rectangle. The repeat distances along the [001] and [1$\bar{1}$0] directions are 8 and 2, respectively. It is evident that this unit cell is not the primitive unit cell of the surface structure, however, which is oblique. The oblique cell cannot be described using the Wood notation and therefore must be specified using the second method, which is the matrix notation first proposed by Park and Madden (1968). In the matrix method, the matrix $\mathbf{G}$ specifies the surface unit mesh relative to the substrate unit mesh, according to

$$\begin{pmatrix}\mathbf{a}'\\ \mathbf{b}'\end{pmatrix}=\begin{pmatrix}G_{11}&G_{12}\\ G_{21}&G_{22}\end{pmatrix}=\begin{pmatrix}\mathbf{a}\\ \mathbf{b}\end{pmatrix},$$

where $\mathbf{a}$ and $\mathbf{b}$ are substrate unit vectors and $\mathbf{a}'$ and $\mathbf{b}'$ are surface unit vectors. The unit cell specified in this way for the Kr/Cu{110} structure is

$$\text{Cu}\{110\}\text{-}\begin{pmatrix}4&1\\0&2\end{pmatrix}\text{-5Kr}.$$

Surface structures are classified as commensurate when the determinant of the matrix $\mathbf{G}$ is an integer and incommensurate when det($\mathbf{G}$) is irrational. Higher-order commensurate (HOC) structures, in which overlayer atoms or molecules occupy more than one type of site, have rational, noninteger det(**G**). Another type of structure often observed in physisorption systems is termed a uniaxial incommensurate lattice (UIC). In such a structure, the spacing of the overlayer is commensurate (or higher-order commensurate) in one direction, but is nominally incommensurate along the other axis. Such structures can be indexed using the matrix method described above. While the distinction between commensurate and incommensurate structures may seem clear for short distances, it can be difficult to distinguish between a truly incommensurate structure and a HOC structure with long spatial period. Beyond some period, the distinction becomes meaningless, at least in terms of experimental studies, where the extent of the "perfect" structure is limited.

APPENDIX C: A BRIEF REVIEW OF LATTICE DYNAMICS

For crystalline condensed matter, which is a dense, strongly interacting, strongly correlated many-body system, the frequency spectrum for small-amplitude atomic displacements has an explicit solution. The normal coordinates for the harmonic solid give a description in terms of independent decoupled variables and lead to closed forms for the statistical mechanics. The quanta of excitations are *phonons*. While the utility of such a formulation was recognized early by Born and von Kármán (Born, 1975), it took decades before it was implemented on a routine basis to calculate the normal modes of 3D crystals (Born and Huang, 1954). We outline the calculation for monolayers and discuss its applicability in this appendix.

Let the Hamiltonian of the N-atom monolayer solid have the form

$$H = \sum_{j=1}^{N} \mathbf{p}_j^2/2m + \sum_{i<j} \phi(|\mathbf{r}_i - \mathbf{r}_j|) + \sum_{j=1}^{N} V_s(\mathbf{r}_j). \qquad \text{(C1)}$$

It is assumed that atoms (or molecules) interact by pair potentials and that the supporting substrate is the source of the external potential V_s. In the harmonic approximation, the potential energies are expanded to second order in the displacements $\mathbf{u}_j$ from the equilibrium positions $\mathbf{r}_{je}$, $\mathbf{u}_j = \mathbf{r}_j - \mathbf{r}_{je}$. The frequencies $\omega(\mathbf{q})$ and polarization vectors $\mathbf{u}(\mathbf{q})$ of the normal modes of wave vector $\mathbf{q}$ are obtained from the eigenvalues and eigenvectors of the dynamical matrix $\mathbf{D}$,

$$\mathbf{D}(\mathbf{q}) = \nabla\nabla V_s + \sum_{j\neq 0} [1 - \exp(\imath \mathbf{q}\cdot \mathbf{r}_{je})] \nabla\nabla \phi(r_{je}), \qquad \text{(C2)}$$

$$\mathbf{D}(\mathbf{q})\mathbf{u}(\mathbf{q}) = m\omega^2(\mathbf{q})\mathbf{u}(\mathbf{q}). \qquad \text{(C3)}$$

For a Bravais lattice with all atoms in equivalent positions, the dispersion relation $\omega(\mathbf{q})$ has three branches, which will be denoted S, LA, and SH. At least at small wave numbers q and more generally for high-symmetry azimuths of the wave vector $\mathbf{q}$, the vibrations can be classified by their polarizations. The shear horizontal (SH) [transverse acoustic (TA)] and longitudinal acoustic (LA) branches have motions mainly in the monolayer plane with polarizations $\mathbf{u}(\mathbf{q})$ nearly parallel and perpendicular, respectively, to $\mathbf{q}$ for small $|\mathbf{q}|$. The S branch is mainly perpendicular to the plane and its frequency ω_S generally has very little dispersion except for an effect of dynamic coupling to substrate vibrations that is illustrated in Fig. 11. Dispersion is observed for ω_S for bilayer and trilayer solids and is a strong diagnostic of the presence of such phases (Gibson and Sibener, 1985, 1988).

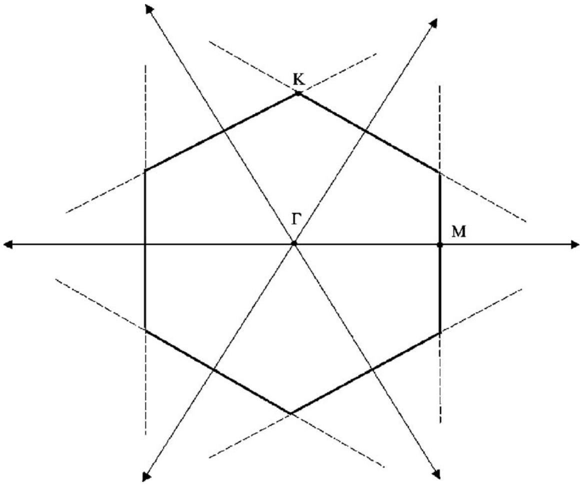

FIG. 30. Brillouin zone for the triangular lattice. The six equal length primitive reciprocal-lattice vectors are shown as arrows. The perpendicular bisectors are drawn as dotted lines and they form the boundary of the first Brillouin zone. The center is denoted by Γ, a corner of the boundary by K, and a midpoint of the boundary wall by M. The normal modes of the monolayer lattice have pure SH and LA polarizations along the ΓM and ΓK azimuths. From Bruch *et al.*, 1997.

The reciprocal lattice of a triangular lattice is itself a triangular lattice. The first Brillouin zone for this triangular lattice is shown in Fig. 30, with three high-symmetry points identified: the Γ point at the center of the zone, the M point at the midpoints of a wall of the zone, and the K point at the corners of the zone. The azimuths ΓM and ΓK are high-symmetry axes and the polarizations of the phonons are precisely SH and LA along these axes. There is a degeneracy $\omega_{\mathrm{SH}} = \omega_{\mathrm{LA}}$ at the K points. In the experimental spectrum for Xe/Pt(111) shown in Fig. 12, the axes of the lattice are slightly misaligned relative to the scattering plane and the scan does not pass precisely through the K point.

The description in terms of small-amplitude displacements typically is most accurate at rather low temperatures. At temperatures near the melting temperature, and for quantum solids with intrinsically large root-mean-square displacements even in the ground state, anharmonic processes must be included. Approximations for these conditions in 3D solids were reviewed by Klein and Venables (1976). For monolayers, there is a further condition in which strongly anharmonic solids are encountered, namely the dilated commensurate lattices stabilized by substrate corrugation (Bruch and Novaco, 2000).

Nevertheless, vibrations perpendicular to the monolayer plane typically remain harmonic over a wide temperature range and lead to characteristic exponential (with temperature) Debye-Waller attenuations of diffraction and inelastic-scattering intensities, Sec. IV.C.3. The net thermal effect of vibrations in the monolayer plane is incorporated in the internal partition function of cell model approximations, which are remarkably useful for estimating properties such as thermal expansion (Bruch *et al.*, 1997). An early application of the cell model to Kr and Xe/graphite was given by Price and Venables (1976) and elaborated upon by Schabes-Retchkiman and Venables (1981).

LIST OF ACRONYMS AND ABBREVIATIONS

AES	Auger electron spectroscopy
AFM	atomic force microscope
BLAG	buffer-layer-assisted growth
C	commensurate solid
CCD	charge-coupled device
CN	n-C_NH_{2N+2} alkane series
DFT	density functional theory
EXAFS	extended x-ray absorption fine structure
FEM	field emission microscopy
FTIR	Fourier transform infrared spectroscopy
GCMC	grand canonical Monte Carlo simulation
GGA	generalized gradient approximation
HAS	helium-atom scattering
HOC	higher order commensurate solid
I	incommensurate solid
IA	incommensurate aligned solid
INS	inelastic neutron scattering
IR	incommensurate rotated solid
IRAS	infrared reflection absorption spectroscopy
LA	longitudinal acoustic mode
LDA	local-density approximation
LEED	low-energy electron diffraction
LITD	laser-induced thermal desorption
LOD	linear optical diffraction
MC	Monte Carlo simulation
MD	molecular dynamics simulation
PBE	Perdew-Burke-Ernzerhof functional
PEEM	photoemission electron microscopy
PLS	power law solid
PW91	Perdew-Wang 1991 functional
QCM	quartz crystal microbalance
QHAS	quasielastic helium-atom scattering
QMS	quadrupole mass spectrometry
QNS	quasielastic neutron scattering[42]
RHEED	reflection high-energy electron diffraction
SH	shear horizontal, transverse, branch
SPLEED	spin-polarized low-energy electron diffraction
STM	scanning tunneling microscope
SWNT	single-walled carbon nanotube
TDS	thermal desorption spectroscopy
TEM	transmission electron microscopy
THEED	transmission high-energy electron diffraction
TOF	time of flight
TPD	temperature programmed desorption
TPRS	temperature programmed reaction spectroscopy
VHRE	very-high-resolution ellipsometry
2D	two dimensions
3D	three dimensions

REFERENCES

Abraham, F. F., J. Q. Broughton, P. W. Leung, and V. Elser, 1990, “Second-layer solidification of ^{3}He on graphite: A numerical study,” Europhys. Lett. **12**, 107–112.

Ala-Nissila, T., R. Ferrando, and S. C. Ying, 2002, “Collective and single particle diffusion on surfaces,” Adv. Phys. **51**, 949–1078.

Alexandrowicz, G., 2005, “Helium spin echo spectroscopy: Measuring the dynamics of atoms, molecules and surfaces,” Ph.D. thesis (University of Cambridge, England).

Alexandrowicz, G., and A. P. Jardine, 2007, “Helium spin-echo spectroscopy: Studying surface dynamics with ultra-high-energy resolution,” J. Phys.: Condens. Matter **19**, 305001.

Alfè, D., and M. J. Gillan, 2006, “Absolute rate of thermal desorption from first-principles simulation,” J. Phys.: Condens. Matter **18**, L451-L457.

Alkhafaji, M. T., and A. D. Migone, 1991, “Vapor-pressure study of the melting of two-dimensional argon adsorbed on BN,” Phys. Rev. B **43**, 8741–8743.

Alkhafaji, M. T., P. Shrestha, and A. D. Migone, 1994, “Adsorption-isotherm study of monolayer films of N_2 on BN,” Phys. Rev. B **50**, 11088–11092.

Altman, E. I., and R. J. Colton, 1993, “Determination of the orientation of C_{60} adsorbed on Au(111) and Ag(111),” Phys. Rev. B **48**, 18244–18249.

Amelinckx, S., and P. Delavignette, 1960, “Electron-optical study of basal dislocations in graphite,” J. Appl. Phys. **31**, 2126–2135.

Annett, J. F., and R. Haydock, 1984, “Anticorrugating effect of hybridization on the helium diffraction potential for metal surfaces,” Phys. Rev. Lett. **53**, 838–841; **57**, 1382(E) (1986).

Annett, J. F., and R. Haydock, 1986, “Hybridization interaction between helium and a metal surface,” Phys. Rev. B **34**, 6860–6868.

Antczak, G., and G. Ehrlich, 2005, “The beginnings of surface diffusion studies,” Surf. Sci. **589**, 52–66.

Antonov, V. N., J. S. Palmer, A. S. Bhatti, and J. H. Weaver, 2003, “Nanostructure diffusion and aggregation on desorbing rare-gas solids: Slip on an incommensurate lattice,” Phys. Rev. B **68**, 205418.

Antonov, V. N., J. S. Palmer, P. S. Waggoner, A. S. Bhatti, and J. H. Weaver, 2004, “Nanoparticle diffusion on desorbing solids: The role of elementary excitations in buffer-layer-assisted growth,” Phys. Rev. B **70**, 045406.

Antonov, V. N., P. Swaminathan, J. A. N. T. Soares, J. S. Palmer, and J. H. Weaver, 2006, “Photoluminescence of CdSe quantum dots and rods from buffer-layer-assisted growth,” Appl. Phys. Lett. **88**, 121906.

Arnold, T., S. Chanaa, S. M. Clarke, R. E. Cook, and J. Z.

---

[42] This is sometimes denoted QENS, but QENS may also refer to a spectrometer at the Intense Pulsed Neutron Source (IPNS) at Argonne National Laboratory.

Larese, 2006, “Structure of an *n*-butane layer adsorbed on magnesium oxide (100),” Phys. Rev. B **74**, 085421.

Arnold, T., R. E. Cook, S. Chanaa, S. M. Clarke, M. Farinelli, P. Yaron, and J. Z. Larese, 2006, “Neutron scattering and thermodynamic investigations of thin films of *n*-alkanes adsorbed on MgO(100) surfaces,” Physica B **385-386**, 205–207.

Arnold, T., R. E. Cook, and J. Z. Larese, 2005, “Thermodynamic investigation of thin films of ethane adsorbed on magnesium oxide,” J. Phys. Chem. B **109**, 8799–8805.

Arnold, T., C. C. Dong, R. K. Thomas, M. A. Castro, A. Perdigon, S. M. Clarke, and A. Inaba, 2002, “The crystalline structures of the odd alkanes pentane, heptane, nonane, undecane, tridecane and pentadecane monolayers adsorbed on graphite at submonolayer coverages and from the liquid,” Phys. Chem. Chem. Phys. **4**, 3430–3435.

Arnold, T., R. K. Thomas, M. A. Castro, S. M. Clarke, L. Messe, and A. Inaba, 2002, “The crystalline structures of the even alkanes hexane, octane, decane, dodecane and tetradecane monolayers adsorbed on graphite at submonolayer coverages and from the liquid,” Phys. Chem. Chem. Phys. **4**, 345–351.

Asada, H., and M. Masuda, 1989, “Bilayer model for zero order desorption,” Surf. Sci. **207**, 517–524.

Asada, H., and H. Sekito, 1992, “Desorption from multilayers,” Surf. Sci. **273**, 139–146.

Ashino, M., A. Schwarz, T. Behnke, and R. Wiesendanger, 2004, “Atomic-resolution dynamic force microscopy and spectroscopy of a single-walled carbon nanotube: Characterization of interatomic van der Waals forces,” Phys. Rev. Lett. **93**, 136101.

Avgul, N. N., and A. V. Kiselev, 1970, “Physical adsorption of gases and vapors on graphetized carbon blacks,” in *Chemistry and Physics of Carbon*, edited by P. L. Walker, Jr. (Dekker, New York), Vol. 6, pp. 1–124.

Aziz, R. A., U. Buck, H. Jónsson, J.-C. Ruiz-Suárez, B. Schmidt, G. Scoles, M. J. Slaman, and J. Xu, 1989, “Two- and three-body forces in the interaction of He atoms with Xe overlayers adsorbed on (0001) graphite,” J. Chem. Phys. **91**, 6477–6493; **93**, 4492(E) (1998).

Azzouz, M., H. J. Kreuzer, and M. R. A. Shegelski, 2002, “Microscopic derivation of the master and Fokker-Planck equations for surface diffusion,” Phys. Rev. B **66**, 125403.

Babič, D., C. Schmitt, and C. Bechinger, 2005, “Colloids as model systems for problems in statistical physics,” Chaos **15**, 026114.

Bagus, P. S., V. Staemmler, and C. Wöll, 2002, “Exchangelike effects for closed-shell adsorbates: Interface dipole and work function,” Phys. Rev. Lett. **89**, 096104.

Bai, M., K. Knorr, M. J. Simpson, S. Trogisch, H. Taub, S. N. Ehrlich, H. Mo, U. G. Volkmann, and F. Y. Hansen, 2007, “Nanoscale observation of delayering in alkane films,” Europhys. Lett. **79**, 26003.

Bär, T., T. Burns, and K. Knorr, 1997, “Growth kinetics of Ar monolayers physisorbed on graphite (001),” Surf. Sci. **383**, 362–369.

Barker, J. A., and C. T. Rettner, 1992, “Accurate potential energy surface for Xe/Pt(111): A benchmark gas/surface interaction potential,” J. Chem. Phys. **97**, 5844–5850; **101**, 9202(E) (1994).

Barth, J. V., 2000, “Transport of adsorbates at metal surfaces: From thermal migration to hot precursors,” Surf. Sci. Rep. **40**, 75–149.

Bauer, E., H. Poppa, G. Todd, and P. R. Davis, 1977, “The adsorption and early stages of condensation of Ag and Au on W single-crystal surfaces,” J. Appl. Phys. **48**, 3773–3787.

Baumgartl, J., M. Brunner, and C. Bechinger, 2004, “Locked-floating-solid to locked-smectic transition in colloidal systems,” Phys. Rev. Lett. **93**, 168301.

Becker, K. E., and K. A. Fichthorn, 2006, “Accelerated molecular dynamics simulation of the thermal desorption of *n*-alkanes from the basal plane of graphite,” J. Chem. Phys. **125**, 184706.

Bée, M., 1988, *Quasielastic Neutron Scattering* (Hilger, Bristol).

Bée, M., 2003, “Localized and long-range diffusion in condensed matter: State of the art of QENS studies and future prospects,” Chem. Phys. **297**, 121–141.

Beeby, J. L., 1971, “The scattering of helium atoms from surfaces,” J. Phys. C **4**, L359–L362.

Behm, R. J., C. R. Brundle, and K. Wandelt, 1986, “The underlayer influence on photoemission and thermal desorption of xenon adsorbed on Ag(111),” J. Chem. Phys. **85**, 1061–1073.

Betancourt, A. E., and D. M. Bird, 2000, “First-principles calculation of the interaction energy of $(\sqrt{3}\times\sqrt{3})R30°$ Xe/Pt(111),” J. Phys.: Condens. Matter **12**, 7077–7088.

Bienfait, M., B. Asmussen, M. Johnson, and P. Zeppenfeld, 2000, “Methane mobility in carbon nanotubes,” Surf. Sci. **460**, 243–248.

Bienfait, M., J. P. Coulomb, and J. P. Palmari, 1987, “Diffusivity of a two-dimensional lattice fluid: CH_4 adsorbed on MgO(100),” Surf. Sci. **182**, 557–566.

Bienfait, M., and J. M. Gay, 1991, “Surface melting and diffusion,” in *Phase Transitions in Surface Films 2*, edited by H. Taub, G. Torzo, H. J. Lauter, and S. C. Fain, Jr. (Plenum, New York), pp. 307–325.

Bienfait, M., J. M. Gay, and J. M. Blank, 1988, “Surface premelting of thin films of methane,” Surf. Sci. **204**, 331–344.

Bienfait, M., and J. A. Venables, 1977, “Kinetics of adsorption and desorption using Auger electron spectroscopy: Xe/(0001) graphite,” Surf. Sci. **64**, 425–436.

Bienfait, M., P. Zeppenfeld, N. Dupont-Pavlovsky, M. Muris, M. R. Johnson, T. Wilson, M. DePies, and O. E. Vilches, 2004, “Thermodynamics and structure of hydrogen, methane, argon, oxygen, and carbon dioxide adsorbed on single-wall carbon nanotube bundles,” Phys. Rev. B **70**, 035410.

Bienfait, M., P. Zeppenfeld, J. M. Gay, and J. P. Palmari, 1990, “Surface melting of the close-packed (111) face of methane thin films condensed on graphite,” Surf. Sci. **226**, 327–338.

Birgeneau, R. J., and P. M. Horn, 1986, “Two-dimensional rare gas solids,” Science **232**, 329–336.

Bloss, E., and A. F. G. Wyatt, 2000, “Surface diffusion of solid hydrogen,” J. Low Temp. Phys. **119**, 743–764.

Boas, C., T. Becker, M. Kunat, U. Burghaus, and C. Wöll, 2001, “Comment on ‘Effect of structural anisotropy and lateral strain on the surface phonons of monolayer xenon on Cu(110),’ ” Phys. Rev. B **64**, 037401.

Boas, C., M. Kunat, U. Burghaus, B. Gumhalter, and C. Wöll, 2003, “Determination of the lateral Xe-Xe potential in a single xenon layer adsorbed on Cu(110) from surface phonon dispersion measurements,” Phys. Rev. B **68**, 075403.

Born, M., 1975, *My Life* (Scribner’s, New York), Chap. 12.

Born, M., and K. Huang, 1954, *Dynamical Theory of Crystal Lattices* (Oxford University Press, Oxford, England).

Bouldin, C., and E. A. Stern, 1982, “Extended x-ray absorption fine-structure study of Kr-grafoil submonolayers,” Phys. Rev. B **25**, 3462–3473.

Boutchko, R. D., and L. W. Bruch, 1999, “Brownian friction of gas molecules on the graphite surface,” Phys. Rev. B **59**, 10992–10995.

Boutchko, R. D., and L. W. Bruch, 2004, “Dynamics of monolayer xenon adsorbed on Pt(111),” Phys. Rev. B **70**, 195422.

Boyd, D. A., F. M. Hess, and G. B. Hess, 2002, “Infrared absorption study of physisorbed carbon monoxide on graphite,” Surf. Sci. **519**, 125–138.

Boyd, D. A., Y. Xia, and G. B. Hess, 2004, “Use of IR spectroscopy to study compression of a physisorbed monolayer on graphite,” Bull. Am. Phys. Soc. **49**, 1345, paper W32-2.

Brand, J. L., M. V. Arena, A. A. Deckert, and S. M. George, 1990, “Surface diffusion of *n*-alkanes on Ru(001),” J. Chem. Phys. **92**, 5136–5143.

Braun, J., D. Fuhrmann, A. Šiber, B. Gumhalter, and C. Wöll, 1998, “Observation of a zone-center gap in the longitudinal mode of an adsorbate overlayer: Xenon on Cu(111),” Phys. Rev. Lett. **80**, 125–128.

Bretz, M., 1977, “Ordered helium films on highly uniform graphite—finite size effects, critical parameters, and the three-state Potts model,” Phys. Rev. Lett. **38**, 501–505.

Bretz, M., J. G. Dash, D. C. Hickernell, E. D. McLean, and O. E. Vilches, 1973, “Phases of ^{3}He and ^{4}He monolayer films adsorbed on basal-plane oriented graphite,” Phys. Rev. A **8**, 1589–1615.

Briquez, S., S. Picaud, C. Girardet, P. N. M. Hoang, J. Heidberg, and A. Voßberg, 1998, “Adsorption of ortho and para H_2 on NaCl(001),” J. Chem. Phys. **109**, 6435–6449.

Brivio, G. P., and M. I. Trioni, 1999, “The adiabatic molecule-surface interaction: Theoretical approaches,” Rev. Mod. Phys. **71**, 231–265.

Brockhouse, B. N., 1995, “Nobel Lecture: Slow neutron spectroscopy and the grand atlas of the physical world,” Rev. Mod. Phys. **67**, 735–751.

Bruch, L. W., 1985, “Zero temperature calculations of the states of a monoatomic two-dimensional solid adsorbed on an fcc (110) surface,” Surf. Sci. **150**, 503–557.

Bruch, L. W., 1986, “Entropy of thin solid layers,” J. Chem. Phys. **84**, 6479–6482.

Bruch, L. W., 1988, “Zone center gap in the frequency spectrum of a commensurate monolayer,” Phys. Rev. B **37**, 6658–6662.

Bruch, L. W., 1991, “Signatures and consequences of the substrate corrugation,” in *Phase Transitions in Surface Films 2*, edited by H. Taub, G. Torzo, H. J. Lauter, and S. C. Fain, Jr. (Plenum, New York), pp. 67–82.

Bruch, L. W., 1994, “Zone-center frequency gap of a commensurate quantum monolayer solid,” Phys. Rev. B **49**, 7654–7659.

Bruch, L. W., 1997, “Comment on ‘Experimental determination of a longitudinal phonon dispersion curve in a quasi-two-dimensional system,’ ” J. Chem. Phys. **107**, 4443–4444.

Bruch, L. W., 2000, “Ohmic damping of center-of-mass oscillations of a molecular monolayer,” Phys. Rev. B **61**, 16201–16206.

Bruch, L. W., 2001, “The $\sqrt{7}R19.1°$ superlattice of Ar/Ag(111),” Phys. Rev. B **64**, 033407.

Bruch, L. W., 2003, “Topography and energy variation in physisorbed layers,” Phys. Rev. B **68**, 235420.

Bruch, L. W., 2004, “Corrugation energy for octane on Cu(111),” J. Chem. Phys. **121**, 11388–11389.

Bruch, L. W., 2005, “Evaluation of the van der Waals force for atomic force microscopy,” Phys. Rev. B **72**, 033410.

Bruch, L. W., M. W. Cole, and E. Zaremba, 1997, *Physical Adsorption: Forces and Phenomena* (Oxford University Press, Oxford, England). Corrected reprinting by Dover Publications, Inc. (Mineola, New York, 2007).

Bruch, L. W., and J. M. Gottlieb, 1988, “Calculations of the shear modulus of a two-dimensional quantum solid,” Phys. Rev. B **37**, 4920–4929.

Bruch, L. W., A. P. Graham, and J. P. Toennies, 1998, “Vibrations of the commensurate monolayer solid Xe/Pt(111),” Mol. Phys. **95**, 579–585.

Bruch, L. W., A. P. Graham, and J. P. Toennies, 2000, “The dispersion curves of the three phonon modes of xenon, krypton, and argon monolayers on the Pt(111) surface,” J. Chem. Phys. **112**, 3314–3332.

Bruch, L. W., and F. Y. Hansen, 1997, “Mode damping in a commensurate monolayer solid,” Phys. Rev. B **55**, 1782–1792.

Bruch, L. W., and F. Y. Hansen, 1998, “Monolayer solid of N_2/Ag(111),” Phys. Rev. B **57**, 9285–9292.

Bruch, L. W., and F. Y. Hansen, 2005, “Excitation of the shear horizontal mode in a monolayer by inelastic helium atom scattering,” J. Chem. Phys. **122**, 114714.

Bruch, L. W., and A. D. Novaco, 2000, “Anharmonic effects on monolayer phonons,” Phys. Rev. B **61**, 5786–5792.

Bruch, L. W., and J. A. Venables, 1984, “Geometrical considerations in monolayer physisorption,” Surf. Sci. **148**, 167–186.

Brunauer, S., P. H. Emmett, and E. Teller, 1938, “Adsorption of gases in multimolecular layers,” J. Am. Chem. Soc. **60**, 309–319.

Brunet, F., R. Schaub, S. Fédrigo, R. Monot, J. Buttet, and W. Harbich, 2002, “Rare gases physisorbed on Pt(111): A low-temperature STM investigation,” Surf. Sci. **512**, 201–220.

Bruschi, L., G. Fois, A. Pontarollo, G. Mistura, B. Torre, F. Buatier de Mongeot, C. Boragno, R. Buzio, and U. Valbusa, 2006, “Structural depinning of Ne monolayers on Pb at $T < 6.5$ K,” Phys. Rev. Lett. **96**, 216101.

Calbi, M. M., M. W. Cole, S. M. Gatica, M. J. Bojan, and G. Stan, 2001, “Condensed phases of gases inside nanotube bundles,” Rev. Mod. Phys. **73**, 857–865.

Calisti, S., J. Suzanne, and J. A. Venables, 1982, “A LEED study of adsorbed neon on graphite,” Surf. Sci. **115**, 455–468.

Caragiu, M., T. Seyller, and R. D. Diehl, 2001, “The adsorption geometry of Ag(111)-$(\sqrt{7}\times\sqrt{7})R19.1°$-4 Ar,” Surf. Sci. **475**, 89–95.

Caragiu, M., T. Seyller, and R. D. Diehl, 2002, “Dynamical LEED study of Pd(111)-$(\sqrt{3}\times\sqrt{3})R30°$-Xe,” Phys. Rev. B **66**, 195411.

Caragiu, M., T. Seyller, and R. D. Diehl, 2003, “Adsorption geometry of Cu(110)-(12×2)-14 Xe,” Surf. Sci. **539**, 165–170.

Carlin, A., L. Bruschi, M. Ferrari, and G. Mistura, 2003, “Observation of depinning phenomena in the sliding friction of Kr films on gold,” Phys. Rev. B **68**, 045420.

Carlsson, A. F., and R. J. Madix, 2001, “Intrinsic and extrinsic precursors to adsorption: Coverage and temperature dependence of Kr adsorption on Pt(111),” J. Chem. Phys. **114**, 5304–5312.

Carpick, R. W., and J. D. Batteas, 2004, “Scanning probe studies of nano-scale adhesion between solids in the presence of liquids and monolayer films,” in *Handbook of Nanotechnology*, edited by B. Bhushan (Springer, Berlin), pp. 603–628.

Cassuto, A., 1988, “On the validity of the desorption-rate version of the Langmuir isotherm proposed by K. Nagai,” Surf. Sci. **203**, L656–L658.

Celestini, F., D. Passerone, F. Ercolessi, and E. Tosatti, 2000, "Reentrant layering in rare gas adsorption: Preroughening or premelting," Phys. Rev. Lett. **84**, 2203–2206.

Chan, M., N. Mulders, and J. Reppy, 1996, "Helium in aerogels," Phys. Today **49** (8), 30–37.

Chan, M. H. W., A. D. Migone, K. D. Miner, and Z. R. Li, 1984, "Thermodynamic study of phase transitions of monolayer N_2 on graphite," Phys. Rev. B **30**, 2681–2694.

Chen, J.-R., and R. Gomer, 1980, "Mobility and two-dimensional compressibility of Xe on the (110) plane of tungsten," Surf. Sci. **94**, 456–468.

Chen, X.-R., A. Oshiyama, and S. Okada, 2003a, "Scanning tunneling microscopy images of argon monolayer on a monolayer graphite surface," Chem. Phys. Lett. **371**, 528–533.

Chen, X.-R., A. Oshiyama, and S. Okada, 2003b, "First-principles calculation for scanning-tunneling-microscopy images of Kr adsorbed on a monolayer graphite surface," Phys. Rev. B **67**, 033408.

Chen, X.-R., X.-L. Zhou, J. Zhu, and Q.-Q. Gou, 2003, "Xenon atoms adsorption on graphite sheet: First-principles calculations," Phys. Lett. A **315**, 403–408.

Chesters, M. A., and J. Pritchard, 1971, "LEED and surface potential study of carbon monoxide and xenon adsorbed on Cu(100)," Surf. Sci. **28**, 460–468.

Chickos, J. S., and W. E. Acree, Jr., 2002, "Enthalpies of sublimation of organic and organometallic compounds, 1910–2001," J. Phys. Chem. Ref. Data **31**, 537–698.

Chickos, J. S., and W. Hanshaw, 2004a, "Vapor pressures and vaporization enthalpies of the *n*-alkanes from C_{21} to C_{30} by correlation gas chromatography," J. Chem. Eng. Data **49**, 77–85.

Chickos, J. S., and W. Hanshaw, 2004b, "Vapor pressures and vaporization enthalpies of the *n*-alkanes from C_{31} to C_{38} by correlation gas chromatography," J. Chem. Eng. Data **49**, 620–630.

Chinn, M. D., 1977, "Low-energy electron diffraction from epitaxial solid krypton layers on graphite," Ph.D. thesis (University of Washington–Seattle).

Chinn, M. D., and S. C. Fain, Jr., 1977, "Structural phase transition in epitaxial solid krypton monolayers on graphite," Phys. Rev. Lett. **39**, 146–149.

Choi, B. I., H. S. Nham, S. Y. Kwon, J. C. Kim, H. S. Youn, and T. K. Lim, 2005, "Multilayer adsorption of krypton on graphite using an ellipsometric technique," J. Korean Phys. Soc. **47**, 836–483.

Choi, B. I., H. S. Nham, H. S. Youn, and T. K. Lim, 2006, "Multilayer adsorption of argon on graphite by using an ellipsometric technique," J. Korean Phys. Soc. **49**, 2338–2347.

Chung, T. T., and J. G. Dash, 1977, "N_2 monolayers on graphite: Specific heat and vapor pressure measurements thermodynamics of size effects and steric factors," Surf. Sci. **66**, 559–580.

Clarke, S., G. Bihlmayer, and S. Blügel, 2001, "Chemical effects in rare gas adsorption: FLAPW calculations for Ag(001)$c(2\times2)$-Xe," Phys. Rev. B **63**, 085416.

Classen, J., K. Eschenröder, and G. Weiss, 1996, "Structural relaxation and surface diffusion of quench-condensed hydrogen films," Physica B **219-220**, 678–680.

Clugston, M. J., 1978, "The calculation of intermolecular forces. A critical examination of the Gordon-Kim model," Adv. Phys. **27**, 893–912.

Coffey, T., and J. Krim, 2005, "Impact of substrate corrugation on the sliding friction levels of adsorbed films," Phys. Rev. Lett. **95**, 076101.

Coffey, T. S., 2004, "Nanotribology fundamentals: Predicting the viscous coefficient of friction," Ph.D. thesis (North Carolina State University, Rayleigh).

Cohen, D., and Y. Zeiri, 1992, "A theoretical study of the surface diffusion of large molecules. I. *n*-alkane-type chains on W(100)," J. Chem. Phys. **97**, 1531–1541.

Colbourn, E. A., and A. E. Douglas, 1976, "The spectrum and ground state potential curve of Ar_2," J. Chem. Phys. **65**, 1741–1745.

Colwell, J. H., E. K. Gill, and J. A. Morrison, 1963, "Thermodynamic properties of CH_4 and CD_4: Interpretation of the properties of the solids," J. Chem. Phys. **39**, 635–653.

Comsa, G., K. Kern, and B. Poelsema, 1992, "Physisorbed rare gas adlayers studied with helium scattering," in *Helium Atom Scattering from Surfaces*, edited by E. Hulpke (Springer, Berlin), pp. 243–263.

Coppersmith, S. N., D. S. Fisher, B. I. Halperin, P. A. Lee, and W. F. Brinkman, 1982, "Dislocations and the commensurate-incommensurate transition in two dimensions," Phys. Rev. B **25**, 349–363.

Coulomb, J. P., and M. Bienfait, 1986, "Diffusive motions in 2D phases of ethane adsorbed on graphite," J. Phys. (Paris) **47**, 89–95.

Coulomb, J. P., M. Bienfait, and P. Thorel, 1979, "Evidence of two kinds of two-dimensional adsorbed fluids by mobility measurements," Phys. Rev. Lett. **42**, 733–735.

Coulomb, J. P., M. Bienfait, and P. Thorel, 1981, "Mobility measurements of two kinds of two-dimensional fluids. Methane adsorbed on graphite," J. Phys. (Paris) **42**, 293–306.

Coulomb, J. P., Y. Larher, M. Trabelsi, and I. Mirebeau, 1994, "Neutron diffraction investigation of the structure of the C_2D_2 film physisorbed upon MgO(100)," Mol. Phys. **81**, 1259–1264.

Coulomb, J. P., T. S. Sullivan, and O. E. Vilches, 1984, "Adsorption of Kr, Xe, and Ar on highly uniform MgO smoke," Phys. Rev. B **30**, 4753–4760.

Crawford, R. K., 1977, "Melting, vaporization and sublimation," in *Rare Gas Solids*, edited by M. L. Klein and J. A. Venables (Academic, London), Vol. 2, Chap. 11, pp. 663–728.

Cui, J., S. C. Fain, Jr., H. Freimuth, H. Wiechert, H. P. Schildberg, and H. J. Lauter, 1988, "Modulated structures for incommensurate monolayer solid phases of D_2 physisorbed on graphite," Phys. Rev. Lett. **60**, 1848–1851.

Curtarolo, S., W. Setyawan, N. Ferralis, R. D. Diehl, and M. W. Cole, 2005, "Evolution of topological order in Xe films on a quasicrystal surface," Phys. Rev. Lett. **95**, 136104.

Cyr, D. M., B. Venkataraman, and G. W. Flynn, 1996, "STM investigations of organic molecules physisorbed at the liquid-solid interface," Chem. Mater. **8**, 1600–1615.

Dai, P., Z. Wu, T. Angot, S. K. Wang, H. Taub, and S. N. Ehrlich, 1999, "Synchrotron x-ray-diffraction study of the structure and growth of Xe films adsorbed on the Ag(111) surface," Phys. Rev. B **59**, 15464–15479.

Daillant, J., and M. Alba, 2000, "High resolution x-ray scattering measurements: I. Surfaces," Rep. Prog. Phys. **63**, 1725–1777.

Daly, C., and J. Krim, 1996, "Sliding friction of solid xenon monolayers and bilayers on Ag(111)," Phys. Rev. Lett. **76**, 803–806.

D'Amico, K. L., J. Bohr, D. E. Moncton, and D. Gibbs, 1990, "Melting and orientational epitaxy in argon and xenon monolayers on graphite," Phys. Rev. B **41**, 4368–4376.

D'Amico, K. L., and D. E. Moncton, 1986, "X-ray study of orientational epitaxy in rare gas monolayers on graphite," J. Vac. Sci. Technol. A **4**, 1455–1458.

Dash, J. G., 1975, *Films on Solid Surfaces* (Academic, New York).

Dash, J. G., 1988, "Phase transitions at interfaces: Roughening, surface melting, and triple point wetting," in *Solvay Conference on Surface Science*, edited by F. W. de Wette (Springer, Berlin), pp. 142–167.

Dash, J. G., 2002, "Melting from one to two to three dimensions," Contemp. Phys. **43**, 427–436.

Dash, J. G., and R. D. Puff, 1981, "Phase transitions in heterogeneous films," Phys. Rev. B **24**, 295–309.

Da Silva, J. L. F., and C. Stampfl, 2007, "Nature of xenon adsorption on graphite: On-top versus hollow site preference," Phys. Rev. B **76**, 085301.

Da Silva, J. L. F., C. Stampfl, and M. Scheffler, 2003, "Adsorption of Xe atoms on metal surfaces: New insights from first-principles calculations," Phys. Rev. Lett. **90**, 066104.

Da Silva, J. L. F., C. Stampfl, and M. Scheffler, 2005, "Xe adsorption on metal surfaces: First-principles investigations," Phys. Rev. B **72**, 075424.

Day, P., M. Lysek, M. LaMadrid, and D. Goodstein, 1993, "Phase transitions in argon films," Phys. Rev. B **47**, 10716–10726.

Dayo, A., W. Alnasrallah, and J. Krim, 1998, "Superconductivity-dependent sliding friction," Phys. Rev. Lett. **80**, 1690–1693.

DeKieviet, M., D. Dubbers, C. Schmidt, D. Scholz, and U. Spinola, 1995, "^{3}He spin echo: New atomic beam technique for probing phenomena in the neV range," Phys. Rev. Lett. **75**, 1919–1922.

den Nijs, M., 1991, "Interplay between surface roughening, preroughening, and reconstruction," in *Phase Transitions in Surface Films 2*, edited by H. Taub, G. Torzo, H. J. Lauter, and S. C. Fain, Jr. (Plenum, New York), pp. 247–267.

DeOliveira, M. J., and R. B. Griffiths, 1978, "Lattice-gas model of multiple layer adsorption," Surf. Sci. **71**, 687–694.

Dham, A. K., W. J. Meath, A. R. Allnatt, R. A. Aziz, and M. J. Slaman, 1990, "XC and HFD-B potential energy curves for Xe-Xe and related physical properties," Chem. Phys. **142**, 173–189.

Diama, A., and A. D. Migone, 1999, "Multilayer Kr films adsorbed on BN," Phys. Rev. B **60**, 16103–16108.

Diama, A., M. Simpson, H. Taub, F. Y. Hansen, R. M. Dimeo, D. A. Neumann, K. W. Herwig, and U. G. Volkmann, 2007, "Studies of dynamical layering in adsorbed organic films," in *Quasi-Elastic Neutron Scattering Conference 2006 (QENS2006) Proceedings*, edited by P. E. Sokol, H. Kaisser, D. Baxter, R. Pynn, D. Bossev, and M. Leuschner (Materials Research Society, Warrendale, PA), pp. 89–95.

Diehl, R. D., and S. Chandavarkar, 1989, "The use of a flat suppressor in low-energy electron diffraction," J. Phys. E **22**, 651–656.

Diehl, R. D., N. Ferralis, K. Pussi, M. W. Cole, W. Setyawan, and S. Curtarolo, 2006, "The ordering of a Xe monolayer on quasicrystalline Al-Ni-Co," Philos. Mag. **86**, 863–868.

Diehl, R. D., and R. McGrath, 1997, "Current progress in understanding alkali metal adsorption on metal surfaces," J. Phys.: Condens. Matter **9**, 951–968.

Diehl, R. D., W. Setyawan, N. Ferralis, R. A. Trasca, M. W. Cole, and S. Curtarolo, 2007, "Ordering of rare gas films on a decagonal Al-Ni-Co quasicrystal," Philos. Mag. **87**, 2973–2980.

Diehl, R. D., T. Seyller, M. Caragiu, G. S. Leatherman, N. Ferralis, K. Pussi, P. Kaukasoina, and M. Lindroos, 2004, "The adsorption sites of rare gases on metallic surfaces: A review," J. Phys.: Condens. Matter **16**, S2839–S2862.

Dienwiebel, M., P. Zeppenfeld, J. Einfeld, G. Comsa, F. Picaud, C. Ramseyer, and C. Girardet, 2000, "Effect of the diffusion anisotropy on the nucleation and growth of xenon on Cu(110)," Surf. Sci. **446**, L113–L119.

Dimon, P., P. M. Horn, M. Sutton, R. J. Birgenau, and D. E. Moncton, 1985, "1st-order and continuous melting in a 2-dimensional system: Monolayer xenon on graphite," Phys. Rev. B **31**, 437–447.

Dion, M., H. Rydberg, E. Schröder, D. C. Langreth, and B. I. Lundqvist, 2004, "van der Waals density functional for general geometries," Phys. Rev. Lett. **92**, 246401.

Douliez, J.-P., A. Léonard, and E. J. Dufourc, 1995, "Restatement of order parameters in biomembranes: Calculation of C-C bond order parameters from C-D quadrupolar splittings," Biophys. J. **68**, 1727–1739.

Driver, S. M., and D. A. King, 2007, "Methanethiolate structural phases on Cu{111} observed using a novel fibre-optic low-energy electron diffraction instrument," Surf. Sci. **601**, 510–517.

Drummond, M. L., B. G. Sumpter, W. A. Shelton, and J. Z. Larese, 2006, "Density functional investigation of the adsorption of a methane monolayer on an MgO(100) surface," Phys. Rev. B **73**, 195313.

Ehrlich, G., and F. G. Hudda, 1959, "Interaction of rare gases with metal surfaces. I. A, Kr and Xe on tungsten," J. Chem. Phys. **30**, 493–512.

Eigler, D. M., and E. K. Schweitzer, 1990, "Positioning single atoms with a scanning tunneling microscope," Nature (London) **344**, 524–526.

Elliott, G. S., D. H. Wei, K. J. Wu, and S. D. Kevan, 1993, "Substrate-mediated dispersion interaction effects in the properties of a physisorbed gas," J. Chem. Phys. **99**, 4152–4159.

Ellis, J., and A. P. Graham, 1997, "The use of quasielastic helium atom scattering to study correlated motion in adsorbate overlayers," Surf. Sci. **377-379**, 833–842.

Ellis, J., A. P. Graham, and J. P. Toennies, 1999, "Quasielastic helium atom scattering from a two-dimensional gas of Xe atoms on Pt(111)," Phys. Rev. Lett. **82**, 5072–5075.

Ellis, T. H., G. Scoles, U. Valbusa, H. Jónsson, and J. H. Weare, 1985, "Hydrogen atom scattering from physisorbed layers. I. Diffraction," Surf. Sci. **155**, 499–534.

Enevoldsen, A. D., F. Y. Hansen, A. Diama, L. Criswell, and H. Taub, 2007, "A comparative study of normal and branched alkane monolayer films of relevance to nanolubrication. I. Structure," J. Chem. Phys. **126**, 104703.

Enevoldsen, A. D., F. Y. Hansen, A. Diama, H. Taub, R. M. Dimeo, D. A. Neumann, and J. R. D. Copley, 2007, "A comparative study of normal and branched alkane monolayer films of relevance to nanolubrication. II. Dynamics," J. Chem. Phys. **126**, 104704.

Etters, R. D., 1989, "Structures and phase transitions of simple molecular solids," in *Simple Molecular Systems at Very High Density*, Vol. 186 of NATO Advanced Studies Institute, Series B: Physics, edited by A. Polian, P. Loubeyre, and N. Boccara (Plenum, New York), pp. 109–139.

Etters, R. D., and B. Kuchta, 1998, "The character of melting for simple molecules deposited on graphite," J. Low Temp. Phys. **111**, 271–286.

Ewing, G. E., 1993, "Excitons and high resolution infrared spectroscopy of adlayers on ionic surfaces," in *Adsorption on Ordered Surfaces of Ionic Solids and Thin Films*, edited by E. Umbach and H. J. Freund (Springer-Verlag, Berlin), pp. 57–67.

Fain, S. C., Jr., C. A. Polwarth, S. L. Tait, C. T. Campbell, and R. H. French, 2006, "Simulated measurement of small metal clusters by frequency-modulation non-contact atomic force microscopy," Nanotechnology **17**, S121–S127.

Farrar, J. M., T. P. Schafer, and Y. T. Lee, 1973, "Intermolecular potentials of symmetric rare gas pairs from elastic differential cross section measurements," in *Transport Phenomena—1973*, edited by J. Kestin, AIP Conf. Proc. No. 11 (AIP, Melville, NY), pp. 279–295.

Faul, J. W. O., U. G. Volkmann, and K. Knorr, 1990, "Ellipsometric thickness and coverage of physisorbed layers of Xe, Kr, Ar and N_2 on graphite," Surf. Sci. **227**, 390–394.

Felici, R., M. Pedio, F. Borgatti, S. Iannotta, M. Capozi, G. Ciullo, and A. Stierle, 2005, "X-ray-diffraction characacterization of Pt(111) surface nanopatterning induced by C_{60} adsorption," Nat. Mater. **4**, 688–692.

Fernandez-Canoto, D., and J. Larese, 2007, "Thermodynamic investigations of thin *n*-heptane films adsorbed on magnesium oxide (100) surfaces," Bull. Am. Phys. Soc. **52**, 1 (March), paper N 18-2.

Ferralis, N., R. D. Diehl, K. Pussi, M. Lindroos, I. Fisher, and C. J. Jenks, 2004, "Low-energy electron diffraction study of Xe adsorption on the ten-fold decagonal Al-Ni-Co quasicrystal surface," Phys. Rev. B **69**, 075410.

Ferralis, N., H. I. Li, K. J. Hanna, J. Stevens, F. M. Pan, and R. D. Diehl, 2007, "Structural and thermal properties of Xe on the Pb(111) surface studied by low-energy electron diffraction," J. Phys.: Condens. Matter **19**, 056011.

Ferry, D. P. ., N.M. Hoang, J. Suzannet, J. P. Biberian, and M. A. Van Hove, 1997, "Structure of physisorbed molecules on an oxide surface from potential calculations and dynamical low-energy electron diffraction analysis: acetylene on MgO(100)," Phys. Rev. Lett. **78**, 4237–4240.

Fichthorn, K. A., and R. A. Miron, 2002, "Thermal desorption of large molecules from solid surfaces," Phys. Rev. Lett. **89**, 196103.

Firment, L. E., and G. A. Somorjai, 1977, "Surface structure of normal paraffins and cyclohexane monolayers and thin crystals grown on the (111) crystal face of platinum: A low-energy electron diffraction study," J. Chem. Phys. **66**, 2901–2913.

Firment, L. E., and G. A. Somorjai, 1978, "Low-energy electron diffraction study of the surface of thin crystals and monolayers of normal paraffins and cyclohexane on the Ag(111) crystal surface," J. Chem. Phys. **69**, 3940–3952.

Flenner, E., and R. D. Etters, 2002, "Behavior of partial monolayers of argon adlayers deposited on graphite," Phys. Rev. Lett. **88**, 106101.

Flenner, E., and R. D. Etters, 2006, "Properties of argon adlayers deposited on graphite from Monte Carlo calculations," Phys. Rev. B **73**, 125419.

Freeman, D. E., K. Yoshino, and Y. Tanaka, 1974, "Vacuum ultraviolet absorption spectrum of the van der Waals moledule Xe_2. I. Ground state vibrational structure, potential well depth, and shape," J. Chem. Phys. **61**, 4880–4889.

Frieß, W., H. Schlichting, and D. Menzel, 2007, "Desorption energies of rare gases on some close-packed transition metal surfaces" (unpublished).

Freitag, A., and J. Z. Larese, 2000, "Layer growth of methane on MgO: An adsorption isotherm study," Phys. Rev. B **62**, 8360–8365.

Fuhrmann, D., L. Criswell, H. Mo, U. G. Volkmann, K. W. Herwig, H. Taub, and F. Y. Hansen, 2000, "Diffusive motion in model soft matter systems: Quasielastic neutron scattering study of short- and intermediate-length alkane layers," Physica B **276-278**, 345–346.

Fuhrmann, D., R. Gerlach, H.-G. Rubahn, and C. Wöll, 1999, "Structure and phase transitions of ultrathin films of alkanes adsorbed on Cu(111)," Surf. Sci. **424**, 145–154.

Fuhrmann, D., and A. P. Graham, 2004, "Spectroscopy of the conformational disorder in molecular films: Tetracosane and squalane on Pt(111)," J. Chem. Phys. **120**, 2439–2444.

Fuhrmann, D., and C. Wöll, 1996, "Damping of external molecular vibrations at surfaces: Alkanes on Cu(111) and Pb(111)," Surf. Sci. **368**, 20–26.

Fuhrmann, D., and C. Wöll, 1997, "The melting of a two-dimensional lattice of flexible rod-shaped molecules: Structure and dynamics studied by He atom scattering," Surf. Sci. **377-379**, 544–549.

Fuhrmann, D., and C. Wöll, 1998, "The microscopic origins of sliding friction: A spectroscopic approach," New J. Phys. **1**, 1.1–1.9.

Gai, Z., B. Wu, J. P. Pierce, G. A. Farnan, D. J. Shu, M. Wang, Z. Y. Zhang, and J. Shen, 2002, "Self-assembly of nanometer-scale magnetic dots with narrow size distributions on an insulating substrate," Phys. Rev. Lett. **89**, 235502.

Gangwar, R., N. J. Collela, and R. M. Suter, 1989, "Thermodynamics of freezing in two dimensions: The compressibility of monolayer xenon on graphite," Phys. Rev. B **39**, 2459–2471.

Gatica, S. M., M. J. Bojan, M. W. Cole, M. M. Calbi, and J. K. Johnson, 2007, "Adsorbed gases in bundles of carbon nanotubes: Theory and simulation," in *Adsorption by Carbons*, edited by E. Bottani and J. M. D. Tascon (Elsevier, Amsterdam), Chap. 15.

Gay, J. M., A. Dutheil, J. Krim, and J. Suzanne, 1986, "A LEED study of methane films adsorbed on graphite in the monolayer range," Surf. Sci. **177**, 25–35.

Gay, J. M., J. Suzanne, and R. Wang, 1986, "Phase transitions, thermodynamics and structural analysis of ethane films adsorbed on graphite," J. Chem. Soc., Faraday Trans. 2 **82**, 1669–1684.

Gellman, A. J., 2005, "Oligomer desorption during heterogeneous catalytic synthesis of polymers," Catal. Today **105**, 144–151.

Gerlach, R., A. P. Graham, J. P. Toennies, and H. Weiss, 1998, "A helium atom scattering study of the structure and dynamics of a Xe monolayer on NaCl(001)," J. Chem. Phys. **109**, 5319–5326.

Giancarlo, L. C., and G. W. Flynn, 1998, "Scanning tunneling and atomic force microscopy probes of self-assembled, physisorbed monolayers: Peeking at the peaks," Annu. Rev. Phys. Chem. **49**, 297–336.

Gibson, K. D., C. Cerjan, J. C. Light, and S. J. Sibener, 1988, "Elastic helium scattering studies of ordered overlayers of Ar, Kr, and Xe physisorbed on Ag(111)," J. Chem. Phys. **88**, 7911–7941.

Gibson, K. D., and S. J. Sibener, 1985, "Helium scattering studies of the surface structure and dynamics of rare-gas crystals," Faraday Discuss. Chem. Soc. **80**, 203–215.

Gibson, K. D., and S. J. Sibener, 1988, "Inelastic helium scattering studies of the vibrational spectroscopy and dynamics of ordered Ar, Kr, and Xe multilayers physisorbed on Ag(111)," J. Chem. Phys. **88**, 7893–7910.

Glachant, A., and U. Bardi, 1979, "Thermodynamics and kinetics of Xe monolayer adsorption on Cu(100) by LEED and AES," Surf. Sci. **87**, 187–202.

Glachant, A., M. Bienfait, and M. Jaubert, 1984, "Uniaxial compressibility of a complete monolayer of Xe adsorbed on Cu(110)," Surf. Sci. **148**, L665–L670.

Glebov, A. L., V. Panella, J. P. Toennies, F. Traeger, H. Weiss, S. Picaud, P. N. M. Hoang, and C. Girardet, 2000, "Experimental and theoretical studies of acetylene layers adsorbed on KCl(001)," Phys. Rev. B **61**, 14028–14036.

Gnecco, E., R. Bennewitz, T. Gyalog, and E. Meyer, 2001, "Friction experiments on the nanometre scale," J. Phys.: Condens. Matter **13**, R619–R642.

Godfrin, H., and H. J. Lauter, 1995, "Experimental properties of ^{3}He adsorbed on graphite," in *Progress in Low Temperature Physics*, edited by W. P. Halperin (North-Holland, Amsterdam), Vol. XIV, Chap. 4, pp. 213–320.

Gomer, R., 1959, "Adsorption and diffusion of argon on tungsten," J. Phys. Chem. **63**, 468–472.

Gomer, R., 1990, "Diffusion of adsorbates on metal surfaces," Rep. Prog. Phys. **53**, 917–1002.

Gordon, M. B., 1986, "Comment on 'Complete wetting on strong substrates: Xe/Pt(111),' " Phys. Rev. Lett. **57**, 2094.

Gordon, R. G., and Y. S. Kim, 1972, "Theory for the forces between closed-shell atoms and molecules," J. Chem. Phys. **56**, 3122–3133.

Gottlieb, J. M., 1990, "Energy and structure of uniaxial incommensurate monolayer solids: Application to Xe/Pt(111)," Phys. Rev. B **42**, 5377–5380.

Gottlieb, J. M., and L. W. Bruch, 1991, "Uniaxial incommensurate rare-gas-monolayer solids. II. Application to Xe/Pt(111)," Phys. Rev. B **44**, 5759–5765.

Graham, A. P., 2003, "The low energy dynamics of adsorbates on metal surfaces investigated with helium atom scattering," Surf. Sci. Rep. **49**, 115–168.

Graham, A. P., M. F. Bertino, F. Hofmann, J. P. Toennies, and C. Wöll, 1997, "Experimental determination of a longitudinal phonon dispersion curve in a quasi-two-dimensional system," J. Chem. Phys. **106**, 6194–6197; **107**, 4445 (1997).

Green, M. J., B. J. Barner, and R. M. Corn, 1991, "Real-time sampling electronics for double modulation experiments with Fourier transform infrared spectrometers," Rev. Sci. Instrum. **62**, 1426–1430.

Grimm, B., H. Hövel, M. Bödecker, K. Fieger, and B. Reihl, 2000, "Observation of domain-wall dynamics in rare-gas monolayers at $T=5$ K," Surf. Sci. **454-456**, 618–622.

Grimm, B., H. Hövel, M. Pollmann, and B. Reihl, 1999, "Physisorbed rare-gas monolayers: Evidence for domain-wall tilting," Phys. Rev. Lett. **83**, 991–994.

Gumhalter, B., 2001, "Single- and multiphonon atom-surface scattering in the quantum regime," Phys. Rep. **351**, 1–159.

Gustafsson, K., and S. Andersson, 2006, "Dipole active vibrations and dipole moments of N_2 and O_2 physisorbed on a metal surface," J. Chem. Phys. **125**, 044717.

Hall, B., D. L. Mills, P. Zeppenfeld, K. Kern, U. Becher, and G. Comsa, 1989, "Anharmonic damping in rare-gas multilayers," Phys. Rev. B **40**, 6326–6338.

Hamichi, M., A. Q. D. Faisal, J. A. Venables, and R. Kariotis, 1989, "Lattice parameter and orientation of xenon on graphite at low pressures," Phys. Rev. B **39**, 415–425.

Hamichi, M., R. Kariotis, and J. A. Venables, 1991, "Diffraction profiles of xenon on graphite at low temperatures," Phys. Rev. B **43**, 3208–3214.

Hansen, F. Y., and L. W. Bruch, 2001, "Molecular diffusion in monolayer and submonolayer nitrogen," Phys. Rev. B **64**, 045413.

Hansen, F. Y., L. Criswell, D. Fuhrmann, K. W. Herwig, A. Diama, R. M. Dimeo, D. A. Neumann, U. G. Volkmann, and H. Taub, 2004, "Intramolecular diffusive motion in alkane monolayers studied by high-resolution quasielastic neutron scattering and molecular dynamics simulations," Phys. Rev. Lett. **92**, 046103.

Hansen, F. Y., V. L. P. Frank, H. Taub, L. W. Bruch, H. J. Lauter, and J. R. Dennison, 1990, "Corrugation in the nitrogen-graphite potential probed by inelastic neutron scattering," Phys. Rev. Lett. **64**, 764–767.

Hansen, F. Y., K. W. Herwig, B. Matthies, and H. Taub, 1999, "Intramolecular and lattice melting in *n*-alkane monolayers: An analog of melting in lipid bilayers," Phys. Rev. Lett. **83**, 2362–2365.

Hansen, F. Y., and H. Taub, 1991, "A molecular dynamics study of the effect of steric properties on the melting of quasi two-dimensional systems," in *Phase Transitions in Surface Films 2*, edited by H. Taub, G. Torzo, H. J. Lauter, and S. C. Fain, Jr. (Plenum, New York), pp. 153–168.

Hansen, F. Y., and H. Taub, 1992, "Melting mechanism in monolayers of flexile rod-shaped molecules," Phys. Rev. Lett. **69**, 652–655.

Hansen, F. Y., and H. Taub, 2004, "Analysis of the center of mass-, rotational- and intramolecular diffusive motions in a monolayer film of intermediate-length alkane molecules adsorbed on a solid surface," in *Proceedings of the 3rd International Symposium on Slow Dynamics in Complex Systems*, edited by M. Tokuyama and I. Oppenheim, AIP Conf. Proc. No. 708 (AIP, Melville, NY), pp. 233–236.

Hassel, M., K. Svensson, J. Bellman, S. Andersson, and M. Persson, 2002, "Photodesorption of physisorbed hydrogen molecules," Phys. Rev. B **65**, 205402.

Heidberg, J., E. Kampshoff, R. Kühnemuth, O. Schönekäs, and M. Suhren, 1990, "High resolution infrared spectroscopy of adsorbates on ionic crystal surfaces," J. Electron Spectrosc. Relat. Phenom. **54-55**, 945–960.

Heidberg, J., A. Voßberg, M. Hustedt, M. Thomas, S. Briquez, S. Picaud, and C. Girardet, 1999, "Monolayers of ortho-H_2, para-H_2, para-D_2 and normal-H_2 adsorbed on NaCl(001) single crystal surfaces," J. Chem. Phys. **110**, 2566–2578.

Heidberg, J., M. Warskulat, and M. Folman, 1990, "Fourier-transform-infrared spectroscopy of carbon monoxide physisorbed on highly oriented graphite," J. Electron Spectrosc. Relat. Phenom. **54/55**, 961–970.

Heiney, P. A., P. W. Stephens, R. J. Birgenau, P. M. Horn, and D. E. Moncton, 1983, "X-ray scattering study of the structure and freezing transition of monolayer xenon on graphite," Phys. Rev. B **28**, 6416–6434.

Hepburn, J., G. Scoles, and R. Penco, 1975, "A simple but reliable method for the prediction of intermolecular potentials," Chem. Phys. Lett. **36**, 451–456.

Herman, P. R., P. E. LaRocque, and B. P. Stoicheff, 1988, "Vacuum ultraviolet laser spectroscopy. V. Rovibronic spectra of Ar_2 and constants of the ground and excited states," J. Chem. Phys. **89**, 4535–4549.

Hernández, M. I., J. Campos-Martínez, S. Miret-Artés, and R. D. Coalson, 1994, "Lifetimes of selective-adsorption resonances in atom-surface elastic scattering," Phys. Rev. B **49**, 8300–8309.

Herwig, K. W., B. Matthies, and H. Taub, 1995, "Solvent effects on the monolayer structure of long *n*-alkane molecules adsorbed on graphite," Phys. Rev. Lett. **75**, 3154–3157.

Herwig, K. W., J. C. Newton, and H. Taub, 1994, "Structure and growth of butane films adsorbed on graphite," Phys. Rev. B **50**, 15287–15297.

Herwig, K. W., Z. Wu, P. Dai, H. Taub, and F. Y. Hansen, 1997, "Quasielastic neutron scattering and molecular dynamics simulation studies of the melting transition in butane and hexane monolayers adsorbed on graphite," J. Chem. Phys. **107**, 5186–5196.

Hess, G. B., 1991, "Multilayer physisorbed films on graphite," in *Phase Transitions in Surface Films 2*, edited by H. Taub, G. Torzo, H. J. Lauter, and S. C. Fain, Jr. (Plenum, New York), pp. 357–389.

Hess, G. B., 2002, "Tunable Fermi resonance in a C_2F_6 monolayer on graphite," J. Chem. Phys. **116**, 6777–6781.

Hess, G. B., B. L. Ellis, and Y. Li, 2006, "Mixing in a solid monolayer: $SF_6+C_2F_6$ on graphite," March meeting of the American Physical Society, paper W12-12.

Hess, G. B., T. Hopkins, and Y. Xia, 2005, "Co-adsorption of CF_4 and SF_6 on graphite," Bull. Am. Phys. Soc. **50**, 1441, paper X34-11.

Highland, M., and J. Krim, 2006, "Superconductivity dependent friction of water, nitrogen and superheated He films adsorbed on Pb(111)," Phys. Rev. Lett. **96**, 226107.

Hilgers, G., M. Potthoff, N. Müller, and U. Heinzmann, 1995, "Structure investigations of Xe-adsorbate layers by spin-polarized low-energy electron diffraction II. $(\sqrt{3}\times\sqrt{3})R30°$-Xe/Pd(111) and the dilute phase of Xe/Pd(111)," Surf. Sci. **322**, 207–220.

Hirschfelder, J. O., C. F. Curtiss, and R. B. Bird, 1964, *Molecular Theory of Gases and Liquids* (Wiley, New York).

Hong, H., C. J. Peters, A. Mak, R. J. Birgeneau, P. M. Horn, and H. Suematsu, 1987, "Commensurate-incommensurate and rotational transitions of monolayer xenon on single-crystal graphite," Phys. Rev. B **36**, 7311–7314.

Hong, H., C. J. Peters, A. Mak, R. J. Birgeneau, P. M. Horn, and H. Suematsu, 1989, "Synchrotron x-ray study of the structures and phase transitions of monolayer xenon on single-crystal graphite," Phys. Rev. B **40**, 4797–4807.

Horch, S., P. Zeppenfeld, and G. Comsa, 1995a, "A scanning tunneling microscopy study of the adsorption of Xe on Pt(111) up to one monolayer," Appl. Phys. A: Mater. Sci. Process. **60**, 147–153.

Horch, S., P. Zeppenfeld, and G. Comsa, 1995b, "Temperature dependence of the xenon-layer morphology on platinum (111) studied with scanning tunneling microscopy," Surf. Sci. **331-333**, 908–912.

Horch, S., P. Zeppenfeld, R. David, and G. Comsa, 1994, "An ultrahigh vacuum scanning tunneling microscope for use at variable temperature from 10 to 400 K," Rev. Sci. Instrum. **65**, 3204–3210; **66**, 3717(E) (1995).

Horn, J. M., Z. Song, D. V. Potapenko, J. Hrbek, and M. G. White, 2005, "Characterization of molybdenum carbide nanoparticles formed on Au(111) using reactive-layer assisted deposition," J. Phys. Chem. B **109**, 44–47.

Hosomi, N., M. Suzuki, and M. Hieda, 2004, "Slippage of ^{4}He films adsorbed on grafoil," J. Low Temp. Phys. **134**, 37–42.

Hosomi, N., A. Tanabe, M. Hieda, and M. Suzuki, 2005, "Low-friction state of ^{4}He films adsorbed on grafoil," J. Phys. Chem. Solids **66**, 1532–1534.

Hostetler, M. J., W. L. Manner, R. G. Nuzzo, and G. S. Girolami, 1995, "Two-dimensional melting transitions of rod-like molecules analyzed by reflection-absorption infrared spectroscopy," J. Phys. Chem. **99**, 15 269–15 278.

Hövel, H., T. Becker, D. Funnemann, B. Grimm, C. Quitmann, and B. Reihl, 1998, "High-resolution photoemission combined with low-temperature STM," J. Electron Spectrosc. Relat. Phenom. **88-91**, 1015–1020.

Hövel, H., B. Grimm, and B. Reihl, 2001, "Modification of the Shockley-type surface state on Ag(111) by an adsorbed xenon layer," Surf. Sci. **477**, 43–49.

Howie, A., and P. R. Swann, 1961, "Direct measurements of stacking fault energies from observations of dislocation nodes," Philos. Mag. **6**, 1215–1226.

Huang, C., D. A. MacLaren, J. Ellis, and W. Allison, 2006, "Experimental determination of the helium-metal interaction potential by interferometry of nanostructured surfaces," Phys. Rev. Lett. **96**, 126102.

Huang, L., S. J. Chey, and J. H. Weaver, 1998, "Buffer-layer-assisted growth of nanocrystals: Ag-Xe-Si(111)," Phys. Rev. Lett. **80**, 4095–4098.

Hückstädt, C., S. Schmidt, S. Hüfner, F. Forster, R. Reinert, and M. Springborg, 2006, "Work function studies of rare-gas/noble metal adsorption systems using a Kelvin probe," Phys. Rev. B **73**, 075409.

Human, D., X. F. Hu, C. J. Hirschmugl, J. Ociepa, G. Hall, O. Jagutzki, and K. Ullmann-Pfleger, 2006, "Low energy electron diffraction using an electronic delay-line detector," Rev. Sci. Instrum. **77**, 023302.

Igarashi, S., Y. Abe, Y. Irie, T. Hirayama, and I. Arakawa, 1998, "Ellipsometry and low energy electron diffraction study of the layer growth of xenon physisorbed on Ag(111) surface," J. Vac. Sci. Technol. A **16**, 974–978.

Igarashi, S., A. Tosaka, T. Hirayama, and I. Arakawa, 2003, "Lateral compression of a Xe film physisorbed on Ag(111)," Langmuir **19**, 4627–4632.

Inaba, A., Y. Koga, and J. A. Morrison, 1986, "Multilayers of methane adsorbed on graphite," J. Chem. Soc., Faraday Trans. 2 **82**, 1635–1646.

Irawan, T., D. Boecker, F. Ghaleh, C. Yin, B. von Issendorff, and H. Hövel, 2006, "Metal clusters on rare gas layers—Growth and spectroscopy," Appl. Phys. A: Mater. Sci. Process. **82**, 81–86.

Ishi, S., and B. Viswanathan, 1991, "Adsorption of xenon atoms on metal surfaces," Thin Solid Films **201**, 373–402.

Israelachvili, J. N., 1992, "Adhesion, friction and lubrication of molecularly smooth surfaces," in *Fundamentals of Friction: Macroscopic and Microscopic Processes*, edited by I. L. Singer and H. M. Pollock (Kluwer, Dordrecht), pp. 351–385.

Jablonski, A., S. Eder, K. Markert, and K. Wandelt, 1986, "Two-dimensional gas-solid phase transition of xenon adsorbed on different metal substrates," J. Vac. Sci. Technol. A **4**, 1510–1513.

Jalkanen, J. P., and F. Zerbetto, 2006, "Interaction model for the adsorption of organic molecules on the silver surface," J. Phys. Chem. B **110**, 5595–5601.

Jardine, A. P., S. Dworski, P. Fouquet, G. Alexandrowicz, D. J. Riley, G. Y. H. Lee, J. Ellis, and W. Allison, 2004, "Ultrahigh-resolution spin-echo measurement of surface potential energy landscapes," Science **304**, 1790–1793.

Jardine, A. P., J. Ellis, and W. Allison, 2002, "Quasi-elastic helium atom scattering from surfaces: Experiment and interpretation," J. Phys.: Condens. Matter **14**, 6173–6191.

Jardine, A. P., J. Ellis, and W. Allison, 2004, "Effects of resolution and friction on the interpretation of QHAS measurements," J. Chem. Phys. **120**, 8724–8733.

Jardine, A. P., P. Fouquet, J. Ellis, and W. Allison, 2001, "Hexapole magnet system for thermal energy ^{3}He atom manipulation," Rev. Sci. Instrum. **72**, 3834–3841.

Jayanthi, C. S., F. Celestini, F. Ercolessi, and E. Tosatti, 2000, "Disordered flat phase separation of the Lennard-Jones fcc(111) surface," Surf. Sci. **460**, L503–L509.

Jean, N., M. I. Trioni, G. P. Brivio, and V. Bortolani, 2004, "Corrugating and anticorrugating static interactions in helium-atom scattering from metal surfaces," Phys. Rev. Lett. **92**, 013201.

Jin, A. J., M. R. Bjurstrom, and M. H. Chan, 1989, "Thermodynamic evidence of first-order melting of Xe on graphite," Phys. Rev. Lett. **62**, 1372–1375.

Johnson, D. E., J. M. Phillips, and J. Z. Larese, 1997, "Search for evidence of commensurate argon-on-graphite films near monolayer completion," Phys. Rev. B **56**, 6462–6465.

Jupille, J., H.-J. Ehrhardt, D. Fargues, and A. Cassuto, 1990, "Study of xenon layers on a Cu(111) surface," Faraday Discuss. Chem. Soc. **89**, 323–328.

Kariotis, R., J. A. Venables, and J. J. Prentis, 1988, "The free energy of domain wall fluctuations in xenon on graphite," J. Phys. C **21**, 3041–3046.

Kern, K., and G. Comsa, 1988, "Physisorbed rare gas adlayers," in *Chemistry and Physics of Solid Surfaces VII*, edited by R. Vanselow and R. F. Howe (Springer, Berlin), pp. 65–108.

Kern, K., and G. Comsa, 1991, "Modulated structures of adsorbed rare gas monolayers," in *Phase Transitions in Surface Films 2*, edited by H. Taub, G. Torzo, H. J. Lauter, and S. C. Fain, Jr. (Plenum, New York), pp. 41–65.

Kern, K., R. David, P. Zeppenfeld, and G. Comsa, 1988, "Registry effects in the thermodynamic quantities of Xe adsorption on Pt(111)," Surf. Sci. **195**, 353–370.

Kern, K., P. Zeppenfeld, R. David, and G. Comsa, 1987, "Incommensurate to high-order commensurate phase transition of Kr/Pt(111)," Phys. Rev. Lett. **59**, 79–82.

Kern, K., P. Zeppenfeld, R. David, and G. Comsa, 1988, "Two-dimensional phase transitions studied by thermal He scattering," J. Vac. Sci. Technol. A **6**, 639–645.

Kern, K., P. Zeppenfeld, R. David, R. L. Palmer, and G. Comsa, 1986, "Impurity-quenched orientational epitaxy of Kr layers on Pt(111)," Phys. Rev. Lett. **57**, 3187–3190.

Kern, K., P. Zeppenfeld, R. Palmer, and G. Comsa, 1987, "Symmetry breaking commensurate-incommensurate transition of monolayer Xe physisorbed on Pt(111)," Solid State Commun. **62**, 391–394.

Kerner, G., and M. Asscher, 2004, "Buffer layer assisted laser patterning of metals on surfaces," Nano Lett. **4**, 1433–1437.

Kerner, G., Y. Horowitz, and M. Asscher, 2005, "Diffusion of buffer layer assisted grown gold nanoclusters on Ru(100) and $p(1\times2)$-O/Ru(100) surfaces," J. Phys. Chem. B **109**, 4545–4553.

Kerner, G., O. Stein, Y. Lilach, and M. Asscher, 2005, "Sublimative desorption of xenon from Ru(100)," Phys. Rev. B **71**, 205414.

Kim, H.-Y., J. Sofo, D. Velegol, M. W. Cole, and A. A. Lucas, 2007, "van der Waals forces between dielectric nanoclusters," Langmuir **23**, 1735–1740.

Kim, J., Z. Dohnálek, J. M. White, and B. D. Kay, 2004, "Reactive growth of nanoscale MgO films by Mg atom deposition onto O_2 multilayers," J. Phys. Chem. B **108**, 11666–11671.

Kim, S. B., J. Ma, and M. H. W. Chan, 1993, "Phase diagram of ^{3}He-^{4}He mixture in aerogel," Phys. Rev. Lett. **71**, 2268–2271.

Kimmel, G. A., M. Persson, Z. Dohnálek, and B. D. Kay, 2003, "Temperature independent physisorption kinetics and adsorbate layer compression for Ar adsorbed on Pt(111)," J. Chem. Phys. **119**, 6776–6783.

King, D. A., 1975, "Thermal desorption from metal surfaces: A review," Surf. Sci. **47**, 384–402.

Kirchner, E. J. J., A. W. Kleyn, and E. J. Baerends, 1994, "A comparative study of Ar/Ag(111) potentials," J. Chem. Phys. **101**, 9155–9163.

Kiselev, A. V., and D. P. Poshkus, 1976, "Molecular-statistical calculation of the thermodynamics characteristics of saturated and unsaturated hydrocarbons on graphitized thermal carbon black," J. Chem. Soc., Faraday Trans. 2, **72**, 950–966.

Klein, M. L., and J. A. Venables, 1976, *Rare Gas Solids* (Academic, London), Vol. I.

Klein, M. L., and J. A. Venables, 1977, *Rare Gas Solids* (Academic, London), Vol. II.

Kreuzer, H. J., and S. H. Payne, 1988a, "Non-equilibrium thermodynamics of a two phase adsorbate," Surf. Sci. **198**, 235–262.

Kreuzer, H. J., and S. H. Payne, 1988b, "Desorption from a two-phase adsorbate: Zero or fractional order," Surf. Sci. **200**, L433–L440.

Kreuzer, H. J., and S. H. Payne, 1997, "Theories of the adsorption-desorption kinetics on homogeneous surfaces," in *Equilibria and Dynamics of Gas Adsorption on Heterogeneous Solid Surfaces*, edited by W. Rudzinski, W. A. Steele, and G. Zgablich (Elsevier Science, Amsterdam), pp. 153–200.

Kruchten, F., K. Knorr, U. G. Volkmann, H. Taub, F. Y. Hansen, B. Matthies, and K. W. Herwig, 2005, "Ellipsometric and neutron diffraction study of pentane physisorbed on graphite," Langmuir **21**, 7507–7512.

Krzyzowski, M. A., P. Zeppenfeld, and G. Comsa, 1995, "Resonant states of helium atoms scattered from the Pt(110)-(1×2) surface," J. Chem. Phys. **103**, 8705–8712.

Lal, M., and D. Spencer, 1974, "Interactions of alkanes with graphite," J. Chem. Soc., Faraday Trans. 2 **70**, 910–919.

Lander, J. J., and J. A. Morrison, 1967, "A LEED investigation of physisorption," Surf. Sci. **6**, 1–32.

Larese, J. Z., L. Frazier, M. A. Adams, T. Arnold, R. J. Hinde, and A. Ramirez-Cuesta, 2006, "Direct observation of molecular hydrogen binding to magnesium oxide (100) surfaces," Physica B **385-386**, 144–146.

Larese, J. Z., D. Martin y Marero, D. A. Sivia, and C. J. Carlile, 2001, "Tracking the evolution of interatomic potentials with high resolution inelastic neutron spectroscopy," Phys. Rev. Lett. **87**, 206102.

Larher, Y., 1971, "Formation of the first layer of argon, krypton, and xenon on a number of layer-like halides by two-dimensional condensation," J. Colloid Interface Sci. **37**, 836–848.

Larher, Y., 1979, "The critical exponent β associated with the two-dimensional condensation in the second adlayer of argon on the cleavage face of cadmium chloride," Mol. Phys. **38**, 789–795.

Larher, Y., 1992, "Monolayer adsorption of Ar, Kr, Xe, and CH_4 on layered halides," in *Surface Properties of Layered Structures*, edited by G. Benedek (Kluwer, Dordrecht), pp. 261–315.

Larher, Y., and F. Angerand, 1988, "The roughening transition of the densest crystal face of Ar, Kr, CO and CH_4 derived from multilayer adsorption studies," Europhys. Lett. **7**, 447–451.

LaRocque, P. E., R. H. Lipson, P. R. Herman, and B. P. Stoicheff, 1986, "Vacuum ultraviolet laser spectroscopy. IV. Spectra of Kr_2 and constants of the ground and excited states," J. Chem. Phys. **84**, 6627–6641.

Lazić, P., R. Brako, and G. Gumhalter, 2007, "Structure and dynamics of Xe monolayers adsorbed on Cu(111) and Pt(111) studied in the density functional approach," J. Phys.: Condens. Matter 19, 305004.

Lazić, P., Z. Crljen, R. Brako, and G. Gumhalter, 2005, "Role of van der Waals interactions in adsorption of Xe on Cu(111) and Pt(111)," Phys. Rev. B **72**, 245407.

Leatherman, G. S., and R. D. Diehl, 1997a, "LEED study of the physisorption of N_2 or CO on Ag(111)," Langmuir **13**, 7063–7067.

Leatherman, G. S., and R. D. Diehl, 1997b, "Rare gas coadsorption with K or Cs on Ag(111)," Surf. Sci. **380**, 455–467.

Leatherman, G. S., R. D. Diehl, M. Karimi, and G. Vidali, 1997, "The epitaxial rotation of 2D rare gas lattices on Ag(111)," Phys. Rev. B **56**, 6970–6974.

Lehner, B., M. Hohage, and P. Zeppenfeld, 2000, "Kinetic Monte Carlo scheme for studying desorption processes," Surf. Sci. **454**, 251–255.

Lehner, B., M. Hohage, and P. Zeppenfeld, 2002, "Kinetic Monte Carlo investigation of Xe adsorption and desorption in Pt(111) and Pt(997)," Phys. Rev. B **65**, 165407.

Lehner, B., M. Hohage, and P. Zeppenfeld, 2003a, "The influence of weak adsorbate interactions on desorption," Chem. Phys. Lett. **369**, 275–280.

Lehner, B., M. Hohage, and P. Zeppenfeld, 2003b, "The influence of long-range lateral interactions on the thermodynamics and kinetics of thermal desorption," Chem. Phys. Lett. **379**, 568–573.

Lei, R. Z., A. J. Gellman, and B. E. Koel, 2004, "Desorption energies of linear and cyclic alkanes on surfaces: Anomalous scaling with length," Surf. Sci. **554**, 125–140.

Leinböck, B., B. Krömker, H. Wiechert, and M. Hofmann, 2000, "Orientational ordering of N_2O molecules on graphite (0001): A novel commensurate pinwheel structure," Phys. Rev. Lett. **84**, 1954–1957.

Leitner, T., J. Kattner, and H. Hoffmann, 2003, "Infrared reflection spectroscopy of thin films on highly oriented pyrolytic graphite," Appl. Spectrosc. **57**, 1502–1509.

Lemmon, E. W., and A. R. H. Goodwin, 2000, "Critical properties and vapor pressure equation for alkanes C_nH_{2n+2}: Normal alkanes with $n \leq 36$ and isomers for $n=4$ through $n=9$," J. Phys. Chem. Ref. Data **29**, 1–39.

Lewis, S. P., M. V. Pykhtin, E. J. Mele, and A. M. Rappe, 1998, "Continuum elastic theory of adsorbate vibrational relaxation," J. Chem. Phys. **108**, 1157–1161.

Li, H. I., K. H. Hanna, R. D. Diehl, and W. Moritz, 2007, "The structure of a C_{60} monolayer on Ag(111)," Bull. Am. Phys. Soc. **52**, 1 (March), paper X19-5; http://meetings.aps.org/link/BAPS.2007.MAR.X19.5

Li, M., J. R. Manson, and A. P. Graham, 2002, "Experimental and theoretical investigation of the multiple phonon excitation of monolayer film modes with helium atom scattering: Kr/Pt(111)," Phys. Rev. B **65**, 195404.

Li, Y. J., O. Takeuchi, D. N. Futaba, H. Oigawa, K. Miyake, H. Shigekawa, and Y. Kuk, 2002, "Characteristic adsorption of Xe on a Si(111)-(7×7) surface at low temperature," Phys. Rev. B **65**, 113306.

Li, Y. J., O. Takeuchi, D. N. Futaba, H. Oigawa, K. Miyake, H. Shigekawa, and Y. Kuk, 2003, "Characteristic intra- and interunit interactions of Kr atoms adsorbed on the Si(111)-(7×7) surface," Phys. Rev. B **68**, 033301.

Liebsch, A., S. Goncalves, and M. Kiwi, 1999, "Electronic versus phononic friction of xenon on silver," Phys. Rev. B **60**, 5034–5043.

Linde, P., and S. Andersson, 2006, "High-resolution resonance measurements of the physisorption interaction," Phys. Rev. Lett. **96**, 086103.

Lysek, M. J., M. A. LaMadrid, P. K. Day, and D. L. Goodstein, 1993, "Heat capacity of multilayer methane on graphite: Phase transitions in the first four layers," Phys. Rev. B **47**, 7389–7400.

Maboudian, R., 1998, "Surface properties in MEMS technology," Surf. Sci. Rep. **30**, 207–269.

Manson, R., and V. Celli, 1970, "Inelastic scattering of nonpenetrating particles," Surf. Sci. **24**, 495–514.

Marmier, A., Ch. Ramseyer, C. Girardet, J. Goerge, P. Zeppenfeld, M. Büchel, R. David, and G. Comsa, 1997, "Adsorption and structure of N_2 on Cu(110)," Surf. Sci. **383**, 321–339.

Marsico, V., M. Blanc, K. Kuhnke, and K. Kern, 1997, "Discrete row growth at vicinal surfaces," Phys. Rev. Lett. **78**, 94–97.

Marti, C., T. Ceva, B. Croset, C. de Beauvais, and A. Thomy, 1986, "The SF_6 monolayer on graphite by x-ray diffraction," J. Phys. (Paris) **47**, 1517–1522.

Martin, C., J. P. Coulomb, and M. Ferrand, 1996, "Direct measurement of the translational mobility of deuterium hydride molecules in a model microporous material: $AlPO_4$-5 zeolite," Europhys. Lett. **36**, 503–508.

Martin, C., N. Tosi-Pellenq, J. Patarin, and J. P. Coulomb, 1998, "Sorption properties of $AlPO_4$-5 and SAPO-5 zeolite-like materials," Langmuir **14**, 1774–1778.

Maruyama, M., M. Bienfait, F. C. Liu, Y. M. Liu, O. E. Vilches, and F. Rieutard, 1993, "Quasi-liquid molecular layer at solid hydrogen surfaces," Surf. Sci. **283**, 333–337.

Marx, D., and H. Wiechert, 1996, "Ordering and phase transitions in adsorbed monolayers of diatomic molecules," Adv. Chem. Phys. **95**, 213–394.

Mason, B. F., and B. R. Williams, 1984, "Dispersion behavior in physisorbed Xe on KCl," Surf. Sci. **148**, L686–L690.

Mason, B. L., S. M. Winder, and J. Krim, 2001, "On the current status of quartz crystal microbalance studies of superconductivity-dependent sliding friction," Tribol. Lett. **10**, 59–65.

Matsui, T., H. Kambara, and H. Fukuyama, 2002, "STM observations of 2D Kr and Xe adsorbed on graphite," J. Low Temp. Phys. **126**, 373–378.

Matsumoto, Y., S. Murakawa, D. Tsuji, C. Bäuerle, H. Kambara, and H. Fukuyama, 2004, "Preliminary heat-capacity measurements of 2D solid ^{3}He adsorbed on graphite preplated with ^{4}He," J. Low Temp. Phys. **134**, 61–66.

Matthies, B. E., 1999, "Diffraction studies of *n*-alkane films adsorbed on graphite," Ph.D. thesis (University of Missouri–Columbia).

McLachlan, A. D., 1964, "van der Waals forces between an atom and a surface," Mol. Phys. **7**, 381–388.

McTague, J. P., and A. D. Novaco, 1979, "Substrate-induced strain and orientational ordering in adsorbed monolayers," Phys. Rev. B **19**, 5299–5306.

Meixner, D. L., and S. M. George, 1993a, "Coverage dependent surface diffusion of noble gases and methane on Pt(111)," Surf. Sci. **297**, 27–39.

Meixner, D. L., and S. M. George, 1993b, "Surface diffusion of xenon on Pt(111)," J. Chem. Phys. **98**, 9115–9125.

Menzel, D., 1975, "Desorption phenomena," in *Interactions on Metal Surfaces*, edited by R. Gomer (Springer-Verlag, Berlin), pp. 101–142.

Menzel, D., 1982, "Thermal desorption," in *Chemistry and Physics of Solid Surfaces IV*, edited by R. Vanselow and R. Howe (Springer-Verlag, Berlin), pp. 389–406.

Meyer, A., R. Dimeo, P. Gehring, and D. Neumann, 2003, "The high-flux backscattering spectrometer at the NIST Center for Neutron Research," Rev. Sci. Instrum. **74**, 2759–2777.

Migone, A. D., 2007, "Adsorption on carbon nanotubes: Experimental results," in *Adsorption by Carbons*, edited by E. Bottani and J. M. D. Tascon (Elsevier, Amsterdam), Chap. 16.

Migone, A. D., M. T. Alkhafaji, G. Vidali, and M. Karimi, 1993, "Thermodynamic study of argon films adsorbed on boron nitride," Phys. Rev. B **47**, 6685–6696.

Miranda, R., S. Daiser, K. Wandelt, and G. Ertl, 1983, "Thermodynamics of xenon adsorption on Pd(s)[8(100)×(110)]: From steps to multilayers," Surf. Sci. **131**, 61–91.

Mo, H., 2004, "Neutron and x-ray scattering study of intermediate-length alkane films adsorbed on solid surfaces," Ph.D. thesis (University of Missouri–Columbia).

Mo, H., H. Taub, U. G. Volkmann, M. Pino, S. N. Ehrlich, F. Y. Hansen, E. Lu, and P. Miceli, 2003, "A novel growth mode of alkane films on a SiO_2 surface," Chem. Phys. Lett. **377**, 99–105.

Mo, H., S. Trogisch, H. Taub, S. N. Ehrlich, U. G. Volkmann, F. Y. Hansen, and M. Pino, 2004, "Studies of the structure and growth mode of dotriacontane films by synchrotron x-ray scattering and molecular dynamics simulations," J. Phys.: Condens. Matter **16**, S2905–S2910.

Moog, E. R., and M. B. Webb, 1984, "Xenon and krypton adsorption on palladium (100)," Surf. Sci. **148**, 338–370.

Morishige, K., K. Inoue, and K. Imai, 1996, "X-ray study of Kr, Xe, and N_2 monolayers on boron nitride," Langmuir **12**, 4889–4891.

Moroz, I., H. Ambaye, and J. R. Manson, 2004, "Molecule scattering from insulator and metal surfaces," J. Phys.: Condens. Matter **16**, S2953–S2966.

Mowforth, C. W., T. Rayment, and R. K. Thomas, 1986, "Long-period commensurate structures near the incommensurate-commensurate phase transition in xenon layers adsorbed on graphite observed by x-ray diffraction," J. Chem. Soc., Faraday Trans. 2 **82**, 1621–1634.

Müller, J. E., 1990, "Interaction of the Pt(111) surface with adsorbed Xe atoms," Phys. Rev. Lett. **65**, 3021–3024.

Mursic, Z., M. Y. M. Lee, D. E. Johnson, and J. Z. Larese, 1996, "A computer-controlled apparatus for performing high-resolution adsorption isotherms," Rev. Sci. Instrum. **67**, 1886–1890.

Nabighian, E., and X. D. Zhu, 2000, "Diffusion of Xe on Ni(111)," Chem. Phys. Lett. **316**, 177–180.

Nagai, K., 1985, "Rate expression incorporating interactions between reactants: Application to zero order desorption spectra," Phys. Rev. Lett. **54**, 2159–2162.

Nagai, K., 1988, "Reply to the Comment by A. Cassuto: On the validity of the desorption-rate version of the Langmuir isotherm proposed by K. Nagai," Surf. Sci. **203**, L659–L662.

Nagler, S. E., P. M. Horn, T. F. Rosenbaum, R. J. Birgeneau, M. Sutton, S. G. J. Mochrie, D. E. Moncton, and R. Clarke, 1985, "Orientational order in xenon fluid monolayers on single crystals of exfoliated graphite," Phys. Rev. B **32**, 7373–7383.

Nalezinski, R., A. M. Bradshaw, and K. Knorr, 1995, "Orientational phase transitions in polar physisorbed molecules: An IRAS study of dichlorodifluoromethane on graphite," Surf. Sci. **331-333**, 255–260.

Nalezinski, R., A. M. Bradshaw, and K. Knorr, 1997, "A vibrational spectroscopy study of the orientational ordering in CH_3Cl monolayers physisorbed on graphite," Surf. Sci. **393**, 222–230.

Narloch, B., and D. Menzel, 1997, "Structural evidence for chemical contributions in the binding of the heavy rare gases on a close-packed transition metal surface: Xe or Kr on Ru(001)," Chem. Phys. Lett. **270**, 163–168.

Narloch, B., and D. Menzel, 1998, "The geometry of xenon and krypton on Ru(001): A LEED IV investigation," Surf. Sci. **412–413**, 562–579.

Neugebauer, J., and M. Scheffler, 1993, "Mechanisms of island formation of alkali-metal adsorbates on Al(111)," Phys. Rev. Lett. **71**, 577–580.

Niedermayer, T., H. Schlichting, D. Menzel, S. H. Payne, and H. J. Kreuzer, 2005, "Thermal and nonthermal kinetics of helium monolayers on Pt(111)," Phys. Rev. B **71**, 045427.

Nuttall, W. J., K. P. Fahey, M. J. Young, B. Keimer, R. J. Birgeneau, and H. Suematsu, 1993, "A synchrotron x-ray diffraction study of the structural phase behaviour of multilayer xenon on single-crystal graphite," J. Phys.: Condens. Matter **5**, 8159–8176.

Nuttall, W. J., D. Y. Noh, B. O. Wells, and R. J. Birgeneau, 1994, "Synchrotron x-ray scattering study of the pressure melting of near-monolayer xenon on single-crystal graphite at 140 K," Surf. Sci. **307-309**, 768–774.

Nuttall, W. J., D. Y. Noh, B. O. Wells, and R. J. Birgeneau, 1995, "Isothermal melting of near monolayer xenon on single-crystal graphite," J. Phys.: Condens. Matter **7**, 4337–4350.

Ogletree, D. F., G. S. Blackman, R. Q. Hwang, U. Starke, G. A. Somorjai, and J. E. Katz, 1992, "A new pulse counting low-energy electron diffraction system based on a position sensitive detector," Rev. Sci. Instrum. **63**, 104–113.

Ostertag, C., A. Oelsener, M. Schicketanz, O. Schmidt, G. H. Fecher, and G. Schönhense, 1996, "Circular dichroism in photoemission from Xe and Kr on Pt(111)," Surf. Sci. **352-354**, 179–183.

Paik, S. M., and I. K. Schuller, 1990, "New calculational method for epitaxial energy: Application to an axial commensurate interface," Phys. Rev. Lett. **64**, 1923–1926; **66**, 395(E) (1991).

Panella, V., R. Chiarello, and J. Krim, 1996, "Adequacy of the Lifshitz theory for certain thin adsorbed films," Phys. Rev. Lett. **76**, 3606–3609.

Park, J.-Y., U. D. Ham, S.-J. Kahng, Y. Kuk, K. Miyake, K. Hata, and H. Shigekawa, 2000, "Modification of surface state dispersion upon xenon adsorption: A scanning tunneling microscope study," Phys. Rev. B **62**, R16341–R16344.

Park, J.-Y., S.-J. Kahng, U. D. Ham, Y. Kuk, K. Miyake, K. Hata, and H. Shigekawa, 1999, "Adsorption and growth of Xe adlayers on the Cu(111) surface," Phys. Rev. B **60**, 16934–16940.

Park, J. Y., D. F. Ogletree, M. Salmeron, R. A. Ribeiro, P. C. Canfield, C. J. Jenks, and P. A. Thiel, 2005, "High frictional anisotropy of periodic and aperiodic directions on a quasicrystal surface," Science **309**, 1354–1356.

Park, R. L., and H. H. Madden, 1968, "Annealing changes on the (100) surface of palladium and their effect on CO adsorption," Surf. Sci. **11**, 188–202.

Paserba, K. R., and A. J. Gellman, 2001, "Effects of conformational iosmerism on the desorption kinetics of n-alkanes from graphite," J. Chem. Phys. **115**, 6737–6751.

Patton, D. C., and M. R. Pederson, 1997, "Application of the generalized-gradient approximation to rare-gas dimers," Phys. Rev. A **56**, R2495–R2498; **71**, 019906(E) (2005).

Payne, S. H., and H. J. Kreuzer, 1988, "Non-equilibrium thermodynamics of a two phase adsorbate: Lattice gas and van der Waals models," Surf. Sci. **205**, 153–176.

Payne, S. H., and H. J. Kreuzer, 1989, "Analysis of thermal desorption data," Surf. Sci. **222**, 404–429.

Persson, B. N. J., and A. Nitzan, 1996, "Linear sliding friction—On the origin of the microscopic friction for Xe on silver," Surf. Sci. **367**, 261–275.

Persson, B. N. J., E. Tosatti, D. Fuhrmann, G. Witte, and C. Wöll, 1999, "Low-frequency adsorbate vibrational relaxation and sliding friction," Phys. Rev. B **59**, 11777–11791.

Petersen, M., S. Wilke, P. Ruggerone, B. Kohler, and M. Scheffler, 1996, "Scattering of rare-gas atoms at a metal surface: Evidence of anticorrugation of the helium-atom potential energy surface and the surface electron density," Phys. Rev. Lett. **76**, 995–998.

Phillips, J. M., 1984, "Methane adsorbed on graphite. II. A model of the commensurate-incommensurate transitions," Phys. Rev. B **29**, 5865–5871.

Phillips, J. M., and J. G. Dash, 2005, "Thermal disorder, fluctuations, growth and fragmentation of finite one-dimensional atomic chains," J. Stat. Phys. **120**, 721–735.

Phillips, J. M. and J. Z. Larese, 1997, "Microscopic structure and transitions in xenon multilayer films," Phys. Rev. B **56**, 15938–15946.

Picaud, F., V. Pouthier, C. Ramseyer, and C. Girardet, 1999, "Influence of steps on atomic adsorption and sequential growth above vicinal surfaces," Surf. Rev. Lett. **6**, 669–681.

Pierce, M., and E. Manousakis, 1999, "Path-integral Monte Carlo simulation of the second layer of ^{4}He adsorbed on graphite," Phys. Rev. B **59**, 3802–3814.

Pitt, I. G., R. G. Gilbert, and K. R. Ryan, 1995, "The application of transition state theory to gas-surface reactions in Langmuir systems," J. Chem. Phys. **102**, 3461–3473.

Poelsema, B., L. K. Verheij, and G. Comsa, 1983, "Direct evidence for two-dimensional Xe gas-solid phase transition on Pt(111) by means of thermal He scattering," Phys. Rev. Lett. **51**, 2410–2413.

Polian, A., P. Loubeyre, and N. Boccara, 1989, *Simple Molecular Systems at Very High Density*, Vol. 186 of NATO Advanced Studies Institute, Series B: Physics (Plenum, New York).

Poon, H. C., X. F. Hu, S. E. Chamberlin, D. K. Saldin, and C. J. Hirschmugl, 2006, "Structure of the hydrogen stabilized MgO(111)-(1×1) surface from low energy electron diffraction (LEED)," Surf. Sci. **600**, 2505–2509.

Potthoff, M., G. Hilgers, N. Müller, U. Heinzmann, L. Haunert, J. Braun, and G. Borstel, 1995, "Structure investigations of Xe-adsorbate layers by spin-polarized low-energy electron diffraction. I. $(\sqrt{3}\times\sqrt{3})R30^\circ$-Xe/Pt(111)," Surf. Sci. **322**, 193–206.

Pouthier, V., C. Ramseyer, C. Girardet, K. Kuhnke, V. Marsico, M. Blanc, R. Schuster, and K. Kern, 1997, "Discrete-row growth of xenon adsorbed on the vicinal Pt(997) surface: Comparison between theory and experiment," Phys. Rev. B **56**, 4211–4223.

Price, G. L., and J. A. Venables, 1976, "A theory of the phase transitions in solid krypton and xenon monolayers on graphite," Surf. Sci. **59**, 509–532.

Pussi, K., J. Smerdon, N. Ferralis, M. Lindroos, R. McGrath, and R. D. Diehl, 2004, "Dynamical low-energy electron diffraction study of graphite (0001)-$(\sqrt{3}\times\sqrt{3})R30^\circ$-Xe," Surf. Sci. **548**, 157–162.

Ramseyer, C., C. Girardet, F. Bartolucci, G. Schmitz, R. Franchy, D. Teillet-Billy, and J. P. Gauyacq, 1998, "N_2 monolayer and bilayer adsorbed on Ag(110) at 15 K: Structure and orientational ordering," Phys. Rev. B **58**, 4111–4119.

Ramseyer, C., C. Girardet, P. Zeppenfeld, J. Goerge, M. Büchel, and G. Comsa, 1994, "Xe monolayer adsorption on Cu(110): Experiments and interaction calculations," Surf. Sci. **313**, 251–265.

Ramseyer, C., V. Pouthier, C. Girardet, P. Zeppenfeld, M. Büchel, V. Diercks, and G. Comsa, 1997, "Influence of mode polarizations on the inelastic He-scattering spectrum: High-order commensurate Xe monolayer adsorbed on Cu(110)," Phys. Rev. B **55**, 13203–13212.

Regnier, J., J. Menaucourt, A. Thomy, and X. Duval, 1981, "Proprietés thermodynamique du film d'éthane adsorbé sur graphite," J. Chim. Phys. **78**, 629–633.

Regnier, J., A. Thomy, and X. Duval, 1979, "Comparative study of the first adsorbed layer of xenon and krypton on boron nitride and graphite," J. Colloid Interface Sci. **70**, 105–111.

Rejto, P. A., and H. C. Andersen, 1993, "Interatomic potentials and the phase diagram of Xe/Pt(111)," J. Chem. Phys. **98**, 7636–7647.

Renner, R. L., P. Taborek, and J. E. Rutledge, 2001, "Friction and pinning of nitrogen films on lead substrates near the superconducting transition," Phys. Rev. B **63**, 233405.

Rieder, K. H., G. Parschau, and B. Burg, 1993, "Experimental evidence for anticorrugating effects in He-metal interactions and surfaces," Phys. Rev. Lett. **71**, 1059–1062.

Rieutord, F., R. Simon, R. Conradt, and P. Müller-Buschbaum, 1997, "Surface melting and preroughening of argon: An X-ray reflection study," Europhys. Lett. **37**, 565–570.

Riley, D. J., A. P. Jardine, S. Dworski, G. Alexandrowicz, P. Fouquet, J. Ellis, and W. Allison, 2007, "A refined He-LiF(001) potential from selective adsorption resonances measured with high resolution helium spin-echo spectroscopy," J. Chem. Phys. **126**, 104702.

Rivière, J. C., 1990, *Surface Analytical Techniques* (Oxford University Press, Oxford, England).

Robinson, I., 2007, "Surface structure as a foundation of nanotechnology," http://meetings.aps.org/link/BAPS.2007.MAR.N6.3

Rosenbaum, A. W., M. A. Freedman, and S. J. Sibener, 2006, "Vibrational properties of disordered mono- and bilayers of physisorbed sulfur hexafluoride on Au(111)," J. Phys. Chem. A **110**, 5537–5541.

Roth, M. W., C. L. Pint, and C. Wexler, 2005, "Phase transitions in hexane monolayers physisorbed onto graphite," Phys. Rev. B **71**, 155427.

Rudzinski, W., and T. Panczyk, 2002, "Remarks on the current state of adsorption kinetic theories for heterogeneous solid surfaces: A comparison of the ART and the SRT approaches," Langmuir **18**, 439–449.

Ruiz-Suarez, J. C., M. C. Vargas, F. O. Goodman, and G. Scoles, 1991, "Zero-order desorption of Xe from (0001) graphite: An experimental study and a theoretical model," Surf. Sci. **243**, 219–226.

Sakurai, M., and C. Yamada, 2005, "Dynamics of physisorbed monolayer of methane on Ag(111)," Surf. Sci. **593**, 195–201.

Sakurai, T., X. D. Wang, T. Hashizume, V. Yurov, H. Shinohara, and H. W. Pickering, 1995, "Adsorption of fullerenes on Cu(111) and Ag(111) surfaces," Appl. Surf. Sci. **87/88**, 405–413.

Schabes-Retchkiman, P. S., and J. A. Venables, 1981, "Structural studies of xenon and krypton solid monolayers on graphite using transmission electron diffraction," Surf. Sci. **105**, 536–564.

Schlichting, H., and D. Menzel, 1992, "High resolution, wide range, thermal desorption spectroscopy of rare gas layers: Sticking, desorption kinetics, layer growth, phase transitions and exchange processes," Surf. Sci. **272**, 27–33.

Schlichting, H., and D. Menzel, 1993a, "Techniques for attainment, control, and calibration of cryogenic temperatures at small single-crystal samples under ultrahigh vacuum," Rev. Sci. Instrum. **64**, 2013–2022.

Schlichting, H., and D. Menzel, 1993b, "Techniques for wide range, high resolution and precision, thermal desorption measurements," Surf. Sci. **285**, 209–218.

Schmidt K. J., and K. Christmann, 2001, "The adsorption of xenon on a ruthenium($10\bar{1}0$) surface," Surf. Sci. **492**, 167–184.

Schollmeyer, H., B. Ocko, and H. Riegler, 2002, "Surface freezing of triacontane at SiO_x/air interfaces: Submonolayer coverage," Langmuir **18**, 4351–4355.

Schollmeyer, H., B. Struth, and H. Riegler, 2003, "Long chain n-alkanes at SiO_2/air interfaces: Molecular ordering, annealing, and surface freezing of triacontane in the case of excess and submonolayer coverage," Langmuir **19**, 5042–5051.

Schwarz, A., U. D. Schwarz, S. Langkat, H. Hölscher, W. Allers, and R. Wiesendanger, 2002, "Dynamic force microscopy with atomic resolution at low temperatures," Appl. Surf. Sci. **188**, 245–251.

Schwennicke, C., J. Shimmelpfennig, and H. Pfnür, 1993, "Ordering and phase diagrams of xenon adsorbed on thin epitaxial NaCl(100) films and on Ge(100)," Phys. Rev. B **48**, 8928–8937.

Setyawan, W., N. Ferralis, R. D. Diehl, M. W. Cole, and S. Curtarolo, 2006, "Xe films on a decagonal Al-Ni-Co quasicrystal surface," Phys. Rev. B **74**, 125425.

Setyawan, W., N. Ferralis, R. D. Diehl, M. W. Cole, and S. Curtarolo, 2007, "Noble gas films on a decagonal AlNiCo quasicrystal," J. Phys.: Condens. Matter **19**, 016007.

Seyller, T., M. Caragiu, and R. D. Diehl, 2000, "Low-energy electron diffraction study of krypton on Cu(110)," Surf. Sci. **454-456**, 55–59.

Seyller, T., M. Caragiu, R. D. Diehl, P. Kaukasoina, and M. Lindroos, 1998, "Observation of top site adsorption for Xe on Cu(111)," Chem. Phys. Lett. **291**, 567–572.

Seyller, T., M. Caragiu, R. D. Diehl, P. Kaukasoina, and M. Lindroos, 1999, "Dynamical LEED study of Pt(111)-$(\sqrt{3} \times \sqrt{3})R30°$-Xe," Phys. Rev. B **60**, 11 084–11 088.

Shaw, C. G., and S. C. Fain, Jr., 1980, "Lattice spacing and isosteric heat of argon monolayers below 50 K," Surf. Sci. **91**, L1–L6.

Shaw, C. G., S. C. Fain, Jr., and M. D. Chinn, 1978, "Observation of orientational ordering of incommensurate argon monolayers on graphite," Phys. Rev. Lett. **41**, 955–957.

Shaw, C. G., S. C. Fain, Jr., M. D. Chinn, and M. F. Toney, 1980, "Overlayer-substrate spacing for argon and krypton on graphite determined by LEED intensity analysis," Surf. Sci. **97**, 128–136.

Shen, J., J. P. Pierce, E. W. Plummer, and J. Kirschner, 2003, "The effect of spatial confinement on magnetism: Films, stripes and dots of Fe on Cu(111)," J. Phys.: Condens. Matter **15**, R1–R30.

Sholl, D. S., and R. T. Skodje, 1994, "Diffusion of xenon on a platinum surface: The influence of correlated flights," Physica D **71**, 168–184.

Sholl, D. S., and R. T. Skodje, 1995, "Diffusion of clusters of atoms and vacancies on surfaces and the dynamics of diffusion-driven coarsening," Phys. Rev. Lett. **75**, 3158–3161.

Shrimpton, N. D., and B. Joos, 1989, "Renormalized model for the dynamics of the krypton-on-graphite domain-wall lattice," Phys. Rev. B **40**, 10564–10576.

Šiber, A., B. Gumhalter, J. Braun, A. P. Graham, M. Bertino, J. P. Toennies, D. Fuhrmann, and C. Wöll, 1999, "Combined He-atom scattering and theoretical study of the low-energy vibrations of physisorbed monolayers of Xe on Cu(111) and Cu(001)," Phys. Rev. B **59**, 5898–5914.

Šiber, A., B. Gumhalter, A. P. Graham, and J. P. Toennies, 2001, "He atom scattering and theoretical study of the surface phonons of a simple benchmark system: Xe(111)," Phys. Rev. B **63**, 115411.

Skofronick, J. G., J. P. Toennies, F. Traeger, and H. Weiss, 2003, "Helium atom scattering studies of the structure and vibrations of H_2 physisorbed on MgO(001) single crystals," Phys. Rev. B **67**, 035413.

Smith, E. D., M. O. Robbins, and M. Cieplak, 1996, "Friction on adsorbed monolayers," Phys. Rev. B **54**, 8252–8260.

Sneh, O., and S. M. George, 1994, "Xenon diffusion on a stepped Pt(11,11,9) surface," J. Chem. Phys. **101**, 3287–3297.

Specht, E. D., A. Mak, C. Peters, M. Sutton, R. J. Birgeneau, K. L. D'Amico, D. E. Moncton, S. E. Nagler, and P. M. Horn, 1987, "Phase diagram and phase transitions of krypton on graphite in the extended monolayer regime," Z. Phys. B: Condens. Matter **69**, 347–377.

Stampfl, C., H. J. Kreuzer, S. H. Payne, H. Pfnür, and M. Scheffler, 1999, "First principles theory of surface thermodynamics and kinetics," Phys. Rev. Lett. **83**, 2993–2996.

Steele, W. A., 1974, *The Interaction of Gases with Solid Surfaces* (Pergamon, Oxford).

Stocker, P., J.-M. Gay, M. Bienfait, and G. Coddens, 1997, "Anisotropy of translational diffusion in premelted methane films," Surf. Rev. Lett. **4**, 863–868.

Strandburg, K. J., 1988, "Two-dimensional melting," Rev. Mod. Phys. **60**, 161–207; **61**, 747(E) (1989).

Suter, R. M., N. J. Colella, R. Gangwar, and W. Wang, 1987, "High-precision vapor-pressure isotherms: Apparatus, errors and results," Rev. Sci. Instrum. **58**, 462–467.

Suzanne, J., J. P. Coulomb, and M. Bienfait, 1974, "Transition bidimensionelle du premier ordre: Cas du xénon adsorbé sur la face (0001) du graphite," Surf. Sci. **44**, 141–156.

Suzanne, J., J. P. Coulomb, and M. Bienfait, 1975, "Two-dimensional phase transition in xenon submonolayer films adsorbed on (0001) graphite in the monolayer range," Surf. Sci. **47**, 204–206.

Suzanne, J., and J. M. Gay, 1996, "The structure of physically adsorbed phases," in *Physical Structure of Solid Surfaces*, W. N. Unertl, volume editor, Vol. 1, in the Handbook of Surface

Science, series editors S. Holloway and N. V. Richardson (North-Holland, Amsterdam), Chap. 10, pp. 503–575.

Suzanne, J., J. L. Seguin, H. Taub, and J. P. Biberian, 1983, "A LEED study of ethane films adsorbed on graphite in the monolayer range," Surf. Sci. **125**, 153–170.

Tait, S. L., Z. Dohnálek, C. T. Campbell, and B. D. Kay, 2005, "*n*-alkanes on MgO(001). II. Chain length dependence of kinetic desorption parameters for small *n*-alkanes," J. Chem. Phys. **122**, 164708.

Tait, S. L., Z. Dohnálek, C. T. Campbell, and B. D. Kay, 2006, "*n*-alkanes on Pt(111) and on C(0001)/Pt(111): Chain length-dependence of kinetic desorption parameters," J. Chem. Phys. **125**, 234308.

Takeuchi, O., and H. Shigekawa, 2003, "Thermodynamic analysis of the interaction between Kr adsorbates on Si(111)-7×7 surface." Jpn. J. Appl. Phys., Part 1 **42**, 4890–4893.

Tang, K. T., and J. P. Toennies, 2003, "The van der Waals potentials between all the rare gas atoms from He to Rn," J. Chem. Phys. **118**, 4976–4983.

Tao, J., and J. P. Perdew, 2005, "Test of a nonempirical density functional: Short-range part of the van der Waals interaction in rare-gas dimers," J. Chem. Phys. **122**, 114102.

Tartaglino, U., T. Zykova-Timan, F. Ercolessi, and E. Tosatti, 2005, "Melting and nonmelting of solid surfaces and nanosystems," Phys. Rep. **411**, 291–321.

Taub, H., F. Y. Hansen, L. Criswell, D. Fuhrmann, K. W. Herwig, A. Diama, H. Mo, R. M. Dimeo, D. A. Neumann, and U. G. Volkmann, 2004, "Slow diffusive motions in a monolayer of tetracosane molecules adsorbed on graphite," in *Proceedings of the 3rd International Symposium on Slow Dynamics in Complex Systems*, edited by M. Tokuyama and I. Oppenheim, AIP Conf. Proc. No. 708 (AIP, Melville, NY), pp. 201–204.

Tersoff, J., and D. R. Hamann, 1983, "Theory and application for the scanning tunneling microscope," Phys. Rev. Lett. **50**, 1998–2001.

Tersoff, J., and D. R. Hamann, 1985, "Theory of the scanning tunneling microscope," Phys. Rev. B **31**, 805–813.

Tessier, C., 1984, "Étude thermodynamique et structurale de la fusion bidimensionelle dans les monocouches de gaz rares ou de methane adsorbeés physiquement a la surface de solides lamellaires," Thèse, Université de Nancy (France), issued as Report CEA-R-5250; see table and graphs in Chap. VI, pp. 171–184.

Tessier, C., and Y. Lahrer, 1980, "2D melting in physisorbed monolayers of Ar, Kr, Xe and CH_4," in *Ordering in Two Dimensions*, edited by S. K. Sinha (North-Holland, New York), pp. 163–168.

Thomas, P., J. Gray, X. D. Zhu, and C. Y. Fong, 2003, "Surface diffusion of Xe on Nb(110)," Chem. Phys. Lett. **381**, 376–380.

Thomas, P., E. Nabighian, M. C. Bartelt, C. Y. Fong, and X. D. Zhu, 2004, "An oblique-incidence optical reflectivity difference and LEED study of rare-gas growth on a lattice-mismatched metal substrate," Appl. Phys. A: Mater. Sci. Process. **A79**, 131–137.

Thomy, A., and X. Duval, 1994, "Stepwise isotherms and phase transitions in physisorbed films," Surf. Sci. **299-300**, 415–425.

Thomy, A., X. Duval, and J. Regnier, 1981, "Two-dimensional phase transitions as displayed by adsorption isotherms on graphite and other lamellar solids," Surf. Sci. Rep. **1**, 1–38.

Thorel, P., J. P. Coulomb, and M. Bienfait, 1982, "Rotational diffusion of methane molecules adsorbed on graphite," Surf. Sci. **182**, L43–L47.

Tkatchenko, A., 2006, "Analytic theory of hexagonal monolayer interacting with hexagonal substrate," Phys. Rev. B **74**, 035428.

Tkatchenko, A., 2007, "Commensurate monolayers on surfaces: Geometry and ground states" Phys. Rev. B **75**, 235411.

Tkatchenko, A., and O. A. von Lilienfeld, 2006, "Adsorption of Ar on graphite using London dispersion forces corrected Kohn-Sham density functional theory," Phys. Rev. B **73**, 153406.

Toennies, J. P., and F. Traeger, 2007, "The structures and vibrations of H_2 monolayers on NaCl, MgO and LiF: Similarities and differences," J. Phys.: Condens. Matter **19**, 305009.

Toennies, J. P., and R. Vollmer, 1989, "Helium scattering studies of the dynamics of a xenon-monolayer-covered graphite single-crystal surface," Phys. Rev. B **40**, 3495–3499.

Tomassone, M. S., J. B. Sokoloff, A. Widom, and J. Krim, 1997, "Dominance of phonon friction for a xenon film on a silver (111) surface," Phys. Rev. Lett. **79**, 4798–4801.

Tosaka, A., and I. Arakawa, 2006, "The comparative study of two dimensional condensation of Xe and Kr physisorbed on Ag(111) and Ag(100)," Surf. Sci. **600**, 1071–1076.

Traeger, F., and J. P. Toennies, 2004, "Helium atom scattering studies of the structures and vibrations of the H_2, HD, and D_2 monolayers on NaCl(001)," J. Phys. Chem. B **108**, 14710–14725.

Trasca, R. A., N. Ferralis, R. D. Diehl, and M. W. Cole, 2004, "The adsorption of Xe and Ar on quasicrystalline Al-Ni-Co," J. Phys.: Condens. Matter **16**, S2911–S2921.

Tribe, L., 2006, "Wave packet calculations for helium scattering by a xenon monolayer," Chem. Phys. **327**, 468–473.

Trischberger, P., H. Dröge, S. Gokhale, J. Henk, H. P. Steinrück, W. Widdra, and D. Menzel, 1997, "One-dimensional xenon band structures on hydrogen modified and stepped platinum surfaces," Surf. Sci. **377-379**, 155–159.

Trogisch, S., M. J. Simpson, H. Taub, U. G. Volkmann, M. Pino, and F. Y. Hansen, 2005, "Atomic force microscopy measurements of topography and friction on dotriacontane films adsorbed on a SiO_2 surface," J. Chem. Phys. **123**, 154703.

Unguris, J., L. W. Bruch, E. R. Moog, and M. B. Webb, 1979, "Xe adsorption on Ag(111): Experiment," Surf. Sci. **87**, 415–436.

Unguris, J., L. W. Bruch, E. R. Moog, and M. B. Webb, 1981, "Ar and Kr adsorption on Ag(111)," Surf. Sci. **109**, 522–556.

Utrera, L., and R. Ramirez, 1992, "Molecular dynamics simulation of Xe diffusion on the Si(100)-2×1 surface," J. Chem. Phys. **96**, 7838–7847.

Velasco, E., and G. H. Peters, 1995, "Effect of substrate potential strength on the melting temperature of a hexane monolayer adsorbed on graphite," J. Chem. Phys. **102**, 1098–1099.

Venables, J. A., 2000, *Introduction to Surface and Thin Film Processes* (Cambridge University Press, Cambridge, England).

Venables, J. A., and M. Bienfait, 1976, "On the reaction order in thermal desorption spectroscopy," Surf. Sci. **61**, 667–672.

Venables, J. A., and P. S. Schabes-Retchkiman, 1978, "On the geometry of dislocations in close-packed adsorbed solid monolayers," J. Phys. C **11**, L913–L918.

Vidali, G., G. Ihm, H.-Y. Kim, and M. W. Cole, 1991, "Potentials of physical adsorption," Surf. Sci. Rep. **12**, 133–181.

Villain, J., and M. B. Gordon, 1983, "Static properties of physisorbed monolayers in their solid phases," Surf. Sci. **125**, 1–50.

Vogt, B., B. Kessler, N. Müller, G. Schönhense, B.

Schmiedeskamp, and U. Heinzmann, 1991, “Spin-resolved photoemission from Xe on Pd(111) in the dilute phase: The model case of singly adsorbed atoms,” Phys. Rev. Lett. **67**, 1318–1321.

Volkmann, U. G., and K. Knorr, 1989, “Ellipsometric study of krypton physisorbed on graphite,” Surf. Sci. **221**, 379–393.

Volkmann, U. G., H. Mannebach, and K. Knorr, 1998, “Ellipsometric study of multilayer growth and wetting of $C_2Cl_2F_4$ physisorbed on graphite,” Langmuir **14**, 4904–4907.

Volkmann, U. G., M. Pino, L. A. Altamirano, H. Taub, and F. Y. Hansen, 2002, “High-resolution ellipsometric study of an *n*-alkane film, dotriacontane, adsorbed on a SiO_2 surface,” J. Chem. Phys. **116**, 2107–2115.

von Przychowski, M. D., H. Wiechert, G. K. L. Marx, and G. Schönhense, 2003, “Real-space observation of xenon adsorption and desorption kinetics on graphite (0001) by photoemission electron microscopy,” Surf. Sci. **541**, 46–58.

Waddill, G. D., C. M. Aldao, I. M. Vitomirov, S. G. Anderson, C. Capasso, and J. H. Weaver, 1989, “Ag and Co cluster deposition on GaAs(110): Fermi level pinning in the absence of metal-induced gap states and defects,” J. Vac. Sci. Technol. B **B7**, 950–957.

Waddill, G. D., I. M. Vitomirov, C. M. Aldao, S. G. Anderson, C. Capasso, J. H. Weaver, and Z. Liliental-Weber, 1990, “Abrupt interfaces with novel structural and electronic properties: Metal-cluster deposition and metal-semiconductor junctions,” Phys. Rev. B **41**, 5293–5305.

Waddill, G. D., I. M. Vitomirov, C. M. Aldao, and J. H. Weaver, 1989, “Cluster deposition on GaAs(110): Formation of abrupt, defect-free interfaces,” Phys. Rev. Lett. **62**, 1568–1571.

Wang, L. L., and H. P. Cheng, 2004a, “Rotation, translation, charge transfer, and electronic structure of C_{60} on Cu(111) surface,” Phys. Rev. B **69**, 045404.

Wang, L. L., and H. P. Cheng, 2004b, “Density functional study of the adsorption of a C_{60} monolayer on Ag(111) and Au(111) surfaces,” Phys. Rev. B **69**, 165417.

Wataru, K., J. Taniguchi, M. Hieda, and M. Suzuki, 2005, “Slippage of He-4 films adsorbed on porous gold,” J. Phys. Chem. Solids **66**, 1535–1538.

Weaver, J. F., A. F. Carlsson, and R. J. Madix, 2003, “The adsorption and reaction of low molecular weight alkanes on metallic single crystal surfaces,” Surf. Sci. Rep. **50**, 107–199.

Weber, W. J., and D. L. Goodstein, 1999, “Theory and observation of displacement phenomena in coadsorbed films,” Phys. Rev. Lett. **83**, 3888–3891.

Weber, W. J., and D. L. Goodstein, 2002, “Coadsorption phase diagram for Kr/CCl_4 on graphite,” Phys. Rev. B **66**, 165419.

Weber, W. J., and D. L. Goodstein, 2006, “Coadsorption phase diagram for CH_4/CCl_4 on graphite,” Phys. Rev. B **73**, 195424.

Wei, D. H., D. C. Skelton, and S. D. Kevan, 1996, “Lateral interactions and corrugation in physisorption systems: $CH_4/Cu(100)$,” J. Chem. Phys. **105**, 7808–7814.

Weiss, P. S., and D. M. Eigler, 1992, “Adsorption and accommodation of Xe/Pt(111),” Phys. Rev. Lett. **69**, 2240–2243.

Wetterer, S., D. J. Lavrich, T. Cummings, S. L. Bernasek, and G. Scoles, 1998, “Energetics and kinetics of the physisorption of hydrocarbons on Au(111),” J. Phys. Chem. B **102**, 9266–9275.

Whitlock, P. A., G. V. Chester, and B. Krishnamachari, 1999, “Quantum Monte Carlo simulation of the second layer helium film on graphite,” Comput. Phys. Commun. **121-122**, 460–465.

Widdra, W., 2001, “Electronic band structures of low-dimensional adsorbate systems: Rare-gas adsorption on transition metals,” Appl. Phys. A: Mater. Sci. Process. **72**, 395–404.

Widdra, W., P. Trischberger, W. Frieß, D. Menzel, S. H. Payne, and H. J. Kreuzer, 1998, “Rare-gas thermal desorption from flat and stepped platinum surfaces: Lateral interactions and the influence of dimensionality,” Phys. Rev. B **57**, 4111–4126.

Wiechert, H., 2003, “Adsorption of molecular hydrogen isotopes on graphite and boron nitride,” in *Landolt-Börnstein Group III, Vol. 42: Physics of Covered Solid Surfaces*, edited by H. P. Bonzel (Springer, Berlin), A.3.6.2, pp. 166–300.

Wiechert, H., B. Leinböck, M. Bienfait, and M. Johnson, 2003, “Diffusive motions in HD films physisorbed on graphite,” Physica B **329-333**, 426–428.

Wong, A., and X. D. Zhu, 1996, “An optical differential reflectance study of adsorption and desorption of xenon and deuterium on Ni(111),” Appl. Phys. A: Mater. Sci. Process. **63**, 1–8.

Wood, E. A., 1964, “Vocabulary of surface crystallography,” J. Appl. Phys. **35**, 1306–1312.

Woodruff, D. P., and T. A. Delchar, 1994, *Modern Techniques of Surface Science* (Cambridge University Press, Cambridge, England).

Wu, Z., 1997, “Diffraction studies of structure and growth of films adsorbed on the Ag(111) surface,” Ph.D. thesis (University of Missouri–Columbia).

Wu, Z., S. N. Ehrlich, B. Matthies, K. W. Herwig, P. Dai, U. G. Volkmann, F. Y. Hansen, and H. Taub, 2001, “Growth of *n*-alkane films on a single-crystal substrate,” Chem. Phys. Lett. **348**, 168–174.

Wüest, A., U. Hollenstein, K. G. de Bruin, and F. Merkt, 2004, “High-resolution vacuum ultraviolet laser spectroscopy of the $C\ 0_u^+ \leftarrow X\ 0_g^+$ transition of Xe_2,” Can. J. Chem. **82**, 750–761.

Wüest, A., and F. Merkt, 2003, “Determination of the interaction potential of the ground electronic state of Ne_2 by high-resolution vacuum ultraviolet laser spectroscopy,” J. Chem. Phys. **118**, 8807–8812.

Yan, X. M., J. Ni, M. Robbins, H. J. Park, W. Zhao, and J. M. White, 2002, “Silver nanoparticles synthesized by vapor deposition onto an ice matrix,” J. Nanopart. Res. **4**, 525–533.

Yang, G., A. D. Migone, and K. W. Johnson, 1991, “Automated apparatus for the determination of the specific heat and the thermal diffusivity of nonconducting solids using ac techniques,” Rev. Sci. Instrum.. **62**, 1836–1839.

Yang, S., L. Ouyang, J. M. Phillips, and W. Y. Ching, 2006, “Density-functional calculation of methane adsorption on graphite (0001),” Phys. Rev. B **73**, 165407.

Yang, S., and J. M. Phillips, 2007, “The geometric and electronic structure of commensurate $4Ar/Ag(111)\text{-}\sqrt{7}\times\sqrt{7}R19.1^\circ$ by density functional theory.” Phys. Rev. B **75**, 235408.

Yaron, P. N., and J. Z. Larese, 2006, “Thermodynamic investigation of *n*-hexane thin films adsorbed on magnesium oxide,” Langmuir **22**, 7203–7207.

Yoo, K., A. P. Li, Z. Y. Zhang, H. H. Weitering, F. Flack, M. G. Lagally, and J. F. Wendelken, 2003, “Fabrication of Ge nanoclusters on Si with a buffer layer-assisted growth method,” Surf. Sci. **546**, L803–L807.

Yoo, K., Z. Y. Zhang, and J. F. Wendelken, 2003, “A novel growth approach of ultrasmall Ge and Si nanoclusters on a Si(100) substrate without a wetting layer,” Jpn. J. Appl. Phys., Part 2 **42**, L1232–L1234.

Yoon, J., and M. H. W. Chan, 1997, "Superfluid transition of ^{4}He in porous gold," Phys. Rev. Lett. **78**, 4801–4804.

Youn, H. S., X. F. Meng, and G. B. Hess, 1993, "Multilayer adsorption of xenon, krypton, and argon on graphite: An ellipsometric study," Phys. Rev. B **48**, 14556–14576.

Zambano, A. J., S. Talapatra, K. Lafdi, M. T. Aziz, W. McMillin, G. Shaughnessy, A. D. Migone, M. Yudasaka, S. Iijima, F. Kokai, and K. Takahashi, 2002, "Adsorbate binding energy and adsorption capacity of xenon on carbon nanohorns," Nanotechnology **13**, 201–204.

Zambano, A. J., S. Talapatra, and A. D. Migone, 2001, "Binding energy and monolayer capacity of Xe on single-wall carbon nanotube bundles," Phys. Rev. B **64**, 075415.

Zeppenfeld, P., 2001, "Noble gases on metals and semiconductors. Adsorption of noble gases," in Landolt-Börnstein New Series: Physics of Covered Solid Surfaces, Vol. III/42, Part A1, *Adsorbed Layers on Surfaces* (Springer, Berlin), pp. 67–115.

Zeppenfeld, P., U. Becher, K. Kern, R. David, and G. Comsa, 1992, "Structure of monolayer Ar on Pt(111): Possible realization of a devil's staircase in two dimensions," Phys. Rev. B **45**, 5179–5186.

Zeppenfeld, P., M. Büchel, J. Goerge, R. David, G. Comsa, C. Ramseyer, and C. Girardet, 1996, "Structure and phase transitions of xenon monolayers on Cu(110)," Surf. Sci. **366**, 1–18.

Zeppenfeld, P., R. David, G. Comsa, C. Ramseyer, and C. Girardet, 2001, "Reply to 'Comment on Effect of structural anisotropy and lateral strain on the surface phonons of monolayer xenon on Cu(110),' " Phys. Rev. B **64**, 037402.

Zeppenfeld, P., R. David, C. Ramseyer, P. N. M. Hoang, and C. Girardet, 2000, "Adsorption and structure of N_2 on Pt(111)," Surf. Sci. **444**, 163–179.

Zeppenfeld, P., J. Goerge, V. Diercks, R. Halmer, R. David, G. Comsa, A. Marmier, Ch. Ramseyer, and C. Girardet, 1997, "Orientational ordering on a corrugated substrate: Novel pinwheel structure for N_2 on Cu(110)," Phys. Rev. Lett. **78**, 1504–1507.

Zeppenfeld, P., S. Horch, and G. Comsa, 1994, "Interaction of xenon at surface steps," Phys. Rev. Lett. **73**, 1259–1262.

Zerrouk, T. E. A., M. Hamichi, R. H. Milne, J. D. H. Pilkington, and J. A. Venables, 1993, "THEED of sub-monolayer phases of xenon adsorbed on graphite," Inst. Phys. Conf. Ser. **138**, 221–224.

Zerrouk, T. E. A., M. Hamichi, J. D. H. Pilkington, and J. A. Venables, 1994, "Observation of solid-hexatic-liquid phase transitions of submonolayer xenon on graphite by transmission-electron diffraction," Phys. Rev. B **50**, 8946–8949.

Zhang, Q. M., and J. Z. Larese, 1991, "Melting of monolayer argon adsorbed on a graphite substrate," Phys. Rev. B **43**, 938–946.

Zhang, Q. M., and J. Z. Larese, 1995, "Freezing transitions and order-disorder processes in multilayer xenon films on graphite," Phys. Rev. B **52**, 11335–11338.

Zhao, X., S. Kwon, R. D. Vidic, E. Borguet, and J. K. Johnson, 2002, "Layering and orientational ordering of propane on graphite: An experimental and simulation study," J. Chem. Phys. **117**, 7719–7731.

Zhdanov, V. P., 1986, "On one of the ways of application of the lattice-gas model to describe the kinetics of desorption," Surf. Sci. **171** L461–L463.

Zhu, D.-M., and J. G. Dash, 1988, "Evolution of multilayer Ar and Ne films from two-dimensional to bulk behavior," Phys. Rev. B **38**, 11673–11687.

Zhu, J. F., H. Ellmer, H. Malissa, T. Brandstetter, D. Semred, and P. Zeppenfeld, 2003, "Low-temperature phases of Xe on Pd(111)," Phys. Rev. B **68**, 045406.

Zhu, X. D., 1992, "Optical diffractions as probes to surface diffusion of adsorbates," Mod. Phys. Lett. B **6**, 1217–1235.

Ziouzia, F., J. Nyki, B. P. Cowan, and J. Saunders, 2004, "Heat capacity of the second layer of ^{3}He adsorbed on graphite pre-plated with a ^{4}He monolayer," J. Low Temp. Phys. **134**, 85–90.